A Novel Wearable Assistive Device for Jaw Motion Disability Rehabilitation

A thesis presented in partial fulfillment of the requirements for the degree of

Doctor of Philosophy
in
Engineering

at
Massey University, Auckland
New Zealand

Xiaoyun Wang

2014.07

Abstract

Temporomandibular disorder (TMD) is a group of dysfunctions in the masticatory system that cause muscle stiffness and weakened masticatory ability. TMD is commonly suffered by a considerate percentage of the population, impairs oral hygiene and brings inconveniences to a great number of patients. The therapeutic exercise with significant efficacy is widely advised among patients in the treatment of the mandibular hypomobility to reduce pain and increase the inter-incisal opening of the mouth. This thesis proposes a novel wearable device to passively assist to deliver the mandibular movement.

The mandible, attached to the skull via masticatory muscles and pivoted at the condyles at the temporomandibular joint (TMJ), can be simplified as moving in the two-dimensional sagittal plane. A planar four-bar linkage was synthesized to reproduce the specified normal jaw motion in terms of incisor and condyle trajectory on the coupler point to meet the kinematic specification. Adjustable lengths of the links were used to achieve a group of trajectories of any possibility. The prototype of the linkage has been fabricated, integrated with the sensory units and electronic hardware into a Mechatronic system.

The dynamics of the entire system was analyzed, along with the model thoroughly built up in Simulink, to facilitate further controller design. A closed-loop control scheme based on the device was proposed, and it is able to achieve the accurate position control to the crank to ensure the position of the jaw to be notified. A series of experiments with the device has been carried to evaluate the performance of the controller, with the control algorithm implemented into a micro-controller based board.

The exoskeleton was then evaluated in terms of the kinematic and dynamic interaction in the hybrid human-machine system, in which the condyle movement was recorded by AG500 tracking machine. Simulation and experimental methods were respectively developed to investigate the joint force which is in-vivo inaccessible. Simulation was conducted by adding the dynamic model of the mandible into the linkage model with controller. A test-rig was designed to mount the skull and the jaw replicas which simulated the counterparts in human body. Experiments were carried to evaluate the joint force and the performance of the controller; results obtained from both simulations and experiments have indicated the force level inside the TMJ is rather small compared with the one in the circumstance where maximum chewing force is applied.

Acknowledgement

At the moment of approaching to the completion of the PhD study, looking over what's been going through in the past four years, memories during the whole doctoral journey all crowded into my mind, full of best and worst scenes. From losing direction at the beginning, to the struggling whilst getting in the research till the persistence to the last moment, they showed up in silence to me every time when I came across difficulty. It would likely not finish the thesis without the help and support from people around me, to some of whom it is only possible to mention here.

First and foremost I wish to express my heartfelt gratitude to my supervisors, Prof. Peter Xu, A/Prof. Johan Potgieter and Prof Olaf Diegel, for their valuable guidance along the whole pathway to my completion of doctorate research, for their encouragement to every my unconfident attempt across the study, for their patience and tolerance to my occasional stagnation with a problem, and also for their concern for my life.

This thesis was partly funded by Foundation for Research, Science and Technology (FRST), New Zealand. I would like to thank the opportunity that was given to me in participating into this competitive team.

To staff at SEAT labs, Mr. Paul Thornton and Mr. Joe Wang, I am grateful for your kindly assistance in fabricating the mechanical parts and electronic boards, in purchasing the materials and parts. My gratitude also goes to the staff, Hongyan Yao, at IFNHH, Massey University, who provides rewardless help to me in the operation of the tracking machine.

Last but not least, I wish to thank my parents, who are living thousands of miles away in China. Their love provided my inspiration and was my driving force. I owe them everything and wish I could show them just how much I love and appreciate them. Special gratitude goes to my husband, Jing Chen, whose love and encouragement allowed me to finish this journey. He already has my heart so I will just give him a heartfelt "thanks." I also want to thank to my in-laws for their unconditional support.

One must choose in life between boredom and suffering. Thanks to the doctoral experience, which always reminds me the last perseverance I am still striving on.

Declaration

The author declares that this is her own work except where due acknowledgement has been given. It is being submitted for the PhD in Engineering to Massey University, New Zealand.

This thesis describes the research carried out by the author at School of Engineering and Advanced Technology, Massey University, New Zealand from February 2009 to November 2013, supervised by Prof. Peter Xu, A/Prof. Johan Potgieter and Prof. Olaf Diegel.

List of Publications

Wang, X., Xu, W., Potgieter, J., & Diegel, O. (2010). "A jaw exoskeleton for jaw motion disability rehabilitation: System conceiving and mechanism synthesis," in Proceedings of the 25th International Conference on CAD/CAM, Robotics and Factories of the Future (CARs&FOF), 2010. (pp. 1 - 12).

X. Y. Wang, W. L. Xu, K. Etzel, J. Potgieter, and O. Diegel, "Mechanism design and analysis of a wearable device for rehabilitation of temporomandibular disorder," in Robotics and Biomimetics (ROBIO), 2010 IEEE International Conference on, 2010, pp. 1674-1679.

X. Wang, P. Xu, J. Potgieter, and O. Diegel, "Review of the biomechanics of TMJ," in Mechatronics and Machine Vision in Practice (M2VIP), 2012 19th International Conference, 2012, pp. 381-386.

X. Y. Wang, J. Potgieter, W. L. Xu, and O. Diegel, " Development of Jaw Exoskeleton for Rehabilitation of Temporomandibular Disorders " in Robot Intelligence Technology and Applications, The 2nd International Conference on, 2013.

Table of Contents

List of Figures

List of Tables

Definitions and Abbreviations

2D	two-dimensional	HMI	human-machine interaction
3D	three-dimensional	HMS	human-machine system
ADC	analog-digital converter	ICR	instantaneous center of rotation
AG	articulograph	IDE	integrated development environment
CMP	continuous passive motion	IP	incisor point
CNS	central nervous system	KC	kinematic center
CP	condylar point	LSB	least significant bit
CPG	central pattern generator	LSQ	least square
CS	coordinate system	MCU	microcontroller unit
CSA	cross-sectional area	MDA	multi-body dynamic analysis
CVA	cerebrovascular accident	MRI	magnetic resonance image
DAC	digital-analog converter	PCSA	physiological cross-sectional areas
DAQ	data acquistion	ROM	range of motion
DLC	dimeric link chain	STD	standard deviation
DOF	degree of freedom	TMD	temporomandibular joint disorders
EMG	electromyography	TMJ	temporomandibular joint
FEA	finite element analysis	UI	user interface
FHA	Finite helical axis	VR	virtual reality
GUI	graphic user interface	WAD	wearable assistive device

Chapter 1: Introduction

1.1 The Concept of Wearable Assistive Robot

The emergence of the wearable assistive device (WAD) traced back to half a century ago, merely motivated to assist human movement in a wearable way, through providing external forces to either augment insufficient human strength or reduce the fatigue on body. Its development has been getting an exponential increase only until the latest decade with some key supporting technology enabled. Generally, the wearable assistive robots have been designed with an anthropomorphic mechanism of the corresponding body part, as wrapped outside of the wearer like exoskeletons of some insects, so the WADs are also called exoskeletal robots, or exoskeletons.

When compared to platform-based assistive device, the exoskeleton robot is not only characterized of portability that advances in adapting to the ambulatory occasion or the limited space. The anthropomorphic structure inherited the flexibility from human secures the mutual coordination of movement; and technically, the physical interaction enables the exoskeleton to detect wearer's motion and recognize one's intention in order to intelligently finish a certain task. Therefore, evolved from the original concept, modern exoskeletons are anticipated to carry further autonomous assistance on top of simple force supplement.

In terms of the assistive modes, the exoskeletons have been developed basically along two separate paths, oriented to able-bodied and disabled subjects respectively. The former category of devices is used to alleviate the metabolic cost in the load-carrying applications where a heavy load is externally borne, targeted at boosting wearer's capability to carry load during a relative long period; while the latter one is used to propel the immobile limb to move properly in the passive manner, focused on either replenishing weak mobility of feeble limbs under the wearer's guidance or piloting paralyzed limbs to exercise meaningful therapy for the rehabilitative purpose. In days of the world facing dramatically growing aging population, the latter group working as active orthotic device has been getting more attentions on providing aid and therapy that would benefit the post-stroke population with paralyzed limbs, in order to improve healthcare and create a decent life. Originally, many exoskeletons have been applied to wear on the extremities catering to both kinds of subjects, such as BLEEX [1], MIT-exoskeleton [2], obtaining success in augmenting physical capability in military and civilian areas, and SAM [3] for medical use, respectively.

Nevertheless, the notion of exoskeleton has extended its application field into other parts of the body, such as hands and shoulder, of either two usages. Built up with the parallel structure analogue to the anatomical counterpart, that device ensures to avoid collision intrinsically and a further autonomous control based on the sensing technology attached on the wearing body.

1.2 Background of the Jaw Disability

The masticatory system plays a rather crucial role in human digestion system as it is the key access for people to take in indispensable nutrition to maintain the health and the unique apparatus to articulate speech. The accomplishment of the masticatory function completely relies on delivering unaffected jaw movement; and due to its irreplaceability, the masticatory system would become compromised in the function realization if the mandibular movement is impaired and not able to reach normal range of motion (ROM), causing mandibular hypomobility.

The reduced range of motion usually appears among the patients with temporomandibular disorder (TMD), which is a collective term generally encompassing a group of dysfunctions in the masticatory system that cause muscle stiffness and weakened masticatory ability, accompanied with pain and clicking sound [4]. Mandibular hypomobility may hardly be spotted that makes it too negligible to treatment, but severely impairs speech and oral hygiene and brings inconveniences and discomforts to a great number of patients [5]. Although studies of the prevalence of the TMD reported different values of the proportion in the general population in terms of their samples, the TMD sufferers commonly occupied a considerate percentage of the population around the world [6].

1.2.1 Description of Disabled Jaw Movement

In fact, there is no uniform description of disabled jaw movement in terms of the way to define and exact range to scope. The mandibular motion by the jaw providing basic functionality, which plays the most essential portions to transport speech and mastication, can be derived to set as the potential range of disability. Troubles in opening the mouth inevitably exist in every move that sufferers experience functional disability and the jaw opening capacity is also viewed as one of the important parameters with which to evaluate the function of the TMJ and muscle status [7]. Referenced to an orthogonal coordination system (denoted in Figure 1-1), mouth opening and closing requires sagittal movement of the jaw, and grinding food involves lateral motion [8]. Qualitatively, the motions in the sagittal

plane and vertical rotation (yaw) have been examined to vary independently to the others, so these motions are the necessary components of the masticatory functionality [9, 10].

Based on the general description of patients suffering from TMD, the mandibular hypomobility related to jaw movement can be concluded to have several main formats some of which are represented in quantitative measures: 1) restricted opening range (fail to open the mouth more than 20mm), 2) deviation of the jaw, 3) ceased chewing function, 4) distorted chewing pattern. These symptoms can be sorted into those of the scope of TMD.

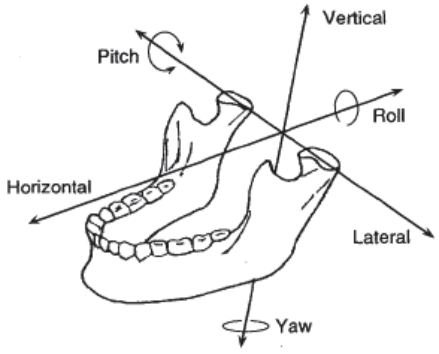

Figure 1-1 The jaw's 3D orientation and position [10]

1.2.2 Jaw Etiology

The etiology of TMD remains to be not very clear yet, but more than one diagnosis are claimed likely to trigger mandibular hypomobility, which could be classified into musculoskeletal and neuromuscular causes, depending on the dysfunction that takes place. The jaw mobility loss due to musculoskeletal reasons usually occurs on the joint, accompanied with joint ankylosis, resulting from external wound [11]. The neuromuscular reasons on the other often associate with neurologic abnormalities in the area of central nervous system (CNS) and brainstem in communication with the masticatory muscles which lose the functional control from the upper level and then go into spasm and trismus [12].

Joint ankylosis can arise after trauma and surgeries on the temporomandibular joint (TMJ), such as displaced fracture dislocation of condyle and orthognathic surgery [13-15], because the damage on the soft tissue may cause degradation of surrounding tissue that leads to adhesion formation and stiffness which even worsens the metabolic activity on the joint and further restrains its mobility [16, 17]. The irradiation unintentionally infiltrating to the masticatory area by radiotherapy in treating the head and neck cancer also brings severe limited jaw movement though with significant curative effect on the tumor on the bright side. The normal tissue around TMJ could get damaged within irradiated area, which inevitably influences the function of masticatory components to some extent [18]. 17%-41% of patients

of taking radiotherapy was reported suffering from limited jaw opening and 12% long-term trismus patients has been found due to taking radiation therapy [11].

Neurologic impairments such as brainstem hemorrhage and infarction on either brain hemisphere that come from head injury or stroke, can be accountable to the disabled jaw movement concerning masticatory muscles which usually behave with trismus and spasm that induces restrained and distorted chewing pattern [19-23]. But the occurrence of jaw disability caused by stroke presents a relative low percentage, only 2 out of 100 subjects counted quantitatively exhibiting jaw deviation from midline and muscle weakness, another 15 in 100 having ipsilateral hemiparesis in one study [24]. The small occurrence has also been implied by another study that reveals no substantial TMD or muscle weakness found among unilateral hemiplegic patients and probably can be explained that upper motor neuron innervation of the jaw muscles is usually bilateral [25].

In contrast to the opening failure, the jaw movement may exhibit difficulties in chewing and speech in the manner of weakness of voluntary muscles and abnormal fatigue on exertion caused by a neuromuscular disease of myasthenia gravis on the masticatory muscles [26]. Approximately 4% of the total number of patients who suffer from myasthenia gravis are found to experience difficulty in chewing hard food, reflecting on the lower electromyographic (EMG) activity compared with that from normal subjects [27]; and even after a period of drug treatment the jaw is also reported in need of some physical support during meals while muscle weakness is still able to feel [28, 29].

Based on the causes to disabled jaw motion, various diagnoses can be categorized into three groups, injured musculoskeletal, handicapped neuromuscular, and impaired neuromuscular.

1.2.3 Rationales for Disabled Jaw Rehabilitation

The crippled jaw motion that interferes with function conveying of the masticatory system may lead to chewing disturbances, poor oral hygiene, and nutrition loss, bringing distress to patients' lives physically and mentally [5]; from the physiological view in addition, long-term joint immobilization will deteriorate shrunk muscular strength and also speed up joint and muscle degeneration, to the detriment of future motion and function restoration [30]. Therefore, the treatment to the restricted movement is urgently required for disabled jaw recovery to free patients from misery.

Medication has traditionally been involved in treating the hypomobility, such as botulinum toxin for alleviating trismus following stroke, so as well the surgical treatment of removing the

ectopic bone after trauma to avoid further exacerbation [11, 23]. Physical therapy has been recommended to be used singly or in conjunction with other treatments in the process of rehabilitation, including several modalities such as icing or thermal packs, acupuncture, biofeedback, laser therapy and exercise. While no significant evidences were indicated by the use of other modalities, in light of the definite effectiveness to relieve the pain and restore oral function, the exercise has gained more support of usage in an appropriate way (active or passive) to improve the muscular conditions [31, 32].

The rationales that explain the effectiveness of exercise to improve mandibular hypomobility were not directly pointed out, but have been suggested among case studies, and basically summarized to lie in two aspects, musculoskeletal rehabilitation and neuromuscular one, oriented to the components where the loss takes place respectively.

To the jaw disability caused on the musculoskeletal level, immobilized TMJ exposing negative effect on connective tissues that transport fluid and control metabolic processes is to primarily blame the loss of passive and active motion among patient because of adhesion formation in the surrounding tissues [17]. Continuous passive motion (CPM) formulated from years of clinical practice, has significant effectiveness in pain elimination and range of motion restoration. CPM is prescribed to execute exercise immediately post-trauma and through passively moving a synovial joint without muscle exertion reaching gradually to a designated range of motion for a long-lasting period, CPM boosts metabolic activity to promote joint nutrition and stimulate healing progress of articular cartilage and tendons [33, 34].

CPM can help the joint restore the decreased ROM, reduce the detrimental effect of immobilization to the lowest extent and virtually accelerate flood flow and enhance elasticity, but the practice of CPM therapy also requires to follow a protocol that ensures the duration and time suitable for the current status of the immobile joint [34]. Originally applied upon the knee, CPM therapy has been taken advantage of its potentials to deliver exercise for the joint rehabilitation to an extended arena of body parts, some of which receive CPM therapy via specially designed CPM devices to eliminate manual work drawbacks based on the rationale of CPM, also obtaining significant clinical evidences [35, 36].

The exercise training that has long been used in course of rehabilitation to the paralyzed limbs due to brain injuries has displayed considerable effect in regaining the lost movement back to normal state, which has been evidenced clinically [37, 38], since rehabilitation in the form of exercise following brain damage stimulates cerebral reorganization in the brain cortex that is

able to re-establish the control to the limb which loses the connection with the impaired counterpart [39]. The plasticity in the brain cortex is capable to undergo changes throughout the whole life, even post-injury to the cortex, the process being referred to be the cortical reorganization, which is only incurred with both a stimulus and an area of healthy cortex [40]. Moreover, the cortical plasticity that in normal adult brains appears to be skill-dependent shows up changes with learning of new skills rather than only with repetitive use, making the exercise training offer exclusive benefit to the rehabilitation [41].

In light of this, the disturbed jaw motion affected by the neuromuscular level involves brain deficits occurring in the area pertaining to the regulation of the mastication that causes disruption to control masticatory muscles. The mastication as known is of complex rhythm movement which pattern of mastication is intrinsically generated by CPG that resides in brainstem, and the face primary motor cortex which takes part in the voluntary jaw movements plays an essential role in fine control of the mastication [42]. The plasticity has been found to go through some changes after cortical disruption and masticatory exercise on the other way is able to lift the cerebral blood circulation on the area of the primary cortex and activate metabolism of the brain function [43]. Therefore, appropriate masticatory movement would promote the cortical plasticity to reshape its representation through the course of learning masticatory task [44, 45]. The physical exercise in the skill-related form could be recruited in the rehabilitation to the restricted movement of the jaw.

1.2.4 Efficacy of Therapeutic Exercise

Prior to our summarization of the rationales of rehabilitation by physical therapy, the therapeutic exercise had already been found to create significantly efficacy in the treatment of the mandibular hypomobility to reduce pain and increase the inter-incisal opening of the mouth [11]. The exercise for training the jaw was largely mentioned in the cases of joint ankylosis following post-irradiation or post-surgery [14, 18, 46, 47], though a few cases of TMD caused by brain injury and disc displacement were also reported to take advantage of exercise to improve limited jaw movement [48, 49]. In the course of the training, stretching devices were normally offered, and able to carry out both active and passive exercise, for the purpose of reinforcing muscular force and activating TMJs, respectively [48]. Among them outstands the [1]Therabite® Jaw Motion Rehabilitation System™, which was broadly adopted to assess the effectiveness of the exercise in clinical trials; also reported a manual device

[1] Therabite® Jaw Motion Rehabilitation System™: for more information, please visit http://www.therabite.com/

dedicated to dilating the mouth for the hypomobility treatment, presenting the efficacy by its clinical usage [50].

While focusing on the efficacy the exercise brings by some implementations, the exercise protocols could not be averted from our sights as well, owing to the cause-and-effect relation. The exercise underlines its delivery by practicing duration, frequency, range magnitude, and gradually intensified program etc., which could be modulated individually in each clinical trial. But the exercise generally lasts at least two weeks to reveal the effects, and the duration is even advised to be prolonged after reaching desired distance in order to prevent the relapse [46]. In view of this, the exercise device highlights its advantages in offering self-adjustable movement range and featuring self-operation compared with traditional methods [50]. The outcome after the exercise has been remarkable in several aspects; quantitatively, the proportion who gets the effect on receiving therapies exceeds more than half of the total subjects across all trials, and the increased opening ranges averages more around 10mm; qualitatively, pain amid jaw moving disappeared to a large extent and the effectiveness of the exercise also brings with the enhancement for quality of life in terms of the functional recovery of the mouth [46]. In addition, the adverse effect from safety consideration was rarely reported in our reviews of cases where therapeutic exercise was applied. Only one research reported the ineffectiveness of the physical exercise for improving jaw opening range, which only took place in a different circumstance that the exercise was carried during the radiotherapy [51].

1.3 Motivation and Research Challenges

In light of the high proportion of effectiveness in restoration of mandibular range of motion with the aid of the exercise, the therapeutic exercise by delivery from physiotherapists or current devices has widely been promoted to practice among the patients simply for dealing with the lost jaw motion. The ideal approach to carry exercise would be mirrored in two sides, to get rid of the downsides of traditional methods, as well as reinforce the bright sides that are functionally called for in the treatment; more clearly, on one hand to make up for the shortage of therapists which may indirectly compromise the eventual efficacy to the patients; on the other hand, to offer the individually tailored therapy that is technically substantial for a complete treatment, including a variety of the protocols at the different stages of course, the duration of each therapy and the total practicing time; meanwhile, to enable proper therapy to be done in daily routine, and operating out of clinic; and as a bonus function to take part in the assistance of chewing in case of being needed.

Motivated by above multi-side expectations, there is no more appropriate to conceive a novel device to fulfill widely applicable operations, particularly in the context that few devices that have been specially developed to provide exercise training protocols. Inspired by the notion of exoskeleton that is characterized of non-conflicting mechanism, multiple control modes and high portability, an autonomous device is anticipated into development to behave in the similar way of exoskeleton that is worn externally on the user, to provide and therapeutic exercise and assistance for daily usage.

However, there are still some challenges have much to face in the successful way to a complete delivery of a specific device. Apart from many common barriers associated with the development of the exoskeleton, such as the misaligned joints, and the portable power supply, lack of which could severely compromise the performance of devices, the jaw exoskeleton is still puzzled by a problem to be attached onto the chin with a compact structure which never happened to exoskeletons on the other parts of body. That could impose more limitations in its implementation means. Different from other joints in the human body that are generally treated as a single hinge, the TMJ that has a much complicated moving workspace requires an appropriate representation in the device to ensure no impairment imposed from the exercise. The individual variance places one more challenge for universally applicable expectation of the device. Back to the device, lightweight structure brings comfort of wearing, at the same time ensures fast response to the feedback signals to be acquired from wearer owing to the low inertia. Therefore, detailed design methodology involves full understanding to human masticatory system trading off with the actual implementation.

1.4 Aims and Objectives

In this thesis, appropriate techniques are taken advantage of to fulfill the aim of the research, which ultimately is to develop an unprecedented wearable assistive device (jaw exoskeleton) that is expected worn on the jaw to execute exercise for the purpose of rehabilitation of jaw motion disorders during daily routines. It can be further divided into following objectives:

1. Investigation of the mandibular movement and construction of a proper mechanism;

   The mandibular movement is too complicated to be reflected fully by the device, so a proper kinematic pattern representative of the forced exercise for the jaw is indispensible to suit the application based on the understanding to human masticatory system. The mechanism based on the kinematic pattern of the mandibular movement will be proposed and it underlies further kinematic and dynamic analysis.

2. Mechatronic design and development of a wearable device;

   The construction of the jaw exoskeleton into prototype will consider featuring lightweight and wearable to materialize the above mechanism in the structure and the mobility of the control scheme implementation; the sensory unit will also be incorporated into the system at critical locations in order to detect the body movement, completing the system to achieve the autonomous operation.

3. Motion control of the jaw exoskeleton;

   Appropriate motion control of the exoskeleton represents the variety of the exercise in terms of concerned variables, such as force and position, and the integrated control relies on a robust algorithm which is able to process the feedback signals from the sensory unit and then convert the corresponding information to controlling command after decision making.

4. Investigation of the human-machine interaction.

   Before the device gets on wearing by human, the safety and reliability should be inspected in terms of the wearers; and it is reflected by representative kinematic and dynamic performances by simulations and experiments, since the human-machine interaction directly indicates the impact from the device to the wearer.

1.5 Significance and Major Contributions

Revolving around the objectives of this thesis, six major contributions to knowledge in the area of wearable assistive device specifically applied to jaw disability rehabilitation will be established in the research work stated in the remaining chapters, as summarized below:

1. By investigating the in-vivo jaw movement, the kinematic pattern pertaining to the functional rehabilitation is formulated by decomposing the joint movement, which is not limited in description of the entire jaw movement, but focused on the typical one borne in this application instead, as the specification for the mechanism design.

2. The rigid-body guidance is introduced to formulate the typical movement of the jaw, which derives the synthesis objective of motion generation. The path of the instantaneous center of rotation contributes as one of the constraint to the synthesis process, regulating the moment to stay between super-sensitive and super-stable position.

3. The Mechatronic system of the jaw exoskeleton is designed and fabricated as the first prototype. The mechanical structure composed of adjustable links allows a great adaptability of the device to the population; the electronic hardware is tailored to fit the portable application; and the sensory units are seamlessly integrated into the device.

4. The dynamics of the jaw exoskeleton as the foundation of the controller design is analyzed in a simulation model which consists of the linkage, the motor and the controller. A bottom control scheme is developed to achieve the position control, which is validated by experiments under a series of predefined motion profiles.

5. The masticatory system is modeled under the environment of rigid-body movement. Each component is assigned with meaningful physical properties, and the material of the components is represented by modeling the mechanic properties if applicable. The implicit and explicit connection between human and the device are modeled by simplified contact. The influence is evaluated when the linkage model produces the whole human-machine interaction. Instead of focusing on the biomechanical properties, the contribution lies in investigating effect on the TMJ imposed from external force.

6. A set of experimental test-rig is built up to mimic the real loading condition the exoskeleton will bear. A pair of inverse-engineered jaw and skull replicas is mounted. The experiment to measure the internal joint force subject to the exoskeleton is conducted to obtain the effect from the exoskeleton.

1.6 Organization of the Thesis

This thesis presents the researching path on the wearable assistive technology specifically applied on the jaw, from thought conceiving of device, via the implementation by the prototype, to verification of reliability. Within this arena, the whole structure of the thesis is organized as states below.

Chapter 2 firstly offers an overview of the human masticatory system from a biological perspective, covering its properties in the area of kinematics, dynamics and biomechanics that would form the footstone for the device development. Then a history of the previous devices specially developed for mastication delivery is pictured technically by analyzing each design concept and its implementation. In light of the expectation to the jaw exoskeleton, some key technology in the field of mechanism synthesis and control strategy whose spectrum is narrowed down to fit this application undergoes a general review.

Chapter 3 starts the design process from identifying the fundamental specifications for constructing the mechanism, followed by the mechanism synthesis through which the fundamental structure of the device is formed. Along with the requirement of the adjustability to adapt the diversity of the population, the mechanism is evaluated in terms of the trajectory generation.

The whole Mechatronic design scheme of the jaw exoskeleton is fully elaborated in Chapter 4, where the hardware is focused on. With considerations in the practical operation, the mechanical parts of the device are designed, integrated with configuration of the controller hardware, and installation of the sensory units.

Dynamic performance of the device prototype is investigated in Chapter 5, presented with analytical calculation and simulation in SolidWorks. A model built up in SimMechanics/Simulink is composed of fully converted SolidWorks assembly, the motor and the controller. Control scheme is firstly verified in the Simulink model, amid the tuning of the parameters of the controller, which is transplanted into the micro-controller based control board. The basic trials at three experimental scenarios are tested on the controller.

Chapter 6 focuses on the evaluation of the jaw exoskeleton via simulation and experiment, for the purpose of verification of the satisfaction of the design requirement, and investigation of the man-machine interaction that seriously concerns the safety. The dynamics of the masticatory system that is modeled in Simulink is combined with the linkage model with proper contact means to evaluate the impact to the TMJ in the simulation. The joint force inside the TMJ is further tested based on a custom built test-platform.

Chapter 7 summarizes the work and the achievement in this thesis, and points out some missing aspects amid the research, finally recommends the direction for future research.

Chapter 2: Literature Review

Understanding the masticatory system underlies the development of the jaw exoskeleton, and it lies in not only the pattern of the mandibular movement, but also its behaviors of each component that associates with functioning jaw. As one of the most complicated systems in humans, it has not yet been fully explored in many interconnected aspects, but previous researches provide us multi-angle prospective in terms of each field of our interests. Therefore, this chapter gives a serious review on the kinematics, dynamics and biomechanics of the masticatory system that awaits justification, with a start of brief introduction of its anatomy and related components.

Though the concept of the jaw exoskeleton appears to be proposed for the first time, similar devices that are termed as jaw motion simulators in this chapter can be found from literature to fulfill part of the function relating to the mastication; and a quick review for such devices will be given in the aspects of the mechanism and applied control strategy, to find out the design mechanics in light of bio-inspiration.

In addition, as envisaged to be operating in the man-in-the-loop mode, the exoskeleton possesses its own requirements penetrating into every corner of the development, such as the construction of the mechanism, the holistic control scheme conceiving, and the hardware composition, correspondingly associated with which will undergo a rough review as well, for the purpose of being differentiated from the principle for the development of common robotic devices. Biomechanics of the masticatory system that will be given an emphasis in the review lays the foundation for further investigation into the interaction between the device and the wearer.

2.1 The Mandibular Kinematics

The jaw movement would be one of the most complicated movements involving human joints owing to the anatomy of the masticatory system and multiple inputs to accommodate neurologic control [45]. Accordingly, the movement has so far been represented by different models, which are claimed to adequate in reflecting its unique features per se and its relationship with morphology. Features in terms of the kinematics may exhibit a large range of variation, affiliated with the associated models.

2.1.1 Human Masticatory System

A. Overview

The human masticatory system is comprised of the maxilla (the upper jaw) and the mandible (the lower jaw) pivoted via both-side temporomandibular joint (TMJ) at each condyle on the mandible, as shown in Figure 2-1. The mandible is actuated to carry out movement by masticatory muscles with respected to the maxilla which composes the whole skull with other bones. Teeth are attached on both sides of jaws to function cutting and grinding food [52].

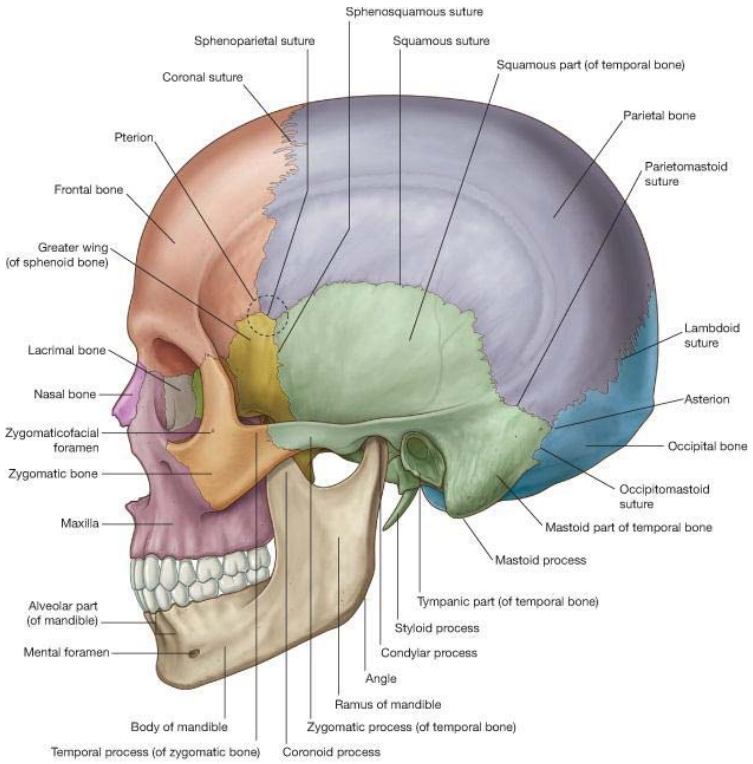

Figure 2-1 Bones of skull and mandible in lateral view [52]

B. Muscular Composition

Muscles that are recruited in mandible actuation are mainly attached between the upper and lower jaw; they are four pairs of muscles, temporalis, masseter, medial pterygoid, and lateral pterygoid, located symmetric across the midline, comprising the major masticatory muscles, as their locations shown in Figure 2-2. Masticatory muscles can drive the mandible to do elevation, depression, protrusion, retraction, and lateral movement by different combinations together with neck muscles, which are attached under the jaw playing a minor role in jaw opening [52]. Basically, the masticatory muscles can be divided groups of elevator and depressor, literally taking part in the movement of mouth-opening and mouth-closing respectively. The elevator muscles, referring to the temporalis, the masseter and medial pteryoid, have radiating shapes with relatively large physiological cross-sectional areas (PCSA)

in common, apt to the chewing circumstance which entails large forces during contraction [53-55]. In contrast to the elevator, the depressor such as digastric, geniohyoid and mylohyoid muscles have small PCSA, not able to generate as large forces as those from the elevator, suitable for the depression that the gravity of jaw is also involved to replenish small forces in the course over long distance. The lateral pterygoid muscles largely provide the actuation for jaw protruding.

The mandibular movement is mainly formed in a three-dimensional space by active contraction of muscles, and can hardly be affected by passive force from components in the masticatory system such as TMJ ligaments [56]. But TMJ ligaments affects greatly to the condylar movement, which can be easily accounted by the adjacent location between them; TMJ ligaments become dominant in restricting the jaw from overstepping the joints when the jaw approaches its boundaries [57].

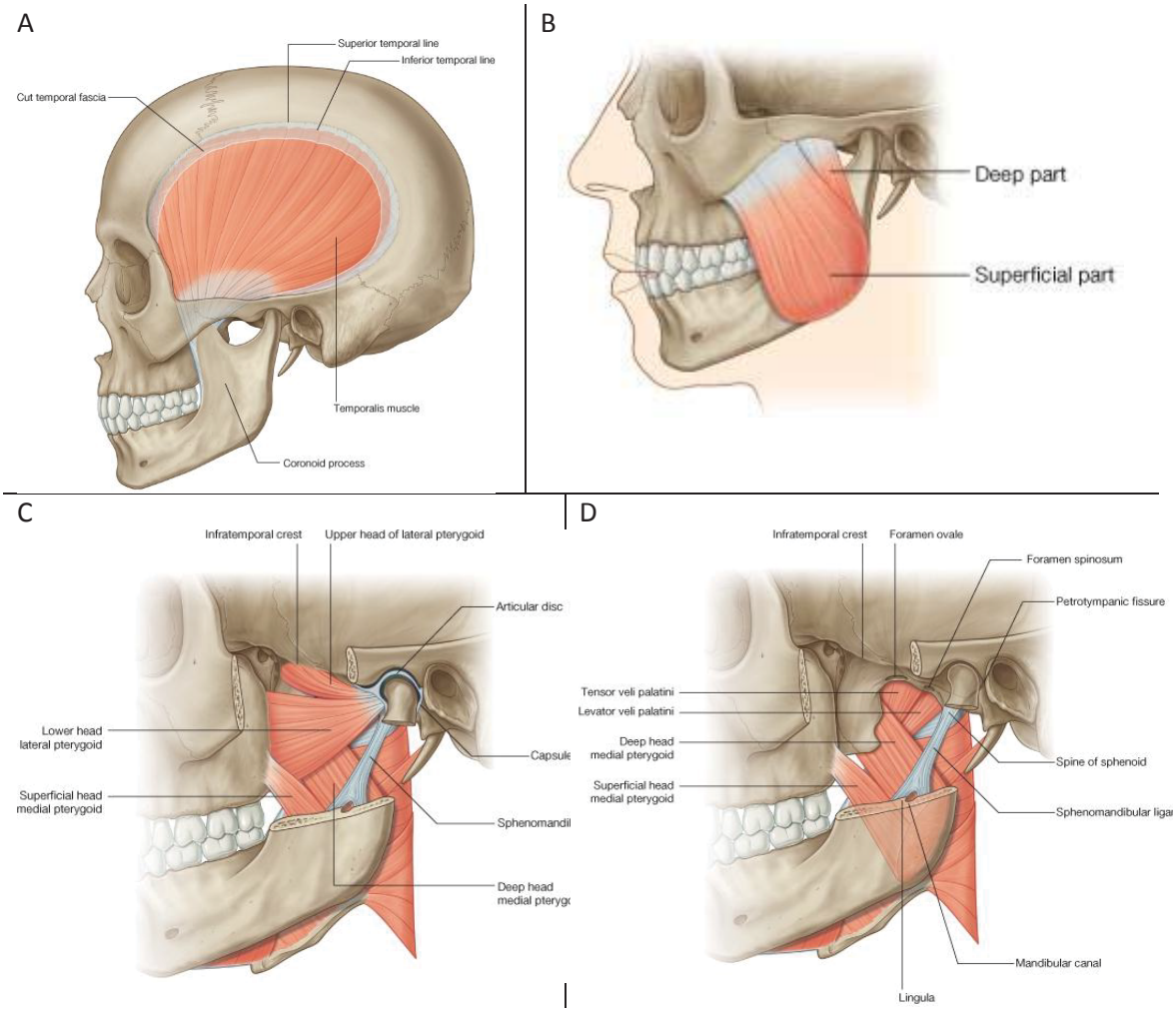

Figure 2-2 Muscles of mastication [52]

C. Temporomandibular Joint

Temporomandibular joint is the two-sided articulation exactly defined between articular tubercle and fossa of the temporal bone and the head of mandible, either side of which forms the superior and the inferior bound of TMJ [52]. Externally surrounded by the capsule, a cavity is formed together with its bounds in the joint, and is filled with synovial fluid, which flows as a lubrication to decrease friction during the mandibular movement, as illustrated in Figure 2-3 (A). A cartilaginous articular disc sits between the mandibular condyle and fossa, separating the synovial cavities into an individual upper and lower part. The articular disc in essential is soft tissue, which spreads the incoming pressure across the whole contact area, allowing to absorb the shocks to the joint and stabilize the condyle during the mandibular movements [58].

Basically the jaw movement on the condylar point does not exhibit along a stationary trajectory though the condyle goes against the superior bound of the joint [56]. Since when the jaw is opening, the upper joint leads the disc to go forward against the fossa and the lower one follows the jaw as a relative pivot allowing the jaw to depress (as illustrated in Figure 2-3 (B)), the TMJ moves in three-dimensional space while presenting variation of the trajectories on the condyle point subject to the slack cavity. The TMJ ligament plays a critical role in the border movement of the jaw, to prevents the condyle from being displaced too far inferiorly and posteriorly and provides some resistance to lateral displacement [58].

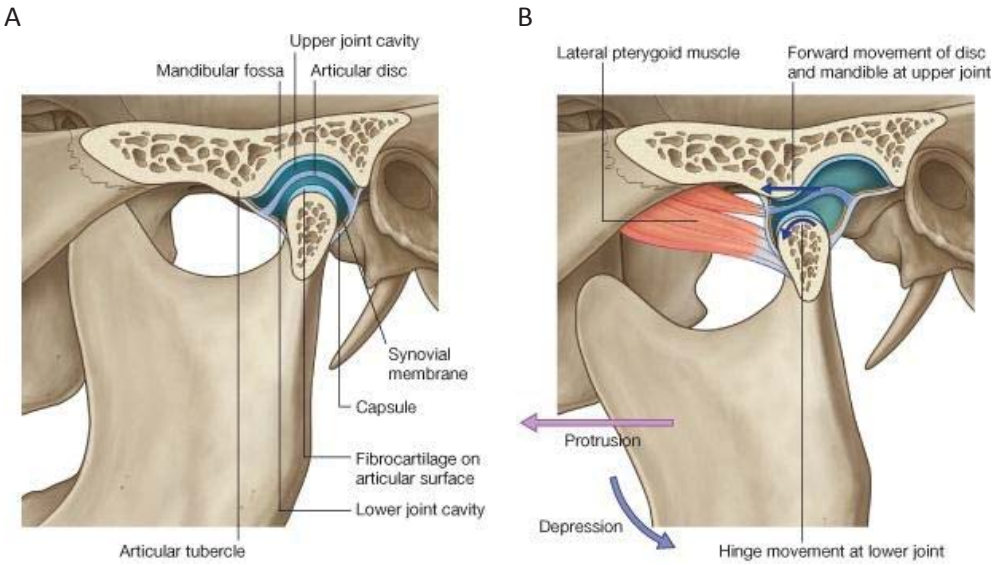

Figure 2-3 The temporomandibular joint in (A) mouth closing position (B) mouth opening position [52]

D. Control of the Masticatory System

The mastication process entails three units in its control: effector organ, sensory input and central nervous system, all are enclosed to produce smooth mastication that is composed of rhythmic cycles of jaw-opening phase and jaw-closing phase, with slow power stroke at the end [42, 59]. Jaw muscles are all innervated by cranial V (trigeminal) motoneurons in brainstem, activated jointly by central pattern generator (CPG), motor cortex and sensory input [42]. Fundamentally, the mastication relies on CPG to generate intrinsic pattern, while reacting to sensory input to regulating masticatory movements in a smooth way by motor cortex which has an effect of fine control.

CPG consisting of groups of neurons in the brainstem generates rhythmic pattern of movement essentially for the mastication; it is subject to the conscious control and peripheral feedback, but its production is not dependent on their afferent information, even in the circumstance without brain cortex and sensory inputs [60]. Therefore, the brainstem CPG generates the intrinsic pattern of mastication that would be most pivotal in CNS for mastication.

The brain cortex takes part in the control of muscles of mastication with the cortical masticatory area (CMA), the face primary motor cortex (face MI) and the face somato-sensory cortex (face SI) [59]. Motor efferent from the CMA is considered as the major source activating the masticatory CPG, which is supported by evidences in patients and animals that showed disrupted activity related to mastication due to cortical damages [61]. Therefore, brain cortex has participated in the voluntary jaw movements, and plays a vital role in fine control of the mastication to maintain the mastication and coordinate of muscle activities as well. Sensory receptors receive sensory information from afferents that broadly spread in the masticatory apparatuses though they are linked to different nerve branch. The peripheral sensory afferents project the acquired information such as movement parameters and muscular forces to cortical area, forming the feedback to the cortex to achieve the fine control of voluntary mastication [62].

2.1.2 Description of the Mandibular Movement

Massive studies have proved that the jaw movement has six degree of freedoms (DOF) in three-dimensional space and the mandible translates against the articular fossa at the condyle while rotating downwards during the jaw opening if regardless of lateral motions. Mandibular kinematics has been studied in many fields, such as orthotic surgery, pathology of TMD and bioengineering, in terms of the range of motion, trajectory of concerned points, and velocity

in each stage and movement pattern. The mandible is universally treated as a rigid-body as it demonstrates little deformation upon normal functional tasks compared with other soft tissues in the masticatory system. Therefore, the spatial jaw movement can entirely be described by the trajectories of non-collinear three points in the mandible, in this circumstance selects the incisor point and condyle points on both sides; if only focusing on movement on the sagittal plane, the projected condylar trajectory always attracts our interest apart from the incisal one.

Before computational models came into sight, the condyle has been represented by anatomically determined points in the assessment of TMJ prostheses; those casually selected points apparently would be very arbitrary and unreliable in evaluating the motion. Kinematical models have been formulated based on discovery from recorded trajectory at incisor and condyle to reflect some features that may induce a pattern to describe the jaw movement. According to the representation, the movement models can be grouped into two ways, which are set up based on absolute or relative reference points in the coordinate system.

Definition of anatomical planes associates with relative movement in body parts. According to the anatomical terminology, three reference planes passing through the body have been indicated. They are coronal plane, sagittal plane, and transverse plane, as the first two shown in Figure 2-4. Additionally, two pairs of terms that will be frequently referred to differentiate the relative locality are anterior and posterior, as well as superior and inferior; the former indicates a relative position in the direction of front to back, while the latter signifies the direction vertically [52].

(A) Sagittal Plane (B) Frontal Plane

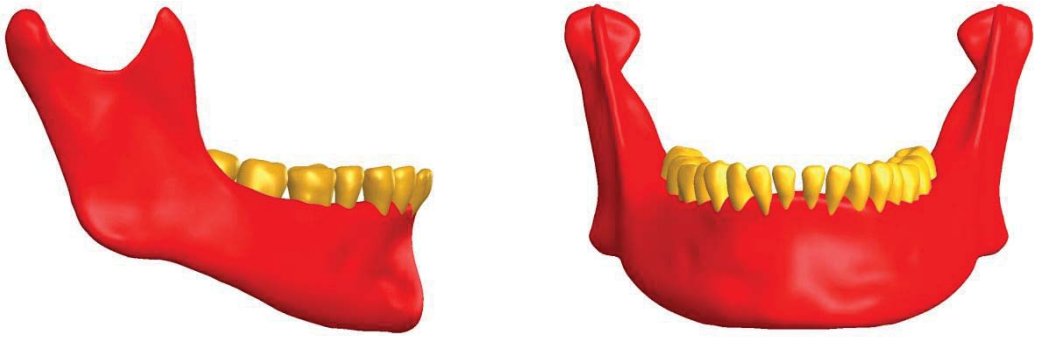

Figure 2-4 The anatomical planes demonstrated on the mandible

A. Absolute Reference Point Based

All methods in this type are more displaying a way to describe the absolute jaw movement basically within the Cartesian coordinate framework, instead of models that are dedicated to

outline a motion pattern. One application exists in setup of a transformation relation in inverse calculation of condyle trajectory from the recorded incisor displacement [63].

1. Cartesian Coordinate Description

Using the Cartesian coordinates is one of the most well-known methods to depict the jaw movement, which combines the translations along the orthogonal axes with the rotations around each axis with respect to a fixed frame (referred to Figure 1-1). The origin of the coordinate system is a stationary point on the skull, usually chosen as the projected condyle to the midline at rest position, or sometimes the head or a point on the temporal bone in the case of coordinate system setup for inverse calculation [64]. This description offers a holistic representation of jaw movement in three-dimensional space without loss of generality; the movement on a specific point can be calculated based on the magnitude in each DOF from original coordinates of the point. In the research of identifying dimensions in jaw motion control, four out of the six decomposed DOFs in Cartesian system are found varying independently and would be essentially controlled in speech and mastication [9]. This description has also crossed widely with researches employing dynamic model of the mandible to study the muscular contribution to a certain jaw movement [55].

2. Non-orthogonal Floating Axis

The non-orthogonal floating axis coordinate system is claimed to describe the jaw natural movement by clinically relevant parameters without speculation of the condylar position [65]. In this description, two Cartesian coordinate frames are set up and initially in coincidence with each other, one being fixed on the mandible (as frame M illustrated in Figure 2-5), able to float with respect to the other (as frame S) which is fixed on the skull as the global reference frame.

During the movement the floating coordinate frame is moving together with the mandible, creating changes from the global one, and the motion is evaluated by six parameterized variables of the rotations around and the translations along three axes of the floating frame. In this way, the spatial relation between the floating and the global frames can be represented with a transformation matrix which is established by the parameterized variables. Therefore, the absolute instantaneous position of concerned point can be calculated through transforming the coordinates from the floating frame to the global one.

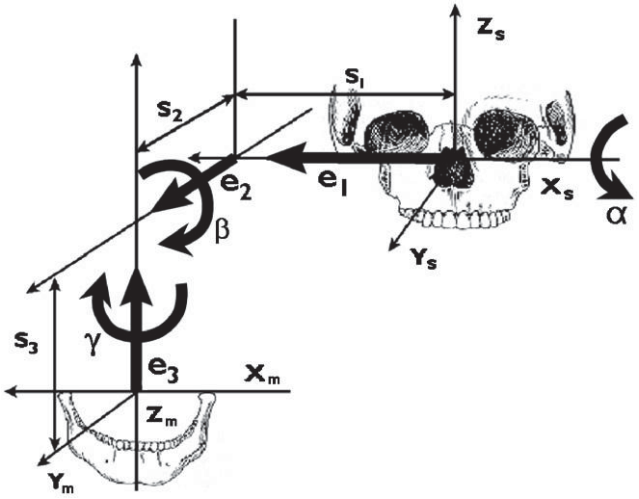

Figure 2-5 Mandible movement described with non-orthogonal floating axis [65]

3. Terminal Hinge Axis

The mandible used to be described to rotate around a fixed shaft during symmetric movement, and the shaft located throughout both sides of condyles with minor shift near the actual boundary is the terminal hinge axis, as figured in Figure 2-6. In fact, the mandible can do the pure rotation around the terminal hinge axis up to an opening distance of 20 mm, still keeping the condyle residing in the posterior area [66]. Therefore, the jaw opening distance can on the other way indicate the inclination angle of the jaw on the sagittal plane. But the existence of the pure rotation remains still unknown in the normal jaw movement, not even to mention during the whole opening range [67]. One application of the TMJ prosthesis which uses a fixed center of rotation as the joint also supports the viewpoint that the traditional terminal hinge poses a restricted range of jaw opening [68].

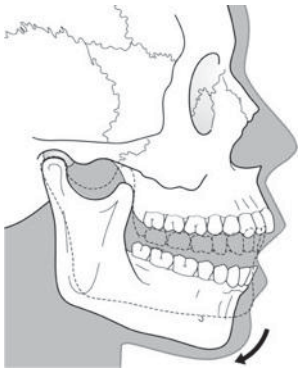

Figure 2-6 Illustration of terminal hinge movement [69]

B. Instantaneous Reference Point Based

The models in this type are prone to describe an intrinsic motion pattern through the observation of the jaw movement, reflected on the trajectories of selected points that are

able to define rigid-body movement, so they are more focusing on discovering the correlation between trajectories of these points with respect to one of them which is generally chosen to be the condyle.

1. Instantaneous Center of Rotation (ICR)

The instantaneous center of rotation (ICR) is a comparatively immovable point at each infinitesimal interval in a rigid-body around which all other points are rotating, bringing an incremental planar displacement (Figure 2-7) [70]. Fixating on jaw movement on the sagittal plane which combines rotation with translation, ICR regularly refer to a relatively stationary point the jaw revolves around instantaneously [71]. In contrast to the terminal hinge defined as an absolutely fixed point on the condyle, the ICR emphasizes a shifting path of axes generated from each displacement increment which if known can be used to easily figure out the jaw movement on other points. Unfortunately, the ICR path has been evaluated to spread at different locations without a specific pattern in the jaw opening to maximum distance, and vary inter-individually in a broad range; but being below the condyle basically has a large occurrence during the entire jaw movement, in consistence with the discovery from terminal hinge [70-72].

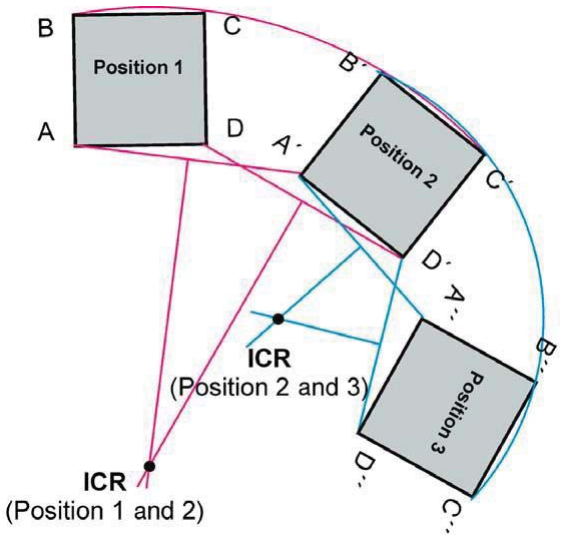

Figure 2-7 Schematic drawing of ICR [70]

2. Kinematic Center (KC)

Kinematic center (KC) also gives relatively stationary reference in the sagittal plane. It is a specialized center of rotation that is constantly located on the condyle and minimally influenced by the mandibular rotation; in this way KC is interpreted as an axis that the mandible revolves around as well as travels translationally along the articular eminence [73,

74]. Therefore, the sagittal planar movement can be characterized to have two DOFs composing of the mandibular rotation around a KC and sliding along the KC path, as pointed in Figure 2-8.

KC is by experiments confirmed to locate superiorly and anteriorly with respect to the lateral pole of condyle; and owning to the jaw protrusion which contains only translational movement, KC could be obtained from seeking the coincident trajectories of points from protrusion and the opening [73]. The ratio of rotation to translation during the open-close movement was not explicitly revealed by a value; according to experimental outcomes, the ratio would be locked between 1 °/mm to 2 °/mm, which only stood for average estimation. However, the location of KC was occasionally reported not in a predictable relationship with condylar anatomy and not even within the contour of the condyle; and the KC path was not either found in consistence along the fossa during the jaw movement [75].

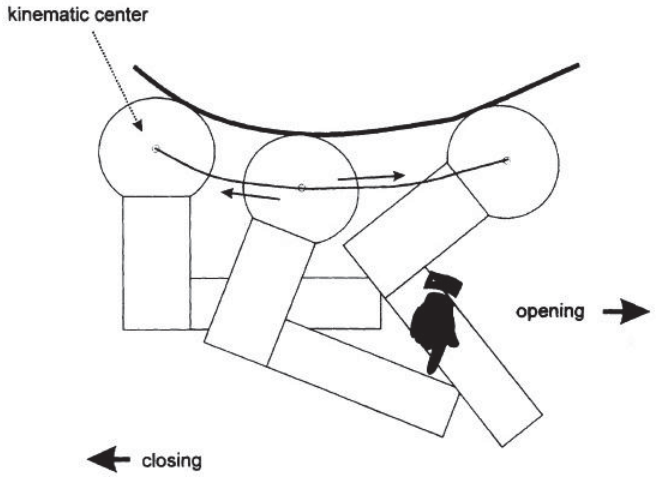

Figure 2-8 Schematic drawing of Kinematic Center [76]

3. Finite Helical Axis (FHA)

Finite helical axis (FHA) can be considered as the concept of ICR in the plane extended to the three-dimensional space to describe spatial jaw movement spanning at a sampled step around a reference axis. The mandible translates along an axis to which only one side of the condylar point is perpendicular, as shown in Figure 2-9 (A), while rotating along this axis which crosses through the condyle transversely [77].

There are four parameters involved in the FHA model to evaluate jaw movement at each sampled step: $d_{CP}, \theta_X, \theta_Y, \theta_Z$, referring to the vector from selected condylar to the axis, the angles between axis and the reference coordinate frame, respectively (as denoted in Figure 2-9 (B)). As the vector d_{CP} can be decomposed into three displacements with respect to the

reference coordinate, FHA can precisely define the jaw movement in space. Symmetric movement generally leads to parallel helical axes medio-laterally oriented, and the spatial movement description with FHA is able to accommodate more information with those parameters to feature asymmetric movement without loss of simplicity, which is reflected on orientation and position changes of helical axes [77-79].

A B

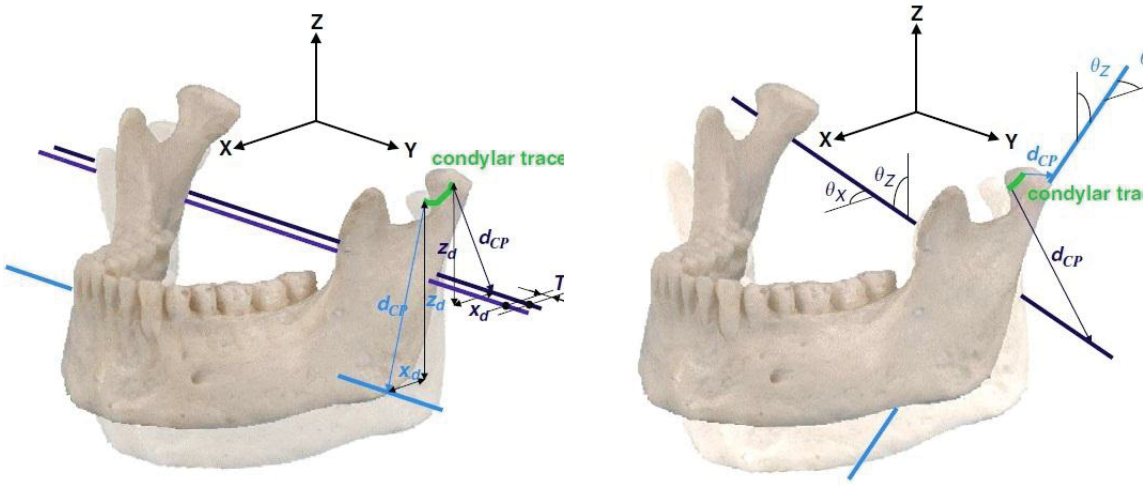

Figure 2-9 Schematic view of helical axis at (A) symmetric movement and (B) unilateral movement [78]

4. Dimeric Link Chain

The mandibular movement is described to rotate around two axes under this method, and Dimeric link chain (DLC) specially refers to a distance constantly maintained between two rotation axes. The mandible rotates around one axis which is called mandibular axis while swinging on a circular path around a fixed maxillary axis at the same time [80]. So the planar movement of three DOFs under this concept is shrunk to two, which are specified by two rotational angles. Jaw movement based on description of DLC was rarely mentioned in the literature, and possible reason could be the difficulty in identifying the location of two axes and defining the rotational angles upon those two axes, though the description was quite precise.

C. Discussion

Apart from the absolute description of the mandibular movement in the 3D space, attempts have always been made to describe the movement by a model that covers as much as features with as few as parameters. Also, a relative rotational center has always been virtualized, empirically chosen as a fixed or relatively stationary point on the condyle. Unfortunately, as to the most prominent points on the mandible, the incisor and the condyle,

no research has disclosed their correlation in terms of the instantaneous position on each trajectory.

2.1.3 Mandible Movement Range and Its Boundary

The function of the mandible is usually evaluated by the range of inter-incisor opening distance. Though each point on the jaw theoretically has a movement boundary subject to the movement, the incisor has been continually chosen in description because of being easy to operate and its standing functionality of the jaw able to reach.

A classic envelope initially described by Posselt demonstrates the boundary movement of the mandible by tracing the maximal reachable displacement on the lower incisor along guided paths, and the three dimensional active space was present by enclosing the projected figures to sagittal, frontal, and horizontal planes, as illustrated in Figure 2-10 [81]. Three extreme paths along which to execute the movement basically encircle the envelope, obtaining approximate range on the point of the incisor. Protrusion sketched with *1-2* composes the superior bound, the irregular curve presumably being caused by convex tubercle in-between in guiding the condyle and occlusal incongruity. Followed by anterior bound, the extreme opening subject to protrusion, illustrated by curve *2-m.o*., involves a pivot movement, which occurs at the farthest position of condyle. The posterior bound, depicted with curve *1-m.o.* is formed by two sections of movement, the first half by *1-H* representing hinge opening where the condyle still resides in the fossa cavity and the second by *H-m.o.* rotating while the condyle translates out of the fossa rendering a forward movement.

The entire border has a great variation in the measurement not only because of inter-individual differences. The maximum jaw opening displacement three-dimensionally measured on the inter-incisor point correlates significantly with the genders and the mandible size, reflecting on the evidence that male gives approximately 10 mm larger spatial opening distance than female, which is also attributed to the bigger size of male mandible than female [82, 83]. But each section of the critical pathway can be approximated within a range. Typically, the maximal protrusion executes about 10 mm anterior translation; the extreme anterior movement gives the uppermost about 50 mm vertical translation; and the hinge movement only opens up to about 20 mm vertically; the lateral movement achieves about 12 mm at the farthest end [84]. The range of envelope at the deepest point *m.o.* can even reach 70 mm in adults in the sagittal plane [85, 86].

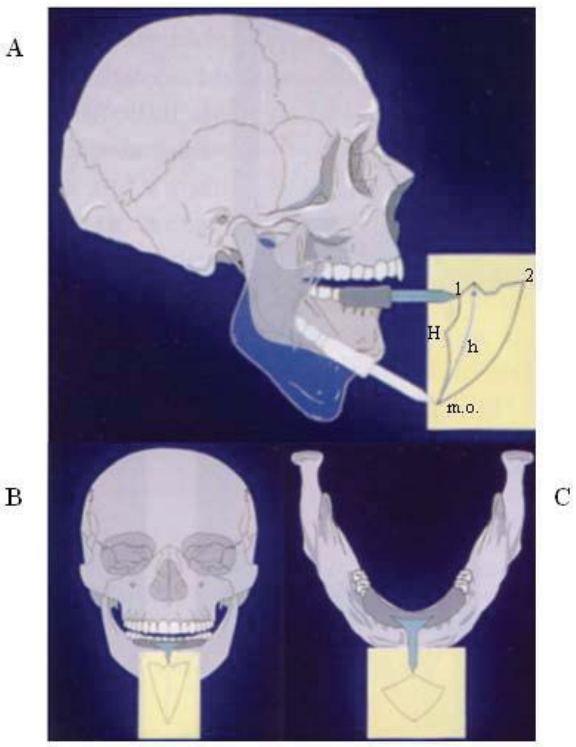

Figure 2-10 Posselt envelope in (A) the sagittal plane (B) the frontal plane (C) the horizontal plane [81]

2.1.4 Features of Condylar Movement

Though condyle point on each side would be the other pivotal points of our concern in the mandible, which is easily recognizable and accessible to acquire the displacement information to complete the rigid-body movement, the boundary of the incisor may not likely corresponds to the maximum displacement on the condyle. The maximum incisor opening displacement has been suggested not in strong dependency on full translation of the condyle and the amount of incisor opening distance is dominantly accountable to the condylar rotation [83, 87]. The condyle is basically moving within a similar envelope like Posselt's, and from a sagittal view it is shaped as a strip. By referencing the critical sections on the incisor trajectory, the condylar path contributing to the incisor counterpart still can be approximately outlined accordingly as follows: the maximal protrusion is derived of about 10 mm anterior condylar translation; the extreme anterior path comes from the peak 30° rotation upon 6 mm more translation; the hinge opening rotates the condyle about 13° in the sagittal plane; subsequent movement reaches the deepest point by finalizing the rest rotation plus translation [84].

A. Condylar Trajectory Length

The condyle varies significantly in its morphology among individuals, so does the translational length inside the TMJ as well, which demonstrates a wide range of inter-individual variance. Unlike the incisor path that can be tracked directly, the same variable on the condyle has been

indirectly obtained by inverse computation from inter-incisor length based on a kinematic model, which commonly selects a point on the condyle as the stationary reference. Until recently the 3D instrumentation has been recruited in the recording of the condylar tracking path. Therefore, the condylar measurement would appreciably exhibit a discrepant outcome of the linear or curvilinear length by different computing methods and reference points.

Regardless of the inter-individuals variance, the shortest distance found in the literature during a jaw-opening movement was indirectly obtained under the model of terminal hinge axis as a reference for condylar tracking, approximate 14.5±2.6 mm of condylar curvilinear pathways [88]. In the case of lateral palpated pole of the condyle as a reference, condyle path was reported 18.2±3.7 mm and 16.2±3.6 mm long for the right and left, respectively [89]. Using kinematic center resulted in a longer curvilinear pathway of 23.2±4.2 mm on the right condyle and 23.1±4.5 mm on the left [74]. 3D opto-electrical instrumentation measured the condylar path of 21 female subjects getting a mean value of 12.8±2.8 mm three-dimensionally and of both genders with 14.6 mm [90].

Though a great inter-individual range, the intra-individual variance of condylar translation was proved to exist only during opening stage rather than including the closing stage [88].

B. Ratio of Rotation to Translation

According to the approximate condylar position deduced from the boundary movement of incisor as well as the TMJ morphology which generally directs the condylar translation, normal jaw movement is likely to recruit a pattern that correlates rotation with translation in terms of condylar movement. Averagely, the maximum inferior-superior translation (≈7 mm) in the sagittal plane was reported to be 1/3-1/2 of the anterior-posterior utmost one (≈20 mm); and a linear correlation between rotation and translation was also found with a mean slope of 1.5°/mm, among which the largest was less than 2°/mm [65, 74].

C. Intra-articular distance

While most researches recorded the condylar movement inside the TMJ, the variance of internal joint clearance had not been noticed in different scenarios of movement. The intra-articular distance firstly proposed based on the KC trajectories refers to the distance between the condyle-disc complex and the articular eminence, which appears to be a TMJ internal clearance when the opening trajectory is not coincident with the closing one, as Figure 2-11 (A) illustrating a discrepancy existing inside of a pair of open-close trajectories on the sagittal plane [76, 77]. Although there are some controversial results from experimental recordings on

the comparison of measured intra-articular distance in the open-close movement, it is universally agreed that loadings on the jaw could decrease the internal space, forcing the condyle closer to the fossa, as shown in Figure 2-11 (B) compared with (A) [64, 75, 76]. Most researches account for the reduction of the intra-articular distance by the fact that the articular disc was being heavily compressed during the closing phase subject to load or mastication. The compressed thickness of the articular disc also explained the TMJ with degenerated disc or clicking sound also showing a reduction of the intra-articular distance [91].

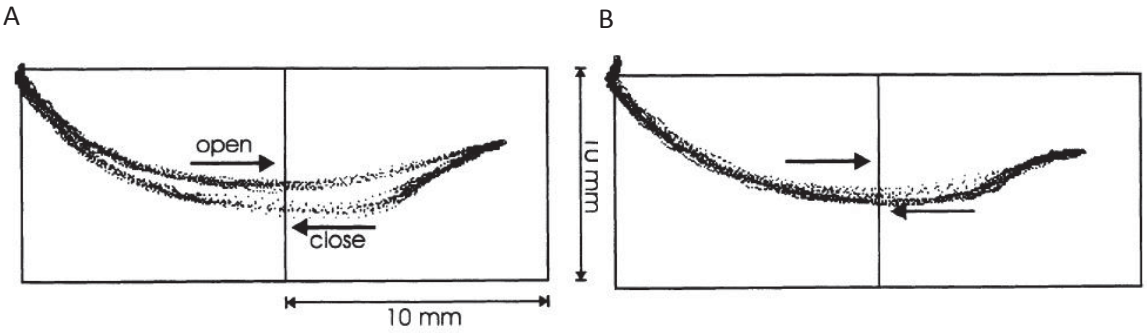

Figure 2-11 Typical sagittal trace of the kinematic center at (A) non-load and (B) low load [76]

2.2 Dynamics of the Masticatory System

The dynamics of the masticatory system discloses the mutual relationship between the mandibular movement and the applied muscular forces subject to passive restraints and morphological features; and dynamic studies rely on the models established in two aspects, the kinematics and the kinetics, contained in the simulation [92].

2.2.1 Dynamic Model of the Masticatory System

Instead of the diversity in the descriptions of the jaw movement, the dynamic model firstly proposed by Koolstra and van Eijden [93] has been built with a similarly ubiquitous construction, which lays a theoretical basis for extensive simulations incorporating muscular forces. The model is composed of a mandible bone considered as a rigid-body; the muscular forces located anatomically, the reaction force from joints and passive components as the movement restraints in the model.

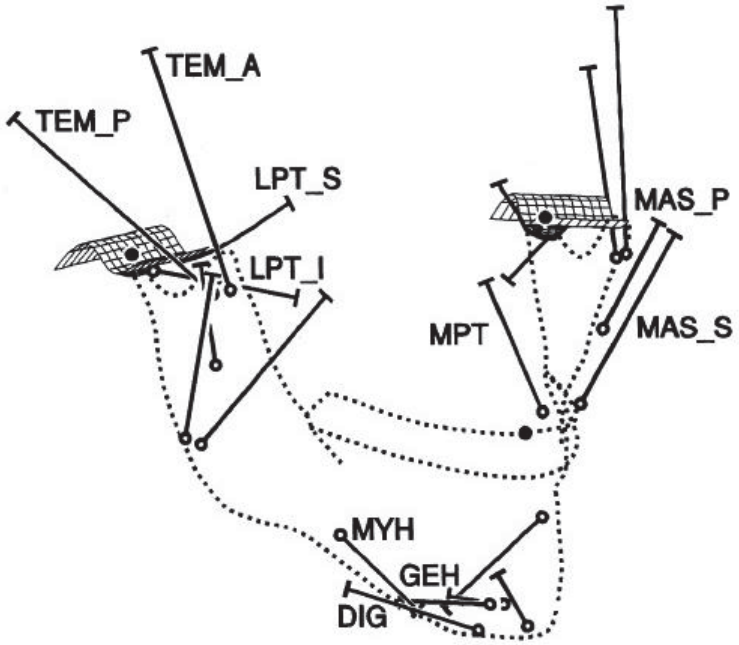

Figure 2-12 Ventro-lateral view of masticatory system [55]

The involved components play a crucial role in the course of model building, lying in not only their morphology, but also the anatomical definition in the model such as the location and orientation, the physiological length, and the PCSA size, which have be acquired by 3D reconstruction of sliced CT images or the direct measurement on a cadaver [92]. The mandible bone is generally simplified to a mass point standing on the center of gravity; its geometry is not so critical as the physical properties that seldom engaged in the simulations; apart from the reconstructed jaw, a polynomial has been created via an iteration to represent the geometry mathematically with the satisfaction of the assigned physical properties [94-96]. Muscles as the dominant actuation involved in the mastication are replaced by one string or a pinnate group in the model along the lines of action that depends on the fan-shaped area; though more than 20 muscle portions participate independently in the mandibular movement, only dominant ones are contained in the model, as shown in Figure 2-12 [96]. The muscular force whose magnitude is configured as the computational variable representing its contraction is estimated in two ways: by the general Hill-type muscular model that correlates the force with activation level plus the sarcomere length, or by distributing the assigned resultant force proportionally to the PCSA of each muscle portion [97, 98]. Muscles denoted in Figure 2-12 can be referred to the literature [55]. Passive components that include the damped structures such as the ligament, cartilaginous disc and the passive muscular forces were not incorporated in the dynamic model initially, but have been accrued in the subsequent studies to investigate the affection to the overall movement. The ligament was included to prevent the jaw from dislocation, behaving as a boundary limit, so was the passive

muscular force that was occasionally recruited but only shown some affection at the largest gape [57].

The mandible is initiated to move subject to the forces and the consequent torques along kinematic definitions in most studies that are given with the guidance against the condyle and morphological constraints. There is no distinct evidence to demonstrate the proportion of contribution from each pair of active muscle to a specific jaw movement, but preliminary study shows that the muscular force has been testified to be minimized or consistent with the minimization of joint loads during the jaw movement [99].

2.2.2 Chewing Force

Muscle force is the dominant motivator to actuate the jaw, while the gravity and TMJ ligaments only take limited part in the mandibular movement, e.g. in the opening phase; so the muscular force exerted in various jaw movements overcomes the resistance from the passive forces of the other group of muscles or the food corresponding to unloaded or loaded circumstance, and should also be restrained within a certain value to avoid too much force damaging the periodontal tissues. Studies that examined the passive resistance of the jaw focused only on the natural opening path and showed that a low resultant force of 5–10 N was sufficient to sustain a wide gape. Values of 15–25 N were necessary to reach maximal displacement [95, 100, 101].

The chewing force has been measured quantitatively amid several studies involving in-vivo trials; the teeth exert chewing force spatially on the food, and the magnitude displays a large variation over these researches, which can be ascribed to the difference of implementing scenarios, such as the position of the sensor and the type of food. Generally, chewing food like biscuits and carrots exerts force about 70-150N on a single tooth [102], while the total bite force at occlusion was given within 190-260N, although the maximal force has been measured up to the range of 500-700N on molars, which occurs in the process of the gosis or grinding teeth to sharpen the cusps [103]. Latest researches on the chewing food in terms of the different factors are not included in the section; but factors that escalate the bite force have been concluded to five criteria, and the magnitude of the force is differentiated spread to the every single tooth. The force on the incisor accounts for 40% and 47% of the force at the molars for biting and chewing respectively [104]. This also explains the distinctive mechanical advantage possessed by the incisors and molars.

2.3 Biomechanical Investigation

Biomechanical study concerns the composition of the components to be investigated, the material properties, and the stress distributions that are influenced by intrinsically the mechanical behaviors and extrinsically the loading conditions. In the masticatory system, the mandible has regularly been considered as a rigid-body without deformation arising to study behaviors of other components. As a matter of fact, it is constantly imposed under forces and torques coming from masticatory muscles and other passive tenders. Little deformation (maximally within the micro-quantity level) showed up in the finite element study when the mandible is subject to normal forces to carry out mastication, the ability to resist moments being owing to the bony geometry and rigid mechanical properties such as elastic modulus [105]. Compared with other components, the articular disc is much vulnerable and susceptible to permanent damage; and most cases of temporomandibular disorder (TMD) is claimed to be accompanied with the perforation and degeneration of the articular disc which are presumably caused by excessive pressure subject [106].

The impact internally upon the articular disc is rarely acquired through invasive measurement in vivo due to the inaccessibility of inside space, but software simulation running the finite element method (FEM) is often used in a non-invasive approach to obtain the required data. If regardless of the mandible, the outcome from FEM studies subject to the simulated mastication scenarios has been extrapolated to the actual situation, it is nevertheless believed that they would show a similar pattern in terms of the TMJ internal loading conditions and deformation. Meanwhile, the accuracy of FEM results in biomechanical study of the TMJ predominately depends on the model build-up in the aspects of morphology representation and parameter selection. The linear model of the articular disc which is broadly applied could not reflect the material property because of its composition, and the interpretation of its function requires a much more complicated representation.

The loadings on the masticatory apparatus have been reported to stand at significant position in modeling and forming the bony parts during human growth. Instead of the biomechanical behaviors of the disc, the TMJ internal loading and stress distribution is extremely concerned to be maintained in reasonable range, especially under the scenario of jaw being subject to an emulated masticatory force, and that information would be very conductive to the development of the jaw exoskeleton and exploration of the coming effects under the same scenarios.

2.3.1 Mechanics of the Masticatory System Components

As an essential parameter, the material feature of each component taking part in the biomechanical study on the TMJ inevitably affects the process of FEA modelling and final results. Of all possibly involved components around TMJ, most researches are aimed at testing the assumed mechanic feature of the articular disc, by means of loading apparatus [107-109]. However, in the FEM dominated researches, the components are more likely to be assumed to have linear elasticity, in order to simplify process of calculation.

As listed in Table 2-1, the bone of the skull and the mandible are generally considered as linear elastic, although in some studies the elasticity differing locally are dealt with different values [105, 110], the bones are still less deformable compared to the articular disc. It should be noted, the elasticity modulus in the mandible also varies from cortical bone to the cancellous bone as applied in some studies, value of the former being larger than that of the latter [110, 111]. The TMJ ligaments and the cartilage are occasionally incorporated in the FEA-based studies, due to the discovery of both being proved to have little influence to the affects little to the disc behaviour. Usually, the former are simulated as linear springs with high stiffness [112], while the latter is often seen as a small size of the articular disc, although it is characterized of compressive properties much well suited to the condyle [113].

Table 2-1 Mechanical properties of TMJ components

	Mechanical properties			
	Elasticity (MPa)	***Poisson's ratio***	***Stiffness (N/m)***	***Source***
Mandible	13700	0.3	--	[110, 111, 114, 115]
	13000	0.3	--	[114, 116]
	17300	0.315	--	[116]
Ligament	0.49	0.49	--	[110, 111]
	--	--	272.4	[117]
Articular disc	0.675	0.125	--	[114]
	6	0.4	--	[118]
	44.1	0.4	--	[110, 111, 114, 115]
		0.5	--	[117]
	0.068 -- 68.0	0.4	--	[119]
Condylar cartilage	0.49	0.49	--	[110, 111, 115]
	0.79	0.49	--	[114]
	0.34—2.34			[113]

The articular disc located between articular fossa in the skull and the condyle in the mandible is considered as a load-absorber by means of its own deformation to expand the contact area of the joint so as to reduce the contact pressure. The thickness of the articular disc is as incongruent as its surface, as reported 3-4 mm in the posterior part of the disc, 1-2mm centrally, 1.5-3mm anteriorly and 3.2±0.77mm in the posteromedial segment to be the thickest part [115]. The disc is primarily composed of macromolecules and fluid, whose different composition of the region presenting tiny difference of the mechanic properties explains regional pressure distribution on the disc [114].

As far as the mechanical behaviour of the disc is concerned, there have been two means to carry out the investigation, namely, by experimentation and by simulation, of which static tests are more commonly used to obtain the elastic characteristics [107-109]. In experiments, the specimens are usually required to be placed within the loading machine to bear the applied force/stress, and the corresponding behaviour under the tests is then obtained through processing. However, the simple single-phase elastic, linearly elastic properties are incapable of describing the mechanical behaviours of the articular disc, since the experimental data exhibit large inconsistence from that of the theoretical model. Several complicated biomechanical model are offered based on the experimental results of the static and dynamic tests. Generally, the mechanical properties of the specimens are firstly obtained under certain experimental protocols; then the outcomes are processed to be fitting into the parameterized mathematical model, in terms of which to compute the exact parameters; subsequently the model is simulated on a FEA study under the same scenarios of the previous static tests to observe the matching.

With this method, biphasic model was constructed to describe the disc in the way of continuum mixture of solid and fluid components exhibiting viscous effect in the interaction of critical boundary. In the context of FEM study, the disc movement derived of coupling of recorded mandibular motion with TMJ morphology reconstructed from data in vivo, was applied in prescription to TMJ disc of biphasic model, where the stress was analysed [118]. The biphasic parameters were chosen from those of human hydrated soft tissue, since the actual material properties of the disc are still lacking. Therefore, this method has some limitations.

The poroelastic material is another method to model the mechanical properties of the disc of hyper-elasticity [119]. In the study, two groups of constants of poroelastic model assigned were executed in the FEM simulation from which the results were obtained to be compared

with the experimental one subject to same loading conditions; the similarity in the variation of the stress, force and energy revealed from comparison demonstrates the poroelastic model is able to describe the dynamic behaviour of the disc.

The viscoelastic material model is capable to take the viscous behaviour responding at a wide range of frequencies into account for the articular disc, which is much suitable to characterize time-dependent behavior under stress. A non-linear multi-mode Maxwell model was used to represent the properties by fitting parameters which were obtained from a cyclic large-strain compression test (Figure 2-13) [107, 120]. Then the Maxwell model is applied to the disc in the FEM study, showing the applicability in order to describe the mechanical response of the TMJ disc cartilage. Viscoelastic properties are often determined with a dynamic mechanical analysis testing where cyclic loading is applied to the specimen.

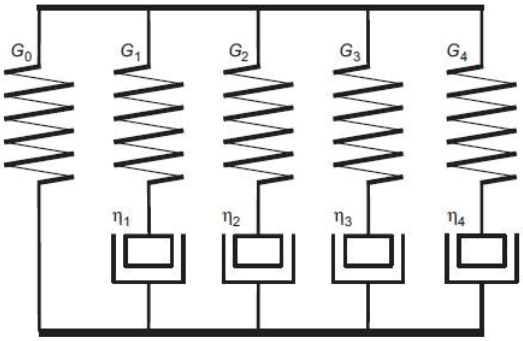

Figure 2-13 Four-mode Maxwell model to represent TMJ disc mechanical property [120]

2.3.2 TMJ loadings

Many literatures have examined the TMJ loading in various ways in both human and primates. Of these studies, Smith et al. [121] have employed a numerical model which had calculated the minimization of mean root square condyle load to maintain a static equilibrium by assigning arbitrary bite force in an iterative way and demonstrated that TMJ is a load-bearing joint over the normal functional positions. The same numerical method was adopted by Nickel et al. [122] to testify whether the load in TMJ exists in the immature TMJ to ensure a static equilibrium and the result has indicated that immature TMJ is loaded as in adult while doing isometric bite and with child growing up, the slope of loading becomes more oblique.

Also the result of Nickel et al. [122] has supported an assumption that appropriate loading in the TMJ contributes to the development of TMJ and cartilage. That is consistent with a review by Tanaka et al. [123] which concluded that remodeling of the joint, fossa and eminence has been accompanied with joint-loading which is supposed to be critical in the growth and maintenance of function and structure of the joint. Besides, neuromuscular control seems also

involved in regulating the relation between joint loads and masticatory muscles forces [99]; as mentioned, the eminence shape and the muscular force have been checked to be consistent with the minimization of joint loads or minimization of muscular force or both in healthy people. Therefore, clinical practice related in TMJ rehabilitation should make sure to minimize the loads to conform to the original criterion in human, which is also suggested in [123].

Since the TMJs bear loads during functional movements, and direct measurement is hard to implement in the human, together with the fact that TMJ loads cannot be extrapolated from primates due to not exact analogue in the structure of TMJ between human and primate, mechanical analysis is developed based on the mathematical models of TMJ in two-dimensionally or three-dimensionally. The mathematical models are generally built as mechanical models in which the application points of muscle force, bite force and joint force are indicated based on anatomical information, invoking either experimental or simulated data. Compared with the study in which the magnitude of each muscle force was calculated only by means of decomposing the resultant force proportionally to cross-sectional area (CSA) of each muscle [124], the instantaneous muscle force calculated from the integrated EMG data combined with CSA is much more accurate than that obtained from CSA only, which represents neurological parameters in mastication [98]. The joint force is obtained through an optimization program with results of 260N and 172N for normal male and female in terms of the maximum bite force of 300N and 210N, respectively. In another study of investigating the relation between TMJ loading and biting-point location, muscle force is also obtained from the combination of EMG data and CSA based on a two-dimensional rigid-body mode of jaw with spring modeled TMJ [125]. TMJ-loading/bite-force ratio instead of absolute magnitude of load has been employed to avoid any difference coming from different simulated condition and input data. And the ratio at molar bite and at premolar bite of 0.477 and 0.904 respectively showed that TMJ loading depends not only on the bite force, also on the biting-point location. The direction of loading is hard to detect, but in 2D model, it is in the articular disc's intermediate zone [98, 125]. In a dynamic study where the jaw is modeled mathematically by nonlinear differential and algebraic equations, the TMJ loading shows a maximally 28 N on the condyle [95].

2.3.3 Stress Distribution on the TMJ

Stress distribution in the TMJ during functional movement has been investigated through building a 2D or 3D finite element model of mandible in many studies [110, 124, 126]. It was considered that stress in the TMJ accounts for the TMJ internal derangement and the

perforation of the articular disc, so stress distribution has also examined among people with TMJ-ID to detect difference between them and normal ones [111, 127].

3D FEM models have been constructed with a resultant input force of 500N to investigate the stress distribution during clenching, and stress was found to distribute in similar pattern in the condyle and gleniod fossa only with less magnitude in fossa, also found larger compressive stresses in the anterior and lateral areas of the TMJ, whereas the tensile stress in the posterior and medial area [111, 124]. That can explain why thinning and perforation of the articular disc occurred in the anterior and lateral area than other regions [128]. Stress distribution is different during mouth opening from clenching; compressive stress was discovered in the contact area in both sides with the highest found in the condyle and tensile stress was found in the remaining area with highest located nearby rim in the gleniod fossa in a study where the finite deformation theory was adopted instead of muscle force in FEM to avoid any uncertainty of muscular proportion towards a motion [126]. Tensile stress functions to maintain normal relations of components in the TMJ. The stress distribution is also affected by the asymmetry of the mandible [127]. Generally, the models of the mandible and the TMJ are formed by the transverse-cut slices or MRI-scanned slices reconstruction, with mechanical properties of components assigned to do the FEM study. The deformation and the compression on the condyle are shaped in two types of loading, from the muscles and from the predefined deformation, while the former is configured in the same way as in the dynamic studies. Without resembled loading from the muscle force due to the uncertainty of muscular proportion towards a function-motion, finite deformations of the condyle in the form of sagittally condylar displacement is specified with certain value of translations to calculate the stress distribution at an incisal opening [126].

The stress and deformation within the TMJ in the studies has been listed and compared, although the scenarios in those studies varied from each other [129]. The pattern of stress distribution got from various studies is similar; since different FE models with loads and assumptions varied in different studies, the magnitude of the stress in the TMJ seems hard to compare and to be concluded with a bound. During clenching, the maximum magnitude of the stress in Tanaka's studies occurred at the condyle in a form of compression of 1.642 MPa. During normal opening and closing, the maximum of stress in Chen's study on the condyle and on the fossa are 4MPa and 4.2Mpa, respectively. These values have been compared with the foregone studies.

2.3.4 Biomechanics of Articular Disc

Generally, the stress on the articular disc has been investigated by means of analyzing FEM model and most FEM models have been constructed in two steps, that is, first to create a mesh of the disc through obtaining the geometry from the cadaver and some transformation of mathematical model, then, to apply mechanical property of the disc to one of the above models [116]. Finite deformation method are commonly used in the only-disc-involved study [130], joint loading from the resultant force are sometimes as an option [131].

The articular disc experienced loads during clenching mainly in the intermediate zone with the largest value of 3MPa located in the posterior of this region and variation of the loading had little effect in the stress distribution [116]. During mouth opening, stress in the disc facing the condyle is much higher than that facing fossa and higher stress was found in the lateral and anterior and posterior regions of the disc [110]. Compared with the stress in the condyle and fossa, pattern of stress distribution is similar, the magnitude in the disc is the smallest among them [111]. The range of the magnitude of the maximal stress in several studies varies from 1MPa to 5MPa.

Also reported is TMJ disc perforation and degeneration of the surface often occurring in the lateral part of the joint, that also conforms to high pressure (excessive and continuous mechanical load) causing the perforation [128]. The stress increases as the coefficient of friction increase and damage to the surface of TMJ will increase the frictional force which will exacerbate the stress cyclically [114]. From this point, minimization of the load and stress in the TMJ complying with neuromuscular control is also verified.

2.3.5 Discussion

The coverage of biomechanical properties of the TMJ is limited in effective representation and the experimental results from the literature cannot be compared as they were obtained under different simulation scenarios. But as to the models and the methodology that are to be used in the future dynamic and biomechanical studies, there are several points to be with our consideration.

All data about the mechanical properties of the articular disc obtained from various experiments are indirectly affected from the sample conditions, including the loading history in the subjects, the preservative environment, the experimental method. There are rarely studies in which the material property is expressed in a funciton to investigate the relationship between itself and the trend of the disc deformation. Even if we assume the computational

models are obtained from well-fitting to the optimal loading data, the information is still quite little to have all the data compared under the same simulation scenarios. As the articular disc exhibits different type of biomechanical properties, which should be reflected in its representation by mathematical model, the reviewed data can give an implication on the application of the data into the FEM-based study.

The combination of MDA and FEM compensates the varying loading condition that is missed in the single FEM-based analysis, and provides a quasi-static load environment to generate finite element outcomes of the concerned components. Quasi-static FEM simulation theoretically does not contain the Newton force formed by the acceleration item, but it is applicable in the study where the acceleration is too small to be ignored, without any influence to the loading output.

The generated outcomes varying in the values are still quite indicative for the future studies. Most studies are showing the similar trend of the stress on the articular disc as well as the other surfaces on the TMJ, while the pattern of the force is also a determinant for the stress distribution. In addition, those values coming from different simulation conditions set limits that can be used as the criteria for further simulation.

2.4 The State-of-the-Art of Jaw Movement Simulators

Many masticatory robots have been developed for the purpose from initially of exploration of the mechanics of the mandibular movement with the bionic substitutes of the components, to lately of the transportation of the masticatory function [132, 133]. Xu has given a thorough overview on the masticatory system and the masticatory robots to date, emphasizing robots with complete degrees of freedom (DOFs) fulfillment in terms of total duplication of the movement [134]. Nevertheless, such devices designed for specific applications perform similar formats of masticatory movement, exhibiting corresponding features in the masticatory process from the perspective of the function; and they share little design specifications in common in terms of each application, leading to distinctive mechanical construction and control algorithms. To study the generalized feature and avoid confusion, the jaw motion simulator discussed herein is broadly referred to devices that have been developed to deliver jaw motion to achieve mastication-related objectives.

This section reviews jaw motion simulators developed to date in terms of mechanisms and control strategies according to mechanisms that are differentiated among different applications, namely, the mechanism of being (1) bio-inspired, (2) quasi-anthropomorphic,

and (3) non-anthropomorphic, matching to the intention of, the replication of the mastication, the rehabilitation and food evaluation, respectively, and directs some attentions to the exceptions of inconsistency between the application and mechanism structure.

2.4.1 Bio-inspired Chewing Devices

This type of devices has been inspired by the kinetic construction in the masticatory system, which is simulated by a parallel mechanism as the prototype of the devices. The mechanism imitative of the anatomy usually consists of a moving platform that emulates the jaw, a fixed base corresponding to the stationary skull and the linear actuators matching muscles of different recruitment combinations from case to case. This bio-inspired structure advances in replication of kinematic features, such as degree of freedom and workspace, as being configured in highly harmony with human counterpart. Devices based on this mechanism are mostly aiming at reconstructing the complicated movement and exploring its potential control principle in terms of the neurologic principles towards a specific motion, rather than chewing that involves too much force. Specially introduced in this section is the most original jaw motion simulator that is able to be found in the literature.

A. The First Jaw Motion Simulator

So far, the first device that was developed to simulate the mandibular movement dates back to the publication in 1967 in which the motion simulator was intended to study the way of dental wear pattern [135], as shown in Figure 2-14.

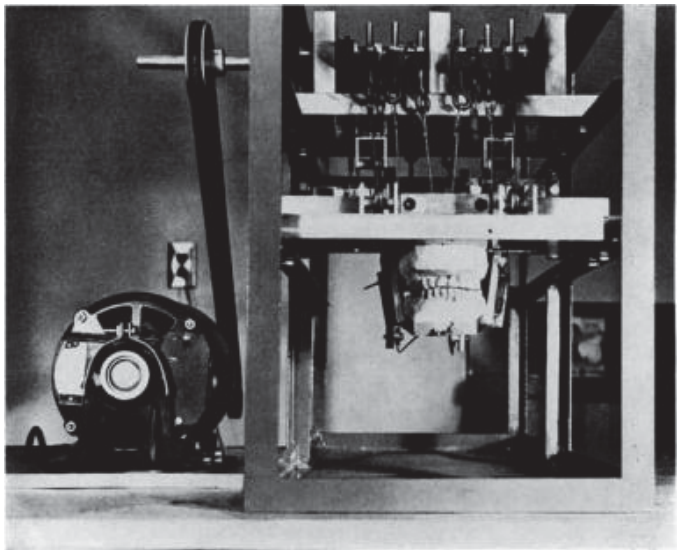

Figure 2-14 Front view of the machine [135]

The machine consisted of a frame as its base on which the cast of the maxillary dentition was fixed with a horizontal occlusal plane and the lower dental one mounted below was driven by

12 cables representing the masticatory muscles of masseter, temporal, pterygoid and digastrics on both side. Twelve cams driven by one electrical motor actuated those cables with pulling force through each rocker arm connected to the cable. Each cam was shaped to have a single activation per revolution, and the varied activation and the dwelling time of different cams were used to roughly simulate the jaw motion according to the EMG signals of each muscles corresponding to the cam. The condyle and the articular eminence on the skull were simply replaced by a metal bar on the machine, but no quantitative measurement of the force on the condyle was implemented. The adjusted cam timing and varied tension on each cable could generate various resultant forces.

B. JSN Series

The JSN series robots were developed by the Niigate University, Japan for the purpose of realizing a humanoid open-close movement [136, 137]. The main structure of the robots consisted of the upper and the lower jaw with occlusal contact, condylar housing that simulated the TMJ, the wire-tendons that were actuated by DC motor and sensors. The wire aligned similarly with the masticatory muscles was connected to the DC motor on one end and connected with the lower jaw on the other end. In the early version JSN/1C; only three muscles were simulated by motors (masseter, lateral pterygoid and digastric) and three more muscles were further incorporated in the latest JSN/2A (anterior pterygoid, internal pterygoid and posterior temporalis) enabling the device to have six DOFs, as illustrated in Figure 2-15. The position of the jaw and the generated muscle force were monitored by a rotary encoder and a cable-tension sensor respectively.

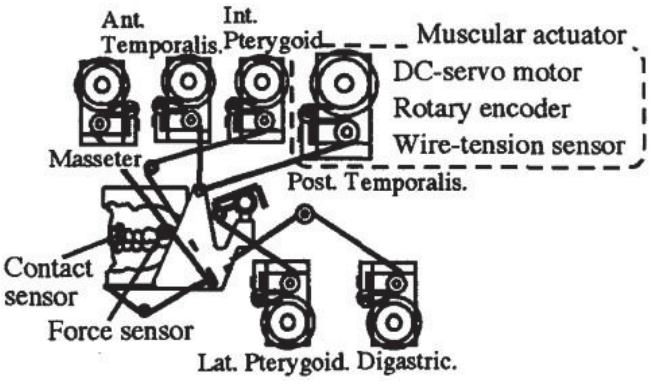

Figure 2-15 Muscular actuator mounted on the JSN/2A [137]

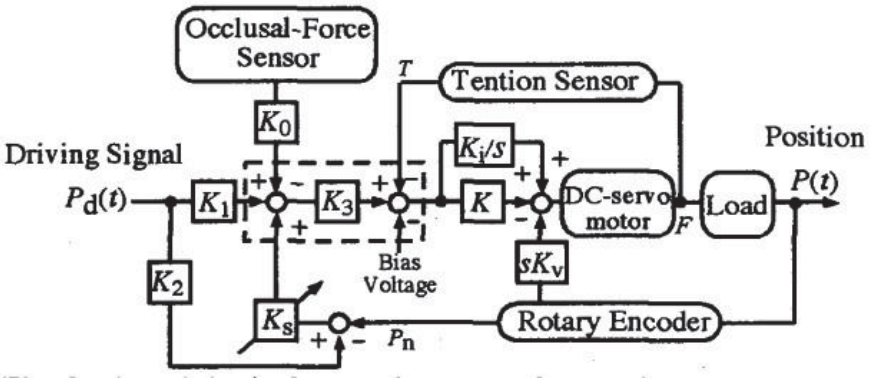

Figure 2-16 Block diagram of the impedance control scheme [137]

Motors that were connected the cable tendon was controlled under an impedance control scheme in order to emulate the actual muscle compliance, in which the impedance ratio was tuned through adjusting parameters in the alpha-gamma linkage. Against the control scheme given in Figure 2-16, the motor was activated by the recorded EMG signals of corresponding muscles at the beginning; then the detected position and force signals in the motor was fed back to be compared with the driving signal under some impedance tuning, so were the biting force that came from sensors installed on the occlusion plane, and the driving signal error can be corrected to form the adaptive control scheme [137]. In the adaptive control scheme, the different muscle signals were regulated clearly to be corrected by certain feedback signals, as there were only one DOF in JSN/1C and 2 DOFs in JSN/2A; therefore, the coordinated muscle movement would be of paramount importance.

C. WJ Series Dental Robot

The WJ series robots were a series of masticatory robots developed as a quantitative model for the purpose of reproducing and evaluating the mandibular movements, the earliest version WJ-1 starting from 1987, which had just a DOF and only was able to perform clenching by a pair of artificial-muscle-actuators (AMAs) [138, 139]. Upgraded from WJ-2, the subsequent models had more than one AMAs (7 in WJ-2 and 9 in WJ-3) that were arranged in alignment with masticatory muscles for bionic replication, to achieve three-DOF movement, based on a kinematic model that each condyle moved translationally along a path while being rotated around by the jaw, as shown in Figure 2-17 (A). The AMA adopted in this system was designed to simulate the muscular motion, and consisted of a set of a servo motor, a gear reduction, a pulley, and wire on each, by which the motor was fastened to the lower jaw to achieve actuation [140].

Each WJ robotic system was composed of four subsystems, i.e. the skeleton, the actuator, the sensor, and the controller; and the skeletal structure in each version was almost similar. The

upper dentition was fixed on the frame and the lower dentition mounted on a bracket that connected the upper dentition with a carbon rod via the right and the left condyles. The carbon rod was constrained to go forward and backward on a virtual planed inclined 40° with respect to the horizontal plane.

The control system in the WJ robots was split into two levels; the bottom one was the single control to muscular actuator in terms of the position and the velocity feedback, while the higher one was responsible for coordination of all AMAs to achieve a specific motion in mastication system level. In the WJ-2, the programmed motion pattern was assigned to each AMA to generate the predefined traced incisor trajectory [138]; the control algorithm was upgraded in WJ-2RII, in which the motion of the robotic jaw was defined in terms of different adaptive motions varied during each phase with reference to the biting force [139]. A large improvement applied in WJ-3R was the controllable stiffness simulating the masticatory muscles, in which a mathematical model representative of the viscosity of the muscle was implemented mechanically by a combination of a helical torsion spring and a rotary damper in WJ-3RII [140, 141].

The performance of the devices has been evaluated in each own criteria in aspects of the control algorithm or nonlinear properties, and the latest WJ-3RIII was assessed in terms of the quantification of the chewing efficiency [142]. Although WJ robot was initially developed to reproduce the jaw movement based on the kinematic model, it has been further utilized in the application of mouth training, serving as a patient robot cooperating with WY dental robot for better understanding the training factors [143].

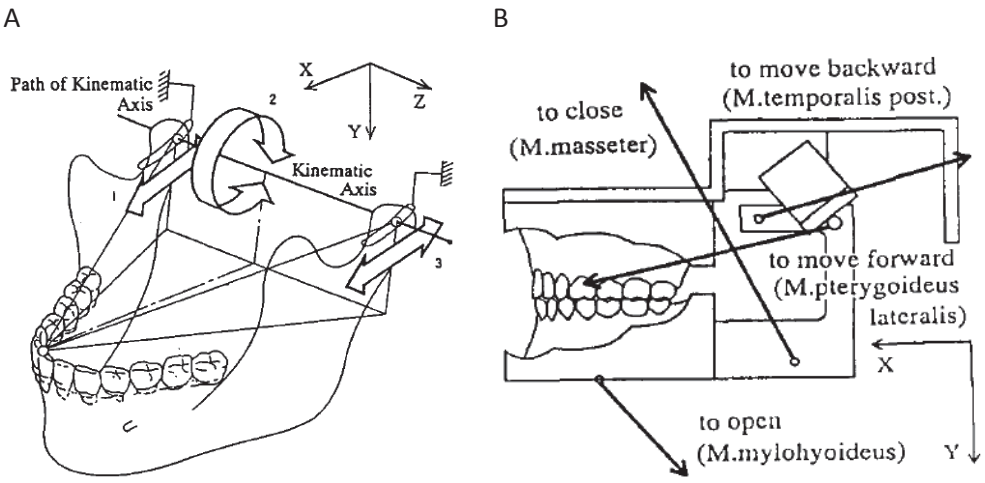

Figure 2-17 WJ robot (A) kinematic model of jaw movement and (B) alignment of AMA in WJ-2 [138]

D. Chewing Robot

The chewing robots developed by Massey University were initially intended to carry out food texture evaluation by delivery of the crush movement. Similar with other bio-inspired robotic jaw, the robots were also composed of a six-DOF parallel mechanism, in which the floating platform as the lower jaw replica awaits for actuation by the masticatory muscles connected to the fixed skull. The first version given in Figure 2-18 (A) recruited three pairs of actuators symmetrically relative to the sagittal plane, but their alignment was not arranged consistently towards the masticatory anatomy; the parallel mechanism that was upgraded to form the foundation of the second robot were assigned in line with major masticatory muscles by floating legs, as the prototype shown in Figure 2-18 (B) [144, 145].

A B

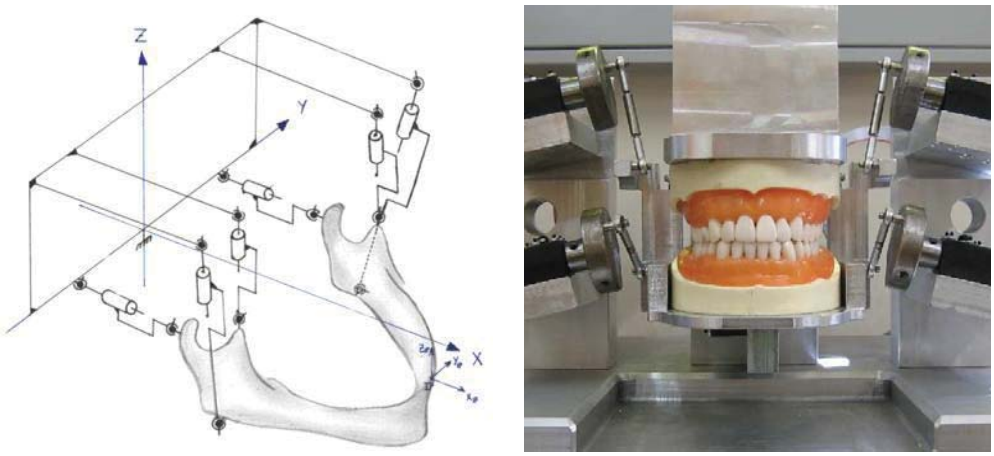

Figure 2-18 Parallel mechanism of the robotic jaw: (A) 3D kinematic sketch and (B) the photo [145]

Since only three groups of the muscles (temporalis, masseter and pterygoid) were included in each side, far less than the involved ones, the deep and superficial in each muscle were combined to a line of muscle action through force-vector calculation, reflected by the position and the orientation of the actuators. The linear actuator was implemented by the slider of a crank slider in terms of the specification of the required force and motion, and the robot turned out to be a 6-RSS parallel mechanism. At the bottom level, all motors were controlled via a six-axis motion control card which is integrated with PID tuning, and illustrative results verified its ability in reproduction of various chewing movement; but no details has been found in the upper level of the control system [146].

E. Dento-Munch Robo-Simulator

Dento-Munch Robo-Simulator built on a six-DOF parallel mechanism was not strictly in line with the dynamic configuration of masticatory muscles, though it was developed for

evaluation of dental wear to replicate typical jaw movement spatially [147]. As shown in Figure 2-19, the floating platform of the Stewart mechanism was attached on the lower jaw, and each leg represented one electrical actuator that executed linearly. The complete assembly of the device contained other periphery modules other than the parallel mechanism itself, which cast high technology in the manufacture engineering. The velocity controller was applied in each actuator at the bottom level; and in the higher level, the force or position control strategy was respectively used corresponding to a contact and non-contact phase within a chewing cycle. Occlusion was positioned to match dental elements while triggering force regulation in maintaining the tooth contact, which did not take place in non-contact stage [148].

A B

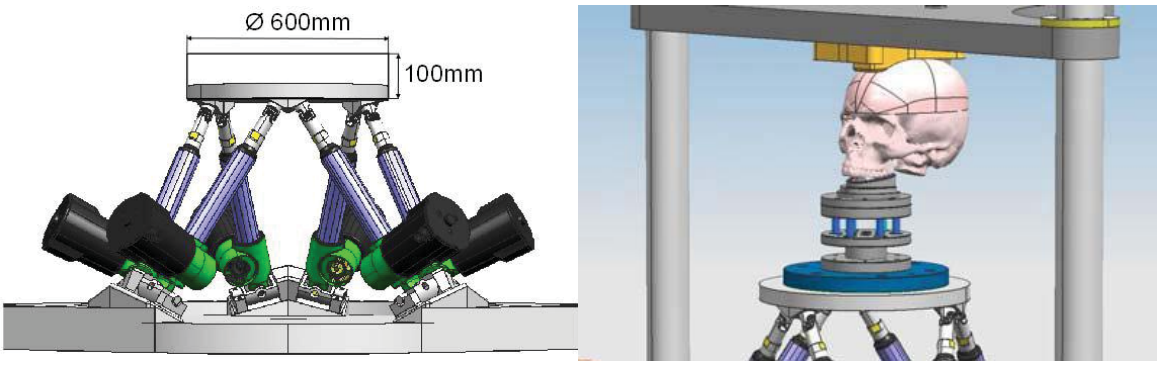

Figure 2-19 Dento-Munch Robo-Simulator (A) based on a parallel mechanism and (B) of complete CAD assembly [147]

2.4.2 Quasi-anthropomorphic Devices for Medical Purpose

Devices for medical use associated with the mastication account for a rather low proportion in jaw motion simulators. Existing devices have been developed to carry out the passive exercise based training to enlarge the inter-incisor opening distance. The feature of the mandibular movement is partially translated in such devices, in the representation of the curvilinear trajectories. Current devices are designed in extremely separate ends in terms of the mechanism, namely, the manual one and the six-DOF parallel one, to fulfill the purpose.

A. Jaw Exerciser

Jaw exercisers that have been developed to prop up the mouth opening distance can be seen as the replacement of the simple mouth gag; and examples of typical commercialized

products include [2]OraStretch™ Press, [3]Dynasplint, and Therabite, as photoed in Figure 2-20 (A, B, C) respectively, as well as the screw-adjusted device introduced in [149].

A

B

C

D

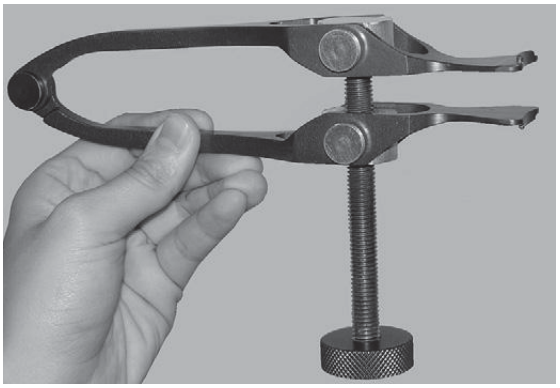

Figure 2-20 Jaw exercisers

Generally, this kind of devices provide passive stretching by forcing the jaw to trace along anatomically correct guidance, behaving as one DOF; and the required force to open the jaw is manipulated by the user, so one can manually control exercise sessions by regulating velocity of the opening motion, the applied force, and the maximal opening range. The stretch pattern in terms of the distance and the complexity totally depends on the shapes of the guiding paths, which are carried in changeable parts offered by Therabite. Reports on the efficacy evaluation in relieve the trismus can be found in use of Therabite and the screw-adjusted device in the postoperative management [46, 50].

[2] Photo is screenshot from: http://www.craniorehab.com/orastretch-press-jaw-motion-rehab.html

[3] Photo is screenshot from: http://www.dynasplint.com/

B. WY Series Dental Robot

The [4]WY (Waseda-Yamanashi) series of robots were developed for patients who suffer from disabled movement on their jaw to deliver physical exercise [150]. The WY series robots were basically built on a similar parallel mechanism which has six DOFs. Take the latest version (also the most advanced) WY-5 as an example, the mechanism was actuated by six linear motors installed on each leg via ball screws; and the floating platform which was a u-shaped end-effector was inserted into user's mouth and drives the lower jaw, while keeping the upper jaw still on the upper mouthpiece that was fixed on the robot, as illustration of the relative position of the patient in training in Figure 2-21. The kinematic configuration was not provided, but apparently the mechanism was not aligned with the location of masticatory muscles; the larger coverage than the one encircled by Posselt envelope signified its ability to generate the same movement range as required. From this perspective, the WY robot was enabled to offer versatile training session compared with a simple mouth gag.

The devices operated subject to a force-feedback based master-slave controller in the treatment, in which the command sent to the patient relied on the two-DOF doctor manipulation (open/close and forward/backward). Then the patient's jaw was propelled to move in responding to the signals while the measured bite force from a force sensor on the mouthpiece signified the subsequent movement according to the algorithm. To monitor any anomaly in the jaw muscle and hence to evaluate robotic therapy, muscular EMG (electromyography) measurements were incorporated into the WY robot. The WJ jaw simulator was tested as the patient robot; clinical training with WY-5 showed a great improvement that has been obtained on the mouth opening distance. [151, 152].

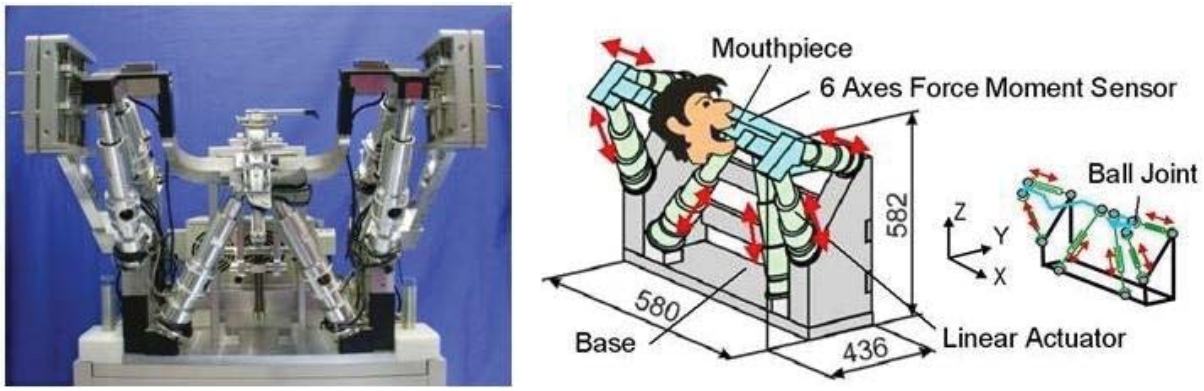

Figure 2-21 [5]WY dental robot

[4] More information can be found in: http://www.takanishi.mech.waseda.ac.jp/top/research/jaws/index.htm

[5] Photos are acquired online, referred in Footnote 4.

2.4.3 Force-oriented Imitation for Food Evaluation

Chewing robots replaying a part or entire mastication have been called in development for better analysing food properties in food industry, in place of the human to get rid of the likely variation in response when it comes to the food evaluation. The fulfilment of chewing motion is instead focused on; making the bionic replication of the anatomical construction is not necessitated; so this type of devices is generally built with non-anthropomorphic mechanism, which features the grinding and clenching during the mastication that is not achievable by generic equipment. Food analyser being the general purpose, the devices were specifically developed for a string of objectives on each own, that falls in the spectrum of chewing motion.

A. Mastication Robot

While the mandibular movement is in pursuit of full reproduction by the conceiving devices, a linkage-based chewing robot was going exactly the opposite way to achieve the typical properties that were representative of the movement. The one-DOF chewing robot originally developed to crush the food for evaluation was built on a four-bar linkage, whose coupler point traced the typical trajectory on the sagittal plane, with the other two links that piloted the coupler point in the lateral direction to achieve lateral movement, as the constructed device shown in Figure 2-22 [146].

The length of some links and the lateral inclination angle formed by the guiding link were all configured to be adjustable, enabling the robot to produce a significantly large family of 3D chewing trajectories at the coupler point. Subsequent work finalized the device by adding food retention apparatus and shock absorber on it, which enhanced the compliance in the force generation, and corresponding control strategy was established based on the fuzzy logic algorithm, to regulate the velocity according to the current force level. The robot has been evaluated in the real trials of the food breakdown by applying the control strategy [153].

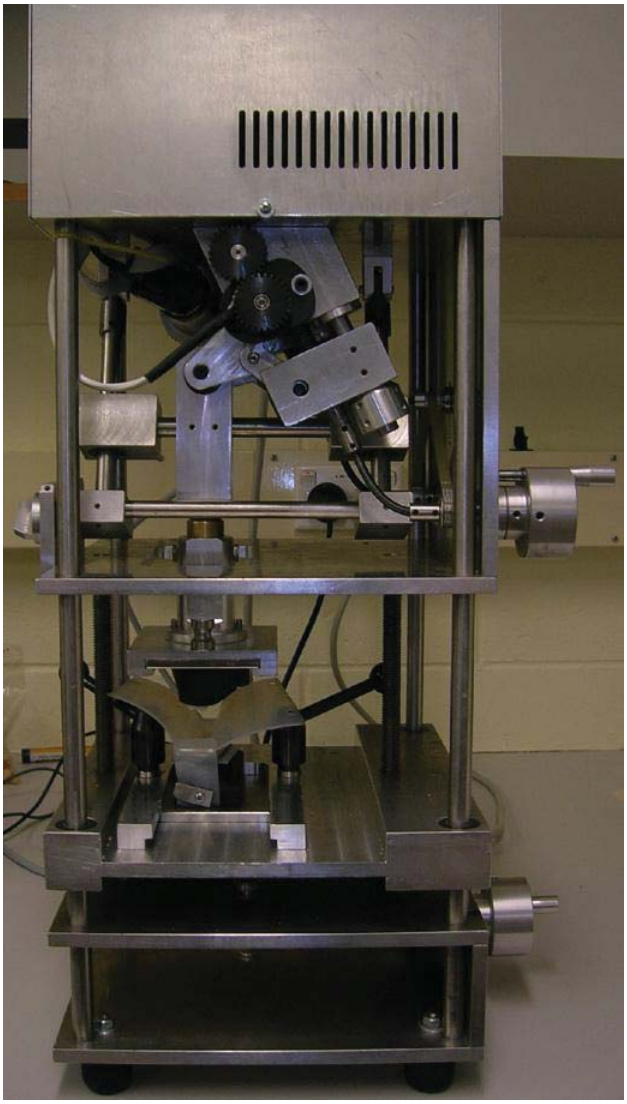

Figure 2-22 Constructed chewing robot [146]

B. The Chewing Simulator

Instead of duplication of chewing motion as other devices, this chewing simulator developed by the University de Bourgogne, France was aimed at creating an intraoral environment to evaluate the in-vitro flavor compound during food breakdown [154]. Therefore, the fulfillment by this device was more focused on the aspect of applied force, and other factors involved in the eating, such as the reproduction of saliva flow, and the frequency. As illustrated in Figure 2-23, the device shaped a cylindrical space that mimicked the oral concave, where the lower jaw and the tongue were actuated by three motors to simulate the shearing and compression by the lower jaw and the flipping by the tongue. The teeth were duplicated from a scanned human molar in arrangement of a ring that were attached to the upper and lower jaw respectively. The internal surface was all layered by a thin cover of polyetheretherketone (PEEK). Device automation was implemented by a host program in LabVIEW that

communicated with the sensors and motors via the combination of DAQ cards and signal conditioning system. Then the whole Mechatronic system was validated through a preliminary study with peanut breakdown in terms of the functionality delivery.

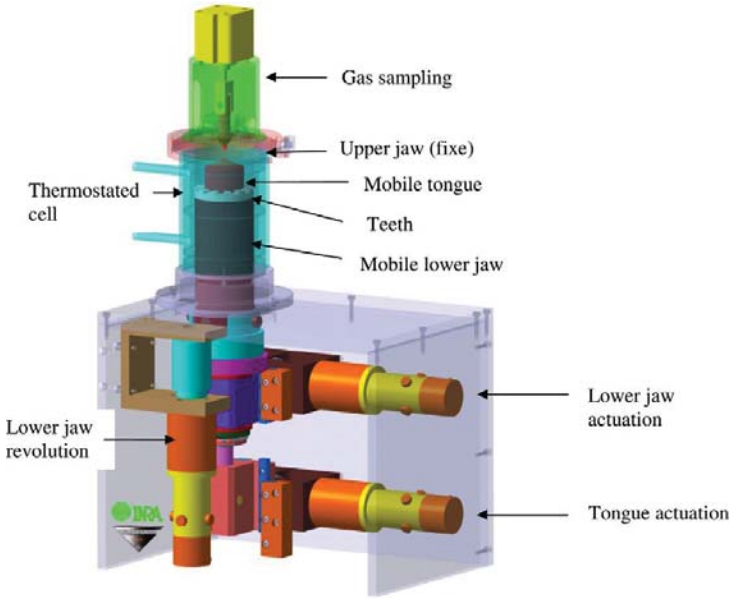

Figure 2-23 3D prototype of the chewing simulator [154]

2.4.4 Discussions

The masticatory system plays a rather irreplaceable role in human digestion system, so the function reconstruction of the masticatory system has attracted a lot of studies in the replication of the jaw movement, which is not only limited to the representation of the mandibular movement by a kinematic model, but also the way to realize the reproduction by means of devices in the field of robotics. Typical devices on achieving mastication-related movement have been reviewed in this section to serve double-side purposes, not only lying in exploring the state-of-the-art of devices to deliver passive jaw motion, but also understanding the bionic construction which is envisaged to underlie the build-up of patient device for following study. The categorization of the objectives of all devices appears to dominate the general consideration in construction of the mechanism.

On the case of bionic device, the pursuit of complete reproduction of the jaw movement account for major motivation at developing such device, together with the exploration of the movement pattern. Kinematic details and biomechanical features hereby have been more likely to be focused on greatly inheriting from human and transforming into design specifications, turning duplication of the entire mandibular movement as the final objective. In another application at which the rehabilitative use is aimed, the device is devoted to propelling the jaw to do passively repetitive movement along the predetermined trajectories

in terms of the functional movement. The appropriate trajectories would be the primary specification set for the crippled jaw. Instead of the anthropomorphic structure, similar mechanisms with the human biomechanics have been usually found in those applications to match workspace. The development of mastication robots in the field of food evaluation stems from the motivation of fulfilling food breakdown in a mimic manner to resemble partial human mastication without too many uncontrollable factors that may affect test results. Initial specified parameters for development, such as chewing angles, masticatory frequency, and the force have been focused on being descriptive of chewing movement, which are not compulsorily delivered by the mechanism with anthropomorphic structure of masticatory system.

The embodiment of the TMJ has rarely been found in the bionic robots, not even mention the other types. The only series devices that contained TMJs were WJ-series robots, in which TMJs on both sides were built in the combination of translation and rotation within a fixed slot. The TMJ modeling in this way simplifies the relation between the jaw motion pattern and the simulated muscular force, but the downside will be the inappropriate replay of the holistic jaw movement. Actuators figurative of muscles differ in the line combination and the placement, but basically share the similar platform, though each device had its own justification on the muscular configuration. Only focusing on the bionic devices, the voluntary mandibular movement has not been carried out by coordination of all participating muscles in terms of a higher neuro-based control scheme. Recorded EMG data have been used to actuate JSN-robots, and the signals reflected the activation level to some extent of resembling the actual jaw movement.

Existing devices for medical use present complete opposition in aspect of the structural complexity, though both have claimed to possess considerable amount of the clinical efficacy in trismus recovery. Differentiated by the mechanism, the WY-series robots can deliver a large adaptability for its large workspace, whereas one-DOF based jaw exercisers have to adapt patients of different jaw sizes and training regime by changing guidance profiles. The force-feedback based algorithm is of our interest, especially in relation with the depressed displacement, but nothing in detail is clearly elaborated.

2.5 Mechanism Structure Synthesis

Kinematic synthesis is a general way to derive the dimension of a specified type of mechanism to fulfill the prescribed specification in terms of functionality, which contains three types of customary tasks, namely, function, path and motion generation. Graphical/geometric

techniques and analytical calculations are two basic means to solve these dimensional problems; the former is assisted with referencing an atlas in the first case to value the mechanism, but ending up with a failure to offer a relative high precision because of inaccurate visual evaluation. The analytical one that involves optimization of a descriptive function of the synthesis problem is able to provide the mechanism with dimensions to achieve high-accuracy satisfaction of the specifications, only downsides lies in a huge amount of computation [155, 156]. The numeric synthesis begins with establishing a common goal function reflecting synthesis problems in a way of mathematically describing the error between the desired points and those tracked by the coupler, which is solved by the global optimization under some structural constraints.

In terms of the fulfillment of the precision, the linkage optimization problem can be partitioned into two groups, i.e., the exact synthesis and the approximate synthesis, split by the number of the goal x function for a determined mechanism. Theoretically all of the prescribed points can be exactly matched up of little errors with the generated linkage in the former case, in which the number of equations is not more than the number of unknowns, projected to up to five points given; whereas the latter one ensures an error of minimum by passing by all the points, during which more goal functions than the unknown variables are formulated, leading to the approximate solutions [155].

2.5.1 Construction of Objective Function

The objective function can be set up to describe synthesis problems generally by means of different approaches, such as complex numbers, vectors, and rotational matrix. In most cases, utilization of the analytical method to solve synthesis problem will eventually turn into the process of solving nonlinear polynomial equations of multi-variables with global searching methods, which are grouped into two common types, namely, numerical method and symbolic method [156, 157].

Computation based on symbolic elimination can only be applied in the exact synthesis, in which all of the solutions are likely to be found amid shrinking multi-variable equations to single-variable ones with triangular substitutes for initial algebraic expressions [158]. But the substitution can be carried out in more than one format amid the elimination, resulting in a rather low efficiency of calculation, plus problems that may occur in the course of calculation such as coefficient expansion and selection of floating points in terms of accuracy, as the latter is worth a thorough consideration due to the result being sensitive to those coefficient generated [159]. In contrast, the numerical method that includes the Newton-Gauss iteration

and global searching algorithms can be broadly applied in solving problems of both approximate and exact synthesis in which the formed polynomial equations go through an iteration starting from an initial guess [157, 160, 161]. The efficiency of numerical computation is comparatively high, but also depends on the selection of the algorithm and the corresponding initial value, since an inappropriate value may lead the iteration to go into the divergence.

2.5.2 Optimization Algorithms

Since most numerical computation rarely avoids solving nonlinear polynomial equations, extended approaches have been developed to advance the synthesis in both aspects of embodying synthesis error and the following optimization to search solutions. For exact synthesis that involves less than five points to be matched, the improvement often falls in the formulation of classic Burmester problem, for example, which has been constructed by symbolical computation of circle-points and center-points independently [156, 162]. For approximate synthesis, the numerical computation finds its way in achieving global optimization to solve nonlinear least-square (LSQ) equations more by upgrading searching algorithm efficiency and finding solutions globally rather than local optima. The synthesis error was also reformulated to LSQ equations in a different symbolical way, for instance proposing a variable-separation method, in which each configuration of the linkage was completely defined by a set of decoupled variables [155]; the contour method that reduced normal equations to two bivariate equations for approximate solutions of rigid-body guidance [157].

Newton iteration that has been widely applied in the course of optimization is rather sensitive to the selection of starting value because of its quadratic convergent speed, particularly to the Newton-Raphson algorithm, whose efficiency in initial value selection can be largely enhanced by introducing Julia set points or a chaotic sequence to generate locate initial points acquired correspondingly from Jacobian of the iterative equations or projection from multiplying two chaotic sequences to find all solutions of the nonlinear questions, respectively [160, 163, 164]. Apart from the effort on the initial start, exact differentiates of the gradient were proposed to signify the relation of the iteration of each step, which was expanded in Taylor's series to convert the formulation of the goal function [165]. Other global searching algorithms that have been developed to optimize LSQ equations include Escaped Particle Swarm Optimization, improved differential evolution (DE), and genetic algorithm (GA) [166, 167]. Natural coordinates were generally used to formulate all types of synthesis, followed by a set of

equations where kinematic analysis would be carried out in the way of minimization of requirements equations [168].

2.5.3 General Procedure in Dimensional Synthesis

Apart from the process of synthesis that goes through a comparison with the atlas in a graphical way stated above, generally solving the problem via a numerical computation based analytical approach starts with establishing an objective function that reflects the intrinsic kinematics of the mechanism, expressed as a minimization of the structural error that is the discrepancy between the given points and the generated ones. The functions are defined by different set of parameters in the mechanism oriented to the specified type of synthesis, and share the same representation of the goal function between each subsequent position with the initial one, i.e.

$$g(x) = \min \mathrm{F(x)} \tag{2-1}$$

Where $F(x) = [f_1(x), f_2(x), \cdots f_n(x)]^T; f_j(x) = [\Gamma(j) - \Gamma(1)]^2; x = [x_1, x_2, \cdots x_n]^T$; is the function to express the jth position of specific link.

Meanwhile, since the objective function in Eq. (2-1) that utilizes structural behaviors of the mechanism fails to implicate some requirements specific to a definite application, the mechanism is often intentionally subject to a series of constraints that carries specifications in functions of design variables, either by equality or inequality. Classification of the constraints has been proposed in different way over the literature, but includes types of the geometry, the kinematics/dynamics, the synthesis, and others specific to the application, for example listed below [162, 167, 168].

1) Prevention of negative lengths of bars;
2) The Grashof condition, to allow for the entire rotation of at least one link;
3) The sequence of input angles, either from highest to lowest or from lowest to highest;
4) The range for the design variables;
5) The range of variation for the input angle;
6) Relations between the gain of an input angle and the adjacent position of the coupler point.

The constraints are incorporated into the objective function of the synthesis by two means, i.e., composing of a penalty function attached behind to express a user-defined requirement

which completes the goal function into an unconstrained one, or evaluating the variables separately in the course of the synthesis being confined within each prescribed range, which type is applied depending on the instruction of the searching algorithm.

$F(x)$ is the nonlinear polynomial equations with respect to x of *n* unknowns and *n* equations. In spite of different way of the synthesis methods as well as the optimization algorithms, steps of optimization will be as follows:

1) Establishing an objective function in the form of Eq. (2-1) to describe the problem
2) Expanding the group of equations of *n* unknowns;
3) Listing all constraints and choosing an appropriate algorithm to search solutions in the course of solving-equations involved optimization;
4) Selecting optimal solutions and their constructions to meet the requirements of designing a planar 4-bar linkage.

2.6 Control Strategy in Exoskeleton

Researches on the exoskeleton devices have been booming for the latest decade, with the topics being focused on the application field of assistance and rehabilitation in terms of the functionality to be delivered; parts of body that are conceived to be surrounded externally have almost been paired with exoskeleton from head to toe, but basically on the extremities [169, 170]. Technical reviews of the control strategies applied in those devices are rarely found in the literature, since instead of the kinematics that is only concerned in the mechanism design, the control strategies differ in the recruitment of different feedback signals, especially the control objectives that vary from different applications. But the control strategy applied in the exoskeletons is comprised of a two-level hierarchical architecture, to be explanatory, the high level controller make decisions of the specific motion that are mapped to lower controller to fulfill a systematic function reflecting the objectives; while the lower one carries out independent control of an actuator in terms of the force and displacement [171].

The control objectives are specified greatly varying across above three categories, as reflected in the aspects of the generated force/torque, the designated range of motion, time and time-derivative of those, deriving from the requirement of each application in terms of each actuator.

The device for strength augmentation aims at scaling down external loads on an able-body wearer for a rather long duration, for the purpose of compressing the power consumption.

Synchronization of the motion is highly preferred for the device along the wearer, which could primarily be regulated by monitoring the movement intention from the detected information, followed by decomposition to each actuator based on a certain algorithm. The control objective can be concluded to fulfill the force/torque required at the bottom level by calculation of a specific motion required force/torque based on detected motion and force distribution. Also intended to power externally, the exoskeleton for assistance focuses the potential users on the ones impaired permanently on the limbs in need of support for enough power and ROM to lead the daily lives. More impedance is expected to adapt the wearer, converting the motion synchronization into the regulation of man-machine interaction in terms of accomplishing the reaction force and predefined movement. Different from targeting only at torque in this case, the control objective is aiming at stiffness diversity in basically achieving both torque and relevant kinematic variable.

Different from assistive exoskeleton, the rehabilitative type that surrounds paralyzed limb carries out meaningful exercises in order to stimulate cortical plasticity, which requires not only repetitive movement inclusive in the exercise, but also movement in a wide range and resistance. Generally, the position is the primary objective the control system is required to reach; in the course of position attainment, the extra force is added in assistive or resistive implementation to correct of the position deviation or train wearer's adaption to strength. Therefore, the appropriate impedance or achievement of force/torque is also essential objective to fulfill in the control system.

In this section, control strategies used in the exoskeletons are not intended to be reviewed seriatim, but generally discussed in the two levels according to the control objectives; more emphasis will be given on the rehabilitative and active-assistive devices as the reference for the jaw exoskeleton. Please note, the control strategy here is referred to the systematic description to cover all of the control algorithms in each level, whereas control algorithm for a single level.

2.6.1 Lower-level Control Algorithm

The lower-level controller is designed specifically for each actuator to achieve the assigned function of the variables, though all actuators literally share the similar control algorithm in the same device. Some exoskeletons operate on more than one mode, which run different algorithms at this level by altering the inherent properties of the controller. By and large, the position and the torque based algorithms are two main categories mostly applied, usage of

which varies from case to case with the help of sensory information, including EMG signals, kinematic and force/torque.

The displacement of a specific joint that is actuated by the device is normally being monitored by positional sensors; the displacement information is then fed back to the controller for further action. The position control of a joint in exoskeleton can usually be found in the rehabilitative applications, where the desired trajectories are pre-planned offline based on normative movement to implement the training modes. The position control algorithms are used in an adaptive way to the specific application, for the purpose of adjusting the force that may be dramatically fluctuated when encountering the resistance. Simple approaches include the gain scheduling to boost the stiffness of the joint and the feed-forward acceleration [172, 173].

The force/torque discussed here in the controller is referred to that specified as a function variable controllable to actuate the joint in the linear/rotary actuator respectively. The variable obtained in the feedback loop is either directly measured from joint force/torque sensors or indirectly converted from joint kinematic variable. Force controller is generally used to exert appropriate force/torque with energy components such as spring or damper mounted in the device. Resistive-induced exercise requires more torque to drive the impaired limb aiming to performing functional training, where the force controller is used to resistively add torque of the estimated or constant amount to the joint [174, 175]. The force based control is widely used in the assistive-based exoskeletons for power augmentation and load-bearing, as the required torque on the closed-loop is directly known for a motion based on the load and voluntary movement [176]. EMG signal measured from the muscles is also engaged proportionally to the define virtual torque fitting into the control algorithm that is applied in Hybrid Assistive Leg (HAL), which reflects the user intention to actuate the knee joint, compensated with the target required joint torque [177, 178].

Impedance control could be the mostly used algorithm in the lower level to adapt the man-machine interaction for rehabilitation since it advances in securing the safety. The desired trajectory offers a string of positions that can be compared to the actual one, and the deviation can derive the force to compensate the contact force. Therefore, the position-based impedance control algorithm that is appropriate to adapt the man-machine interaction can satisfy the requirements on both position achievement and the contact force. Other algorithms, such as adaptive impedance control, and the admittance control can also be found for proper applications.

2.6.2 Higher-level Control Algorithm

The higher-level controller is designed to fulfill the control objective in terms of systematic function; or intuitively speaking, to translate the rehabilitative training or the assistive scheme into a string of movement patterns conveyed by the control parameters. The motion patterns that play a crucial role in decision-making to pass down commands to each actuator have been formulated in different fashions to adapt each specific application. Since a specific motion pattern is sometimes finely divided into several different stages in terms of the phase that composes of the entire periodic cycle, the control scheme applied here is also arranged with a level-based hierarchy that reflects the corresponding motion stages.

The simplest control scheme carries over a pre-programmed motion pattern which is formulated in a function of a position/force variable, in a way to reflect the resembling behavior of periodic movement of that human joint. That has been widely used in the lower-limb exoskeletons and ankle orthosis, which represent the phase-based gait pattern of by defining the gait speed, the duration and the peak; the predefined trajectories that appeared in the upper-limb rehabilitative devices with similar can actually be classified into this type as well, though this scheme has only one level [179].

Finite-state control scheme complicates fixed trajectory based scheme by expanding one pattern to switchable multiple ones, which could be obtained via a much finer representation of the phases in terms of a specific dividing criterion. Jiménez-Fabián and Verlinden [180] gave a thorough review of the control strategy used in the ankle exoskeletons, which exemplified the finite-state machine that are further leveled in terms of regulation of the similar mechanical impedance; similar mechanics is also found in the switching different control laws in accordance with the embodiment of the exercise [173, 179]. The higher-level algorithm representing the motion pattern can be much more complex to emulate the human behavior through fine control regulated by the crucial parameter, by involving motion detection based adaptive controller to achieve decision making, such as the fuzzy controller and neuro-network controller [181, 182].

2.7 Biomechanical Study Methodology

Finite element method (FEM) offers computational models to deal with the biomechanics concerned studies in terms of the musculoskeletal system by digitally reconstructing its mechanical properties and iterative calculation on the discretized structure. When FEM is applied in biomechanical study of the TMJ, ordinary linear model of the articular disc could

not reflect the mechanical property, and the interpretation of its function requires a much more complicated representation. While FEM usually provides static load based stress analysis in the course of mastication though the force condition is continuously varying. Biomechanical behaviors of the TMJ are usually of our concern, such as the mandibular motion contributed from each muscle and the interaction of different components. Traditional approaches to those understanding have great limitations, as theoretically the component is simplified to a mass point by which physical properties are hardly reflected; and experimentally sensors cannot be directly attached to the place where the internal force is generated and expected [92]. Currently, the biomechanical studies of the TMJ are mostly conducted with the assistance of computational-model-based multi-body dynamic analysis (MDA) and finite element analysis (FEA), both of which are predominantly applied in the field of engineering.

MDA is a process to restore the actual loading conditions on a specific component via simulating the rigid-body motions existing among two or more rigid bodies without considering the deformation, and can be further categorized into kinetic analysis and kinematic analysis. Computational models of the mastication system with high emphasis of the morphology are obtained sliced CT-image reconstruction from a real body. The type of contact surface, constraint and joints are also defined in the model, as resembling to the actual state and meanwhile ensuring to form the determinate motion [92, 95, 96]. The jaw muscle is usually simulated to be one or several linear actuators with of firing the predefined scheme in terms of the location and shape. So MDA can basically emulate the loading condition of any scenario with defined parameters upon a computational model, in order to demonstrate the profile of force versus gape.

MDA is also applied in the field of evolutionary study by exploring the biomechanical properties of animal skulls. A lizard skull was modeled by reconstruction of CT-scanned images, with assigned physical features. Muscles were modeled based on Hill-type muscle and attached to connect the skull and the jaw on appropriate location. Passive element of the muscle force and the ligament were also incorporated in the study. The bite scenarios were formed by applying the muscle forces, and the bite forces and joint forces were derived.

FEA works by dividing the geometry of model into finite number of sub-regions, the element, which are bonded via nodes. The model structure is then transformed into mesh which applies the structural and material properties and defines the way the nodes deform, through the node system. When the force is applied, the model is solved in mesh and represented in the form of nodal displacement. In terms of the TMJ, FEA studies varies from the simulation

scenarios, and usually focused on the on the representative function of the articular disc and stress distribution across the contact surfaces under certain loading.

MDA simulates continuous process of the rigid-body motions and aims to obtain the variation of the concerned force during simulation period; while FEA is a static or quasi-static simulation in which the force occurs intermittently at certain moment to obtain the deformation at that moment. Recently FEA studies are combined with MDA method in several literatures, in which the load data provided from MDA solution are directly transferred into FEA to investigate the stress and strain. As in the dynamic simulations, muscle force varying with the gape and other constraints eventually affects the bite force and joint force; both generated from MDA are more realistic than traditional FEA studies in which the applied force cannot be proved correctly fitting at certain gape. To be loaded as the input discretely to the FEA study, the validity of the input data of FEA ensures that of the outcome. This method is firstly proposed in the study of tension distribution in the cartilaginous structure of TMJ [183]. Muscles are modeled as Hill-type with different-level of activations and the cartilage are modeled with a Mooney-Rivlin material model. The combined study method is also used to investigate the mechanics of the macaque and lizard skull [184, 185]. Apart from the definition of the muscle force in the stage of MDA, in the study of injury investigation, the moment simulating impact were also included as part of external force by specifying its acceleration on its center of gravity [186]. Limitations are all referred in all of those combined studies, but mostly mentioned is the simplification of the material representation due to the software capability. As mentioned above, the cartilage layer of the condyle and the disc exhibits viscoelasticity which cannot be modeled in the software. The certain jaw motion contributed by jaw muscles is achieved with the same activation that may not conform to the way that the jaw muscles are recruited to do free movement. The kinematics of the jaw is not specified before simulation or demonstrated after simulation, so the velocity and acceleration of the jaw are not known. Other limitations on the MDA mainly focus on the validity of the dynamic model in which the joint was not usually defined.

2.8 Summary

The literature reviewed in this chapter focuses on the two major parts, namely, the characteristics of the human masticatory system and the technique in the Mechatronic system development. More specifically, the former is unfolded in the aspects of kinematics, dynamics and biomechanics of the mandible, while the latter pays more attention in the state-of-the-art of such devices having similar function or action spot.

As one of the most complicated system in the human body, the masticatory system is a product after thousands of years of human evolution. Multiple pairs of the muscles participating in the mastication and the afferent nerves going into the deep part of the brain all ensures the robustness to keep the only pathway for the intake of the nutrition unobstructed. A complete replication of its anatomy integrated with the neurologic control is hardly achievable by robotic devices; most development of biomimetic devices is more prone to interpret one feature among the complexity. It is predictable that the diversity of understandings in one aspect could not be all justified in the development of the jaw exoskeleton.

For the designing process, more considerations are expected to cast to the motion regain and the related function regeneration, rather than dynamic behaviors. Though a lot of the studies put the emphasis on the pattern of the mandibular movement per se in both 2D and 3D space, the motion in more refined decomposition has not been taken into account; while the common feature agreed by all kinematic studies is envisaged to form the fundamental pattern, which is of the functional importance.

Since the exoskeleton is a recognized means to build this device for users to wear, control strategies commonly applied in developed exoskeletons have been summarized in a level-based architecture. The mechanism that has been used in the devices resembling the extremities is not discussed due to the irrelevance; but the methods related to the linkage synthesis have been systematically reviewed.

As to the TMJ, its movement is usually acquired by transformation of the in-vivo measurement on other spots; meanwhile non-invasive simulation paves the way to investigate the biomechanical and dynamic performance under static loading conditions. Those studies per se are prone to pursue the construction of the computational model in approaching to the human system.

Chapter 3: Mechanism Modeling and Identification

The mechanism of a device could be considered as the skeleton to accommodate substances which are notably dependent. Appropriate representation of the original kinematics stays an important position, particularly in this case of TMJ presenting more complicated movement that other joints in the human; on one hand the mechanism of the TMJ should be able to reflect the intrinsic kinematic features of the masticatory movement, or to say precisely, the movement the device is intended to replicate; while it is also in line with some requirements orientated to the operation and design process.

Only replication of the jaw movement would not be adequate to achieve a significant effectiveness. The therapeutic efficacy relies on motions in meaningful therapeutic exercise according to the clinical studies, for example intensity and resistance modes, which also expand design specifications in terms of kinematics.

Modeling TMJs and mandibular movement lays a foundation to build up the mechanism and further entire device, the process undergoes a trade-off between the full realization of mobility and compliance and simple structure of the device. Some important factors that may not appear on the modeling process impose great impacts on the device design, such as the way of implementation and control system structure subject to constraint of force reaction working on the TMJ. This chapter starts constructing mechanism with investigating mandibular kinematics based on literature review of the masticatory anatomy, gives a full-view of the process of mechanism synthesis, including specifying the design requirements, the type and the dimension synthesis till finalizing the mechanism.

3.1 Planar Kinematics of the Jaw

The jaw is basically able to move with six DOFs in the three-dimensional space, which gives a rather spatial workspace in terms of each point of interest. The workspace of the device movement relies on the chief functional implementation of the jaw, but it does not have to be identical with the mandibular one. Ostry [9] indicated in their studies that the sagittal plane motion is independently varying from other DOFs, composing of the movement necessarily required for daily functionality; additionally, according to the cases showing jaw motion loss, the restricted mouth opening range patients mostly suffer from severely impairing the oral functions also implies the importance of the sagittal movement. The sagittal plane is

appreciably referred to be the primary functional plane for the mandibular movement, within which is to be focused on the movement delivery by the jaw exoskeleton.

3.1.1 General Model of the TMJ

While fixating on the sagittal plane to be where rehabilitation exercise the device provides is located, the jaw movement theoretically contains three DOFs in the plane which have been represented with different combinations of joints, namely, rotating together with sliding. The planar workspace of the movement can be encircled by the border trajectories and filled with the off-the-border free movement paths, the former being constrained by physical contacts while the latter being normally regulated by the nervous control [86]. The mandible is regularly considered as the rigid-body, which in sagittal plane trajectories of two concerned points, usually choosing the condyle point (CP) projected on the sagittal plane and the incisor point (IP)s to lock the exact planar motion.

To evaluate the jaw kinematics in the sagittal plane, a three-DOF TMJ model is built up using an ordinary planar representation without loss of generality, which consists of two orthogonal prismatic joints in the beginning and a revolute joint in the end attached to the jaw, instead of following the concave morphology of TMJ, as illustrated in Figure 3-1. For the kinematic purpose, some assumptions that emphasize the establishment of the model are worth mentioning to ensure the outcome not to be interfered by biomechanical considerations.

1) The articular disc does not undergo any deformation in any dimension;
2) The translation the temporal fossa forces the jaw to do is treated as combination of vertical and horizontal sliding;
3) The assumed area by the translations covers ROM of TMJ;
4) The rotation can be carried out with any magnitude at any point where the translation takes place.

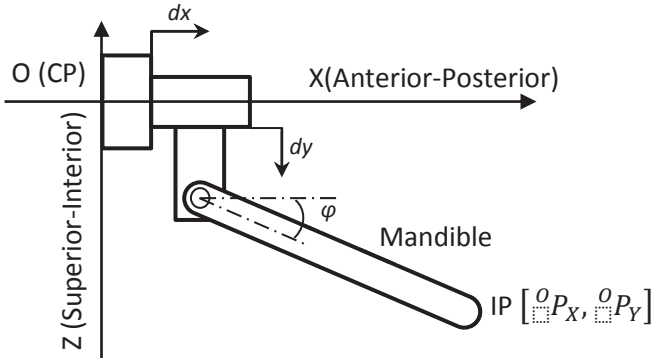

Figure 3-1 Kinematic representation of the TMJ

The origin of the coordinate system sits on a stationary point on the skull where the CP is located at rest. X axis matches along the anterior-posterior direction and Z axis along the superior-inferior direction. The variables defining the corresponding pairs for the revolute joint, horizontal and vertical joints are denoted as *φ, dx, dy* respectively, and the initial state indicating the rest position of jaw from start assigns zero value to each variable. The mandible is illustrated by a bar in Figure 3-1 and IP located at tip side represents the current position.

Under this frame, the IP coordinate denoted as $\left[{}^{O}P_X,\ {}^{O}P_Y\right]$ in the sagittal plane can be written in the algebraic format in Eq. (3-1).

$$\begin{aligned} {}^{O}P_X &= dx + L_{IP}\cos(\alpha+\phi) \\ {}^{O}P_Y &= dy + L_{IP}\sin(\alpha+\phi) \end{aligned} \tag{3-1}$$

Where:

$L_{IP} = \sqrt{{}^{M}\mathrm{x}_{IP}{}^{2} + {}^{M}\mathrm{y}_{IP}{}^{2}}$, L_{IP} is the length of IP with respect to CP at the initial position;

${}^{M}\mathrm{x}_{IP}$, ${}^{M}\mathrm{y}_{IP}$ are the coordinates at X-axis and Y-axis under the tip frame respectively;

$\alpha = \tan^{-1}\frac{{}^{M}\mathrm{y}_{IP}}{{}^{M}\mathrm{x}_{IP}}$, is the inclination angle of the vector pointing to P under the tip frame at the initial position.

Assuming the area covered by trajectories on the IP has already been known, which means the IP coordinates of each pair are given. The inverse kinematics is going through the process starting from eliminating a variable of ϕ with Eq. (3-2) and (3-3). Squaring both sides of them and summing them together in Eq. (3-4), we can get Eq. (3-5).

$${}^{O}P_X - dx = L_{IP}\cos(\alpha+\phi) \tag{3-2}$$

$${}^{O}P_Y - dy = L_{IP}\sin(\alpha+\phi) \tag{3-3}$$

$$\left(\frac{{}^{O}P_X - dx}{L_{IP}}\right)^2 + \left(\frac{{}^{O}P_Y - dy}{L_{IP}}\right)^2 = (\sin(\alpha+\phi))^2 + (\cos(\alpha+\phi))^2 = 1 \tag{3-4}$$

$$\left({}^{O}P_X - dx\right)^2 + \left({}^{O}P_Y - dy\right)^2 = {L_{IP}}^2 \tag{3-5}$$

The first three unknowns turned into two, so one variable (dy) can be expressed with respect to the other (dx), in Eq. (3-6), showing two solutions for (dy). The angular variable ϕ is also obtained by substituting (dx) back into (3-2) and calculated in Eq. (3-7).

$$dy = \pm\sqrt{{L_{IP}}^2 - \left({}^{O}P_X - dx\right)^2} + {}^{O}P_Y \tag{3-6}$$

$$\phi = \cos^{-1}\frac{{}^{O}P_X - dx}{L_{IP}} - \alpha \tag{3-7}$$

3.1.2 Workspace on the Incisor

The joint configuration at each instantaneous position requires at least coordinates of one point on the mandible, and IP is selected here. So prior to processing the inverse kinematics of TMJ model, the precise workspace on the IP should be given as a premise. As no boundary trajectories enclosing the whole area is found in quantitative recording in the literature, the overall workspace evaluated in terms of the IP is rebuilt into a numerical one by contrasting the Posselt envelope to be sampled in the literature and having it scaled to the typical description that is itemized below.

1) The pure protrusion only moves translationally anteriorly about 10 mm;
2) The maximum opening contributes to approximately 50 mm vertical translation;
3) The hinge-opening stays around 13° rotations without condyle sliding.

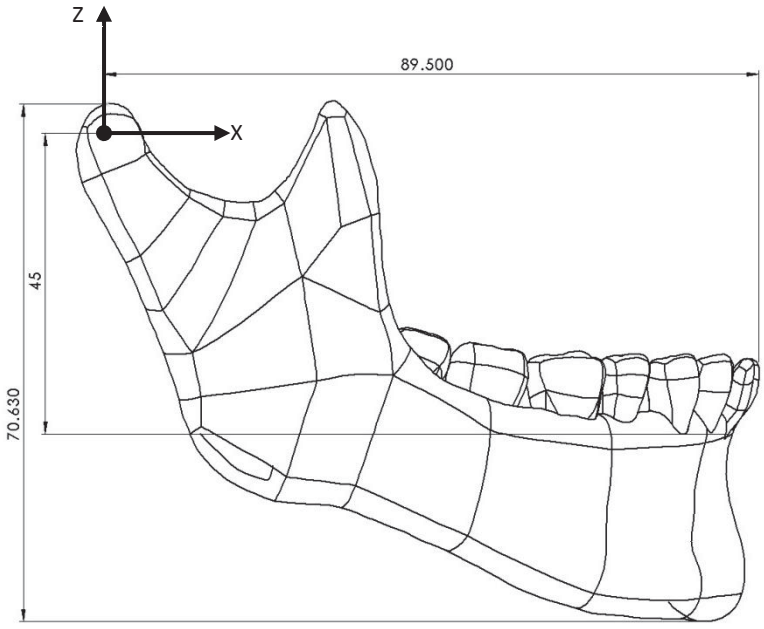

Figure 3-2 Size illustration of the mandible

The size of the mandible also affects the calculating result of joint variables. For the consistency of further calculation, the size of the jaw used in this chapter for the consistency of the calculation is given in Figure 3-2, and was measured from an accurate replica of a human jaw by reconstruction CT slices of a cadaver by [6]Faculty of Dentistry in University of

[6] Faculty of Dentistry, University of Otago, please visit http://dentistry.otago.ac.nz/. Details of the 3D model can refer to Publications under the name of Ichim, I..

Otago. The coordinate frame is still in coincide with the global frame in three-dimensional space, the distance from CP to IP in the anterior-posterior direction being 89.50 mm length and in the superior-inferior direction of 45 mm length.

The original data of Posselt envelope was obtained through sampling points figured in the literature [86]. Instead of directly discretizing the curves to points at selected interval, some critical points on this boundary are chosen to be scaled in this context of parameters about the ROM being already set with exact pairs of coordinates, which are selected to be the rest point, the protrusion point, the hinge terminal point, and the maximum opening point, all of which are marked in (o) in the Figure 3-3. Then the scales on one direction is determined by the ratio of preset length on the selected item to the sampled counterpart, in the circumstance that the maximum vertical length which can be precisely acquired stands for the superior-inferior direction and the protrusion for anterior-posterior direction ($r_x = d_{max}/d_{sample\_v}$, $r_z = d_{protrusion}/d_{sample\_h}$). Other points on the border sampled from the literature are processed based on the same scales (along both axes) to be attached on the new curve to compose of the overall trajectories.

To reflect a more distinct workspace of the jaw in this context rather than the one roughly enclosed by limited sampling points, the border is more sketched by interpolating more points between the sampled pairs. The interpolation by using FFT method can insert specified times the amount of points between the samples of those obtained from Lagrange method, and the process is completed in MATLAB. That could eliminate difficulties in fine discretization brought from sampling. But FFT interpolation requires a periodic value of the variable, which can be satisfied by selecting the whole range of the variable in sequence during an overall circle of jaw movement forming a closed envelope. Some points sampled on the same X-coordinate are given as side-witness points, which are used to verify the rationality of the interpolated points that sections of curves pass through.

Two points are interpolated in-between each adjacent pair of sampled points ((x) marked in the Figure 3-3) and the maximum offset on the same anterior-posterior variable between the selected sampling points and the interpolated counterparts is compared to show less than 0.1 mm clearance. Therefore, the envelope of the border movement on the IP can be expressed by in Figure 3-3.

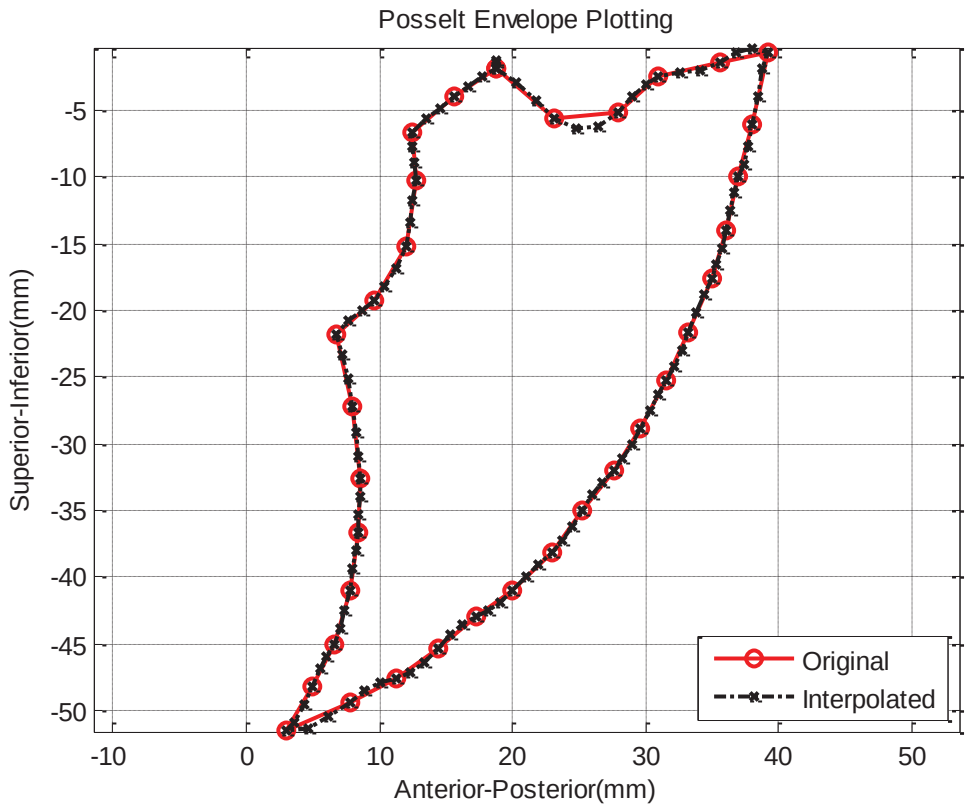

Figure 3-3 The interpolated Posselt envelope plotted in the MATLAB

A couple of facts are believed to implicitly support the feasibility of using the method of scaled range of motion joint with interpolated points to acquire the border trajectories. The classic trajectories have a string of typical and comprehensive description which fits the envelope provided in the literature very properly, and eliminates possible discrepancy brought from individual recording. The generated trajectories also can be verified by referencing those from the same literature which sets a restraint to range of border. However, the downside consists in the likely lack of individual differentiation, as the typical one is intrinsically borne to cover the most common features of border movement; therefore, to avoid the loss of individuality, the jaw movement is recorded in vivo on the IP by using three-dimensional recording machine, [7]Articulograph AG500, in an attempt to acquire a personalized boundary trajectories.

The introduction and configuration to AG500 is to be stated in section 6.5, together with the data post-processing procedure. In this recording scenario, one sensor is glued to the lower incisor for the tracking purpose, and three other sensors are respectively glued to the upper incisor on the skull, outside of left and right ear, as the reference to offset the head motion.

[7] All experiments with using AG500 referred in this thesis were carried out in the IFNHH, Massey University. More information about Articulograph AG500 can be found in: http://www.articulograph.de/.

[8]The subject has a full dentition and has not reported any history of TMD symptoms based on a questionnaire; the size of the jaw was obtained by calculating the relative distances recorded on the incisor, the left and the right ear (assumed to be both sides of condyles) by the machine; the mandible size measured on the X-axis is 74 mm and on the Z-axis 42 mm under the same coordinate frame.

The sagittal movement was carried out in 18 trials of specified protocols, including the protrusion, the normal open-close, and the maximum opening, which was repeated three cycles in each trial. Though the border movement in this circumstance is desirably anticipated to acquire, in order to give an actual profile of individuality, as well as to be compared with the typical one; unfortunately, the subject could not manage herself to beware of achieving defined border movement consciously. The recorded trajectories on the incisor hereby were not ensured to constitute the absolute sagittal-plane boundary, but the subject was following the instruction literally to move her jaw.

The recorded data are given in numerical form after the data are undertaken format conversion (the procedure of data conversion, which avoids undergoing the process of data discretization. However, those data presenting the absolute coordinates of the moving sensors in the AG machine frame should be transformed into the same representation under the current frame before illustrating the composed trajectories. The machine frame in Figure 6-18 inherently set up intrinsically is considered as the global frame, with respect to which a jaw frame can be established on the subject's jaw.

As the sagittal movement actually refers to the XOZ-plane of the jaw frame in accordance with the one set up to represent model in Figure 3-1, instead of attempting to locate the X'OY'-plane at first, the Z-axis of the jaw frame is identified by linking the points recorded on the upper and lower incisor sensors at the moment when the lower one gives the highest Z-value on the machine frame during each trial except protrusion. Note the jaw frame locates its origin at the lower point and stays immobile relative to the machine frame. That avoids gluing sensors to other teeth and subsequent data-processing, also gets rid of the likely deviation of the plane orientation due to irregular occlusion. The lateral motion possibly introduced in the trials could not be evaded based on machine's resolution, making the recorded points not able to link into a planar trajectory. A vector in the X'OY' plane is composed by connecting the origin to the median point among the trajectory after the high-frequency noise is filtered out.

[8] Informed consent was obtained from the subject.

Then the Y-axis points perpendicularly to the cross product of this vector and Y'-axis, and X'-axis is obtained by the cross-product between Y'-axis and Z-axis, as illustrated in Figure 3-4.

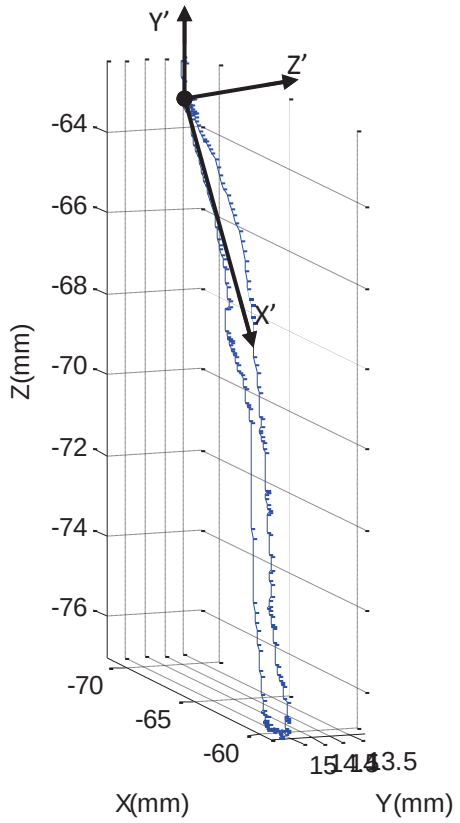

Figure 3-4 illustration of jaw coordinate frame established based on the recorded data

The transformation matrix from machine frame to jaw frame ${}^{AG}_{JAW}T$ in each trial can be written in a generic representation. The coordinates of the points ${}^{JAW}P$ under the jaw frame can be calculated by Eq. (3-8).

$$ {}^{JAW}P = {}^{JAW}_{AG}T \cdot {}^{AG}P \tag{3-8} $$

Where:

${}^{AG}P = [\, P_{OX} \quad P_{OY} \quad P_{OZ}]^T$ are the 3D coordinates of the jaw origin in the machine frame.

${}^{JAW}_{AG}T = \left({}^{AG}_{JAW}T\right)^{-1}$ is inversely calculated from the transformation matrix established in Figure 3-4.

The way to create the jaw frame seemed unable to ensure the X'OY' plane to be exactly the one the largest proportion of the recorded points is located. But in this scenario, the subject was instructed to do normal open-close movement that restrained the lateral displacement within a less than 2 mm strip away from sagittal plane according to the calculated data, so the likely deviation of X'OY' plane derived from this vector evaluated by the function of deviated

angle θ is small enough to hypothesize $\sin\theta \cong \tan\theta$ that the absolute magnitude of a recorded point would approximate the projected length on the plane.

The trajectory in each trial that is comprised of recorded points is transitioned to start from the same position at the origin over all trials, and trajectories recorded on the incisor are plotted in the same sketch on the sagittal plane shown in Figure 3-5. Figure 3-6 depicts the deviation of the lateral motion of each trajectory after transformation into the orthogonal plane (X'O'Y'). Since the spatial trajectory on the incisor could not be avoided even if the jaw movement was consciously controlled, the small margin of the lateral error, as mostly less than ±0.5mm, supports the assumption that the trajectory on the new X'O'Y' plane can be considered to be identical with the original one.

Not all continuous trajectories that have been obtained from the experiments are encompassed in this figure; some exhibiting large lateral motion have been omitted; the coordinates representing the composing points are not those originally recorded which have been processed with a low-pass filter that is fully stated in the section 6.5.3. A GUI for all of the AG data processing is created in the MATLAB to facilitate transformation of the original trajectory into new orthogonal plane, filtering the original data, and plot visualization as shown in Figure 3-7.

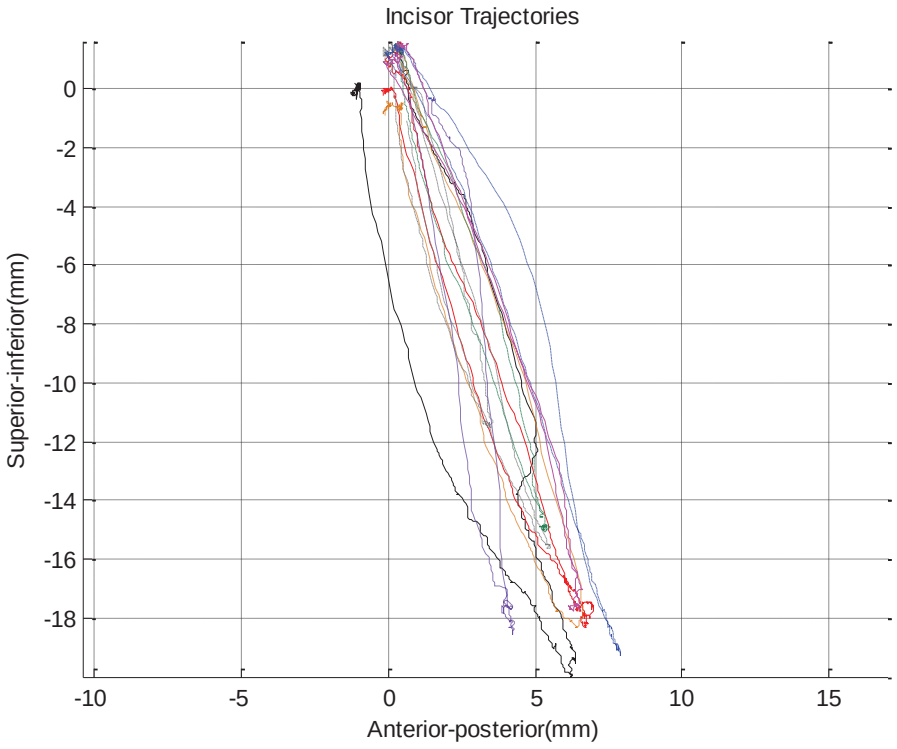

Figure 3-5 The sagittal-plane workspace recorded in vivo

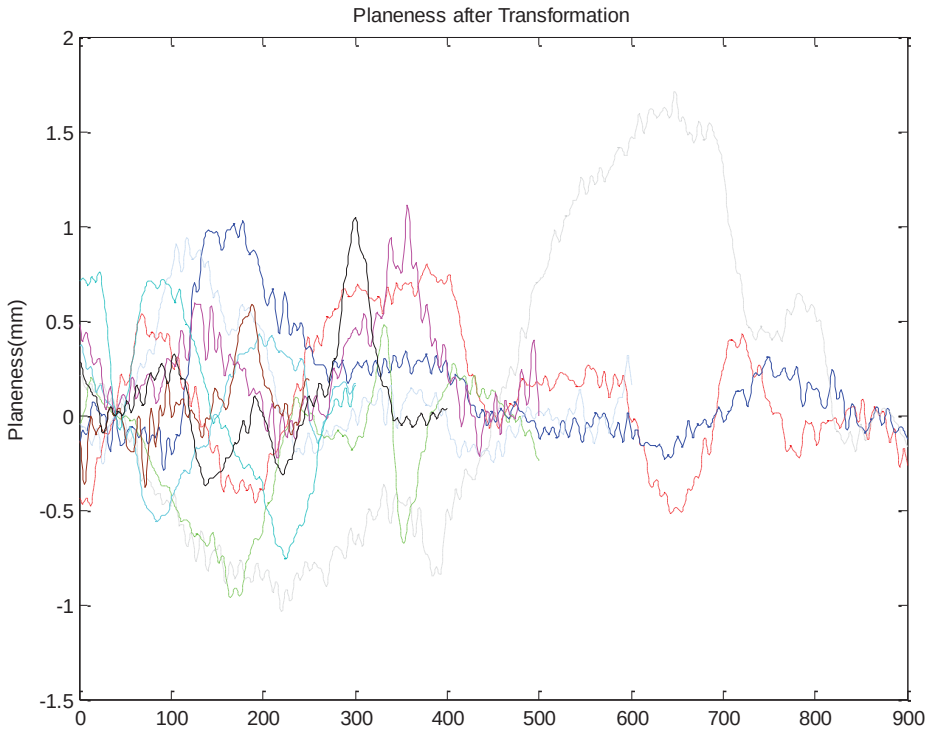

Figure 3-6 The planeness on the z-axis after transformation

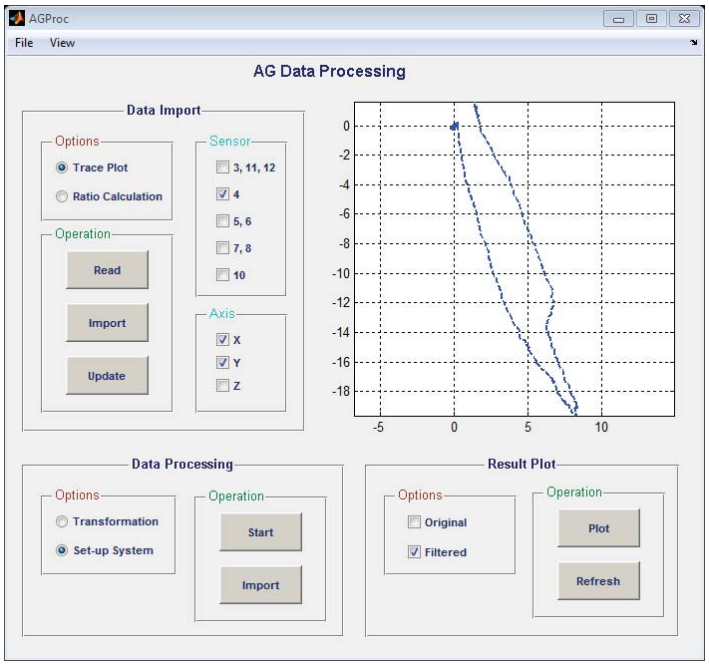

Figure 3-7 A GUI developed for AG data processing

The above two envelopes that encircle a general and an individual workspace of the incisor in the sagittal plane, are invoked into the inverse kinematic study to calculate the joint variables of the kinematic chain. The solved parameters can be hereby imported into forward kinematic expression to outline the workspace of another interesting point on the jaw. As the irregular incisor workspace is barely specified by precise description of range, random points falling within this workspace are stochastically selected to describe the overall scale of IP envelope

based on Monte Carlo method. Basically, X-value of random sample is directly chosen in-between its lower and upper bounds as indicated in Eq. (3-9); the values intersected with the incisor boundary vertically at this random X-value form the lower and upper bounds at the identical sample along the Y direction, as expressed in Eq. (3-10). The vertical lower and upper bounds are generated by linearly interpolating the boundary at each random X-value, as generically expressed in Eq. (3-11). The interpolation for all stochastic samples is processed in MATLAB, and the workspace on the incisor covered by scattered points is illustrated in Figure 3-8 based on a sampling size of 1000.

$$M_X^i = M_{X_{LB}}^i + \left(M_{X_{UB}}^i - M_{X_{LB}}^i\right) \times RAND \tag{3-9}$$

$$M_Y^i = M_{Y_{LB}}^i + \left(M_{Y_{UB}}^i - M_{Y_{LB}}^i\right) \times RAND \tag{3-10}$$

$$M_{Y_{UB}}^i = \max\left(f(x_m) + \frac{f(x_{m+1}) - f(x_m)}{x_{m+1} - x_m}(x - x_m)\right) \tag{3-11}$$

Where:

$M_{X_{LB}}^i, M_{X_{UB}}^i, M_{Y_{LB}}^i, M_{Y_{UB}}^i$ are the lower and upper bounds of the X- and Y-coordinates, respectively; $\mathrm{i} = 1,2,\cdots$ The randomly selected points; the size of the sample pool is λ.

x_m, x_{m+1} are one side of the points nearest to the sample x without special order; $f(x_m), f(x_{m+1})$ are the corresponding boundary Y-values.

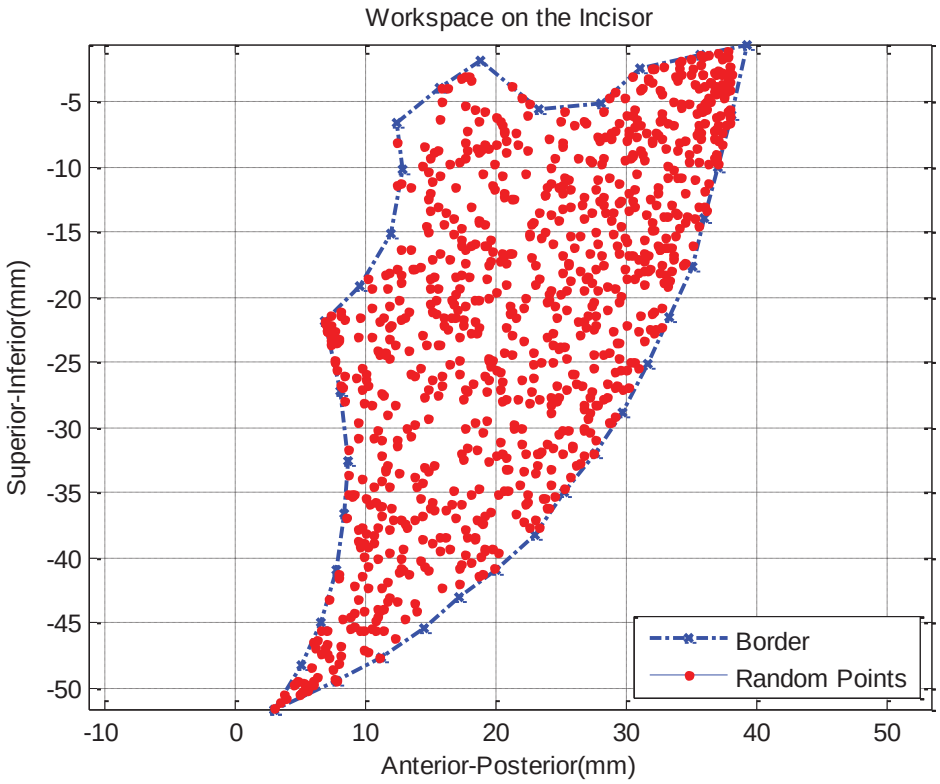

Figure 3-8 The scattered points within incisor point border

The reachable area on the incisor composed of all accessible points of all joint configurations within a specified range has been offered straightly in two means, representative of the generality and the individuality, by which the workspace can be assessed numerically with the result of the maximal displacement in the superior-inferior and the anterior-posterior direction being 52 mm and 20 mm respectively.

3.1.3 Workspace on the Condyle

Theoretically, the workspace on the condyle can be easily sketched with using Monte Carlo method by invoking the joint variables obtained in the inverse kinematic calculation with the known incisor workspace. However, as indicated in Eq. (3-6) and (3-7), solving inverse kinematic problems will incur infinite solutions to the variable configuration due to inadequate position information, and also inevitably involve nonlinear solving subject to an appropriate set of constraint. The coordinates for any point in the jaw can be expressed in Eq. (3-12) with respect to three variables, the forward kinematics is hereby simplified to be formulated with two variables by adding a weight ratio r_s between two translational parameters in the coordinate representation, in order to gain a definite joint configuration particular to a specific motion. As far as the TMJ motion is concerned, the translational movement in the perpendicular direction to the fossa formed by the compression of the articular disc is rather slight in magnitude, and it has been usually considered dependent relative to the one along the fossa. In this joint configuration, the vertical translation dx is treated as a dependent variable with respect to the horizontal one dy, given by the ratio value which is limited within a range of $[0,10]$ according to the literature, as expressed in Eq. (3-13).

$$\begin{bmatrix} {}^{O}P_X \\ {}^{O}P_Y \end{bmatrix} = \begin{bmatrix} f_x(dx, dy, \phi) \\ f_y(dx, dy, \phi) \end{bmatrix} = \begin{bmatrix} dx + L_{IP}\cos(\alpha + \phi) \\ dy + L_{IP}\sin(\alpha + \phi) \end{bmatrix} = \begin{bmatrix} r_s & \cos(\alpha + \phi) \\ 1 & \sin(\alpha + \phi) \end{bmatrix} \cdot \begin{bmatrix} dy \\ L_{IP} \end{bmatrix} \quad (3\text{-}12)$$

Where:

$\mathrm{R}_x, \mathrm{R}_y$ are the parameter matrix with respect to three variables for X- and Y-coordinate, respectably.

$$\begin{bmatrix} dx \\ dy \\ \phi \end{bmatrix} = W \cdot \begin{bmatrix} dx \\ dy \\ \phi \end{bmatrix} = \begin{bmatrix} r_s & 0 & 0 \\ 0 & 1 & 0 \\ 0 & 0 & 1 \end{bmatrix} \cdot \begin{bmatrix} dy \\ dy \\ \phi \end{bmatrix} \quad (3\text{-}13)$$

To avoid the misunderstanding of the way of the kinematic chain simplification in the subsequent calculation, there are some interpretations stating below:

1) The rotation is defined independent of both directions of translation, but the ratio of rotation to translation is limited up to 2.5°/mm at any moment;

2) The ratio (r_s) of the horizontal translation to the vertical one is not essentially specified as a constant, standing for a particular movement pattern at the instantaneous moment;

3) Each of the rotation, horizontal and vertical translation has a displacement range, limited up to the maximum opening of 35°, 30 mm and 10 mm respectively.

Solving the joint configuration for a particular correlation between translational variables turns into the nonlinear minimization of the Eq. (3-5) in which the dx is replaced by $r_s dy$ subject to the range constraints, as the goal function is expressed in Eq. (3-14).

$$\min g(x) = \min\left(\left({}^{O}P_X - r_s dy\right)^2 + \left({}^{O}P_Y - dy\right)^2 - {L_{IP}}^2\right) \tag{3-14}$$

Subject to: $\begin{cases} r_s \in [0,10] \\ dy \in [-3,7] \\ \frac{\partial \phi}{\partial r_s dy} \in [0,3] \end{cases}$.

The condyle in this model is assumed to be represented by a relatively stationary point that only moves translationally without influential from jaw rotation and acts as the revolving center. The condylar boundary that could circle the area of CP movement is not literally corresponding to the incisor border according to the kinematic rules, which means points on the IP boundary could not be only used in the process to form an active area of the condyle. The IP workspace represented in distributed samples is invoked to calculate the CP location inside the TMJ in order to cover the overall CP workspace under the specified r_s. The joint configurations, especially relying on the value of r_s, are not chosen randomly but in accordance with the TMJ morphology summarized from the literature and our measurements, which are summarized in trials, as given in Eq. (3-15).

$$r_s = \begin{cases} [-5,-3], & 0 < dx \leq 5 \\ [0,2], & 5 < dx \leq 20 \end{cases} \tag{3-15}$$

r_s is assigned with a 0.2 interval combination, and the size of the jaw still applies the one used for the random scattering of IP coordinates, and the calculated workspace can only be an indication of the rough shape of the CP workspace without precise implication. Figure 3-9 illustrates the condyle workspace which start from the origin at $[0,0]$. All IP sampling pairs of coordinates are imported in this process and the size is also 1000. The condylar space can be ambiguously speculated in value but in general the active area presents a shape of to 25mm and 8mm respectively.

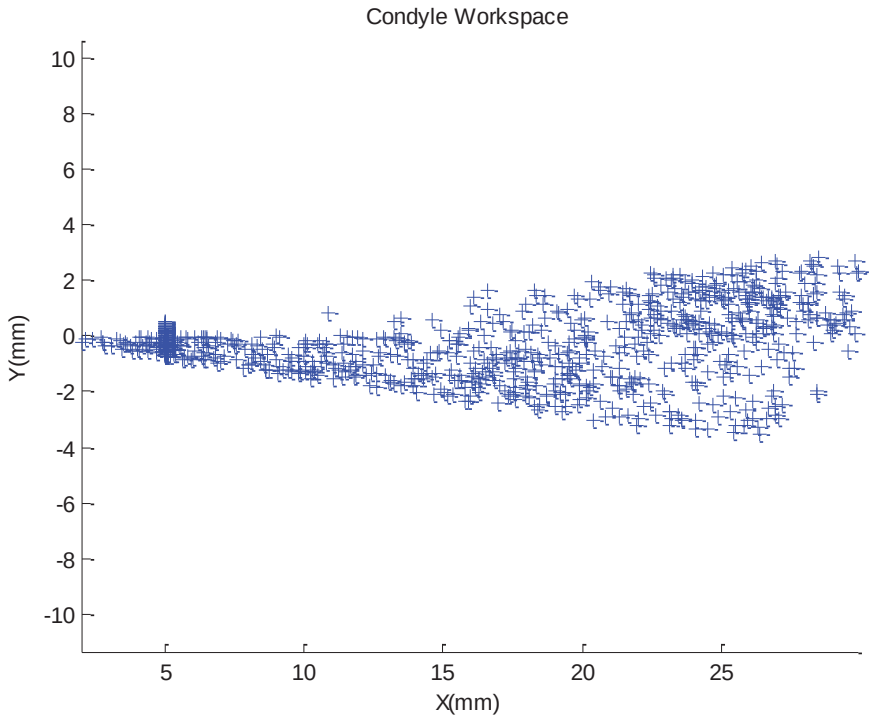

Figure 3-9 The condyle trajectories

3.1.4 Functional Analysis

The kinematic chain set up above universally generalizes the unconstrained movement of a single link in the plane having three DOFs, which is applied to describe the free jaw movement, instead of a specific model that carries typical features; representatively, the condyle position depends on the translational displacements if the condyle is simplified to an single point, while the incisor under the same frame relies on the rotational displacement with respect to it. That provides a way to explore the jaw movement pattern in different functional scenarios based on the kinematic chain, and also gets rid of inherent error due to the variability of the individual fossa-eminence inclination angle.

The anatomy of the masticatory system inflicts the morphological constraints on the mandible in terms of its movement, in both aspects of the workspace and the number of DOF, which is intuitively reflected on the Posselt-envelope shaped incisor boundary. Each pattern of the jaw movement that may embody one masticatory function can generically be represented with a distinctive kinematic mechanism given only rigid-body is concerned. The interaction between the maxilla and mandible occurs at two sites, indispensably on the TMJ side that is pivoting the jaw movement, and optionally on the occlusal plane when the upper teeth are contacting to the lower ones. Apart from the linkage constructed to stand for the TMJ, the tooth occluding is modeled by a two-DOF slider that cusp contacting in the plane restricts one-DOF translation, allowing slight rotation around the pin and slide along the occlusal line, which can

be interpreted in kind as the lower tooth retaining at the touching counterpart still able to translate along and rotate around it.

By means of the above definition, when the teeth keep in tight contact that the jaw does not stay away from occlusal plane, such as protrusion or retrusion, a closed-chain mechanism can be built up to demonstrate the interplay between the maxilla and the mandible in Figure 3-10. Illustratively, this mechanism is a five-bar slider where the mandible is coupled by partial restrictions at both sites of interaction to possess two DOFs. The ground of the mechanism represents the maxilla which is set stationary as the reference on the TMJ at rest and incisor; the slider on the IP iconically represents the occlusal curvature guidance projected on the sagittal plane, which is literally the mandible can translate during protrusion; and the pivot joint on the incisor side refers to the tooth cusp keep in touch with the maxilla on teeth. Note this demonstration is not denoted.

As opposed to the current mechanism, a four-bar linkage was offered by coupling the guidance on both TMJ and incisor to describe the protrusion/retrusion in the literature where mandible was restricted to a resultant one DOF kinematically [187]. However, that one-DOF mechanism clarified the interaction between maxilla and mandible based on the neuromuscular control to TMJ, which is not intentionally avoided here but instead of a purely established kinematic relation. Since a special scenario in which the border movement was carried out while maintaining clenching excluded the affection from the disc compression, this gives explanations for one more number of DOF existence in this contextual mechanism which fully describes each possible TMJ motion, and back up the correctness of the interaction model as well.

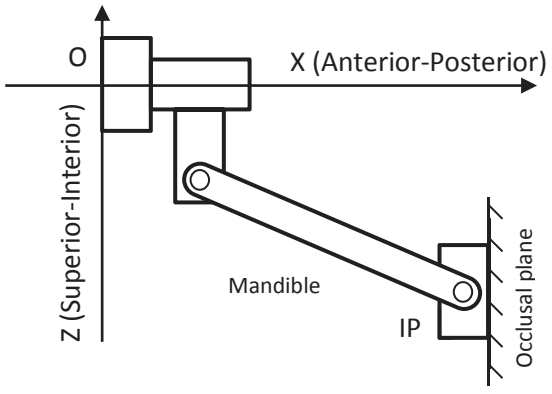

Figure 3-10 The interplay between the mandible and the maxilla during occlusion

Other guided movement of the mandible that is piloted to stick along a trajectory in terms of the incisor theoretically can be modeled to a pivotal slider similar to depiction of the occlusion

that allows rotating around the instantaneous contacting point, such as the boundary movement or chewing. The sliding joint is correspondingly replaced by the curvature of the incisal boundary or the shape of food bolus, and the permission of the disc compression leads to a resultant number of DOF equal to two. Only the distinction lies in the chewing circumstance in which crushable food does not apply to the rigid-body kinematics and hereby presents instantaneous contact between the upper and lower teeth, resulting in a mechanism with varying parameters.

Aside the neurologic control of the muscular system, the normal unloaded jaw movement is not inflicted explicitly with the tangible constraints, and the area evaluated on the incisor can be sketched out by stochastically dropping samples for each joint variable within an designated range, which conforms to the literature, for the purpose of partitioning the active incisal area regarding contribution from each variable. The workspace coverage under two extreme configurations, no anterior-posterior (+) and no superior-inferior (•) translation, is shown in Figure 3-11.

Based on above the sagittal plane focused analysis, it is concluded that the mandible has the ability to move freely with three DOFs, and the morphology of the whole system restricts its movement in terms of the number of DOF, but for a specific purpose the exact pattern is primarily regulated by the neuromuscular system, which is reflected by comparisons between with and without clenching in the similar scenario.

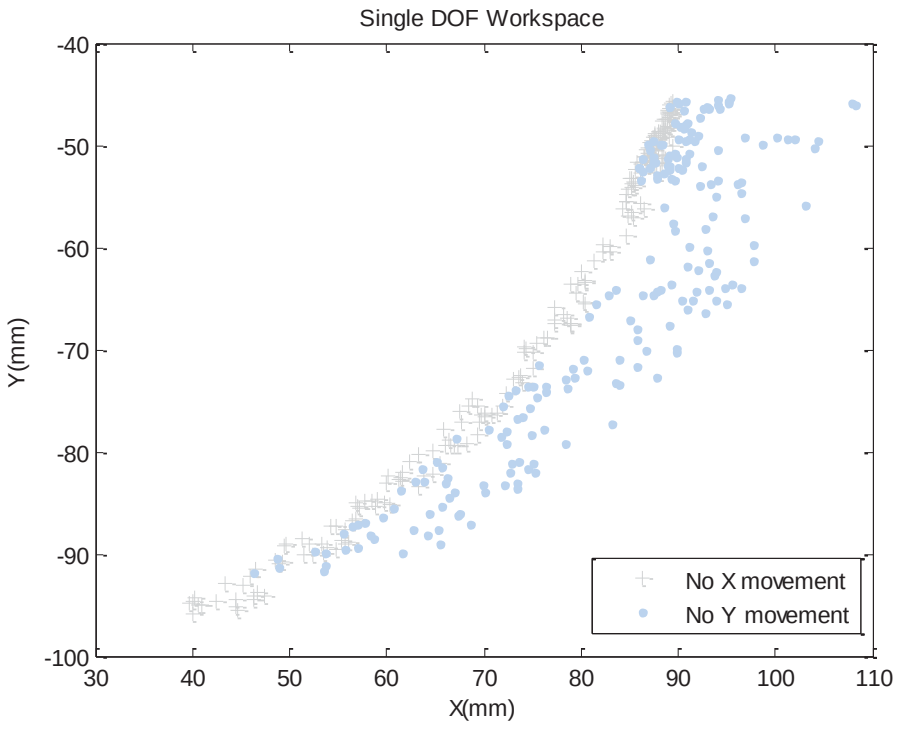

Figure 3-11 Incisor workspace under two extreme configurations

3.2 Mechanism Design Specification

As the device is envisaged to assist the immobile jaw to undertake the exercise which is expected to vary in the protocols to reinforce the therapeutic efficacy, many intrinsic properties of the mandible that may be coupled to the exoskeleton should be taken into account in the course of development in terms of formulating the design specifications, either qualitatively or quantitatively. At the first stage of design, the kinematic representation of the indicated features is only targeted through synthesizing a basic mechanism by referencing given data, as the general requirements regarding device movement are listed in Table 3-1.

Table 3-1 Qualitative specifications of the device

Item	Qualitative Criterion
Trajectory	Trajectories on CP and IP to be followed simultaneously
Range	Largest incisor ROM vertically
Clearance	Within the thickness of the articular disc
Time	Longer than a chewing cycle
Velocity	Smaller than the chewing velocity
Force	A range between minimal force for opening the jaw to maximal force of assisting chewing
Size	No coupling with part of body
Weight	Lightweight

Since the lost motion of the jaw is primarily found to fall within the functional plane, also known as the sagittal plane, the replication of the movement occurring on this plane that is only focused on is intended to be delivered by the mechanism as the fundamental specification that are indispensably ensured. The instantaneous position of the mandible can be exactly defined by those of two points on it according to the rigid-body kinematics, where the IP and CP are selected for hereafter representation since they have been mostly accessed coincidently in the literature. Intuitionistically, the range that the device is designed to offer should be given in accurate value, and can adopt the same variable that is usually used in assessment of the jaw opening distance, i.e. the vertical displacement on the incisor, which is preferable to fit the majority of the population discrepancy with a relative large value. The time and the time-derivatives along the jaw travelling paths will not straightly be outlined to maintain a certain pattern, but they may appear in posing constraints to the optimization function in the mechanism synthesis process so as to accommodate the exercise protocols. Similarly, the force that is essentially required to drive the mandible to move will also place constraints to the optimization in terms of the power efficiency and way of actuation which are of paramount importance for minimization of the device weight.

3.2.1 Mandible Movement Pattern

The movement of the mandible is rather complicated even if only focused on the sagittal plane, in which it is featured of combined sliding along the temporal fossa-eminence surface with rotating during the normal open-close; the jaw movement therefrom used to be simplified to a pure rotation hinged on the TMJ, which has been widely applied in the dental prosthesis as a fixed revolving center [68]. In light of the achievable opening range which was considerably restricted in the vertical distance compared to that obtained under the fixed center opted to be positioned on an average ICR, the pure hinge on the posterior TMJ was considered oversimplified to properly model the jaw movement.

The general model recruiting three variables that capably assesses travelling distance of any point on the jaw facilitates to reveal the inherent pattern which is likely to exist in the way of the correlations in the inside TMJ concerning the jaw movement between each pair. The variables are apparently varying along with the jaw depression in terms of the vertical displacement; and as formulated in Eq. (3-1) of the position for the IP and CP, the ratios of the horizontal displacement versus vertical one, plus the angle versus translation, are herein introduced to define the corresponding relationship during the jaw movement, denoted as $r_t = \frac{dx}{dy}$; $r_a = \frac{dx}{\phi}$ respectively.

Theoretically, with a set of definite values of the correlation, the mandible can be exactly positioned. Usually, the ratios that have been investigated in the literature are given in mean values which are so averaged across the whole trajectory on the IP with respect to that on the CP that only outlining a general mandibular movement trace; but each ratio can be finely valued to spread into the divided phases along the overall travelling distance. Live recordings capable to provide the correlated trajectories under the synchronous time frame are herein preferable to acquire the stepwise ratios. Unfortunately, current resources (AG500 machine) could not support non-invasive tracking of the condylar trace directly in vivo; as an alternative way, two more points on the molars that could define a spatial position of a rigid-body together with the incisor were recruited in trajectory tracking for further computation of the joint variables. In fact, the information of simultaneous trajectories on two points whose positions can be universally expressed in Eq. (3-16) is adequate to solve each instant variable, then through subtraction each corresponding item that is shown in Eq. (3-17) to obtain the ratios in Eq. (3-18).

$$\begin{bmatrix} {}^{O}P_{X1,2} \\ {}^{O}P_{Y1,2} \end{bmatrix} = \begin{bmatrix} dx + L_{P1,2}\cos(\alpha+\phi) \\ dy + L_{P1,2}\sin(\alpha+\phi) \end{bmatrix} \tag{3-16}$$

$$\begin{bmatrix} {}^{O}P_{X2} - {}^{O}P_{X1} \\ {}^{O}P_{Y2} - {}^{O}P_{Y1} \end{bmatrix} = \begin{bmatrix} (L_{P2} - L_{P1})\cos(\alpha+\phi) \\ (L_{P2} - L_{P1})\sin(\alpha+\phi) \end{bmatrix} \tag{3-17}$$

$$\phi = \tan^{-1}\frac{{}^{O}P_{Y2} - {}^{O}P_{Y1}}{{}^{O}P_{X2} - {}^{O}P_{X1}} - \alpha \tag{3-18}$$

Data in the literature that disclosed the rhythm based on each model are also referenced in the form of either giving the corresponding ratios or providing pairs of trajectories on the IP and the CP that were found to appear coincidently with the measurement of the jaw morphology by referencing Eq. (3-12). Since the relationship describing the decomposed magnitudes is barely mentioned in the literature to be present in a unified concept of TMJ rhythm, selected data basically offering ratios of rotation versus slides are found to not entirely conform to the same way those defined in the context. Only couples of articles explicitly indicated the contribution correspondingly from components of the rotation and the translation to the overall movement regarding the incisor opening displacement; so ratios of r_t and r_a are managed to be transformed to adapt those partial apparatuses as provided, for example, the proportions, either of which is attributed to rotation and translation respectively as stated in the literature is formulated in Eq. (3-19).

$$\mathrm{C}_{R/T} = \frac{\mathrm{P}_R}{\mathrm{P}_T} = \frac{L_{IP}\sin(\alpha+\phi)}{dy} = \frac{L_{IP}\sin(\alpha+\phi)}{r_a\phi/r_t} \tag{3-19}$$

Where:

$$\mathrm{P}_R = \frac{L_{IP}\sin(\alpha+\phi)\times 100\%}{r_a\phi/r_t + L_{IP}\sin(\alpha+\phi)};\ \mathrm{P}_T = \frac{r_a\phi/r_t\times 100\%}{r_a\phi/r_t + L_{IP}\sin(\alpha+\phi)}$$

In AG recording trials, the subject was sitting in the chair while maintaining an upright head position, and ordered to relax the jaw and open the mouth naturally as usual till up the limit, as much as in consistency with the motion that was described in the literature. This session was repeated for three times in which GUI for AG data processing coded in the MATLAB was then used to calculate the each ratio based on each selected data group; the mean ratio is then averaged over the values of the corresponding item; note the statistical analysis in terms of standard deviation on the same subject is not carried out. The calculated AG data in the form of r_t and r_a are then reshaped to quantify the relationship in the definition of P_R and P_T, since correlation displayed in this way for the overall trace were already known and could be proof-test the AG recordings data. Then the data in the literature that were not present in numerical format undergo a process of discretization before reconstructed into the specified

TMJ rhythm concept with a speculated assumed morphology of the jaw which was not explicitly given. Then the process is followed by the computation of the relationship in the way adopted in the general jaw movement model.

Table 3-2 Mandible movement rhythms on the sagittal plane

Stage	Phase	T	R	dx	dy	ϕ
Opening	I-i	1	0	[0,3]	[0,3]	0°
	I-ii	0.2-0.5	0.5 mm/°	[3,7]	[3,5]	15°
	II	0.2-0.3	2 mm/°	[7,20]	[0,6]	32°
Close	I	0.2-0.5	2 mm/°	[3,20]	[3,6]	30°
	II	1	--	[0,3]	[0,3]	2°

Table 3-2 lists the stepwise ratios transformed in expression of both definitions that are split into an opening and a closing phase to reveal the likely mandible movement rhythms. According to the resultant ratios, the normal open-close movement also referred to the habitual movement is dominated by mandibular rotation, which accounts for the majority of the jaw opening displacement, in accordance with the discovery from literatures discussed in section 2.1.4.

Each one-way movement can roughly be divided into two phases in terms of the correlation of different value standing for each ratio. Separately, during the opening section, phase I contributes to the starting stage of the jaw opening till the rotational angle to around 15°, in which both rotation and translation are going up linearly on each own, basically approximating to maintain a constant ratio; but can also be finely partitioned with one more ratio that increases proportionally at the very beginning whose duration is too short to neglect. In phase II, the rotation prevails in the depression with an increasing proportion of the instantaneous opening distance, whereas the translation loses the percentage of its contribution at a linearly dropping rate; though the ratio between two values stays approximately invariant as a constant up to the maximal depression, around 2mm/°. The closing section is by and large filled with a symmetrical distribution in terms of each component with respect to the peak point, and can also be depicted by two phases according to the differentiated ratios. The mouth closing movement starts from the maximum opening position with similar values of ratio till phase II; in the very ending part, the rotation hits its bottom value while the translation peaks up to finalize the elevation to occlusion [83]. Figure 3-12 sketches the stepwise relation of vertical displacement of the jaw evaluated on the incisor with respect to rotational and translational movement during depression.

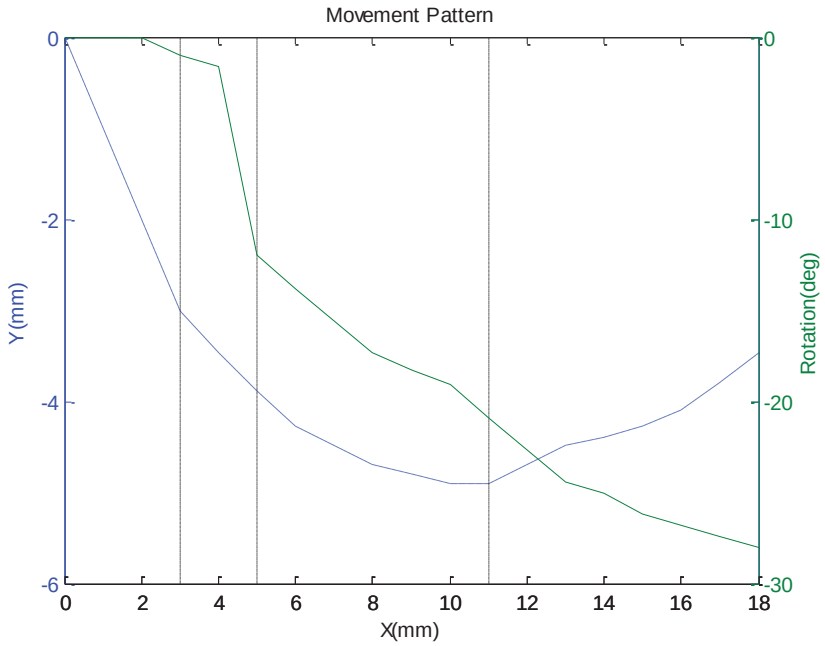

Figure 3-12 Stepwise Phases of the mandible movement on the sagittal plane

The information about the TMJ rhythm in exact values that is chosen here has been obtained on healthy subjects by means of in-vivo 3D tracking systems, which excluded the influence likely coming from the location of different reference points. Subject's mandible size under our trials with AG can be roughly estimated by calculating the distance between the sensors at rest attached on the teeth (incisor and the other two molars) and attached around ears as reference, which were not ensured to be the rest position of condyles. The unloaded jaw is requested to carry out normal movement up to the maximum mouth opening distance during the recording. Measurement in terms of original tracking apparatus and data post-processing was individualized in different researches, but basically concluded with the indirect calculation from trajectories within accessible oral space. Inconsistent discoveries on the contribution of each apparatus appeared occasionally in previous publications, which may result from the inter-individual variation of the movement pattern among subjects or the intra-individual allowance due to joint morphology, exclusive of factors from the methods adopted in movement recording and data computing.

3.2.2 Typical Trajectories

A string of pairs of the IP and CP that assemble each trajectory can be matched together to unveil the inherent rhythm among each pair of apparatuses in a habitual depression-elevation, and they are the other essential component to sketch the continuous movement of the jaw on the sagittal plane an alternatively way. On the contrary, the TMJ pattern is also required to build on one known trajectory to fully define the corresponding counterpart. The trajectories

on the CP and IP either of which respectively is representative of the movement of the jaw and the TMJ, have been given through different in-vivo measurements in the publications; as opposed to the one on the IP which is exposed for easy access, the condyle travelling length inside the TMJ was even individualized by referencing different points given the same action. Only a few of trajectories that have been obtained by three-dimensional tracking instruments are exemplified herein to avoid the interference brought by relative reference points; plus the AG recording data that were adopted to derive the TMJ rhythm can provide the trajectories on the incisor straightly and on the condyle as well indirectly calculated with the trajectories on the molar.

The sagittal trajectories on the condyle generally obtained in normal jaw movement among several studies are illustrated in Figure 3-13, in which the sampling points were linearly linked together from roughly partitioned the original curves. As denoted, all of the condylar trajectories that are derived from the models of floating-axis, kinematic center and the AG recording respectively share a similar one-way length of approximate 20 mm in the anterior-posterior direction and 6 mm in the superior-inferior direction; and those circular-arc shape also fit the description of DLC modeled for neurologic control. Note neither the trajectory is described in an average way by Posselt which is not illustratively meaningful, nor is plotted here the one involving grinding in the mastication.

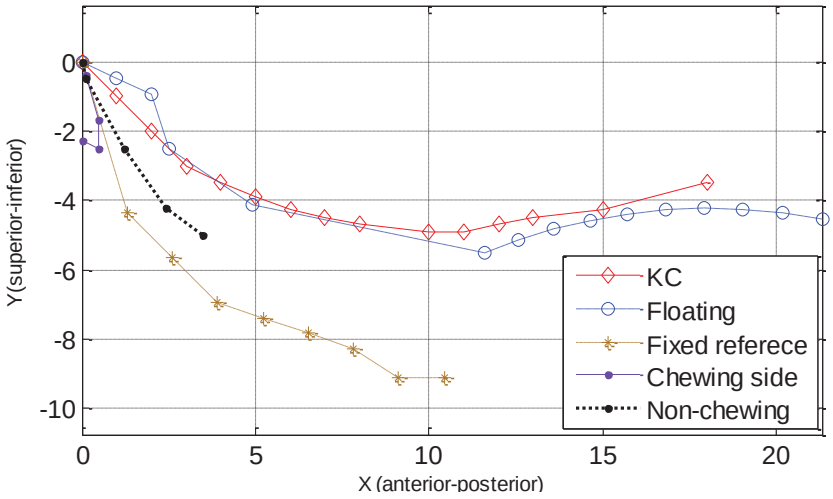

Figure 3-13 Condyle trajectories enumerations

The incisor trajectories acquired accordingly are illustrated in Figure 3-14, which are transitioned to the same starting point to implicitly discard the likely affection from the mandible size. The ones denoted as floating-axis and AG recording match with the corresponding condylar trajectories listed above, while the one is randomly picked among the publications for the comparative purpose. From appearance of the plotted curves, their shape

and each length basically keep a similar pattern, with a vertical 40 mm at least and near 10 mm horizontally.

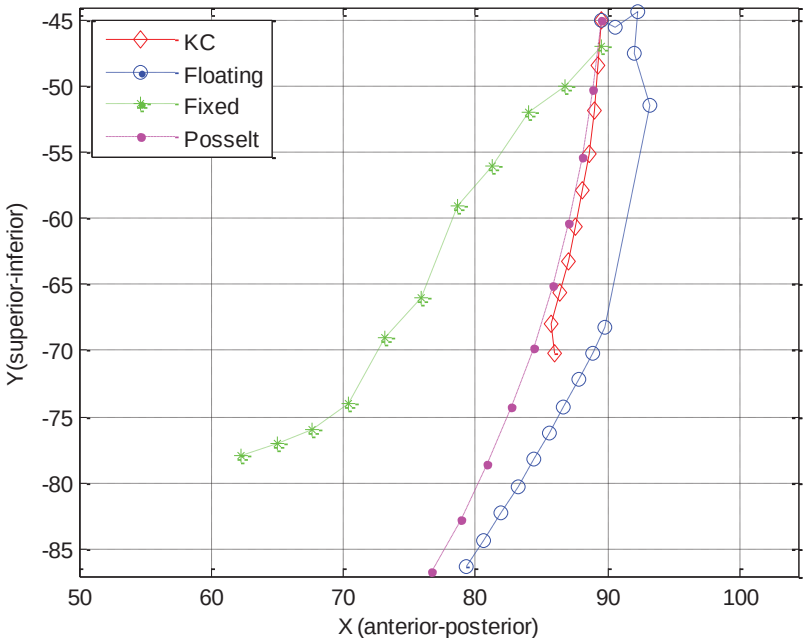

Figure 3-14 Incisor trajectories enumerations

3.2.3 Rigid-body Guidance Movement

Each cycle of mandible open-close may have the ability to exhibit a little variation in the normal unloaded motion if assessed by referencing the incisor, the trajectories however can be found to fall within a small narrow strip on the sagittal plane, as the live trajectories that were recorded on the incisor plotted in Figure 3-5. In fact, during a single cycle, masticatory muscles are only recruited to carry out a definite jaw motion, which is regulated by the neurologic system for specific purpose, behaving to possess one DOF featured by a pair of the trajectories on two points according to the analysis. From the therapeutic perspective, the exercise is preferable to deliver the periodical stretch training in a certain fixed manner for a relative long duration as one protocol before switching to another in order to establish the control in the neuromuscular level or maintain the joint ROM in the musculoskeletal level, instead of keeping altering the pattern in one motion cycle.

Considering the device is expected to drive the mandible repetitively to follow the same trajectories as those at enabled state, a pair of trajectories that pilots the jaw to move along a series of exact position is specified as the first paramount requirement to replicate the jaw movement orientated to a single exercise session by the exoskeleton; and both trajectories on the IP and CP that fall into their own family of trajectories are selected to construct a typical pair for each individual usage whose relative correlation is established based on the inherent

motion rhythm. A vast range of training choices in terms of the guiding traces can be achieved by setting up adjustable links that are broadly applicable in the wearable exoskeleton to adapt the population.

The value of TMJ rhythm varying among separate phases can be assumed piecewise linear upon those sections. Based on a definite trajectory on the condyle that is illustrated in pair with the incisal counterpart upon the same trial, connecting lines signifying each instantaneous orientation of the jaw can be derived to match the coupled trajectories without concerning the jaw size, as seen a typical pair of trajectories illustrated in Figure 3-15, along with the locational correlation between pairs of IPs and CPs shown in Figure 3-16.

Therefore, from the perspective of the planar kinematics, the crippled jaw will be forced to move along a rigid-body guidance shaped by a specified pair of trajectories when subject to the exoskeletal device; conversely the selected way of jaw motion will also be involved in mechanism synthesis as a specification for proximal reproduction.

One point worth mentioning regarding the essence of the human-machine interaction (HMI) is that the jaw can be piloted through the other way of guidance, which known as the path guidance, only engages one incisor trajectory. Different from the rigid-body guidance, one-point contact between the jaw and the device instantaneously places inadequate constraints in attempt of defining the jaw position by a mechanism, which leads to a seemingly free revolving around the point on the incisal trajectory that the mandible is passing by.

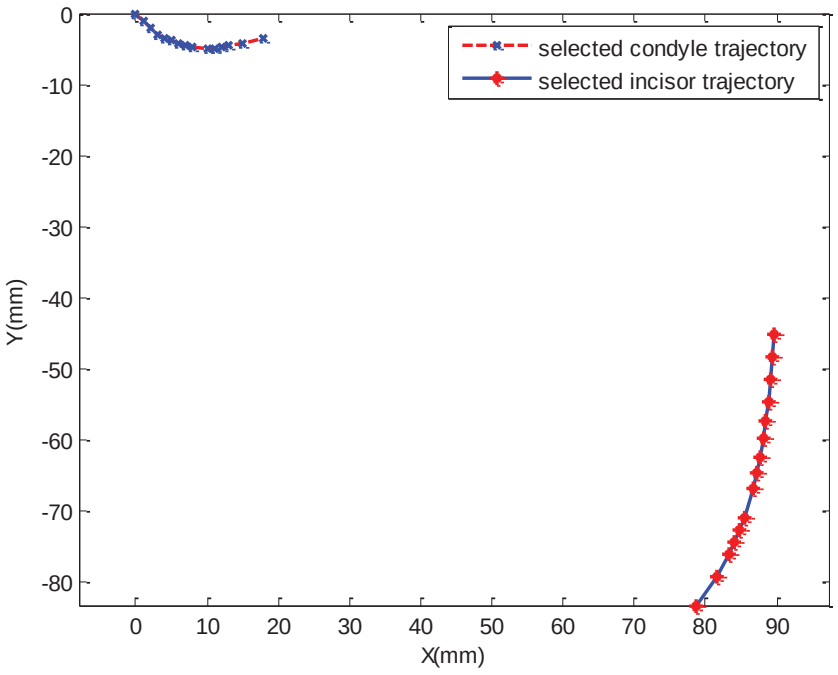

Figure 3-15 A typical pair of synchronous trajectories on the CP and IP

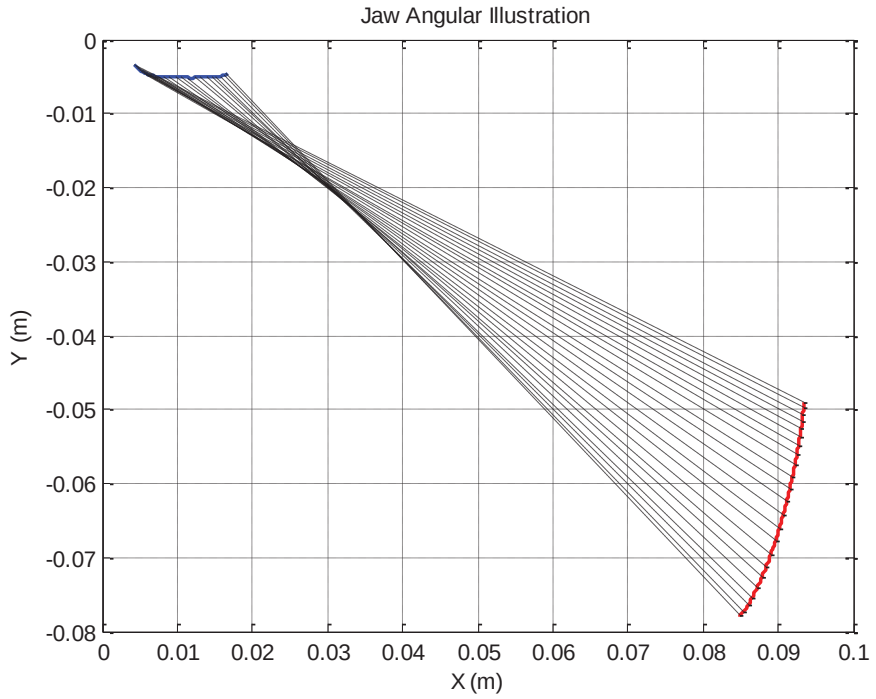

Figure 3-16 Locational Correlation between IP and CP

3.2.4 Specifications in System Realization

Though the fundamental requirement specially referring to a typical pair of trajectories is illustrative provided to fulfill the reproduction of the mandibular movement, relevant kinematic specifications are given explicatively in details amid the therapeutic requirement. Clinical studies usually apply the vertical opening distance of the mouth evaluated on the incisor to define the baseline of the limited jaw movement, which also varies in the specified value of 20 mm to 35 mm in the literature. As the minimal distance to maintain the functionality of the mouth, 20 mm can be set as the least that should be delivered by the device presenting the trajectories on the track. Continuous range of ROM is also expected to be preferably offered instead of the one compromised into stepwise; a gradual increment of the ROM relieves users from sudden discomfort which may occur in the step-by-step varying ROM. The acceptable tolerance which may be present in the device refers to the maximum discrepancy away from the specifications in speaking of each quantified item, particularly to the trajectory inconsistency on the condyle, to avoid the unnatural compression to the articular disc of a thickness of 2mm.

The time of and the time-derivatives along the selected trajectories should be able to be controlled according to the rehabilitation regimes or protocols, which is reflected to the cycle time and velocity of the device to drive the jaw move. As distinguished from normal opening motion, exercise in the beginning may move in low velocity and takes much time on one cycle

because resistance is required to overcome and muscles needs stretching. To avoid any injury in the exercise, time spending in one cycle is specified more than 2s. Since fast chewing cycle consumes around 0.5 second, which gives an estimate velocity for 25mm opening around 100mm/s.

Additionally, the forces applied to hold the jaw and lift the jaw to a certain distance varies with inter-individually amid various circumstances. According to the literature, the minimal force to open the jaw is rather small as being less than 5 N, but adequate to overcome passive muscle force. A much larger resistance that may be accompanied of jaw-opening amid ankylosis TMJ with impedance exercise as one part will allow the force that the mechanism can apply to the jaw will be specified within a range between 10N-30N. Besides, other basic requirements as listed in Table 3-3 include that the device must be lightweight to ease users so that the exercise can be executed without being attached to one locality, that the device must be adjustable to suit the various sizes of jaw and head, and that the device should be able to perform different training protocols chosen by the operator.

Table 3-3 Mechanism design specifications

Items	**Specifications**	**Literature**
Trajectory	Selected typical pair of trajectories simultaneously	--
ROM of incisor	Usually 0mm-20mm	50mm maximally
ROM of condyle	20mm	Vertical 25 mm
	6mm	Horizontal 8 mm
Rotation angle	27°	27°
Tolerance	2.5 mm	--
Force	Minimal 5N; maximal 150N	28N maximally
	General range: 10-40N	10N
Time	>2s a cycle	0.77s
Velocity	< 100mm/s	--
Total weight	< 1000g	--
Motion Plan	Periodicity correspondence	--

3.3 Possible Design Approach

The entire exoskeleton can be partitioned into three parts from the perspective of the mechanism composition, i.e. the actuation, the body, and the attachment, the middle of which is of our concern herein to fulfill the trajectory reproduction of the kinematic specifications. This one-DOF movement can be conveyed by different mechanism solutions, which are grouped into the one-DOF mechanism and kinematically-redundant manipulator in

terms of number of the DOF, as discussed below in the aspects of the structural advantage and corresponding complexity in the control system.

1. Four-bar linkage

The four-bar linkage could be the simplest closed-loop linkage but widely used in a great variety of machines. Links of different length are combined to create different motion formats, so does the selection amid links to be the crank and the ground. Coupler point which is able to produce sixth-order algebraic curves can only approximate the prescribed trajectories, instead of precisely tracing out, which would obviously be engaged to generate replicating a curve through configuration of a linkage in the wake of a rigid-body guidance problem. Only one actuator that drives the crank in the four-bar linkage simplifies the controlling of the whole device, whereas the disadvantage exists in the range of incisor displacement delivered by a full circle of the crank that is hardly adjustable in line with the one generated partially.

2. Cam-linkage mechanism

A cam system is also able to offer the periodical jaw movement of one DOF regarding the given trace transported by the cam follower, which specifically refers to the jaw in this circumstance travelling along the profile. The cam mechanism advances in precise duplication of a curve in the plane or in space, whereas unalterable profile cripples a vast applicability to fit the population. But the way the cam drives the follower is a point contact, which casts only one path trajectory on the jaw to be replicated by the guiding slot, as the path guidance discussed before. The profile is uniquely features of being capable to regulate the control parameters, such as velocity and accelerations, which is also at a cost of compromised variability of the training protocols.

3. Auxiliary joint

The misalignment that is likely to exist between the actual ICR and the forced ICR subject to device movement will cause excessive force and stress on the human-machine interface and the internal injury in the joint. An approach to compensate this offset which is hardly measurable in practice is the addition of an extra joint without actuation, under-actuated joint, which is granted a priority to other solutions; on the downside, the under-actuated DOF will complicate control to the mechanism.

4. Robotic manipulator

A multi-DOF manipulator, in either serial or parallel form, drives the jaw attached on its end-effector. The flexibility and the workspace of the jaw movement can be easily achieved; but multi-DOF borne structure could incur more weight from the mechanism itself and the accessary parts and lower the wearability of device.

3.4 Dimensional Synthesis in Motion Generation

The four-bar linkage intrinsically provides one-DOF repetitive movement, which is usually embodied in a form of a closed-loop curve on a coupler point only if the crank is allowed to do complete rotations. The specified trajectories standing for travelling paths of the condyle and the incisor that are discretized into points can be conveyed by pieces of the curve or the entire one generated by two points on the coupler, which are spread to the separated opening and closing phases or a whole cycle of the jaw movement on the sagittal plane, respectively. The opening and closing phases are selected to share the same piece of trajectory that represents the jaw movement offered by the device, instead of the complete cycle of curve or a pair corresponding to each phase, as listed here are some justifications as follows.

1) Evaluated from the plotted trajectories which have been obtained from the literature and the live recordings, the clearance between the trajectories of opening and closing phases is rather small, maximally measured to be less than 2 mm, though which is theoretically able to be transported by the entire curve.

2) The discrepancy generated in the course of the approximating mechanism might get increasingly widened along with the growth of the number of the sampling points, which inevitably takes place in combining both phases together.

3) The points spreading on the opening and closing phases arranged in sequence are hardly halved for each one to generate the same mechanism correspondingly.

4) Practically speaking, the trajectory conveyed by a partial curve facilitates the adaptability of the device to a vast scope of application with easy operation, since the affection to the other segments amid configuring adjustable links can be neglected in contrast to the one to be carried by an entire curve which may hardly to fit both phases properly.

3.4.1 Objective Function of Motion Generation

As the simplest means, the dimension of a four-bar linkage can be roughly derived by choosing the resemblance in atlas through visual comparison with the prescribed trajectory, and followed by positioning the linkage relative to the reference, which if applicable refers to the mandible here. Approximating a pair of trajectories by atlas could not secure the choice with a required precision. Numeric solution that imposes a group of optimization objectives upon the

mechanism is preferable undertaken in the course of dimensional synthesis, the result of which will inevitably affect some kinematic parameters such as the velocity and the efficiency of the mechanism which could be utilized to impose the constraints in the course of synthesis the mechanism.

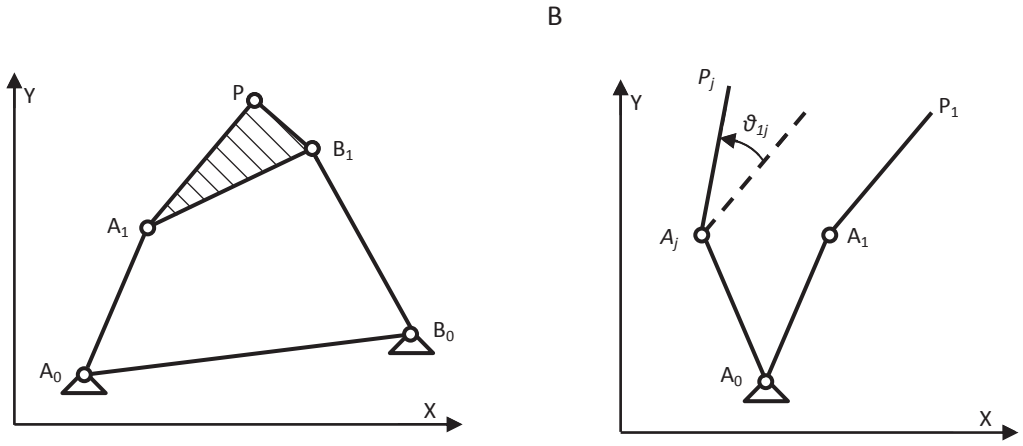

Figure 3-17 Dyad illustration (A) original position (B) other positions

$$P_j - A_j = Q(P_1 - A_1) \tag{3-20}$$

$$A_j = P_j + Q(P_1 - A_1) \tag{3-21}$$

Where, $\mathrm{Q} = \begin{bmatrix} \cos\theta_{1j} & -\sin\theta_{1j} \\ \sin\theta_{1j} & \cos\theta_{1j} \end{bmatrix}$angle θ_{1j} around A from the initial position.

The four-bar linkage as shown in Figure 3-17 (A) can be decomposed into two groups of dyads, denoted as A_0A_1 and B_0B_1, which sharing the identical composition can be considered to have each coupling point go through a string of the given locus. The left-side dyad A_0A_1 that is picked out as shown in Figure 3-17 (B) represents the same formulation of the structural error at both sides of dyad, the feasible outcomes from which can be combined to construct into the four-bar linkage. The relationship of the coupling points amid prescribed positions in a dyad yields an Eq. with substitution of values in the form of the vector.

In Figure 3-17 (B) the coupler point is generally denoted as P (note to differentiate the ones used in the jaw CP and IP), and P_j is denoted as the coordinates of the jth position, all of which spreading over the specified path are given in the specification and expected to be met by the coupler of four-bar linkage; A_j is the jth position of the A correspondingly; the rotation of the coupler can be written in Eq. (3-20) which is converted to express floating crank tip with respect to the prescribed coupler points in Eq. (3-21).The distance between each crank floating tip A_j over all given coupler points and the stationary tip representing the length of the crank, should maintain constant in Eq. (3-22).

$$\left\|A_j - A_0\right\| = \|A_1 - A_0\| \tag{3-22}$$
$$j = 2,3,\cdots,m$$

Therefore the discrepancy between the subsequent crank length and of the initial one expressed in the form of least-square error in Eq. (3-23), formulates the structural error, which is expected to be minimized over all prescribed positions, as written in Eq. (3-24).

$$\begin{aligned} f_j(x) &= \left\|A_j - A_0\right\| - \|A_1 - A_0\| \\ &= \left(A_j - A_0\right)^T \cdot \left(A_j - A_0\right) - (A_1 - A_0)^T \cdot (A_1 - A_0) \end{aligned} \tag{3-23}$$

$$\min F(x) = \sum_{j=2}^{m} f_j^2(x) \tag{3-24}$$

The coordinate of stationary point A_0 in the dyad is denoted as $[x_{A0}, y_{A0}]$, and the coordinate of floating tip A_1 at the initial position is $[x_{A1}, y_{A1}]$; the coordinate of A_0 and A_1 are the unknowns in all equations, as expressed to be $x = [x_1, x_2, x_3, x_4]^T = [x_{A0}, y_{A0}, x_{A1}, y_{A1}]^T$.Substitute A_j of the form of Eq. (3-21) into Eq. (3-23), the length error can be written in Eq. (3-25) with respect to the x ($[x_1, x_2, x_3, x_4]^T$).

$$\begin{aligned} f_j(x) &= M_{j1}x_1x_3 + M_{j2}x_1x_4 + M_{j3}x_2x_3 + M_{j4}x_2x_4 \\ &+M_{j5}x_1 + M_{j6}x_2 + M_{j7}x_3 + M_{j8}x_4 + M_{j9} \end{aligned} \tag{3-25}$$

Where all the coefficients are denoted as follows:

$$\begin{cases} M_{j1} = M_{j4} = 1 - \cos\theta_{1j} \\ M_{j2} = -M_{j3} = \sin\theta_{1j} \\ M_{j5} = x_{P1}\cos\theta_{1j} - y_{P1}\sin\theta_{1j} - x_{Pj} \\ M_{j6} = x_{P1}\sin\theta_{1j} + y_{P1}\cos\theta_{1j} - y_{Pj} \\ M_{j7} = -M_{j5}\cos\theta_{1j} - M_{j6}\sin\theta_{1j} \\ M_{j8} = M_{j5}\sin\theta_{1j} - M_{j6}\cos\theta_{1j} \\ M_{j9} = \left({M_{j5}}^2 + {M_{j6}}^2\right)/2 \end{cases}$$

The $\left[x_{Pj}, y_{Pj}\right]$ and θ_{1j} as known parameters are denoted as the coordinates of the coupler in a natural coordinate system and each corresponding rotated angle with respect to the initial position, respectively provided by the specification by referring to Figure 3-17 (B). The mandible for training is placed to contact with the linkage exactly on the coupler to do the rigid-body guidance movement; the coordinates of the points in the condyle and incisor trajectories are herein given in the relative frame that 15 pairs of the points are linked linearly

on each own track and incremental rotation of each position relative to the initial one is given after calculation as well, and no other interpolation is provided upon the existing data.

To adapt the synthesis process, the CP at the rest position establishes the origin of the coordinate frame for this application, and the size of the jaw for initializing the IP coordinates applies the one referred in section, whose details can be acquired in great precision. Accordingly the initial position of the incisor can be written in the format of $[89.51, -45.01]$ with respect to the condyle of $[0,0]$.

The coordinates of the condyle and incisor that are travelling along each trajectory are respectively denoted as $[CP\_x_j, CP\_y_j]$ and $[IP\_x_j, IP\_y_j]$ at each position $[j]$, sequentially starting from the closed state of the jaw. The IP coordinates are invoked in the optimization equations of Eq. (3-25) to replace $[x_{Pj}, y_{Pj}]$; and the incremental rotation angles at each step of which is denoted as $q_{j1} = q_j - q_1$, calculated from the $q_j = \frac{IP\_y_j - CP\_y_j}{IP\_x_j - CP\_x_j}$ and $q_1 = \frac{IP\_y_1 - CP\_y_1}{IP\_x_1 - CP\_x_1}$ are invoked to substitute all of the θ_{1j}.

Typical performances of the mechanism in terms of the mechanical system rely on its kinematic parameters, which form the constraints directly or indirectly with respect to the synthesis variables. The constraints the mechanism is subject to encircle a set of ranges for each variable in seeking a desirable combination that satisfies the requirements, and are incorporated into the process of the minimization of the objective function in two ways, depending on adopting the form of penalty function attached behind. The constraints are set up in aspects of kinematics and the process of synthesis that specifically embodies on the application based on the current synthesis model, among them the commonly referred ones are listed up in the aspects of the construction.

1) The length of each link L_{crank}, $L_{coupler}$ is restricted within a range of $[5,20]$ for the crank, and $[5,60]$ for the other, and the relation in terms of the length $L_{coupler} > L_{crank}$;
2) Rotational angle of the crank α over all prescribed points is limited within $[0,180]$;
3) θ_{1j} is arranged in sequence of the points concerning j;
4) Structural error $|\varepsilon|$ is specified within a range.

All of the k constraints are arranged in the form of inequality, as $c_i(x_1, x_2, x_3, x_4) \leq 0, i = 1,2,\cdots,k$. Therefore, the complete problem can be formulated by tailing above constraints into the structural error in Eq. (3-26)

$$\min F(x) = \sum_{j=2}^{m} f_j^2(x) + \sum_{i=1}^{k} c_j(x) \tag{3-26}$$

There are four unknowns in the Eq. (3-25) of each position, all of which compose of amount of *(n-1)* equations over the given *n* positions. without consideration of any technical constraints in the four-bar linkage, the number of given points for the exact synthesis should be less than five, more than the number of which the problem turns to approximate synthesis.

Instead of using the derivatives of the completed function that can signify a searching direction in each step of iteration to find the local optima, the nonlinear LSQ equations are optimized by the built-in function in MATLAB. Newton algorithm based iteration is configured in the process of the optimization, which is too sensitive to the initial value to occasionally drive equations falling into a local optimum. As to the precise synthesis, four equations that are formed with five points illustrative of both trajectories on condyle and incisor can be theoretically solvable subject to four unknowns with little error, so the original LSQ function can be simplified to the minimization of each Eq., all of which compose of multi-objective functions, as written in Eq. (3-27). Still, it is also equivalent to minimize the worst-case among multivariable functions in the circumstance of precise synthesis, as expressed in Eq. (3-28), without avoiding of starting at an initial estimate. The solving process takes advantage of built-in functions in MATLAB while being subject to the constraints in the form of equality and inequality. Regarding the approximate synthesis, the optimization is simply undertaken by going through the solving process of LSQ function in MATLAB in order to find the global minimum; any conversion of the objective function is avoided here since local optima could be brought into the multivariable minimization, in which the error could not be globally satisfied.

$$\min F(x) = \min\{[|f_1(x)|, |f_2(x)|, \cdots |f_n(x)|]^T\} \tag{3-27}$$

$$\min F(x) = \min\left\{\max\{[|f_1(x)|, |f_2(x)|, \cdots |f_n(x)|]^T\}\right\} \tag{3-28}$$

Suppose $F(x)$ stands its globally minimum point, which is the necessary conditions of the LSQ objective function, i.e., the *Jacobian* equals to zero, which is written in Eq. (3-29).

$$\frac{\partial F}{\partial x} = 0 \tag{3-29}$$

Namely,
$$\begin{aligned}
&\textstyle\sum_{j=2}^{m} f_{j-1}\left(M_{j1}x_3 + M_{j2}x_4 + M_{j5}\right) = 0\\
&\textstyle\sum_{j=2}^{m} f_{j-1}\left(M_{j3}x_3 + M_{j4}x_4 + M_{j6}\right) = 0\\
&\textstyle\sum_{j=2}^{m} f_{j-1}\left(M_{j1}x_1 + M_{j3}x_2 + M_{j7}\right) = 0\\
&\textstyle\sum_{j=2}^{m} f_{j-1}\left(M_{j2}x_1 + M_{j4}x_2 + M_{j8}\right) = 0
\end{aligned}$$

3.4.2 Consideration in the Application

For general synthesis of the four-bar linkage, coordinates of dyads that are derived from the known trajectory can construct the mechanism to pass by the prescribed points. The final linkage amid dyad combination subject to generic constraints is intended to ensure the applicability to this surrounding; the torque generated by the linkage is preferably pointed as nearly as to the direction during the actual movement, and it can be interpreted into the requirement on the locus of the ICR in company with the movement, which is desirable to be on the same side of the mandibular one during the linkage operation. Conflict inspection is conducted amid the implementation of these constraints in terms of each variable before going into the objective function.

The mandible with the conceiving is bonded to the coupler, behaving as a part, so the centrode of the jaw is actually the one of the coupler. The centrode of the mandible has been confirmed to be constantly varying, rather than staying invariant during its movement. Inherited with denotations and specifications from Figure 3-17, Figure 3-18 illustrates the centrode of the coupler in linkage, i.e. the instantaneous center of the coupler, which can be derived from intersection of instantaneous A_0A_j and B_0B_j, denoted as E, and E_j representing its jth position correspondingly.

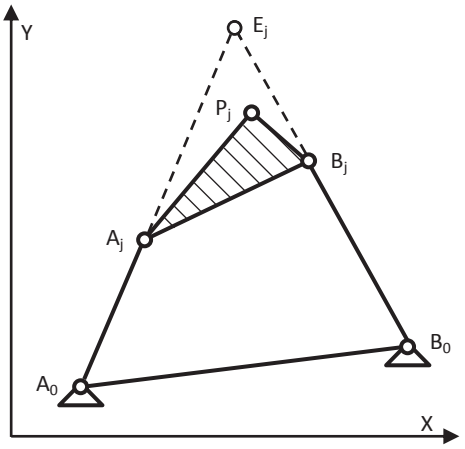

Figure 3-18 The ICR of the coupler

Providing with each given location of coupler coordinates, i.e., A_j and B_j, the coordinates of the centroid E_j can be obtained by solving Eq. (3-30) to derive the locus of the centroid of the coupler, given in Eq. (3-31).

$$\begin{cases} y_E = k_A(x_E - x_{A0}) + y_{A0} \\ y_E = k_B(x_E - x_{B0}) + y_{B0} \end{cases} \tag{3-30}$$

Where, $k_A = \frac{y_{Aj} - y_{A0}}{x_{Aj} - x_{A0}}$; $k_{Bj} = \frac{y_{Bj} - y_{B0}}{x_{Bj} - x_{B0}}$

$$\begin{cases} x_E = \dfrac{k_A x_{A0} - k_B x_{B0} + y_{B0} - y_{A0}}{k_A - k_B} \\ y_E = \dfrac{k_A k_B (x_{A0} - x_{B0}) + y_{B0} - y_{A0}}{k_A - k_B} \end{cases} \tag{3-31}$$

Instead of a definite curve set as the constraint traced by the ICR, the centrode is restricted into a strip of area to form a constraint of creating the linkage, away from the area TMJ would not emerge, since the moment actually generated by the muscles is much larger than that on the rotational hinge. Some inconsistency in the literature is found in terms of the locus of the ICR of the mandible, but it is agreed that the ICR has little chance to reside on the condyle, which has been stated by several live-recording based measurement of the mandibular movement. The ICR locus as mentioned showed up around the area of the mandibular ramus, in the shape of band virtually circling them up. It is difficult to quantify the actual band size since most studies conveyed only qualitative cognition.

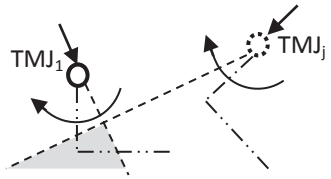

Figure 3-19 General area of the ICR

The lower and upper bound for the coordinates of ICR locus is defined in two ranges to restrict the movement that is applicable in this coordinate system, corresponding to the area with grey shading shown in Figure 3-19, and the far left one as expressed in Eq. (3-32).

$$\begin{cases} x_{LB} \le x_E \le x_{UP} \\ y_{LB} \le y_E \le y_{UB} \end{cases} \tag{3-32}$$

Where,

$\begin{cases} x_{LB} = -20, x_{UB} = 40 \\ y_{LB} = -40, x_{UB} = -60 \end{cases}$ and $\begin{cases} x_{LB} = -100, x_{UB} = 20 \\ y_{LB} = -40, x_{UB} = -60 \end{cases}$ respectively.

3.4.3 Results and Comparisons

With the objective coordinates and the constraints given above, the coordinates of the hinges in the four-bar linkage are derived, as listed in Table 3-4. The length of the synthesized linkage is calculated in Eq. (3-33), for the crank, follower, ground, coupler, and the jaw attaching point, respectively.

Table 3-4 Result of precise synthesis

	Fixed point	Floating point
1st group	A_0 (13.18, -3.60)	A_1 (4.05, -7.99)
2nd group	B_0 (-13.58, -42)	B_1 (2.33, -40.45)

$$\begin{aligned}
\overrightarrow{A_0A_1} &= \overrightarrow{A_1} - \overrightarrow{A_0} \\
\overrightarrow{B_0B_1} &= \overrightarrow{B_1} - \overrightarrow{B_0} \\
\overrightarrow{A_0B_0} &= \overrightarrow{B_0} - \overrightarrow{A_0} \\
\overrightarrow{A_1B_1} &= \overrightarrow{B_1} - \overrightarrow{A_1} \\
\overrightarrow{A_1P_1} &= \overrightarrow{P_1} - \overrightarrow{A_1}
\end{aligned} \tag{3-33}$$

The linkage is then schematically drawn in MATLAB with the given coordinates, as shown in Figure 3-20. The range of the crank rotation based on the range of motion preset by the coordinates of the incisor, can be calculated as about 120°, with respect to the initial IP location. The ICR of the coupler is also computed based on this set of dimension, as incrementally sketched in Figure 3-21, where the rotational range of the crank is assigned to 30°, starting from the given origin. The intersection between the extension of crank and follower depicts a curve of ICR of the coupler, shown in red line.

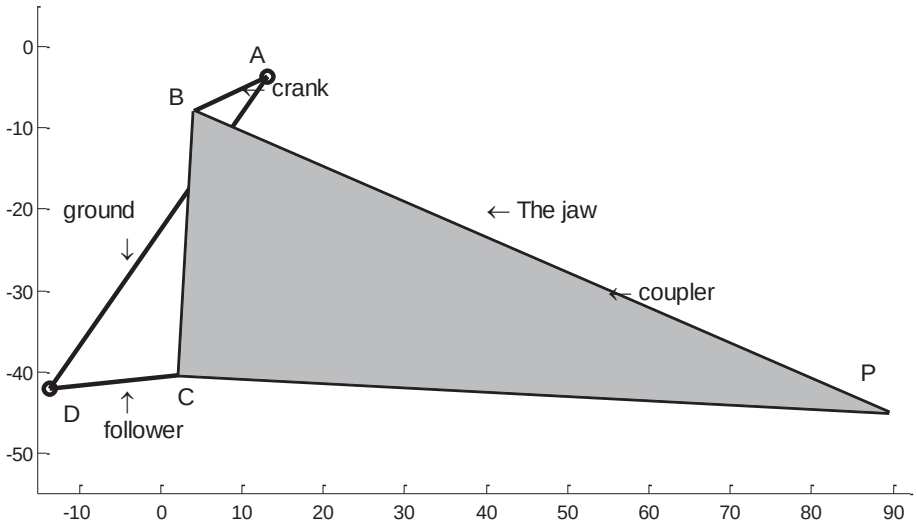

Figure 3-20 Schematic diagram of the linkage

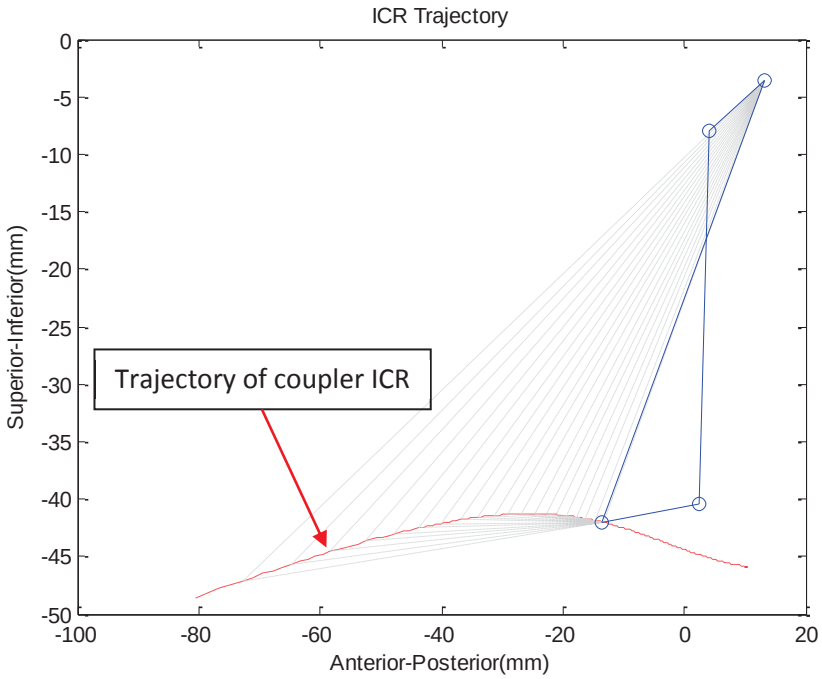

Figure 3-21 ICR trajectory of current four-bar linkage

3.5 Kinematic Simulation of the Mechanism

The mechanism as the skeleton of the device is oriented to the medical treatment which interacts with people of jaw size diversity; therefore the adaptability to individual relies on the adjustability of the mechanism, which is intended to be implemented on the adjustable dimension of some links as conceived.

3.5.1 Trajectories Comparison and Verification

For fast verification of conformation of the linkage design rules, as well as the synthesis results in terms of the trajectory replication, the four-bar linkage is built up in the SimMechanics to obtain the trajectories of some critical points that represents the IP and CP in the specification, as diagramed in Figure 3-22. The mechanism would not be executed into movement if rules in composition of the four-bar linkage were not satisfied, as reflected in the simulation in SimMechanics. Each link is configured in the same coordinate system and assigned with the synthesized coordinates to maintain the consistency with the synthesis result, as shown in Figure 3-23.

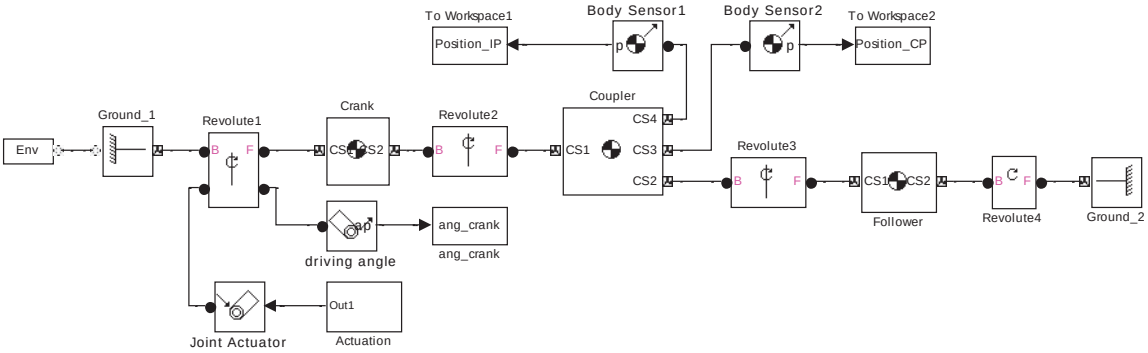

Figure 3-22 Comparison between generated trajectories

A

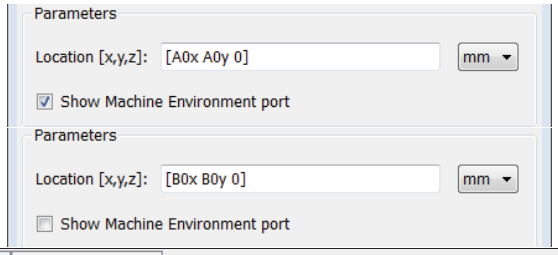

B

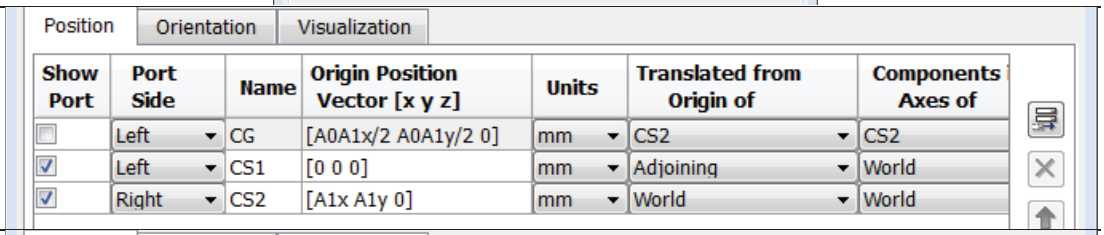

C

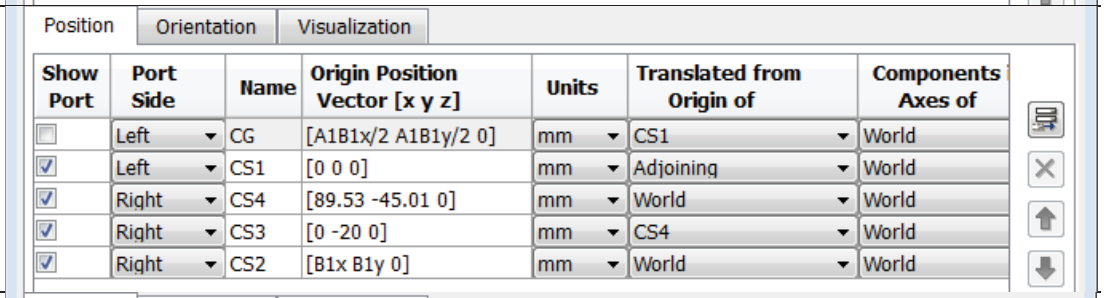

D

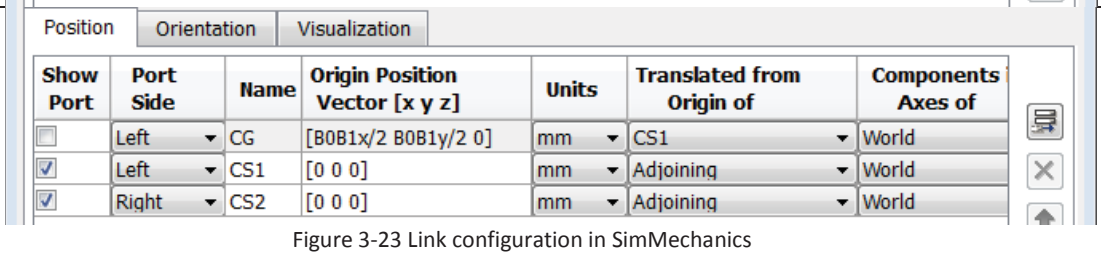

Figure 3-23 Link configuration in SimMechanics

The IP and CP trajectories are then evaluated based on several configurations of the link size in the model as listed in Table 3-5. Blanks in the table mean the default dimension applied, and configuration of No.2 applies the default combination. Figure 3-24 and Figure 3-25 illustrate the trajectories on the IP and CP under different combinations of link size, respectively.

Table 3-5 Simulation scenarios for adjustable linkage

Trial	Coupler	Follower	Ground	Trial	Coupler	Follower	Ground
#1	-2			#3	+2		
#4		+2		#5		+4	
#6		+4	-4	#7		+4	+4

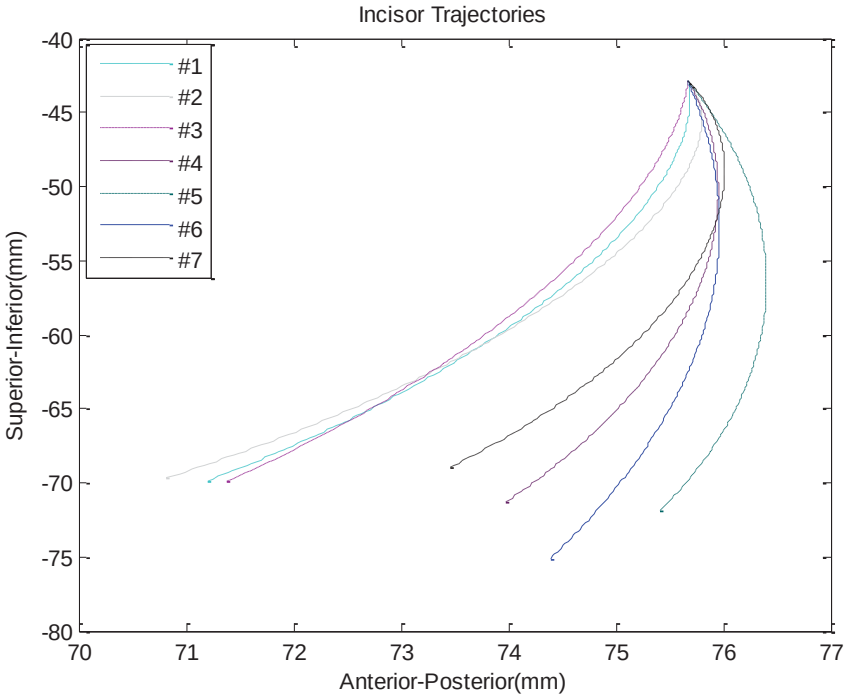

Figure 3-24 Incisor trajectories

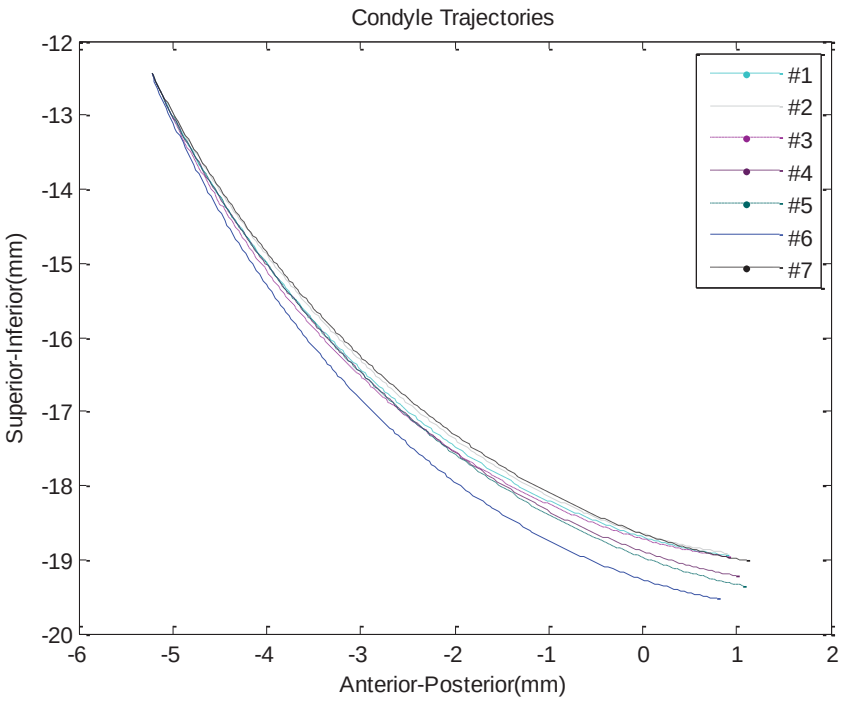

Figure 3-25 Condyle trajectories

The diversity of the range and the slope of the trajectories as generated from different combinations of the link dimension suggest the adjustable linkage has the ability to adapt a family of trajectories reflective of the individualities in terms of the jaw size and motion difference.

3.5.2 Interactive GUI for Linkage Adjustment

The typical pair of the trajectories can be considered as a base, adhering to which the families are derived from within a small variation. An interactive GUI that is created in MATLAB and illustrated in Figure 3-26 facilitates users to adjust the active dimension of some links to achieve the suitable one set. Through tuning slider within a preset range, the trajectories of any point on the coupler can be interactively produced, together the entire linkage diagram in contrast of the one with original size. The adjustability of the linkage via this GUI is reflected on the slope of the curve, the dimension of the curve, as well as the location of the point to critically attach on the jaw.

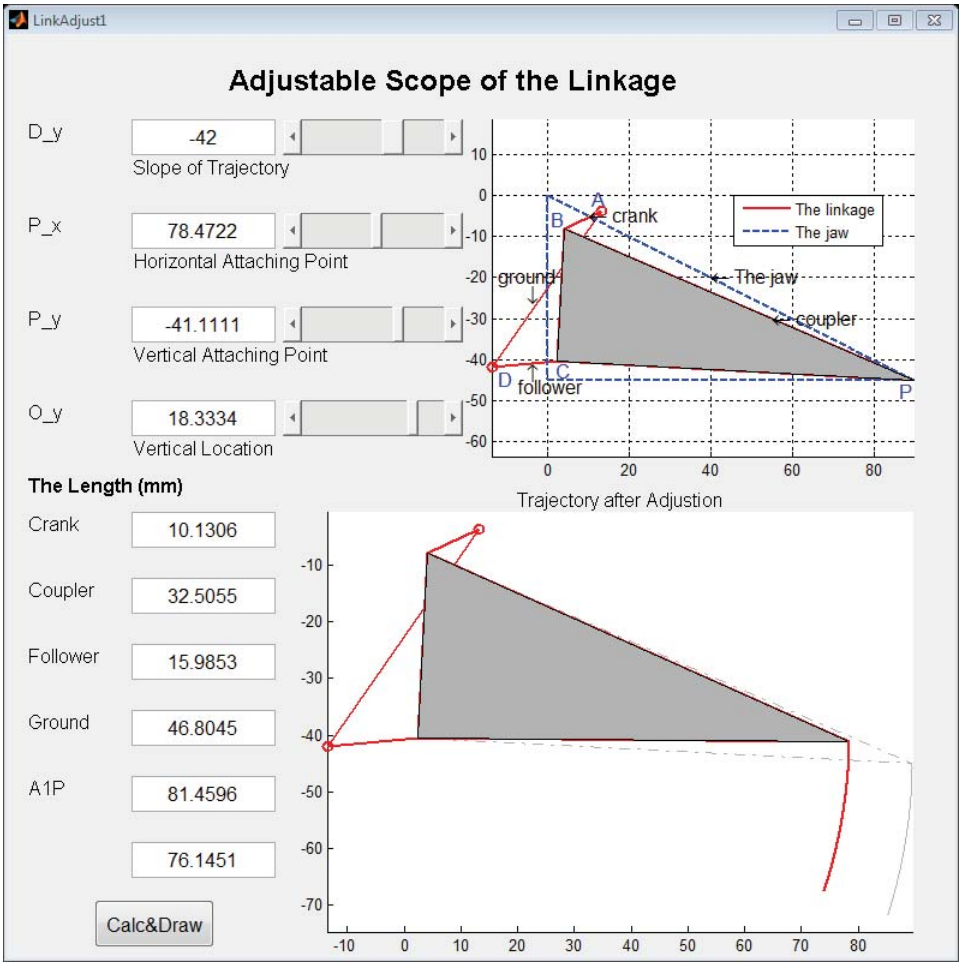

Figure 3-26 GUI for adjusting size of the links in the four-bar linkage

3.6 Chapter Summary

The fundamental structure of the jaw exoskeleton has been synthesized in this chapter, as the mechanism to underlie the integral device design. For the jaw exoskeleton which is highly required in replication of jaw movement, the kinematics of the mandibular system has been thoroughly investigated based on a generic 3-DOF model on the sagittal plane. The inconsistency of the state-of-the-art of the mandibular kinematics lies in establishment of a reasonable model, which has not been considered in this circumstance. Instead, the trajectories of concerned points that are representative of the movement have been specified to be traced by the conceived device, from which, the investigation of the model has been turned into the one oriented to the trajectory.

With consideration of limited operation space around the head, simple mechanism would have the priority in selection, to on the one hand avoid too much weight that may affect the portability, on the other hand, to ease the unnecessary DOF with small ROM. The adjustable the four-bar linkage meanwhile makes up for the requirement to adapt the diversity of the individual. Amid the process the traditional linkage synthesis, the specialized constraint has been imposed on the objective function of global minimization of structural error, which has also lead to a set of acceptable result.

The generated linkage has been evaluated in terms of the kinematics in verification of the design rules and also the trajectory tracking performance. Several configurations of the active link size have been tested in a structural SimMechanics model to illustrate the adjustability and adaptability of the mechanism; and also an interactive GUI program has been developed in the MATLAB to allow users to tune the linkage as reference on their own.

Chapter 4: Mechatronic Construction of Jaw Exoskeleton

The concept of the jaw exoskeleton could not be verified concerning the functionality as claimed if it never leaves the drawing board and has been implemented. The integrated Mechatronic system of the device consists of three subsystems by hardware implementation, i.e. the mechanical, the electronic and the sensory subsystem, which will be fully described in this chapter.

For the mechanical construction, it conforms to the mechanism derived from design specifications, but the delicacy of the parts relies on the practice of the designer and the manufacture, which could impose passive influence to the performance of the device, such as the precision for the subsequent control and motion delivery. The electronic hardware passes the control decision to the actuator based on the feedback acquired from the sensory units that instrument the linkage; and it is envisaged in implementation via offline operation, i.e. microcontroller-based embedded circuit. The sensory units that are used to acquire different physical signals may undergo a difficult selection, since option spectrum is confined by the limited mounting space around the jaw.

This chapter describes the overall construction of the jaw exoskeleton in the hardware level, which starts with proposing the systematic framework of the Mechatronic system, followed by proposing general requirements to meet the performance and functionality spread into each subsystem. The mechanical subsystem is detailed in the part design and the subsequent evaluation towards the device; the electronic subsystem is given in elaboration with building MCU-based circuit for the autonomous manipulation; each sensory unit is completed unfolded in the usage and undergoes calibration which is also given in details as well. Then the whole system is prototyped on the part of hardware and coded, as well as integrated with the mechanical system to evaluate the performance.

4.1 Systematic Conceiving

The hardware of the device is envisaged to include a linkage and the attachment as the main body parts, the sensors to detect the real-time status of the device movement at frequency of 50 Hz to 200 Hz, and the decision making unit that acquires the sensor signals and sends the command away to the actuation. The systematic conceiving of the Mechatronic system of the jaw exoskeleton is illustrated in Figure 4-1.

The training status can be reflected by the forced movement from the instantaneous velocity and the displacement, and the reactive force generated in the contact surface, which reveals the operating status of the linkage and should be strictly monitored. Since the wearer is expected to have the mandible fastened to the attachment on the device, the sensory unit that is deployed on the linkage respectively measures above parameters that are adapted to the context, namely, the displacement of the attachment and the force on the contacting surface.

The motor that directly actuates the crank in the linkage is intended to be instrumented by an encoder that tells the absolute velocity of the crank to the motor controller and further to the system controller; in that way the motor can be initialized with velocity control profiles. The opening distance of the mouth suggests the actual displacement of the coupler, which differentiates the one calculated by the angular displacement of the crank to feedback the discrepancy to the motor controller, to achieve the position control of the exoskeleton on the coupler. In order to secure the safety of the user during continuous movement, the reactive force inside the attachment indicated by the force sensors is conceived to serve as one criterion, within the range of which is accepted, and otherwise action that should be taken to help loose the compression between the jaw and the holder. Hall-effect sensor behaves as a hard stop to confine the movement range, and it is to be mounted at each end of limiting position. The construction of the Mechatronic system can meet all hardware requirements to carry a higher control strategy particularly to the exoskeleton.

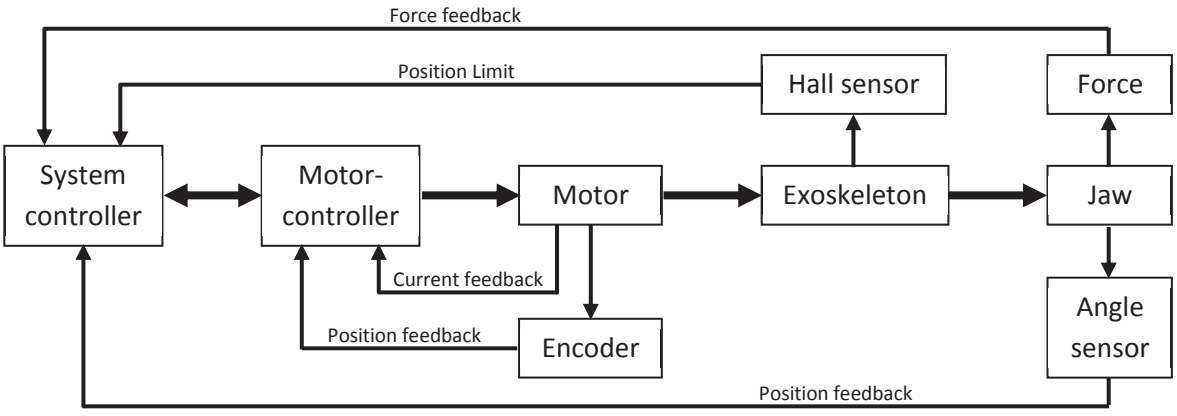

Figure 4-1 The hardware integrated scheme

Based on above conceiving for the device, the integrated design is carried out from a systematic perspective that the development of each subsystem adapts its construction with others. Since the device is intended to be worn by the user, requirements specific to the

exoskeletal devices are qualitatively summarized in Table 4-1 from the manipulation, therapy and safety, which are interpreted into technical specifications falling to each subsystem.

Table 4-1 General requirement for the exoskeleton system

Specific to exoskeleton	Therapy	1	Replicate movements in all direction and cover the whole ROM of required movement;
		2	Move human-body passively and repeatedly
		3	Move human-body according to the state of the patients
		4	Realize various exercise modes including the various directions and various assistance in one direction
		5	Operate simultaneously as a therapy device and an assessment
		6	Maintain natural movement of individual
		7	Simulate a range of virtual environments
	Manipulation	1	easy to control by patients themselves
		2	ease to convert between different modes of exercises
		3	easily adjustable to accommodate a wide range of users
		4	simple to be worn
		5	Energy save
	Safety	1	maintain the identical track of the movement to human natural one
		2	rapid stop/brake
		3	Avoid any stretch beyond the ROM of human
		4	Lightweight
		5	Comfortable attachment
		6	Fully adjustable to accommodate a wide range of users
		7	As few vibration as possible
Common technical Requirements	Mechanical Structure	1	As simple mechanism as possible with compliance
		2	Perform specified movement in limited workspace
		3	Singular configurations must be avoided over the entire workspace
		4	Manipulability of the mechanism should be maximized
		5	Mechanism must not collide with itself or the user
		6	Generate joint torques sufficient to move human body
		7	Back-drivable
		8	High power-to-weight ratio
	Electronic Circuit	1	Compliant conversion within the range of force and velocity
		2	Able to detect the real-time force and velocity
		3	Able to detect the user's intention
		4	Adjust force or position/velocity timely
		5	Passively exert force on the user
	Sensory Unit	1	Real-time performance
		2	Support required sampling frequency
		3	Relatively high precision
		4	Low noisy level

4.2 Mechanical Design

The mechanical construction of the exoskeleton includes the linkage and accessory parts that help to mount the linkage to an appropriate location with respect to the mandible in order to accomplish the specified trajectories, together with above requirements by the four-bar linkage. The device in a wearable mode facilitates the exercise in its delivery which can be executed without being restricted to the locality. As the first test prototype, all of the expected requirements are not necessitated, but the essential functionality that stays of high priority is greatly preferably accomplished, such as the likelihood of the adjustability in the linkage setup which produces a family of trajectories. The motion which is as rigid as the linkage yields that hardly adapts to the interaction with the user in terms of the active force, the compliance is desired of the involvement into the design to tackle the uncertain request of force on top of the positional information, to on the other hand secure the safety and reliability.

Accessory parts generally complete the linkage in the functionality delivery. The proper bearing site places one more consideration in laying out the wearable device, which distributes the weight that virtually burdens users, and especially the way to connect the linkage; particular attachment on the chin has the only actual contact with the user, inflicting direct feeling subject to the wearing of the device.

4.2.1 Four-bar Linkage

Since the dimensioning of the linkage basically adopts the mechanism synthesized to achieve rigid-body motion, the basic design is carried out relatively straightforward so as to match each link of the calculated length, which of adjacency is connected with hinge joints of pins. The length of crank, ground, coupler, and follower is initially configured to the rounded value inversely calculated from the typical pair of trajectories, namely, 5 mm, 49 mm, 30 mm and 20 mm respectively, as illustrated in Figure 4-2. For the first prototype, it is attempted to design parts as small-sized and lightweight as possible, but without causing any mechanical failure on the part.

The linkage is made of aluminium as the material. The link that can slide over the adjacent one is connected by pins, which hold the links together and make the motion frictionless between them. The relative rotation is smoothed by adding bushing in-between each pivot. For the adjusting screws and the guide-bolts as well as for the pins, stainless steel is the choice of material. The bushings are generally made out of acetal. The location and orientation of the

ground is specifically arranged as the basis for the whole linkage with respect to the jaw of rest position according to the synthesis result, as shown in Figure 4-3. The relative position of the linkage suggests the side placement to the user, parallel to the sagittal plane of the human.

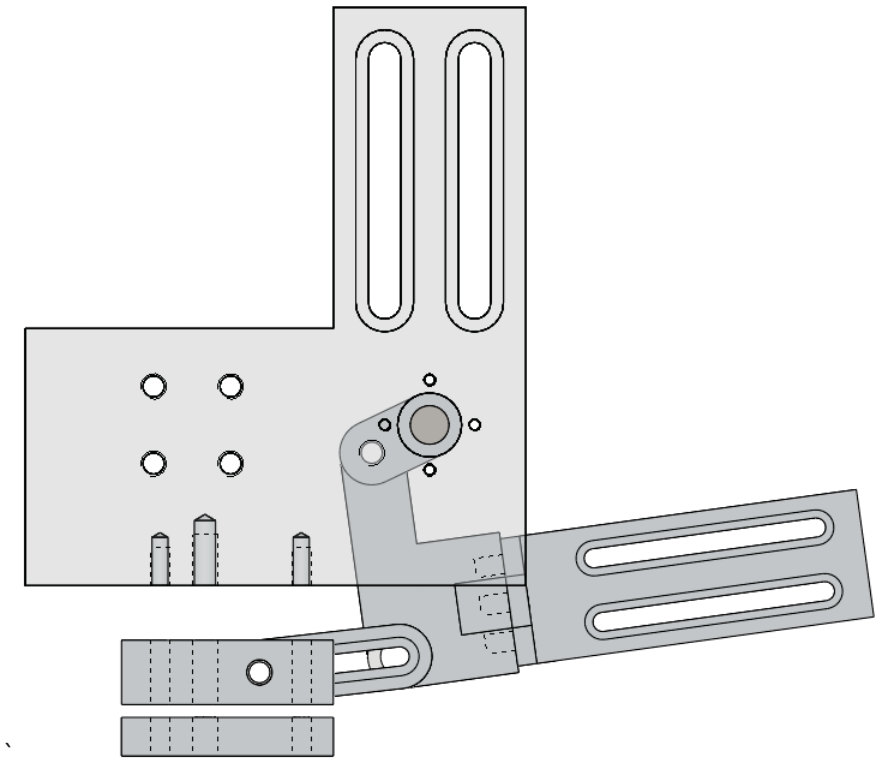

Figure 4-2 The basic design of four-bar linkage

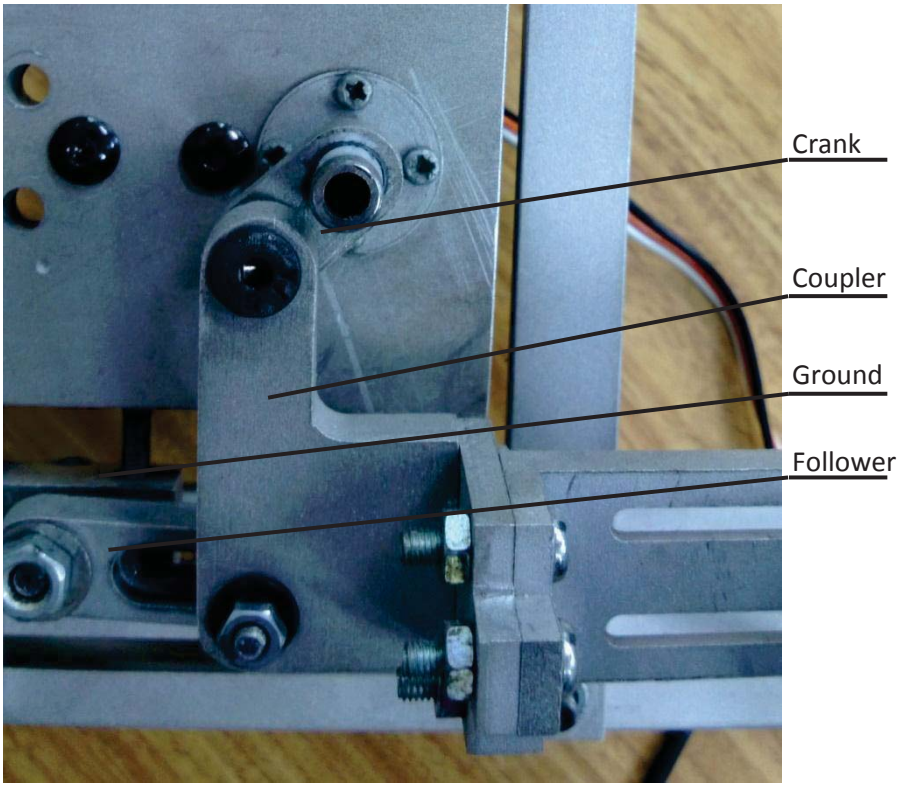

Figure 4-3 Assembly of four-bar linkage

A. Adjustability of the Linkage

The adjustability of the linkage according to the mechanism devise is implemented in the follower, ground, and attaching point on the coupler to the jaw, the first two of which are tuned to alter the shapes of the trajectories while tuning the last fits the position of the jaw size of the wearer. Look-up graph of Figure 3-26 can be referenced to reach out the best fitted trajectory. The follower link is only assigned a small range of alternation as 10mm, which allows the length variable between 16mm and 26mm; the ground link that is designed to be adjustable in the range of 40mm to 60mm, but the way to tune the length is otherwise fulfilled. The attaching site on the coupler can achieve tuning its length relative to the connecting joints in two dimensions in order to adapt the size of the wearer in space, which covers a range of anterior-posterior and superior-inferior at the incisor; while the length is given adjustable in a range of 30mm to 50mm. Structurally, the coupler is secured to cause no collision within the length of tunable range while the device is in operation.

The ground block is fixed on one end to the entire monolithic plate connective to the base, and has the other end floating along the guidance composed of two pins that are fixed to the big plate. The guidance that is mounted vertically can only pilot the other end of the ground link tunable on the vertical direction, which inevitably changes the alignment of the ground link. The height of the movable end can be tuned within 20mm, giving the varying orientation of 16° and the adjustable ground length of 17 mm maximally. The follower link is fabricated with a slotted arm on which has a pin mounted at one end to allow the coupler pivoted via a bushing, as the full block shown in Figure 4-4. The location of the pin on the slot is adjustable to alter the length of the follower, and is lockable to the arm by a screw when the tuning is done.

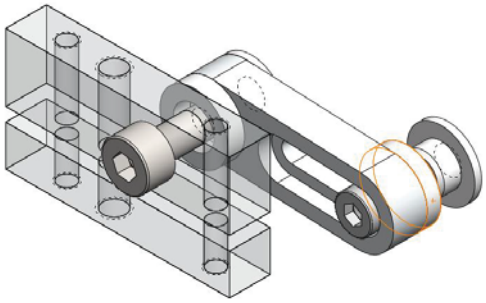

Figure 4-4 Adjustable follower link

B. Actuation Installation

It is preferable to mount the actuator unit away from the linkage which operates on the head to on one hand lower the overall weight of the wearing and on the other hand facilitate adjust

the link length. But considering the experimental attempt in this prototype, a DC motor is chosen to be installed to the rear of the crank. The required moment for the device operation is calculated to select the model of the DC motor in the Simulation/SolidWorks, subject to the velocity profile of the crank which is specified as the motor control input, as shown respectively in Figure 4-5. All of the parts are generally built with assigned proper materials in the software and assembled into the mechanism, and a mandible 3D model of a given 400g is also added to mate the linkage on the attachment. A piecewise constant force of 10N is applied to the attachment vertically directing opposed to each phase of movement. Less than 0.6 Nm moment is required to actuate the linkage according to the simulation in SolidWorks, and a motor and gearbox combination hitting a nominal torque of 1.67 Nm is selected in this application to be installed on the linkage.

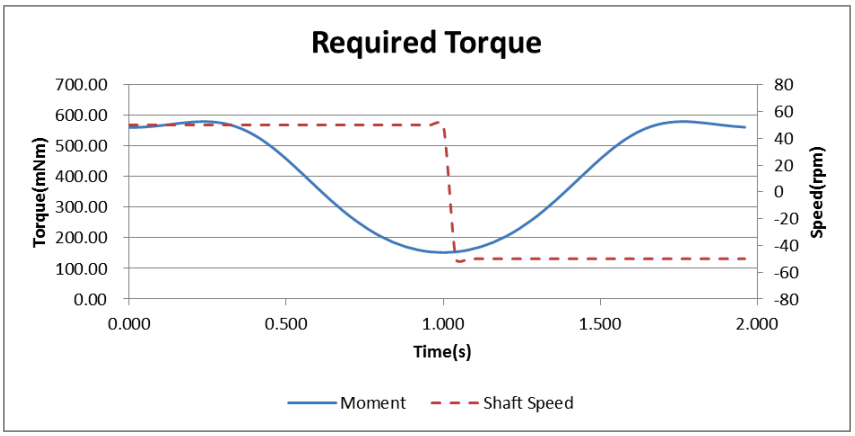

Figure 4-5 The moment corresponded to a velocity profile

4.2.2 Mounting Accessories

The four-bar linkage is the part of the exoskeleton that generates the desired motion. However, the whole exoskeleton consists of more parts like the actuator, and the parts through which it can be attached to the user.

The coupler is fabricated in the most simple and intuitive way to be attached on the jaw that the adjustability in both directions is achieved by an adjusting screw and two guide pins for each one since it can be configured on the coupler itself, as shown in Figure 4-6. The bar linked to the follower and crank link is the actual coupler of the four-bar linkage; and others form the adjustable extension of the coupler link, containing a guiding arm that is directly fastened on the coupler and a guiding screw mounting the attaching-point. Two guiding slots cut on the arm keep the sliding parts from twisting and bending and guide the motion and bear the weight. The guiding pins that are fixed on the guiding arm pilot the movable block,

which straightly connects the attachment by a locking pin on each to locate the attachment. One more screw adjusts the distance in that direction.

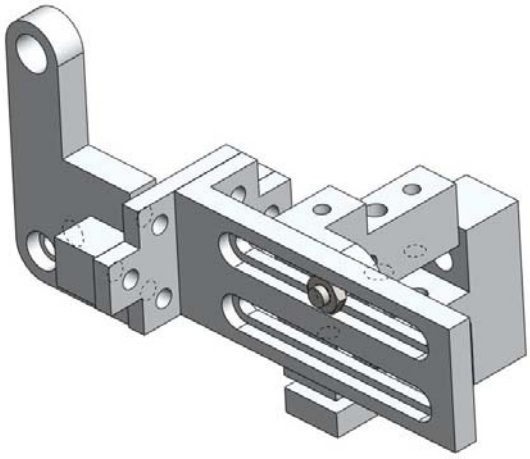

Figure 4-6 Chin attachment on the jaw

The exoskeleton is conceived to be worn on the head to free the hands instead of the hand-hold mode; therefore the linkage is mounted on a monolithic fixed plate which can be hold onto the wearer. To make the whole device wearable and independent from a certain locality, a common helmet is used to fasten the plate to be integrated into the ground of the linkage. This helmet has a stable fit inside and easily adjusted to adapt the head size; and the hard shell is firm enough to bear the weight of the device, as the concept is illustrated in Figure 4-7. Via TMJs the mandible is linked to the skull which is seen as the fixed base, under which as the reference the trajectories on IP and CP are described. The floating parts on the device are attached to the mandible while the stationary parts firmly to the skull, which affiliates the ground in the linkage as well as the helmet. The linkage should be enabled to move along the long axis as one piece of its height to adjustable relative to the jaw, via connective plates cut with slots to the helmet. Since connective plates are counted into the overall weight of the exoskeleton, these accessory parts are designed as lightweight as possible to shrink stress on the wearer. An adjustable range of 50mm to 80mm is basically intended to locate the linkage with respect to the helmet. All of the accessory parts are made out of the aluminum.

The attachment on the device coupled with the jaw accounts for the physical man-machine interaction, and it should have high efficiency and reliability to transform the driving force. An irregular shape of the interface is prototyped from the actual chin in 3D space with some modification to grasp the jaw. It inevitably involves some pliable materials on the attachment to fill up the clearance between contact surfaces. The surface material will be separately modeled as combination of the springs in the Simulink to simulate the elastic feature.

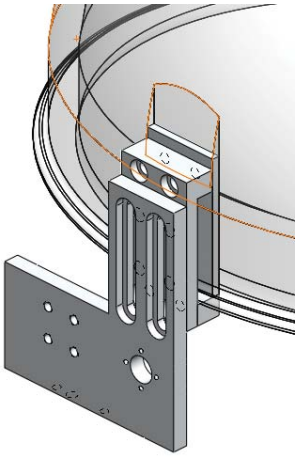

Figure 4-7 Helmet connection

4.2.3 Passive Compliance Design

The crank is actuated following specification of one of the predefined velocity profiles, from the integral of which the mouth opening displacement relative to the rest position can be calculated. The movement purely delivered by four-bar linkage is rigid in terms of force management to the jaw, resulting in poor adaptability to the scenario of a relatively large variation in resistance. The force exertion is desirably regulated on the linkage-based mechanism for double-side consideration, which is to secure the motor operation to adapt the force that may be required to a large resistance to lower the jaw on one hand, and on the other hand to buffer the force generating impact at the opening distance.

Since the force that applies to the jaw via the attachment is prescribed to be 10N as the maximum value, which is used in the selection of the motor, larger force that is likely to occur in the opening phase is intentionally offered via releasing energy conserved with a compliant component. A linear spring behaving as a passive compliance is added into the prototype device. Initially, the spring is not in compression if the actuator can provide adequate force to open the jaw fluently, and the force exerted to the attachment basically approximates the theoretical magnitude provided by the motor based on their relationship.

The initial state of the spring can also be pre-tightened up to 5mm theoretically to provide an initial force, by locking the adjustable screw. Larger force can be provided via gradual spring compression during the opening process, and the generated force conforms to $\mathrm{F}_i = \mathrm{k}_i \mathrm{x}_i$, explanatory to Figure 4-8. The maximum length up by the spring can be compressed is suggested as 8mm, producing the maximum force of by calculation. The length of the spring compression is also limited by a screw to define the acceptable upper boundary for each individual. Figure 4-8 (B) depicts the performance of the spring when subject to a random

force of constant 0.1 N in the aspects of the reaction force and deformative length. The spring recovering time has been found in an inverse relation with the pre-tightened length; the shorter it is pre-tightened the longer it takes, generally in the level of 10^{-3} s, able to be negligible compared to the overall duration of the mandibular motion.

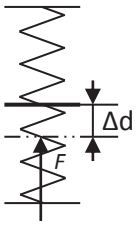

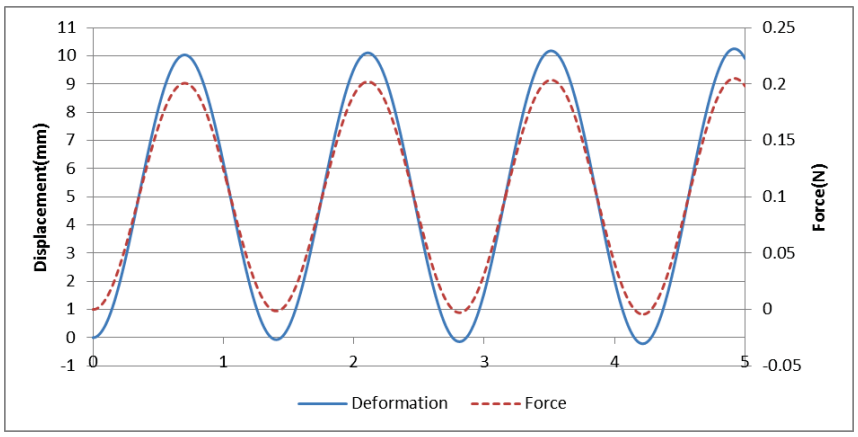

A B

Figure 4-8 Passive compliance

Since two symmetric linkages are arranged on each side of the face, each spring compliance unit can only be placed on top of the attachment to avoid asynchronous paces. The spring unit centers the spring with accessory components, such as the spring locking pins, as shown in Figure 4-9. Apart from the adjustable boundary limits, there is a hard stop along the guidance pin to give a spring compressible length maximally of 12mm, equivalently generating 0.5N, which is believed to give a secure level of force complement. Adjusting screws as referred above are fitted into both ends of the sleeve to adapt the requirements for initial and maximum force.

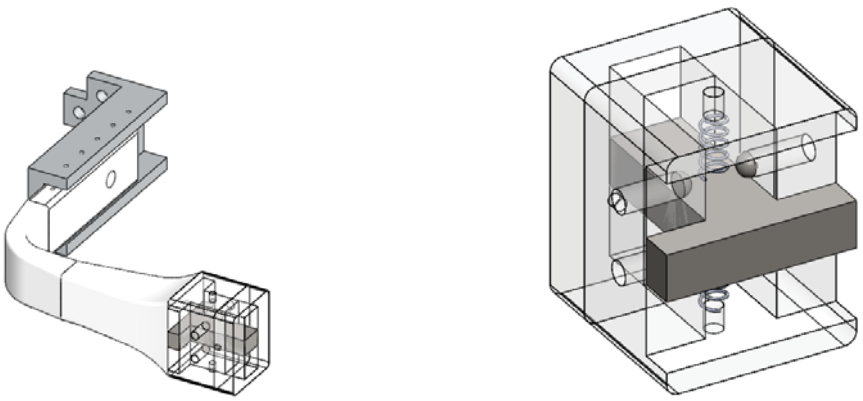

A B

Figure 4-9 Compliant components design

4.2.4 The Entire Jaw Exoskeleton Assembly

The main consideration in the mechanical design lies in the holistic construction of the linkage-based device in terms of the reliability and stability, apart from the movement delivery. The configuration of one linkage that is fixed to the helmet on one side turns into a cantilever to drive the jaw, which could cause unbalanced force to the jaw. Two linkages that are totally mirrored with respect to the centre plane are composed of the main structure of the device, which ensures the synchronic movement. Figure 4-10 shows the assembly of the two four-bar linkages on each side, both of which are connected to the attachment that holds up the chin. Double sides of symmetrical linkages are fixed to the helmet via the connective plate on each side, in this way the stability of the device is easily maintained for frontal force exertion so as well the adequate power upon the mandible. Figure 4-11 gives the fabricated prototype.

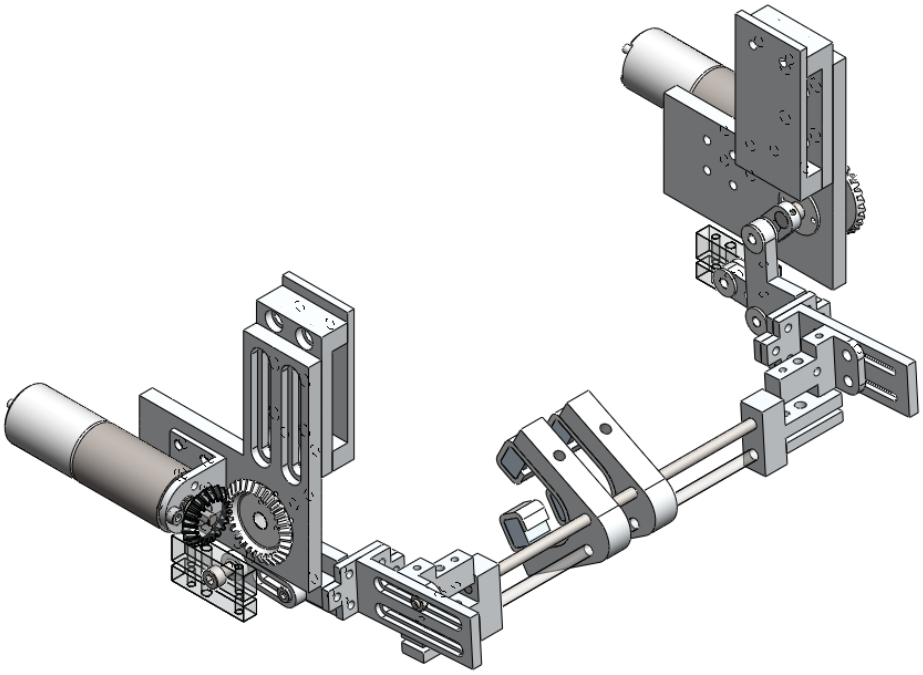

Figure 4-10 The configuration of double four-bar linkage

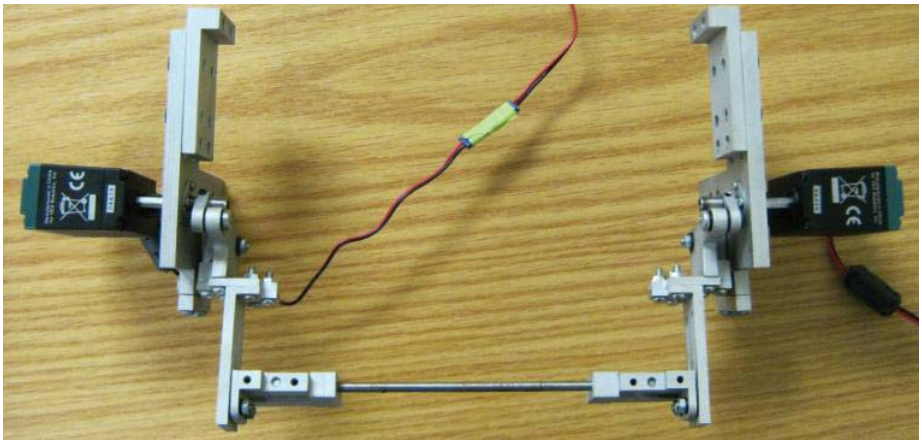

Figure 4-11 Linkage prototype

The overall assembly plus the helmet is illustrated in Figure 4-12 which gives an impression of the envisaged concept of the jaw exoskeleton by placing a mandible bone replica to display wearing condition. The connective plates on both sides are designed with adjustable slots, allowing users to adjust the wearing locality, in order to ensure the linkage is worn on the designated relative position with the jaw.

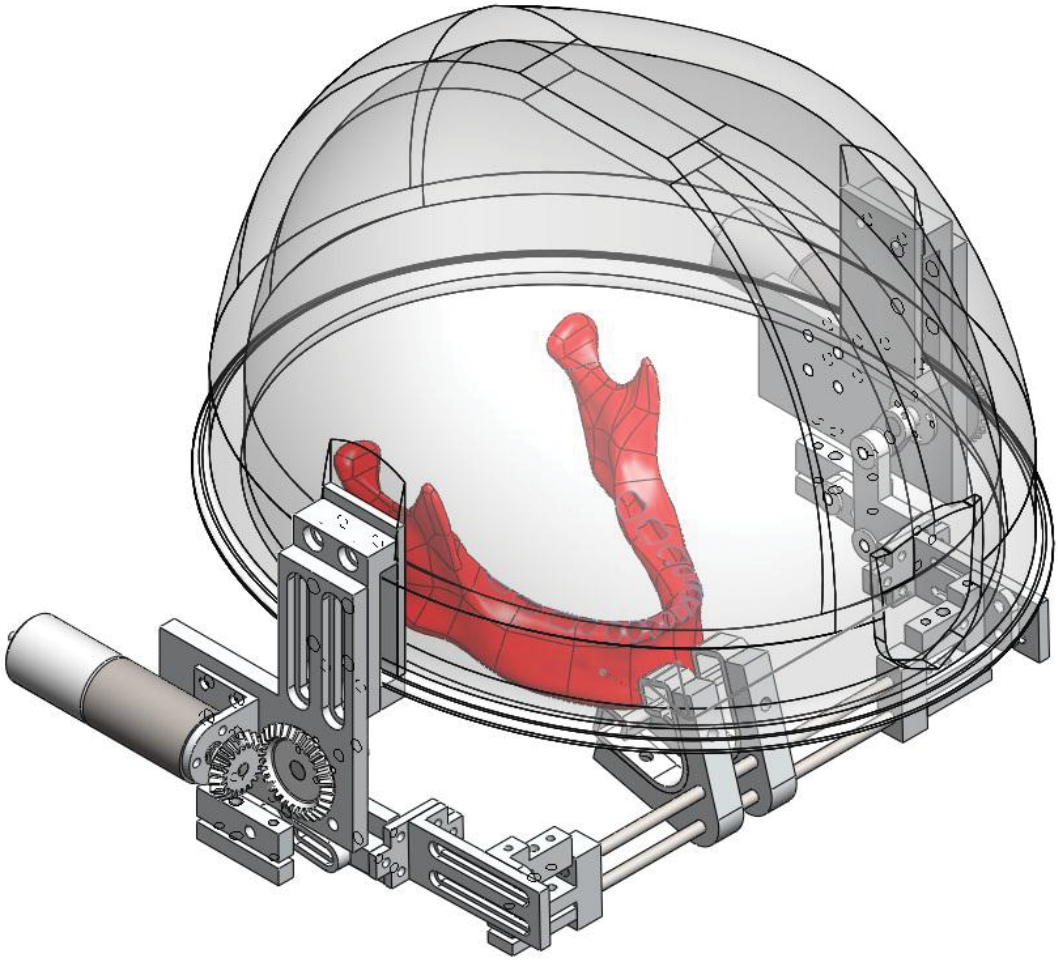

Figure 4-12 Overview of the whole assembly in SolidWorks

4.3 Sensory Subsystem Design

The sensory feedback signals that signify the wearing feeling of user and operating status of device are configured into the hardware implementation of the control system in terms of where it being acquired, forming hardware integrated control system. The position feedback loop compares the crank angle read from encoder with the crank's rotating angle converted from the actual position of the jaw, whose acquisition requires a position sensor. One feedback loop incorporates force signal which is essential as the threshold to trigger the higher controller according to the rules. Meanwhile, for safety reason, a type of limit signal is intended to regulate the boundary of the swing of the crank to avoid either too much

unexpected force clashing the upper teeth or exceeding the bearable mouth-opening distance, in case of the controller being out of order. Given the limited space to fit installation of all sensors on the linkage, the general requirements of selection are summarized as being compact size, independent unit and easy-installed. Technically according to the precision requirement from the controller, the basic specifications of required sensors are listed in Table 4-2.

Table 4-2 Specifications of the required sensor

Type	range	Resolution	Output
Jaw position	0°-90°	0.5°	Analog
Force	0N-50N	1N	Analog
Limit switch	On/off	--	Digital (On/off)

4.3.1 Tilt Angle Measurement Unit

In the device where the compliance is planted inherently, the encoder installed on the motor cannot give the exact position of the jaw on the occasion of activating compliance; while the actual position of the jaw indicates the actual position that is essentially put into the position feedback loop and the higher control loop as an key parameter to tune the system to the desired position. The position of the jaw can be obtained by either directly a sensor installed on the jaw or indirectly calculation from the monitored crank angle. When the device starts from the initial position, with the crank rotating, the mouth increasingly opens, while the angle between the initially horizontal tangent at the bottom point of the chin and the ground is varying monotonously till the opening limit. Hence, the chin angle denoted as γ_c is seen to be an optimal parameter revealing the position of the jaw with respect to the crank angle in this application. The chin angle is actually the varying angle of the coupler in a rigid-body guidance based mechanism. By referring the same denotation, the angular displacement of the coupler θ_3 is expressed as the function of the crank θ_2.

The angular displacement on the chin is implemented by a tilt measuring unit, which comprises of a dual-axis accelerometer ADXL203 and two cascaded amplifiers; [9]ADXL203 can measure both static and dynamic acceleration of two axes that are normal to the direction of the gravity upon the high performance of sensitivity accuracy. General technical characteristics are listed in Table 4-3, where non-relevant specifications in this application are

[9] More information can be referred to the product manual, please visit: http://www.analog.com/static/imported-files/data_sheets/ADXL103_203.pdf.

not given. The tilt measurement utilizes the vector of the gravity as an input acceleration, which projects on the sensing axis produces output voltage component in relation with the angle between the sensing axis and the horizon (parallel to the earth). The dual-axis accelerometer is laid to place two sensing axis in the plane where the tilt occurs as shown in Figure 4-13, so both axes are involved in the measurement of the same tilt angle, i.e. the coupler angular displacement. The angle between one axis and the horizon increases while the other decrease. The sensitivity to angular variance stays highest at the orientation of 0g reading on axis parallel to the ground and shrinks when the angle is increasing. The sensitivity of either axis can be mutually compensating.

The output acceleration of both axes referring to X-axis and Z-axis can be calculated in Eq.(4-1).

$$\begin{cases} A_X = 1g \times \sin\theta \\ A_Y = 1g \times \cos\theta \end{cases} \tag{4-1}$$

Table 4-3 Specification of the ADXL203

Sensor Properties	
Size	5 mm × 2 mm × 2 mm
Package	LCC
Power supply	5 V (operating range 3V-6V)
Shock survival	3500 g
Output	1.5 V-3.5 V
Typical Performance	
Full-scale range	± 1.7 g
Sensitivity (maximum)	1000 mV/g
0g Voltage	2.5 V
Initial 0g output deviation	± 25 mg
Resolution	1 mg at 60 Hz (approximately 0.06° of inclination)
Axis alignment	≤ 0.1°

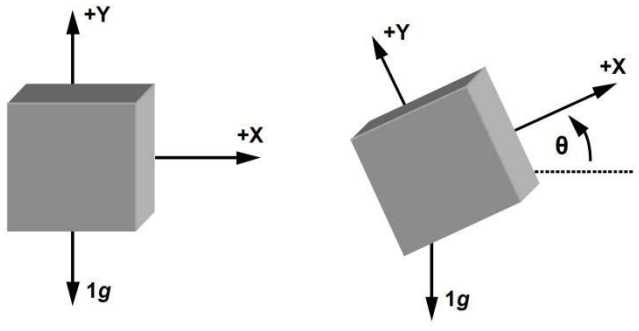

Figure 4-13 Two axes application (adapted from product manual)

The output of the accelerometer is analog voltage, theoretically ranging from 1.5 V to 3.5 V. A built-in ADC in MCU is converting analog information to the digital data readable with input range of 0 to 3.3 V. According to the manual the product has a bias of 100 mV shift of zero-g

and 40 mV/g shift of sensitivity; the worst-case output voltage is ranged within 1.36 V to3.64V, which is shifted to fit the input ADC range via a two-stage amplifier circuit. The first stage amplifies the signal 1.2 times based on common-mode voltage of 2V, while the second one has a gain of 1.1 based on the common-mode voltage 1.7 V. The amplifier carried out by a quad AD8608 has a total gain of 1.32 and the output range is in well accordance to the input range. The amplified voltage corresponding to the output of accelerometer is expressed in Eq. (4-2).

$$V_{amplified} = \left(V_{original} - 2.5\right) \times 1.2 \times 1.1 + 1.7 \tag{4-2}$$

The maximum of amplified voltage and the minimum is calculated as 3.2 V and 0.2 V respectively so the output range of tilt system is 3 V. The resolution of the voltage per least significant bit (LSB) from a 10-bit ADC is expressed:

$$LSB = \frac{3.3V}{2^{10}} = 0.0029V \approx 3mV \tag{4-3}$$

As specified, for the single-axis inclination measurement, the desired inclination resolution of the system derived from the controller precision is 0.4° for a range of 0° to 55°. The output acceleration is trigonometric function of the tilt angle, so the resolution of acceleration is variable, and it can be expressed in terms of the incremental sensitivity of a certain step size in Eq. (4-4).

$$\begin{aligned} \Delta g &= 1g \times (\sin\varphi - \sin(\varphi - \Delta\varphi)) \\ &= \sin\varphi - \sin(\varphi - 0.4°) = 2\cos\left(\frac{2\varphi - 0.4}{2}\right)\sin\frac{0.4}{2} \end{aligned} \tag{4-4}$$

Where: φ is the current angle, $\Delta\varphi$ is the step size.

Therefore, the resolution of the acceleration is monotonously dropping while the angle is growing up. The largest resolution locates at $\varphi = 0°$, $\Delta g = 7mg$ while the least point stays at $\varphi = 55°$, $\Delta g = 4mg$. The minimum resolution is chosen as the constant acceleration per LSB that can be achieved by single-axis measurement. The resolution of the output voltage per constant acceleration is calculated:

$$\Delta V = 1000\, mV/g \times \Delta g = 4mV \tag{4-5}$$

As the output voltage of constant acceleration ΔV is much larger than the resolution LSB that can be distinguished by ADC, the tilt unit is able to meet the requirement from controller. Since two axes that are orientated to in the plane where the inclination occurs are able to yield the acceleration, the effective incremental sensitivity stays roughly constant within the

range of all inclination angles. The resolution of the acceleration can be represented in Eq. (4-7) with respect to an inclination change δ°, i.e.

$$\Delta A_{out} \cong 1g \times \sin\delta \tag{4-6}$$

$$\delta_{min} = \sin^{-1}(\Delta A_{out}) = \sin^{-1}\left(\frac{LSB}{1000\ mV/g}\right) \tag{4-7}$$

The allowed minimum acceleration resolution that can be differentiated by the ADC is calculated as 0.17°, far less than the resolution of the changing angle required by the system accuracy. Then the output voltage denoted as $V_{(X,Y)}$ representing the measured acceleration along each axis in Eq. (4-8) on the identical axis is converted to the angle of inclination, which can be calculated in Eq. (4-9). Since the calculation basically presents the same value, it can also be expressed in Eq. (4-11) by easier approach of using the ratio of two values of Eq. (4-10).

$$V_{(X,Y)} = \left(1000\ mV/g \times A_{(X,Y)}\right) \times 1.32 + 1.7 \tag{4-8}$$

$$\begin{cases} \theta_X = \sin^{-1}\left(\dfrac{V_X - 1.7}{1.32}\right) \\ \theta_Y = \cos^{-1}\left(\dfrac{V_Y - 1.7}{1.32}\right) \end{cases} \tag{4-9}$$

$$\tan\theta = \frac{A_X}{A_Y} \tag{4-10}$$

$$\theta = \tan^{-1}\left(\frac{V_X - 1.7}{V_Y - 1.7}\right) \tag{4-11}$$

Note: a low-pass filter of 50 Hz bandwidth specified is accessorily created along the output by attaching capacitors to the internal 32 KΩ resistors, which is supportive of ADC sampling rate of 200 Hz, and the capacitor of a -3 dB bandwidth is pointed from:

$$f_{cutoff} = 1/\left(2\pi(32k\Omega) \times C_{(X,Y)}\right) \tag{4-12}$$

Where:

$C_{(X,Y)} = 0.1\mu F | f_{cutoff}$

The tilt measuring unit shown in Figure 4-14 is designed to be detachable with interfaces to power supply and output. The circuit board is prototyped as similarly shaped to fit the installation area on the side of the device, given in Appendix Figure 8-1. From of whole assembled device, the circuit board is finely placed on the coupler hand to align one sensing axis at the initial position to the direction of the gravity as much as possible, and the PCB installation can be found in Figure 8-2.

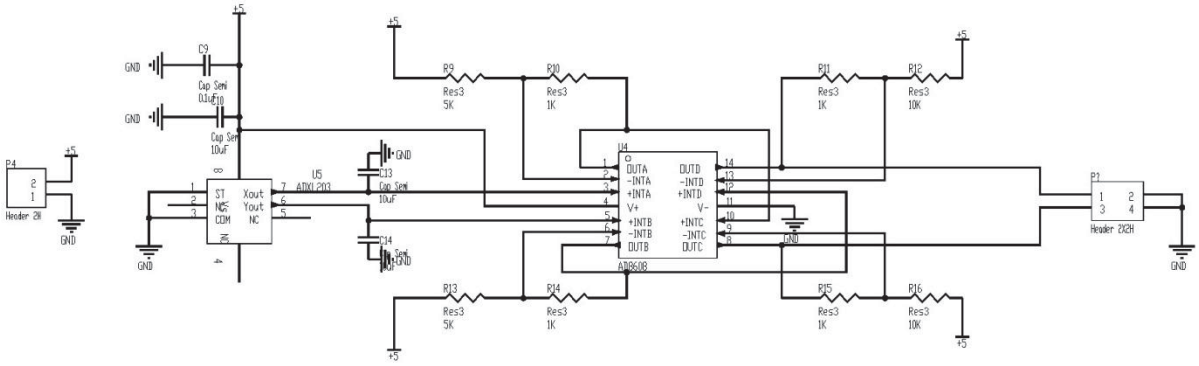

Figure 4-14 Tilt measurement unit circuit

4.3.2 Force Measurement Unit

The force sensor is used to measure the approximate normal force of the contact surface between the jaw and the device, which compares the pre-set acceptable magnitude on one DOF. Considering the direct contact with the jaw of the user, the sensor is preferably characterized of flexibility to fit a complex surface measurement, and small thickness to ease its influence to the functionality of the device. The repeatability and the hysteresis of selected sensor are required of high standard, which comes from periodically repeat usage for exercise. The *FlexiForce* sensor that is featured of an ultra-thin flexible printed circuit is used to accommodate this application, as photoed in Appendix Figure 8-3. It is terminated with solderable male square pins and can be easily connected into a circuit. The key specifications are listed in Table 4-4, as well as the properties of force sensing properties, linearity, hysteresis, drift, and temperature sensitivity, which are met in terms of technical parameters.

Table 4-4 Selected sensor specifications (partially quoted from manual)

Sensor Properties	
Thickness	0.208mm
Sensing Area	9.53mm diameter
Connector	3-pin male square pin (center pin is inactive)
Typical Performance	
Force Ranges	0-110N
Operating Range	-9°C to 60°C
Linearity	<+/- 5%
Repeatability	<+/- 2.5% of full scale (conditioned sensor, 80% force applied)
Hysteresis	<4.5% of full scale (conditioned sensor, 80% force applied)
Drift	<3% per logarithmic time scale (constant load of 90% sensor rating)
Response Time	<5 microseconds

Flexiforce sensor is actually a resistor of large resistance, which inversely-proportional varies to the force applied on the active sensing area. The resistance delivers mV-level voltage

subject to a 10V-input, and the output should undergo the amplification before being conveyed to the controller. The original voltage after passing the sensor is amplified to the range 0-3.3 V in order to match the range of ADC in (the voltage resolution enlarged corresponding to the increasing input force). As shown in Figure 4-15, the circuit built in the Simulink shows the inverse amplification scheme and is simulated to get the appropriate value of electronic components.

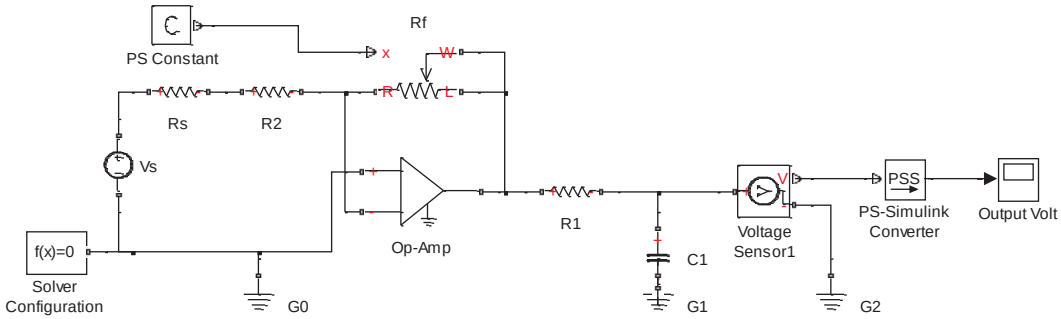

Figure 4-15 Amplifier circuit simulation in the Simulink

The sensitivity of *Flexiforce* sensor can be adjusted by changing a fixed reference resistance (R_f) to ensure the measurable range to fall into the acceptable range, under the reference power V_S. The response time of the sensor is less than 5ms, so 200 Hz of signal acquisition will not cause any signal missing. To avoid high-frequency noise present among acquired signals without losing original data, a low-pass RC filter of 500 Hz cutoff frequency is cascaded after the amplifier. The output voltage of the sensor V_{out} after the amplification is calculated in Eq. (4-13). Since the V_{out} is proportional to the applied force, the force can be inversely calculated from its relationship with the output voltage, which can be established in the calibration of each sensor in Eq. (4-14).

$$V_{out} = V_s \times \frac{R_f}{R_s + R_2} \tag{4-13}$$

$$V_{out} = V_s R_f \times \frac{1}{R_s + R_2} = C_f \frac{1}{R_s + R_2} \propto C_f \cdot F_{applied} \tag{4-14}$$

Flexiforce sensor of two ranges applied here are, 1 lb and 25 lb, i.e. approximately 450g and 10 Kg in metrics; corresponding to maximum force of 4.4N and 100N respectively. The resolution of the ADC supports the force detection of every LSB of 3mV, and is much more precise than the required incremental of the force in this application, though 0.1N is approximately the least magnitude detectable under 100N sensor measurement. The acceptable voltage input to the ADC is configured to 3V according to the converter and 6V with a peripheral circuitry to boost the sensitivity of the sensor with larger range.

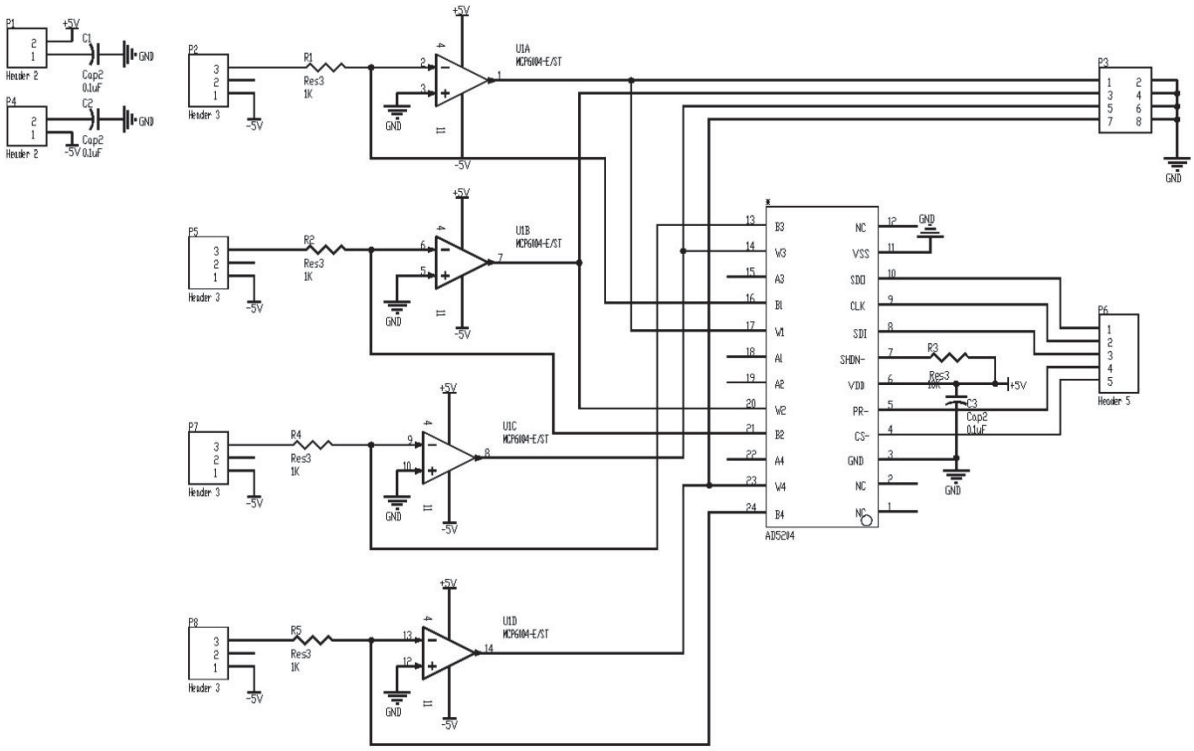

Figure 4-16 *Flexiforce* circuit

Since more than one force sensors are conceived to be mounted in the contact surface plus the occlusal plane, each force measurement unit consisting of four amplifier ports is integrated into a single circuit board with similar power supply and output interface, as shown in Figure 4-16. Two circuit boards are fabricated to accommodate eight sensors. Circuit boards can be seen in Figure 8-4. The circuit board connecting sensors in operation can be seen in Figure 8-5.

4.3.3 Hall-effect Sensor Unit

The safety apparatus that sends immediate stop signal is configured into a switch that acts in an on/off mode subject to the detection of the reach out of the range limit. The limits are set on the top and the bottom bounds along the crank rotational path, where proximity sensing is used to indicate the prescribed limits. Since the crank length is too small to incur cross-detecting over close vicinity, contactless sensing is fulfilled along the travelling path on the coupler. A small magnet is mounted on the desired position on the coupler, which activates the Hall-effect sensors that are fixed on the boundary position of the coupler.

A

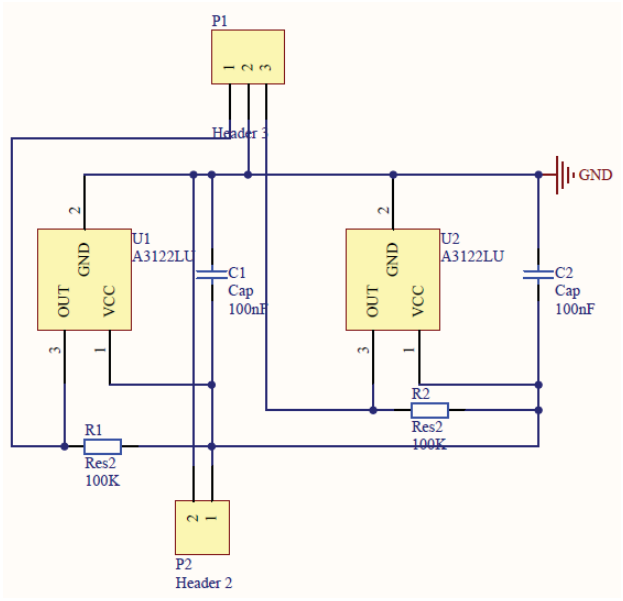

B

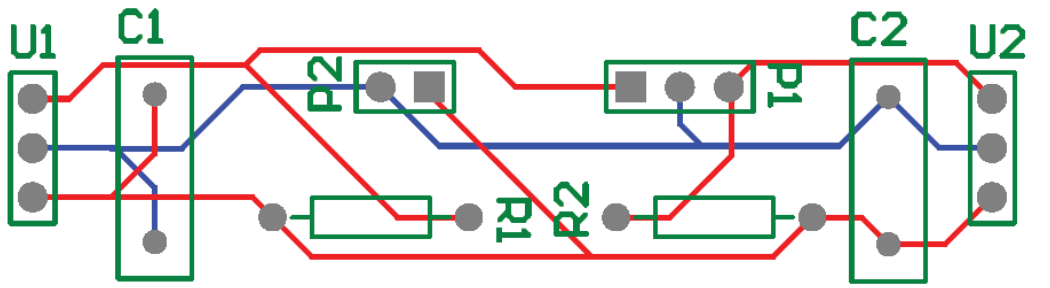

Figure 4-17 Hall-effect switch circuit (A) and circuit board (B)

The Hall-effect sensor operates directly to return a TTL in response to a magnetic field. The circuit is simply designed only to power two Hall-effect sensors with the output port for each for accessing as an analog signal; and a low-pass RC filter of 15 Hz cutoff frequency is affiliated into the circuit, as illustrated in Figure 4-17 (A). The circuit board is fabricated to attach onto the coupler independently in similar shape where two sensors can be firmly mounted, as the board shown in Figure 4-17 (B).

4.3.4 Self-Test of Sensory Subsystem

All sensory units in the device count on the conditioning circuits to convert the measured physical signals into the readable voltage. Since the spatial limit in the head area restricts the adoption of the off-the-shelf products that mostly appear to be too bulky to be installed, the primitive sensors are incorporated in the mechanical parts of the device instead. Therefore, those sensors must undergo a process of calibration for magnitude correctness before put into use.

A. Tilt Measurement Unit Calibration

Calibration of tilt sensors attempts to eliminate the errors in the output, which are derived from three aspects, i.e. the inclination of sensor installing plane, the sensitivity along each axis and the calculation. According to the product manual, the sensitivity that may exhibit difference in two axes due to a mismatch and an offset, results in a carried coefficient involved into the further calculation, as express in Eq. (4-15). Inclination upon the installation of the sensor here refers to the sensing plane (plane XOY referring Figure 4-13) tilt towards the third axis, which could occur during soldering the sensor to circuit board, mounting the board to the device, or wearing the device. So the sensitivity at that power level could be shrunk on both axes due to a tiny angle of the inclination on the plane XOY, leading to the actual rotational angle differing from the calculated one.

$$A_{OUT}[g] = A_{OFF} + (Gain \times A_{ACTUAL}) \tag{4-15}$$

Since the installation-plane inclination could hardly be avoided during the wearing for practice, the likely angle will only be rectified through online calculation of the data acquired in operation. The sensitivity on each axis is calibrated in order to re-establish the relationship between the actual tilt angle and the output voltage. Each axis is firstly placed into a +1g and -1g field to obtain the output voltage of that acceleration, as given in Eq. (4-16); and the sensitivity-related parameters can be calculated in Eq. (4-17) for each axis, which are used to finally calculate the actual sensitivity in Eq. (4-18). By integrating Eq. (4-8), the acceleration at each axis can be expressed in Eq. (4-19) to further calculate the tilt angle in Eq. (4-10).

$$\begin{cases} A_{+1g}[g] = A_{OFF} + (Gain \times 1g) \\ A_{-1g}[g] = A_{OFF} + \big(Gain \times (-1g)\big) \end{cases} \tag{4-16}$$

$$\begin{cases} A_{OFF}[g] = \dfrac{1}{2}\big(A_{+1g}[g] + A_{-1g}[g]\big) \\ Gain = \dfrac{1}{2}\big(A_{+1g}[g] - A_{-1g}[g]\big) \end{cases} \tag{4-17}$$

$$A_{ACTUAL}[g] = (A_{OUT} - A_{OFF})/Gain \tag{4-18}$$

$$A_{ACTUAL(X,Y)} = \left(\frac{V_{(X,Y)} - 1.7}{1.32} - A_{OFF}\right)/Gain_{(X,Y)} \tag{4-19}$$

Where:

$A_{\pm 1g}[g]$ is calculated from the measured voltage V_{+1g} and V_{-1g} based on $\frac{V_{\pm 1g}-1.7}{1.32}$ respectively.

The third-axis inclination shrinks the sensitivity on both axes in a relationship with the tilt angle φ, as expressed in Eq. (4-20); the output acceleration at each axis that associates with

the measured voltage is the component of the actual acceleration projected to the XOY plane, which is formulated in Eq.(4-21). By referencing Eq. (4-10), the angular displacement measured by the two-axis sensor is deduced without being affected from the third-axis inclination.

$$A_{OUT}[g] = A_{ACTUAL}[g] \cdot (1g \times \cos\varphi) = \begin{cases} \sin\theta\cos\varphi, & X-axis \\ \cos\theta\cos\varphi, & Y-axis \end{cases} \quad (4\text{-}20)$$

$$A_{ACTUAL(X,Y)} = A_{OUT(X,Y)}/\cos\varphi = \begin{cases} \sin\theta/\cos\varphi, & X-axis \\ \cos\theta/\cos\varphi, & Y-axis \end{cases} \quad (4\text{-}21)$$

Where: φ is the third-axis inclination angle.

The circuit board is mounted on the larger gear in a two-meshed gear set that rotates around each center, all of which are fixed onto an upright board. The gear teeth ratio is 1:12, which suggests a cycle rotation of the small gear triggers the circuit board rotating by 30°. The calibration is not carried out by incremental rotation, which though is supportive by the setup; only distinctive positions (±1g for both X/Y axes) are chosen to measure the corresponding output voltage.

A NI DAQ card USB-6210 that links the circuit board to PC via USB port is used for calibration to convert the voltage into the readable digital signal flow (setup given in Appendix Figure 8-6). Since the DAQ card supports 16 channels of analog input with 16-bit resolution, higher than the required one to be offered by ADC module, it is able to provide a precise matching relation for all analog converting scenarios through calibration to the electronic system that might be taken advantage to compose of the future control hardware for signal acquisition. Further data processing includes extraction of the data through three modules, i.e. the acquisition, data filter and recording output, which are fulfilled by a program built in the Simulink, as entirely depicted in Figure 4-18 (A). The acquisition module is configured to run in the asynchronous mode and sample the voltage for single-ended input at the rate of 500 Hz, as shown in Figure 4-18 (B). A filter block is affiliated into the program in order to eliminate the noise that may be derived from the interference of multiple channels crossing the ground during the input varying basically via two steps, i.e. a median filter to smooth the signal flow out and then a Butterworth filter to meet the attenuation specifications, as reformatted to output shown in Figure 4-18 (C).

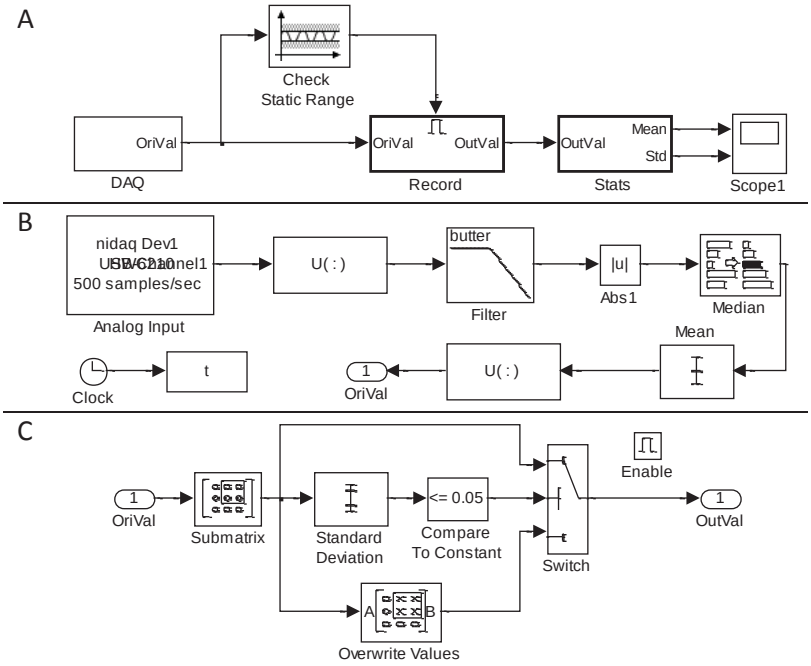

Figure 4-18 Experimental-rig to calibrate the *Flexiforce* sensor

The voltage at each incremental angle averaged to a single value is sketched out for both axes in Figure 4-19, where the theoretical ones are also illustrated for comparison. The actual sensitivity on the X-axis is deviated from the theoretical about 5%, also accompanied with an offset of 5%, since the zero value can hardly be searched; the offset on the Y-axis is adequately small to be neglected. The clearance along both axes hit the peak smaller than 0.05 V, which may bring about 3° error intrinsically. The output curve in Figure 4-20 approaches closely to the theoretical line, with the error at each incremental step shown in dashed line. The error is approximately between -2° to 2°.

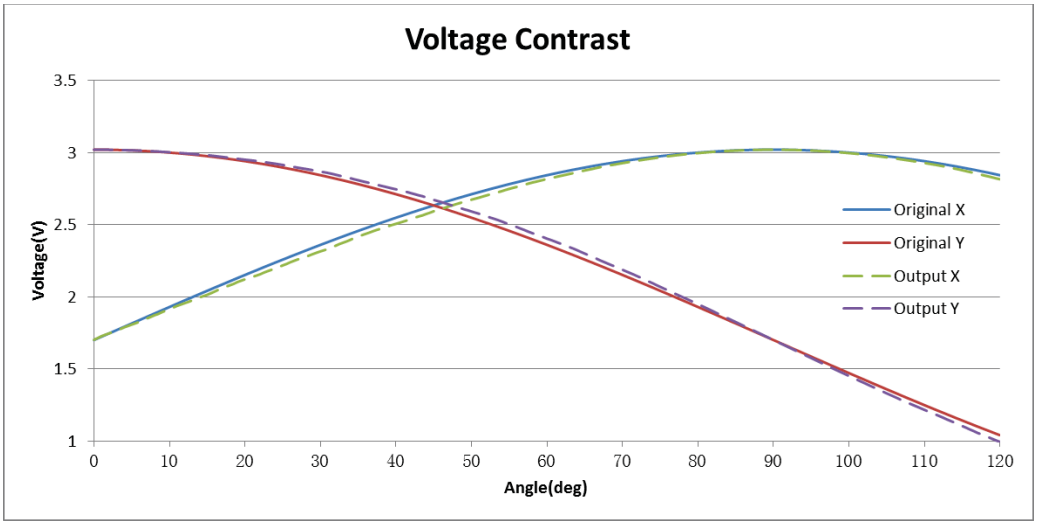

Figure 4-19 The voltage acquired during calibration versus the theoretical one

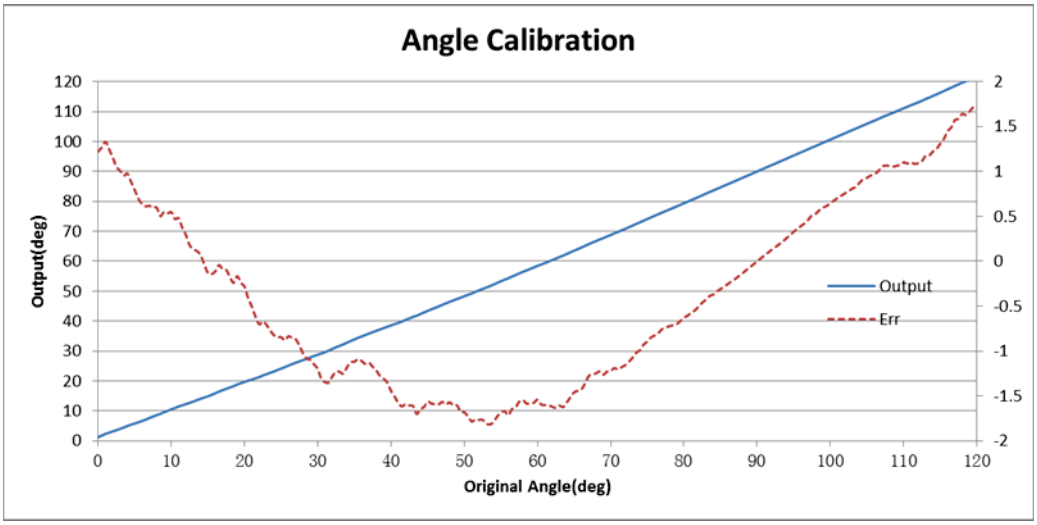

Figure 4-20 The tilt angle after calibration

B. Calibration of *Flexiforce* Sensor

Since *Flexiforce* sensors that are multiply recruited in the device may exhibit small variance in the resistance; each of them is calibrated upon its own conditioning circuit for operational amplifying. As requested, sensors of two measurement ranges are matched to the two circuit boards in each of identical sorts, totally up to six channels of the corresponding voltage outputs. The USB-6210 DAQ card is recruited again together with the corresponding acquisition block built in Simulink for the data processing.

The sensing area can be treated as a single point according to the manual. For the sensor that never experienced loads before, conditioning is essential to be undertaken on the sensor by placing 110% of the maximum loads to be measured for four times, for the purpose of diminishing the effects of drift; each conditioning usually consumes 20s to 30s till the sensor getting stabilized, and the whole conditioning setup in the loading machine that should be identical with the one for calibration. During calibration, each sensor is placed in the workbench of the machine one by one to bear a string of specified loading that increases gradually with a step size 25g and 500g from zero up to 450g and 10kg for the sensor of force ranging to 1 lb and 25 lb, respectively; the corresponding voltage at each loading condition is recorded in MATLAB.

An approximate linearity is illustrative of the force-voltage correlation according to the plotted data, which generally conforms to the physical characteristics of *Flexiforce* sensor. With an acquired voltage, the corresponding force on the sensor can be inversely calculated by linear interpolation or extrapolation; and this correlation can hereby be exactly curve-fitted to an expression of Eq. (4-22).

$$V(i) = aF(i) + b \tag{4-22}$$

Where:

$F(i), V(i)$ represents the loaded force and the mean voltage value of four-time loading, respectively; a, b are constants to stand for the linearity between voltage and force.

A

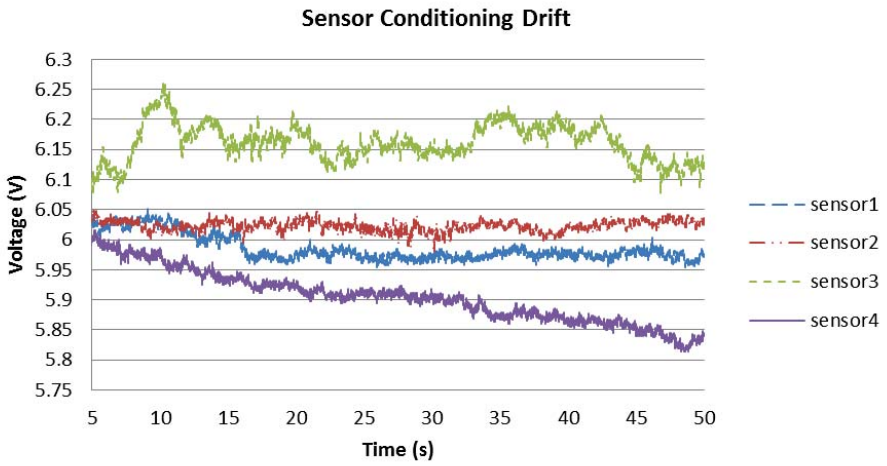

B

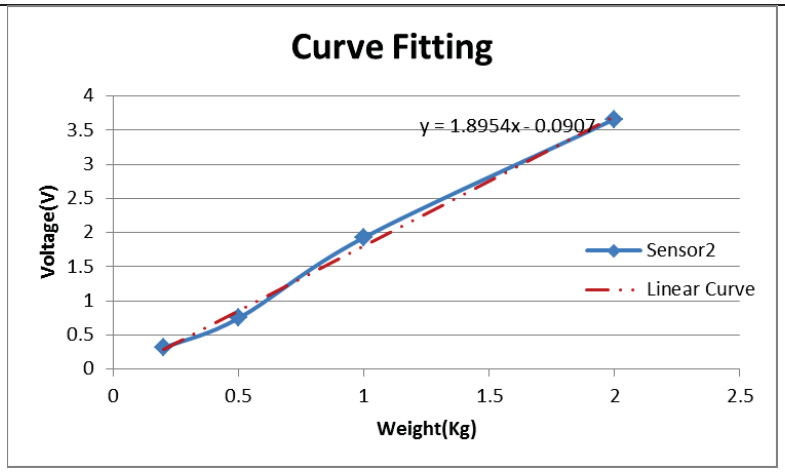

Figure 4-21 Calibration of the force sensors

The curve-fitting is processed in MATLAB to solve the parameters in each sensor, where the least square method is applied by default. Generally, extrapolation that should be avoided in speculating the outranged force would not be involved in the calculation as the calibrated coverage basically fits the force may occurred herein. Meanwhile, as errors are inevitably accompanied in the practice, the sensors have also been investigated in terms of the precision based on the calibrating data, including characteristics of non-linearity, repeatability, and the hysteresis, apart from the drift prior to the calibration in request; according to the manual where the drift rate is given within 3%/logarithmic time, the precision of further calibration for all current sensors subject to the drift is acceptable.

Figure 4-21 illustrates the conditioning drifts of sensors on the top and one group of the relationship established between the acquired voltage and the incrementally applied force on the bottom via curve fitting. A simple GUI coded in MATLAB for easily recording the acquired voltage values at each step of loading which are further averaged over four times to compose of the calibrating point in the curve.

4.4 Construction of the Electronic Subsystem

The electronic subsystem here refers to an independent hardware composition integrated into the device, which can physically run controlling solutions via processing the sensory information and instruct the actuators in compatible formats. The objective of constructing an electronic subsystem is to form an embedded control hardware, which is anticipated to accomplish data acquisition and processing, decision making and signal transmission. It comprises of the overall electronic hardware, not only the microcontroller (MCU) as indicated in Figure 4-1, but also the peripheral interfaces and pathways as well for example the analog-digital converter (ADC). The signal feeds coming from each sensory unit via different interfaces reveal instant wearing condition of the user and operating status of the device, which would be interpreted by controller to send further commands with the signal processed by appropriate filter and amplifier to ensure stability of the system.

4.4.1 Specifications of the Electronic Subsystem

Apart from the functionality mentioned before, this electronic subsystem should also be able to work independently to match the required performance of the control system with corresponding technical specifications in delivering all functions, especially in the aspects of the precision and the real-time response; while it offers communication pathways via which to exchange information and command with a host PC in case of necessary online control and software update. Therefore, this system is designed to have the following performance:

1) ADC unit

   The analog output from sensors requires the subsystem to be equipped with at least six ADC channels. The range of the input voltage depends on programmable gain and original magnitude. 200 sampling points on the path of incisor approximately match the control precision, and it is defined passing by within 2 s for normal usage, so the sampling rate is around 100 Hz, which is the minimum sampling rate required by ADC unit. According to the required resolution per LSB calculated from sensor, referencing ADC of different resolution listed in Table 4-5, ADC unit is preferable to have eight 12-bit channels.

Table 4-5 ADC resolution with different amount of bit

A/D bit	Resolution	LSB (%)	LSB (10 V voltage)
8	256	0.391	39.1mV
10	1024	0.0977	9.77mV
12	4096	0.0244	2.44mV
16	65536	0.0015	0.15mV

2) Versatile interface

Apart from the analog input, the system provides other interfaces such as I2C and SPI, via which to access some sensor signals and create communication pathways, and enhance the extendibility of the system.

3) Filter

Hardware filter is required to be placed in the peripheral circuitry to roughly filter out the high-frequency noise generated in the transmission apart from the software filter process in order to maintain the operation speed of the whole system

4) Controllable user interface (UI)

As the system can run several working programs representing different exercise protocols, between which is expected to be switched by easy operation, a simple but friendly user interface is envisaged to allow users to select the daily program independently according to their rehabilitative conditions.

5) Full-duplex communication and real-time response

The electronic subsystem uploads data acquired from sensors and downloads commands to actuators via UART, acting as the combination of a data acquisition system and a motion control system, in addition to the simplex downloading from PC to update the firmware of the electronic system.

Therefore, the subsystem requires a high-speed real-time response, which ensures the acquired information from sensors to be processed without any loss or passing into the stack and gives command to the motor controller on sequence.

6) Alert

Besides the hard stop activated by limit sensors, the system is able to give indication to any critical state by setting the limits for warning and alarm in software.

7) Dimensions

The dimensions should be kept as compact as possible with low power consumption

4.4.2 The Architecture of the Integrated Hardware

According to the design requirements of the electronic subsystem, the architecture of the overall hardware system is organized as illustrated in Figure 4-22. The scheme adopts an embedded system composed of a MCU and periphery circuits to complete the whole process of signal acquisition, data process and command sending towards the device control. The feedback subsystem acquires signals in analog or digital form, which go into the MCU after being filtered via built-in ADC in MCU or insulator respectively. MCU applies the loaded control algorithm inside to generate a command that is send to the actuator, achieving a closed-loop controlling structure.

A host PC that can communicate with the system via UART is an optional module attached, aiming at switching the system to an alternative online control mode, which enables full-duplex data exchange between the host PC and client under MATLAB. Instead of forming the signal loop with processing all acquired data by embedded unit, it can be replaced by PC to run the control algorithm and gives command to the actuator via the micro-system which serves here as the combination of the acquisition system and motion control system, also achieving the desired closed loop.

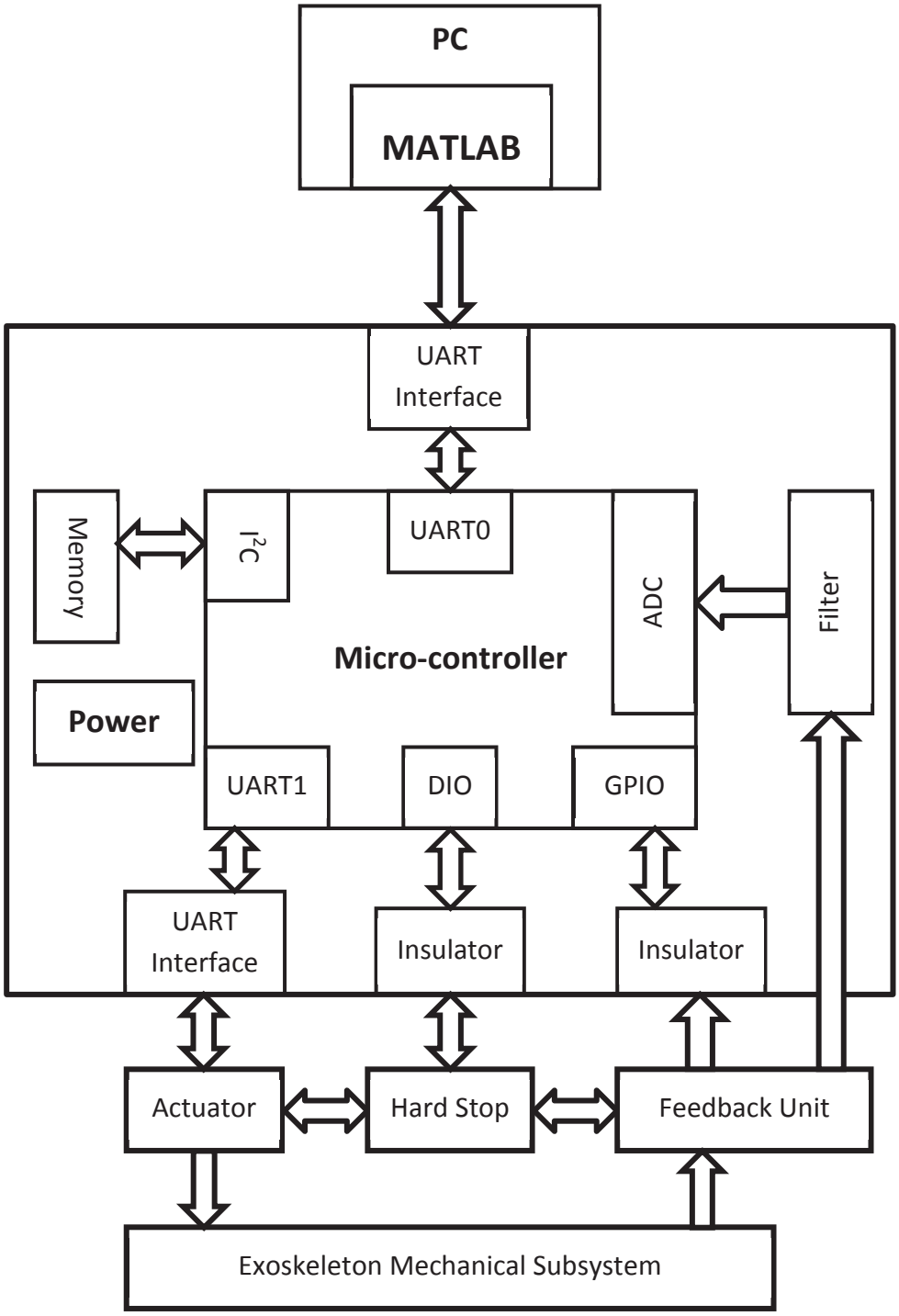

Figure 4-22 Schematic diagram of the hardware system

4.4.3 Key Interfaces Configuration

Considering the performance and function requirements, the electronic subsystem is implemented on an off-the-shelf Cortex-M3 MCU based motherboard, affiliated to the entire peripheral circuitry, some of which are optionally addressed below.

A. Main Board Unit

[10]LM3S1968 board (Appendix Figure 8-7) that supports eight 10-bit ADC channels and other interface passages can basically satisfy the need of communication for the system. Highlight lies in the built-in OLED display and the hibernation module on-board, which drive the board definitive to choose. The former that can be used to visualize the UI offers a simple means to modulate the operation and for user to choose the program, while the latter is able to maintain the non-volatile memory when losing the power.

B. Supporting Peripheral Circuitry

The circuit provides essential power supply for board and all other ICs which run in different voltage levels, ±5 V for OP, 3.3 V for sensors, and 2.5 V for reference voltage, also distinguished in digital or analog mode. LDOs matching those voltage levels are used here to stabilize the required power from external DC power supply. The 3.3 V voltage supply widely used in this circuit is differentiated by capacitors for each pin out and a LC filter separates the digital voltage which is the reference voltage for ADC from the analog one to avoid interference between analog signal and digital signal, as shown in Figure 4-23.

10-bit ADC represents a resolution of 2.9 mV per LSB based on the 3 V reference voltage level. The sensor conditioning circuits of the force and the angle are placed together with the sensors to cut down noise source in wires to be enhanced after amplification. A voltage divider circuit doubling the readable range 3.3 V to 6.6 V is connected before ADC to enlarge the sensitivity. Digital I/O ports are inherently arranged into various standards of transportation for data transmission, and the overall configuration is not detailed here.

The user interface offers a means for user to choose one proper exercise from present options. In the simulation of the control system, two modes of the control algorithm differing in compliance level were applied in three scenarios representing different running speed contained in each mode, which laid the foundation of setup to the operational mode in the electronic hardware. Same speed profiles are also established to provide more options in the compliant level. The compliance can be switched between those two levels to form operation mode together with a selected speed. Apart from the power-up switch, Reset and Return are two switches essentially set up to respond to the emergency, the former to ensure the device able to stop the device at any time, the latter to drive the device back to the initial position.

[10] For more information, please visit http://www.ti.com/tool/ek-lm3s1968.

Indicators carried by LEDs are affiliated on the way of each communication to point out successful connection. An indicator acting as an alarm is connected to a pin which reads the overflow from watchdog timer to observe the state defined from software; once the alarm being lit is caused by overflow from watchdog timer, representing abnormal state of the monitored signal. The peripheral circuitry is communicating with the main processing board with a 8-bit MCU based board, as shown in Figure 4-25, in order to access the signal flow between the MCU and the sensory units and serve as an UI.

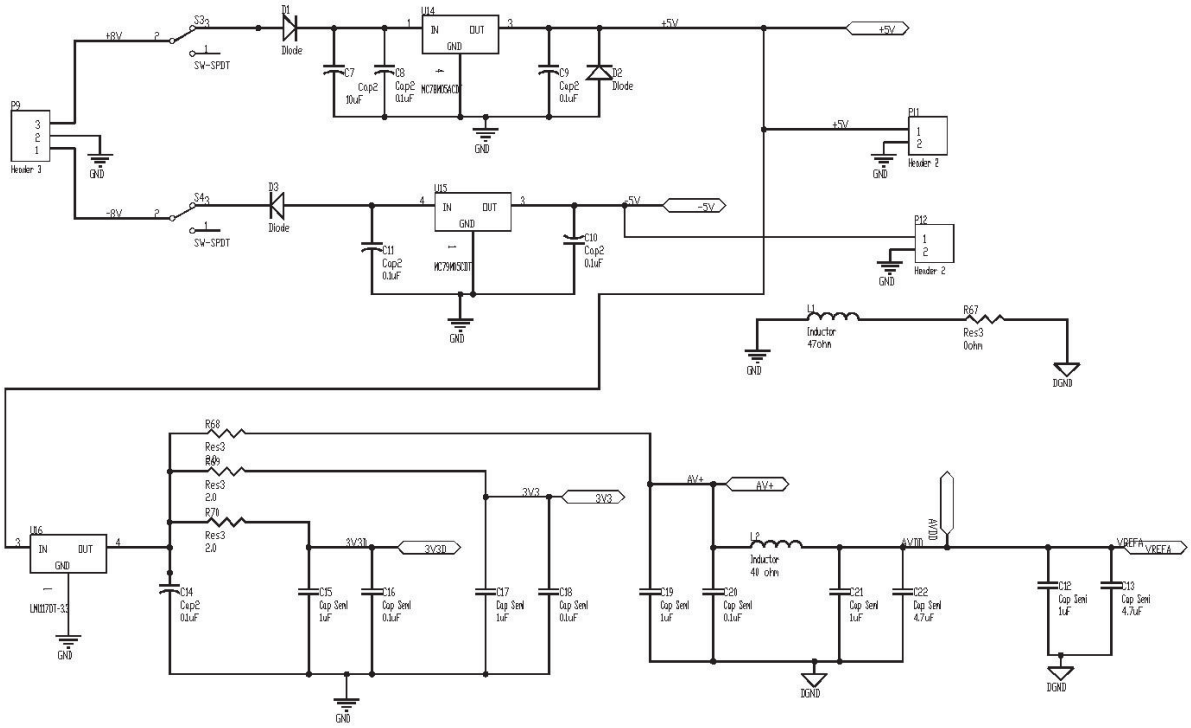

Figure 4-23 Voltage circuit of 3.3 V

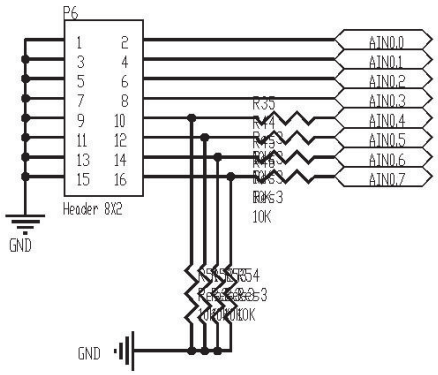

Figure 4-24 ADC circuitry

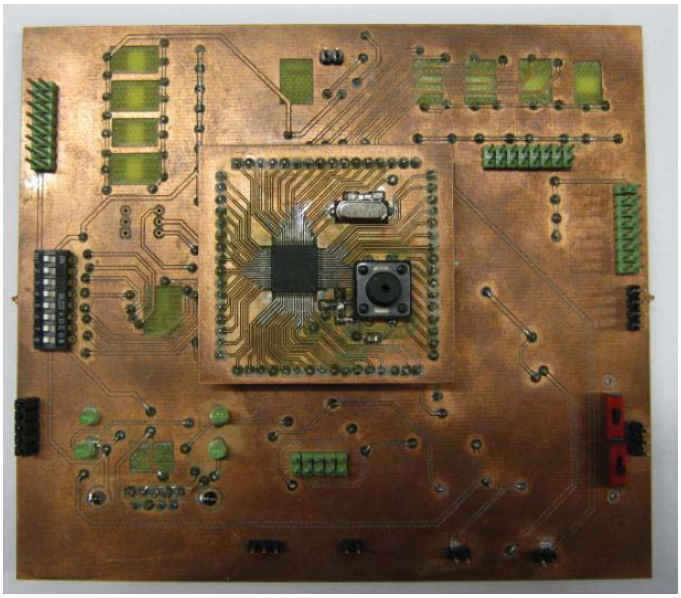

Figure 4-25 Peripheral circuitry board

4.5 Evaluation of Jaw Exoskeleton

As such a Mechatronic system, the jaw exoskeleton could fail in the structure due to many reasons, especially when the device is in operation and encounters a large amount of resistance. The device is tested under extreme conditions of loads to enhance further mechanical structures.

4.5.1 Stress and Strain Analysis

The stress analysis of the four-bar linkage system is done in the Simulation/SolidWorks test if the mechanism can withstand the forces to be applied. The starting position in the opening phase is selected as the analyzing position because it is the initially subject to the impact and inertial forces from the motor. But different scenarios of the stress analysis defined by the crank rotation angle can also be done to test the distribution of the stress at corresponding position. A total force of 200N is applied to the attaching point, and a torque of 0.3 Nm is applied to either side of the gear rigidly connected to the crank shaft to fully investigate the bearing ability of the device.

The stress analysis shows that there is no excessively large stress on the mechanism, as shown in Figure 4-26 with largest amount of the stress occurring at the coupler of the linkage which connects the attaching components and the main structure of the linkage. The corresponding deformation under the same constraints and load is shown in Figure 4-27, and the maximum displacement is concentrating on the extended components out of the main structure fixed on the helmet. As the applied force is located far away from the fixture, the whole linkage may experience larger stress and deformation, especially taking place in the coupler group of

components. From the automatic design check with a safety factor defined manually, Figure 4-28 demonstrats the places under the safety factor.

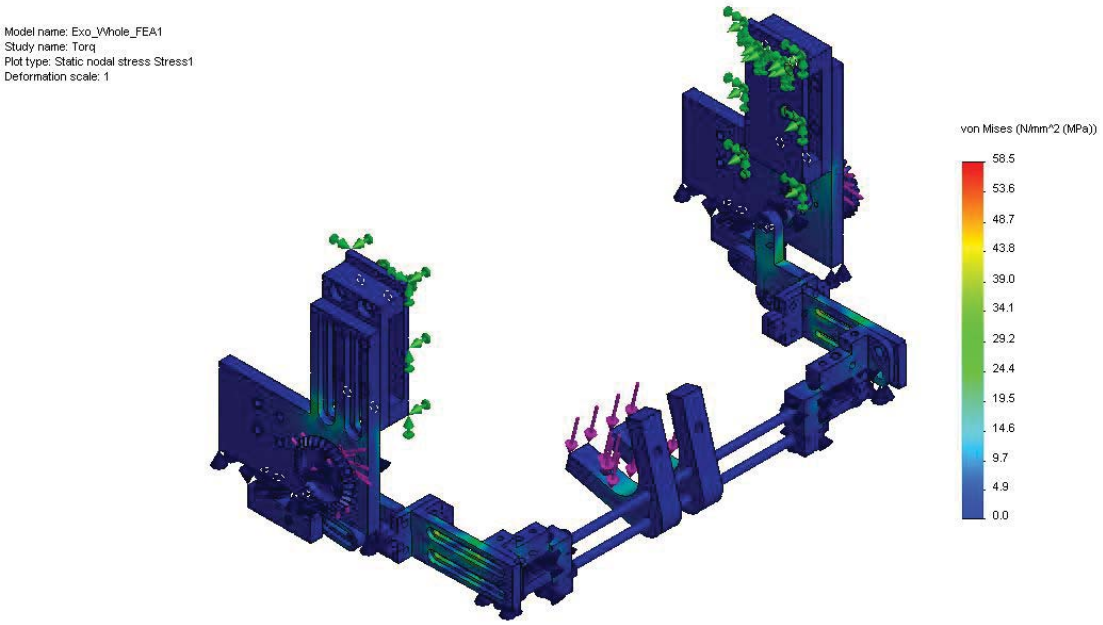

Figure 4-26 The stress analysis of the whole device

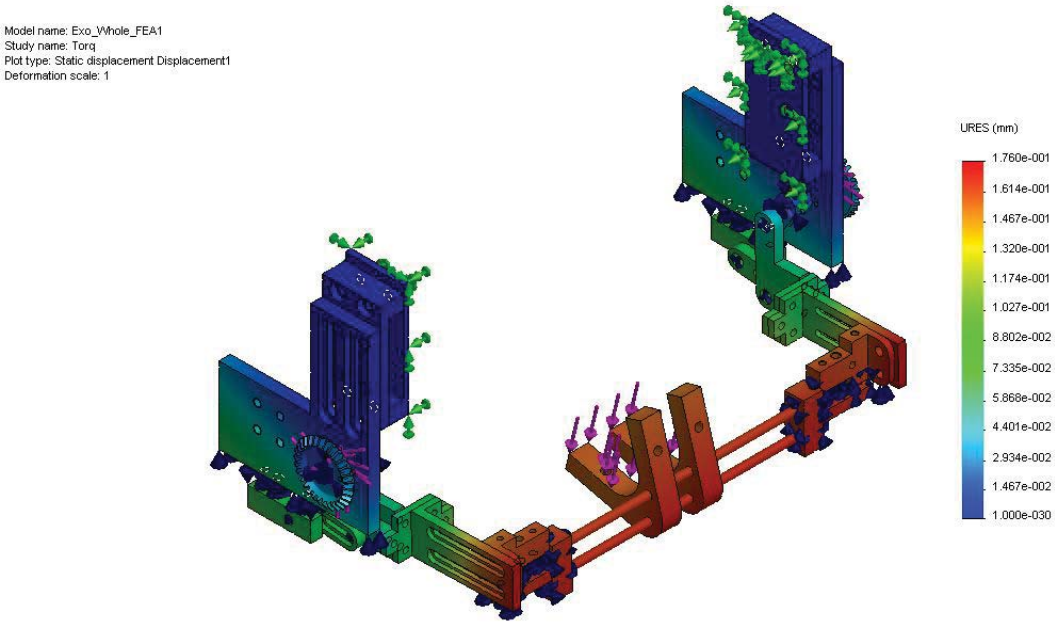

Figure 4-27 Displacement of the deformation of the whole device

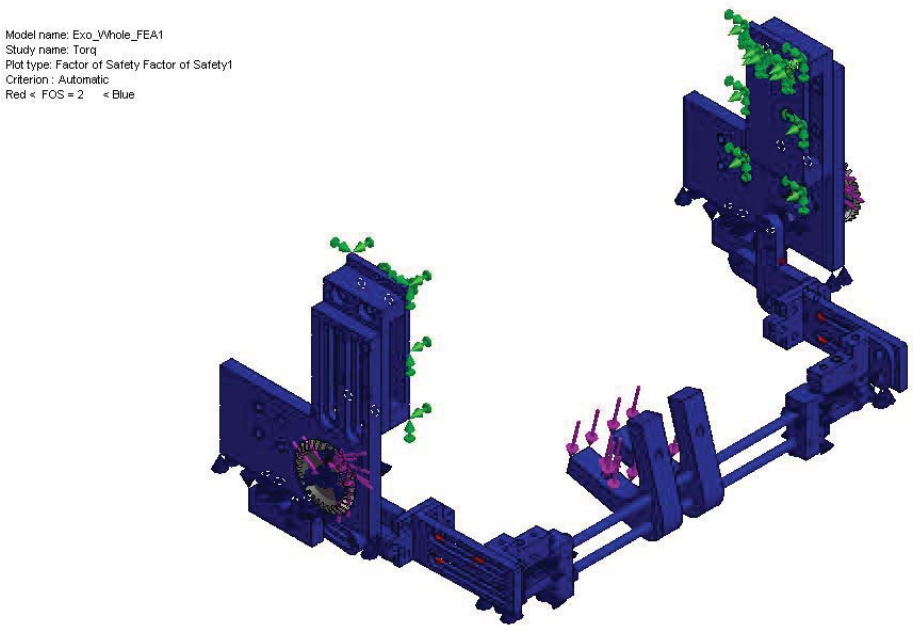

Figure 4-28 Safety factor based analysis of the whole device

Figure 4-29 to Figure 4-31 demonstrates the stress analysis, deformation analysis and placed under safety factor of the coupler group of the components, respectively. As the same scenario with the whole linkage study, the applied force is 100N on one side, instead of the rigid connector; the connecting plates are simulated with the bolt connector. The most loaded area is concentrating on the extending bar of the coupler and the connecting bar of the attachment.

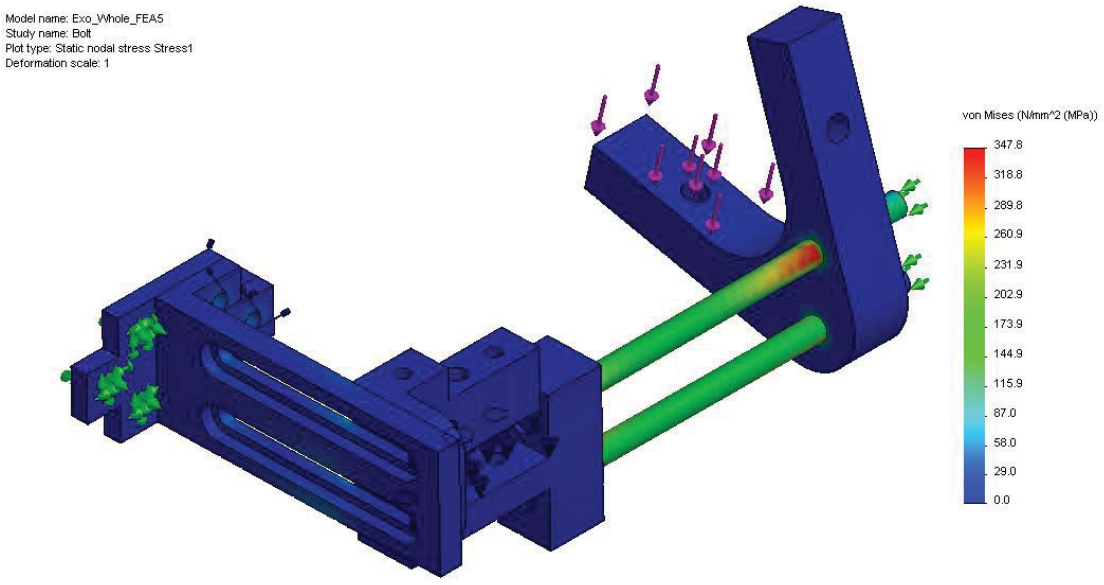

Figure 4-29 The stress analysis of the coupler group

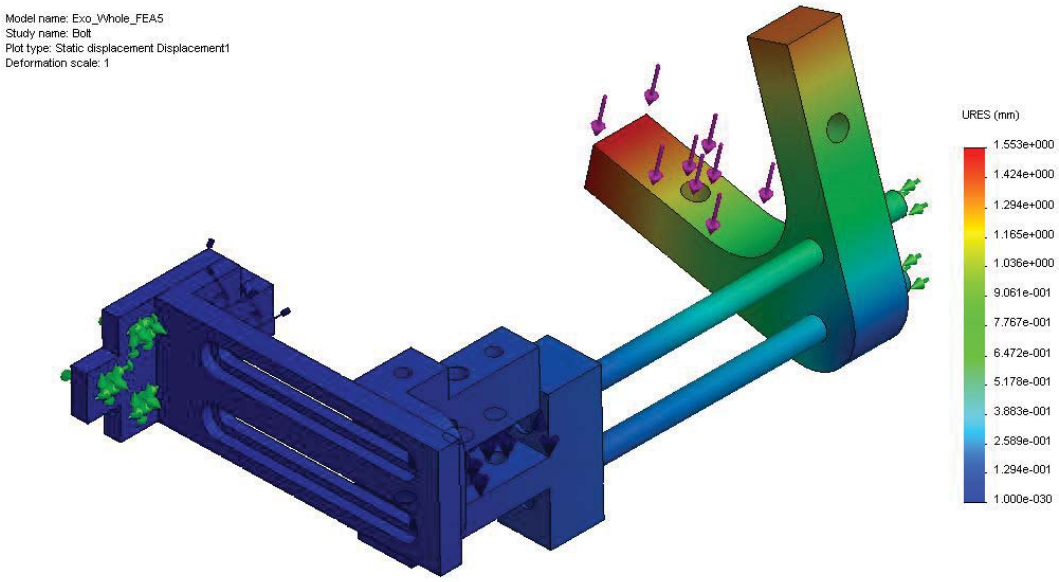

Figure 4-30 Deformation analysis of the coupler group

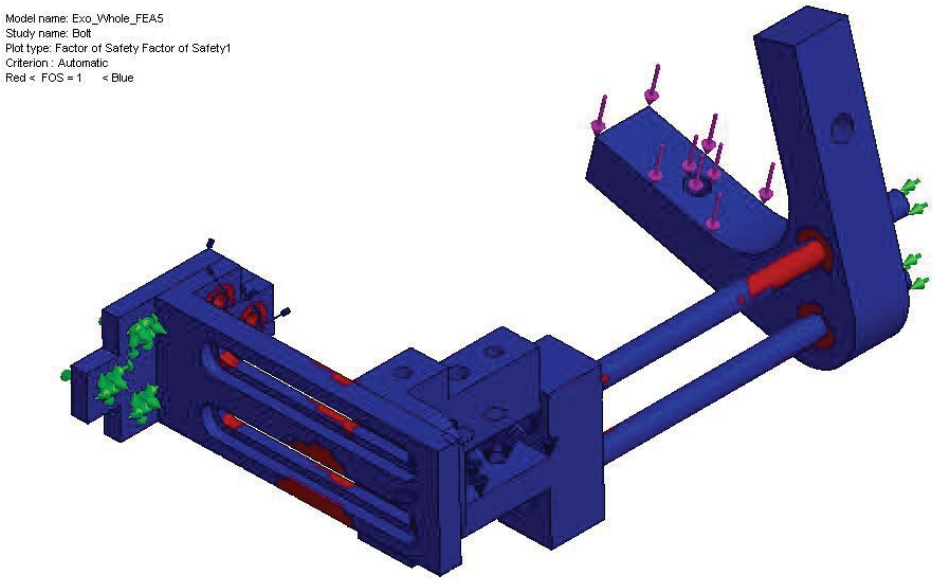

Figure 4-31 The safety factor based analysis of the whole device

4.6 Chapter Summary

The concept of the jaw exoskeleton has been materialized in this chapter under the integrated design thinking; the Mechatronic construction of the device that consists of three subsystems has been entirely built up. From the systematic perspective, the mechanism only provides the basic frame for the mechanical structure, which is required to be incorporated with the control system and the sensory units setup; oriented to this special application that lists some consideration in terms of the space and safety, the sensor installation has inflicted limitation

on its selection; all together have formed the hardware scheme of the device, which meanwhile casted the way to implement the controller in software.

The mechanical subsystem based on the four-bar linkage has been elaborated in the part design; as requested, the links have all been designed in the adjustable manner, which allows adapting to the different size and correlated motion path. Passive compliance as conceived to passively increase the driving force has also been designed, along with the force response of the spring-based unit. The electronic hardware has been built up on an evaluation board, which has been extended with peripheral circuitry to conduct communication and provide the other voltage level in this application. Each sensory unit has been detailed from the selection to operation in the usage.

The system evaluation has been conducted in two parts, i.e. the calibration of the sensors and the safety check of the mechanical structure of the device per se. The mechanism has been prototyped with the aforementioned design in terms of hardware.

Chapter 5: Dynamic Analysis and Motion Control

The device needs more compliance on mechanical parts to secure the interaction with users, which complicates the motion control of the primitive four-bar linkage in fulfillment of a predefined profile. By means of the position and force feedback that tells the immediate operating status, the device is intended to be precisely controlled in accordance with a proper motion profile while dealing with unpredictable joint resistance under a specific strategy. The inhibitory pattern of the mandible is preferably called in embodiment over the hierarchical control system, though the mechanism was designed to be supportive of the piecewise-trajectory based two-phase movement, which originally resulted from downsizing difficulties in the applying adaptability from crank rotation.

As the foundation to implement control strategy, the dynamic analysis taps off this chapter, of the entire linkage complex in the aspects of the kinematics and kinetics, which is computed over several scenarios defined in Simulink, so is the mathematical model of DC motor. The dynamic model of the linkage is formulated to unveil the kinetic energy that will be consumed with respect to a set of the predefined positional protocol. Kinematic analysis in the forward and inverse fashion of the linkage suggests the relationship established between the input crank and the output coupler, which stays important in regulating the mandible motion that is assessed on the incisor. The whole model which is further used to carry control strategies for testing purpose is validated by a series of comparisons with results from SolidWorks calculation of the 3D model applying the same scenarios.

A hierarchical strategy for motion control of the device is proposed based on a CPG neural oscillator, which generates rhythm commands to the actuator periodically. Bottom control algorithm that refers to the profile concerning a control parameter directly sent to the motor is also simulated upon the analytical model along with tuning to the optimized performance. Some typical scenarios will be prescribed to simulate the training practice in terms of the critical parameters is used to validate the control strategy, and the whole process is carried out in the electronic system as well.

5.1 Dynamics of the Linkage System

Dynamic analysis of the linkage complex starts from the kinematic calculation of the analytical model, which also consists of the gear and the compliance affiliated in the linkage. The motor fixed on the ground and the loading condition is not included. Since the attachment is

considered as part of the couplers, which are connected to construct the whole device, the two linkages symmetrically located on each side of the mandible can be simplified to the identical one. Therefore, the entire linkage device is converted into a two-dimensional planar model that is used to undergo the following computation. Meanwhile, the friction within the link is assumed of non-existence.

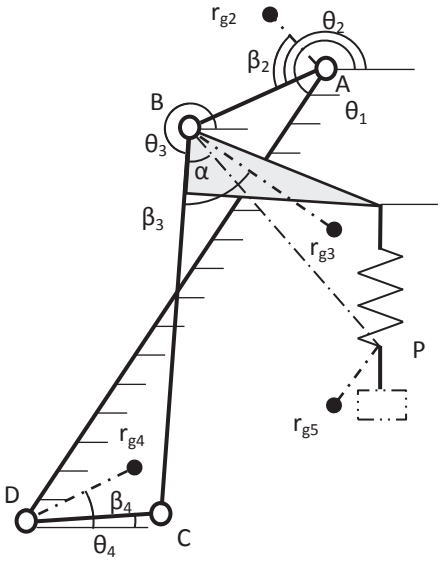

Figure 5-1 Block diagram of the entire linkage complex

Table 5-1 Representation of linkage symbols in the diagram of the four-bar linkage

	Ground	Crank	Coupler		Follower
Denotation	DA	AB	BC	BP	CD
Length	l_{DA}	l_{AB}	l_{BC}	l_{BP}	l_{CD}
Angular displacement	θ_1	θ_2	θ_3	θ_3	θ_4
Mass	N/A	m_{AB}	m_{BC}	m_{BP}	m_{CD}
Moment of inertia	N/A	I_{g2}	I_{g3}	I_{g5}	I_{g4}
Centroid radius	N/A	r_{g2}	r_{g3}	r_{g5}	r_{g4}
Centroid relative angle	N/A	β_2	β_3	β_5	β_4

The whole linkage complex is sketched in a block diagram as shown in Figure 5-1, in which all of the parts are denoted in company with the corresponding physical properties symbols given in Table 5-1. The kinematic variables of the links (coupler, follower and attachment) are derived with respect to a string of positional parameters of the crank as the input, namely $\theta_2, \dot{\theta}_2, \ddot{\theta}_2$ to represent the angular displacement, the velocity and the acceleration,

respectively, to maintain the consistency with the denotation of the mechanism design in Chapter 3. The centroid (center of the mass) of each moving part is also expressed by relative polar representation with a radius and an angle with respect to each adjacent joint.

5.1.1 Kinematic Analysis

The kinematics of the linkage system is analyzed based on the expression of the closed-loop vector in terms of the position with all involved links, as written in Eq. (5-1). $\overrightarrow{l_{CD}}$ is multiplied by itself after singled out in Eq. (5-2) to convert the vector Eq. into scalar expression in Eq. (5-3), which can be written with a transcendental Eq. in (5-4).

$$\boldsymbol{l_{AB} + l_{BC} = l_{CD} + l_{DA}} \tag{5-1}$$

$$\boldsymbol{l_{CD} \cdot l_{CD} = (l_{AB} + l_{BC} - l_{DA}) \cdot (l_{AB} + l_{BC} - l_{DA})} \tag{5-2}$$

$$l_{AB}^2 + l_{BC}^2 + l_{DA}^2 - l_{CD}^2 + 2l_{AB}l_{BC}\cos(\theta_3 - \theta_2) - 2l_{AB}l_{DA}\cos(\theta_2 - \theta_1) - 2l_{DA}l_{BC}\cos(\theta_3 - \theta_1) == 0 \tag{5-3}$$

$$A\sin\theta_3 + B\cos\theta_3 + C = 0 \tag{5-4}$$

Where:

$$\begin{cases} A = 2l_{BC}(l_{AB}\sin\theta_2 - l_{DA}\sin\theta_1) \\ B = 2l_{BC}(l_{AB}\cos\theta_2 - l_{DA}\cos\theta_1) \\ C = l_{AB}^2 + l_{BC}^2 + l_{DA}^2 - l_{CD}^2 - 2l_{DA}l_{AB}\cos(\theta_2 - \theta_1) \end{cases}$$

Then θ_3 can be solved via Eq. (5-5) in Eq. (5-6). With the algebraic expression in Eq. (5-7), θ_4 can be solved in Eq. (5-8).

$$\tan\frac{\theta_3}{2} = \frac{\mathrm{A} \pm \sqrt{A^2 + B^2 - C^2}}{B - C} \tag{5-5}$$

$$\theta_3 = 2\tan^{-1}\frac{\mathrm{A} \pm \sqrt{A^2 + B^2 - C^2}}{B - C} \tag{5-6}$$

$$\begin{cases} l_{AB}\cos\theta_2 + l_{BC}\cos\theta_3 = l_{CD}\cos\theta_4 + l_{DA}\cos\theta_1 \\ l_{AB}\sin\theta_2 + l_{BC}\sin\theta_3 = l_{CD}\sin\theta_4 + l_{DA}\sin\theta_1 \end{cases} \tag{5-7}$$

$$\theta_4 = \sin^{-1}\frac{l_{AB}\sin\theta_2 + l_{BC}\sin\theta_3 - l_{DA}\sin\theta_1}{l_{CD}} \tag{5-8}$$

So, the position of any point P on the coupler can be expressed in Eq. (5-9).

$$\begin{cases} x_P = l_{AB}\cos\theta_2 + l_{BP}\cos(\theta_3 + \alpha) \\ y_P = l_{AB}\sin\theta_2 + l_{BP}\sin(\theta_3 + \alpha) \end{cases} \tag{5-9}$$

The vector loop Eq. (5-1) is then differentiated into Eq. (5-10) to derive the angular velocity of each link, as given in Eq. (5-11) and Eq. (5-13). So the velocity on the coupler point P can be written in Eq. (5-14) along the decomposed direction.

$$\begin{cases}\dot{\theta}_4 l_{CD}\boldsymbol{e}_{CD}^t = \dot{\theta}_2 l_{AB}\boldsymbol{e}_{AB}^t + \dot{\theta}_3 l_{BC}\boldsymbol{e}_{BC}^t \\ 0 = \dot{\theta}_2 l_{AB}\boldsymbol{e}_{AB}^t\boldsymbol{e}_{CD} + \dot{\theta}_3 l_{BC}\boldsymbol{e}_{BC}^t\boldsymbol{e}_{CD}\end{cases} \tag{5-10}$$

$$\dot{\theta}_3 = \frac{\dot{\theta}_2 l_{AB}\sin(\theta_2 - \theta_4)}{l_{BC}\sin(\theta_3 - \theta_4)} \tag{5-11}$$

$$\dot{\theta}_4 l_{CD}\boldsymbol{e}_{CD}^t\boldsymbol{e}_{AB} = \dot{\theta}_3 l_{BC}\boldsymbol{e}_{BC}^t\boldsymbol{e}_{AB} \tag{5-12}$$

$$\dot{\theta}_4 = \frac{\dot{\theta}_3 l_{BC}\sin(\theta_3 - \theta_2)}{l_{CD}\sin(\theta_4 - \theta_2)} \tag{5-13}$$

$$\begin{bmatrix} v_{Px} \\ v_{Py}\end{bmatrix} = \begin{bmatrix}\dot{x}_P \\ \dot{y}_P\end{bmatrix} = \begin{bmatrix} -l_{AB}\sin\theta_2 & -l_{BP}\sin(\theta_3+\alpha) \\ l_{AB}\cos\theta_2 & l_{BP}\cos(\theta_3+\alpha)\end{bmatrix}\begin{bmatrix}\dot{\theta}_2 \\ \dot{\theta}_3\end{bmatrix} \tag{5-14}$$

The angular acceleration of the links can be obtained by differentiating the velocity Eq. (5-10), as written in (5-15) and (5-16); and the concerned item $\ddot{\theta}_3$ can be expressed in Eq. (5-17). The acceleration of the point P on the coupler can be written in Eq. (5-19).

$$l_{CD}\dot{\theta}_4^2\boldsymbol{e}_{CD}^n + l_{CD}\ddot{\theta}_4\boldsymbol{e}_{CD}^t = l_{AB}\dot{\theta}_2^2\boldsymbol{e}_{AB}^n + l_{AB}\ddot{\theta}_2\boldsymbol{e}_{AB}^t + l_{BC}\dot{\theta}_3^2\boldsymbol{e}_{BC}^n + l_{BC}\ddot{\theta}_3\boldsymbol{e}_{BC}^t \tag{5-15}$$

$$\begin{aligned} &l_{CD}\dot{\theta}_4^2\boldsymbol{e}_{CD}^n\boldsymbol{e}_{CD} + l_{CD}\ddot{\theta}_4\boldsymbol{e}_{CD}^t\boldsymbol{e}_{CD} = \\ &l_{AB}\dot{\theta}_2^2\boldsymbol{e}_{AB}^n\boldsymbol{e}_{CD} + l_{AB}\ddot{\theta}_2\boldsymbol{e}_{AB}^t\boldsymbol{e}_{CD} + l_{BC}\dot{\theta}_3^2\boldsymbol{e}_{BC}^n\boldsymbol{e}_{CD} + l_{BC}\ddot{\theta}_3\boldsymbol{e}_{BC}^t\boldsymbol{e}_{CD}\end{aligned} \tag{5-16}$$

$$\ddot{\theta}_3 = \frac{l_{CD}\dot{\theta}_4^2 - l_{AB}\dot{\theta}_2^2\cos(\theta_2-\theta_4) - l_{BC}\dot{\theta}_3^2\cos(\theta_3-\theta_4) - \ddot{\theta}_2 l_{AB}\sin(\theta_2-\theta_4)}{l_{BC}\sin(\theta_3-\theta_4)} \tag{5-17}$$

$$\ddot{\theta}_4 = \frac{-l_{BC}\dot{\theta}_3^2 - l_{AB}\dot{\theta}_2^2\cos(\theta_3-\theta_4) - l_{CD}\dot{\theta}_4^2\cos(\theta_3-\theta_4) + \ddot{\theta}_2 l_{AB}\sin(\theta_3-\theta_3)}{l_{CD}\sin(\theta_3-\theta_4)} \tag{5-18}$$

$$\begin{cases} a_{Px} = -\ddot{\theta}_2 l_{AB}\sin\theta_2 - \dot{\theta}_2^2 l_{AB}\cos\theta_2 - \ddot{\theta}_3 l_{BP}\sin(\theta_3+\alpha) - \dot{\theta}_3^2 l_{BP}\cos(\theta_3+\alpha) \\ a_{Py} = \ddot{\theta}_2 l_{AB}\cos\theta_2 - \dot{\theta}_2^2 l_{AB}\sin\theta_2 + \ddot{\theta}_3 l_{BP}\,cos(\theta_3+\alpha) - \dot{\theta}_3^2 l_{BP}\sin(\theta_3+\alpha)\end{cases} \tag{5-19}$$

Since the inverse kinematics of the linkage can easily be derived to Eq. (5-20) by specifying the variable as the input in the universal expression of the linkage position in (5-3), the concerned set of variables $\theta_2, \dot{\theta}_2, \ddot{\theta}_2$ that specifies the actuation can be derived with respect to the known parameters of $\theta_3, \dot{\theta}_3, \ddot{\theta}_3$, in Eq. (5-22) (5-23) and (5-24).

$$A'\sin\theta_2 + B'\cos\theta_2 + C' = 0 \tag{5-20}$$

$$\tan\frac{\theta_2}{2} = \frac{\mathrm{A}' \pm \sqrt{A'^2 + B'^2 - C'^2}}{B' - C'} \tag{5-21}$$

Where:

$$\begin{cases} A' = 2l_{AB}l_{BC}\sin\theta_3 \\ B' = 2l_{AB}(l_{BC}\cos\theta_3 - l_{DA}) \\ C' = l_{AB}^2 + l_{BC}^2 + l_{DA}^2 - l_{CD}^2 - 2l_{DA}l_{BC}\cos\theta_3\end{cases}$$

$$\theta_2 = 2\tan^{-1}\frac{\mathrm{A}' \pm \sqrt{A'^2 + B'^2 - C'^2}}{B' - C'} \tag{5-22}$$

$$\dot{\theta}_2 = \frac{\dot{\theta}_3 l_{BC} \sin(\theta_3 - \theta_4)}{l_{AB} \sin(\theta_2 - \theta_4)} \quad (5\text{-}23)$$

$$\ddot{\theta}_2 = \frac{l_{CD}\dot{\theta}_4^2 - l_{AB}\dot{\theta}_2^2 \cos(\theta_2 - \theta_4) - l_{BC}\dot{\theta}_3^2 \cos(\theta_3 - \theta_4) - l_{BC}\ddot{\theta}_3 \sin(\theta_3 - \theta_4)}{l_{AB} \sin(\theta_2 - \theta_4)} \quad (5\text{-}24)$$

5.1.2 Dynamic Analysis

The entire mechanism is partitioned into three units to carry out the dynamic study, i.e. the linkage complex, the spring unit, and the gear combination, each of which is analyzed independently. The Lagrange method in (5-25) is used here to formulate the dynamic performance of the mechanism.

$$\frac{d}{dt}\left(\frac{\partial T}{\partial \dot{\theta}_j}\right) - \frac{\partial T}{\partial \theta_j} = Q_j \quad (5\text{-}25)$$

Where:

$T = \sum_{i=1}^{n} \frac{1}{2} m_i \left(\dot{x}_{gi}^2 + \dot{y}_{gi}^2\right) + \sum_{i=1}^{n} \frac{1}{2} I_{gi} \dot{\theta}_i^2$ is the total kinetic energy of a mechanism;

$Q_j = \sum_{i=1}^{n} F_i \frac{\partial r_i}{\partial q_j}$ is the generalized force exerted by all of the external force.

By applying Lagrange's equation into the linkage mechanism, the external load that might be the resistance during mouth opening can be generalized to fit the form in (5-26); and the dynamics of the entire system in Lagrange's can be expressed in Eq. (5-27), in which the left side represents the kinetic energy of totally five parts and the right gives the summation of the force on the mechanism. The torque required from the actuation can be written in (5-28).

$$\tau_{load} = F_P \frac{\partial P}{\partial \theta_2} = F_{Px} \frac{\partial x_P}{\partial \theta_2} + F_{Py} \frac{\partial y_P}{\partial \theta_2} \quad (5\text{-}26)$$

$$\sum_{i=2}^{4} \left\{ m_i \left(\ddot{x}_{gi} \frac{\partial \dot{x}_{gi}}{\partial \dot{\theta}_2} + \ddot{y}_{gi} \frac{\partial \dot{y}_{gi}}{\partial \dot{\theta}_2} \right) + I_{gi} \ddot{\theta}_i \frac{\partial \dot{\theta}_i}{\partial \dot{\theta}_2} \right\} = \tau_{act} - \tau_{load} - g \sum_{i=2}^{4} m_i \frac{\partial \dot{y}_{gi}}{\partial \dot{\theta}_2} \quad (5\text{-}27)$$

$$\tau_{act} = \sum_{i=2}^{4} \left\{ m_i \left(\ddot{x}_{gi} \frac{\partial \dot{x}_{gi}}{\partial \dot{\theta}_2} + \ddot{y}_{gi} \frac{\partial \dot{y}_{gi}}{\partial \dot{\theta}_2} \right) + I_{gi} \ddot{\theta}_i \frac{\partial \dot{\theta}_i}{\partial \dot{\theta}_2} \right\} + g \sum_{i=2}^{4} m_i \frac{\partial \dot{y}_{gi}}{\partial \dot{\theta}_2} + \tau_{load} \quad (5\text{-}28)$$

Where:

$m_i,\ i = 2, \cdots, 4$ are the mass of the link i;

$\left(x_{gi}, y_{gi}\right), i = 2, \cdots, 4$ are the coordinates of the centroid (center of mass) of the link i with respect to the generalized coordinate θ_1 in the linkage.

The acceleration of the centroid of each link is separately derived in Eq. (5-29) to (5-31).

$$\begin{cases} \ddot{x}_{g2} = -r_{g2}\left[\ddot{\theta}_2 \sin(\theta_2 + \beta_2) + \dot{\theta}_2^2 \cos(\theta_2 + \beta_2)\right] \\ \ddot{y}_{g2} = r_{g2}\left[\ddot{\theta}_2 \cos(\theta_2 + \beta_2) - \dot{\theta}_2^2 \sin(\theta_2 + \beta_2)\right] \end{cases} \tag{5-29}$$

$$\begin{cases} \ddot{x}_{g3} = -l_{AB}\left(\ddot{\theta}_2 \sin\theta_2 + \dot{\theta}_2^2 \cos\theta_2\right) - r_{g3}\left[\ddot{\theta}_3 \sin(\theta_3 + \beta_3) + \dot{\theta}_3^2 \cos(\theta_3 + \beta_3)\right] \\ \ddot{y}_{g3} = l_{AB}\left(\ddot{\theta}_2 \cos\theta_2 - \dot{\theta}_2^2 \sin\theta_2\right) + r_{g3}\left[\ddot{\theta}_3 \cos(\theta_3 + \beta_3) - \dot{\theta}_3^2 \sin(\theta_3 + \beta_3)\right] \end{cases} \tag{5-30}$$

$$\begin{cases} \ddot{x}_{g4} = -r_{g4}\left[\ddot{\theta}_4 \sin(\theta_4 + \beta_4) + \dot{\theta}_4^2 \cos(\theta_4 + \beta_4)\right] \\ \ddot{y}_{g4} = r_{g4}\left[\ddot{\theta}_4 \cos(\theta_4 + \beta_4) - \dot{\theta}_4^2 \sin(\theta_4 + \beta_4)\right] \end{cases} \tag{5-31}$$

All of the partial derivatives are given in Eq. (5-32) to (5-35).

$$\begin{cases} \dfrac{\partial\dot{\theta}_3}{\partial\dot{\theta}_2} = \dfrac{l_{AB}\sin(\theta_2 - \theta_4)}{l_{BC}\sin(\theta_4 - \theta_3)} \\ \dfrac{\partial\dot{\theta}_4}{\partial\dot{\theta}_2} = \dfrac{l_{AB}\sin(\theta_2 - \theta_3)}{l_{CD}\sin(\theta_4 - \theta_3)} \end{cases} \tag{5-32}$$

$$\begin{cases} \dfrac{\partial\dot{x}_{g2}}{\partial\dot{\theta}_2} = -r_{g2}\sin(\theta_2 + \beta_2) \\ \dfrac{\partial\dot{y}_{g2}}{\partial\dot{\theta}_2} = r_{g2}\cos(\theta_2 + \beta_2) \end{cases} \tag{5-33}$$

$$\begin{cases} \dfrac{\partial\dot{x}_{g3}}{\partial\dot{\theta}_2} = -l_{AB}\sin\theta_2 - r_{g3}\dfrac{\partial\dot{\theta}_3}{\partial\dot{\theta}_2}\sin(\theta_3 + \beta_3) \\ \dfrac{\partial\dot{y}_{g3}}{\partial\dot{\theta}_2} = l_{AB}\cos\theta_2 + r_{g3}\dfrac{\partial\dot{\theta}_3}{\partial\dot{\theta}_2}\cos(\theta_3 + \beta_3) \end{cases} \tag{5-34}$$

$$\begin{cases} \dfrac{\partial\dot{x}_{g4}}{\partial\dot{\theta}_2} = -r_{g4}\dfrac{\partial\dot{\theta}_4}{\partial\dot{\theta}_2}\sin(\theta_4 + \beta_4) \\ \dfrac{\partial\dot{y}_{g4}}{\partial\dot{\theta}_2} = r_{g4}\dfrac{\partial\dot{\theta}_4}{\partial\dot{\theta}_2}\cos(\theta_4 + \beta_4) \end{cases} \tag{5-35}$$

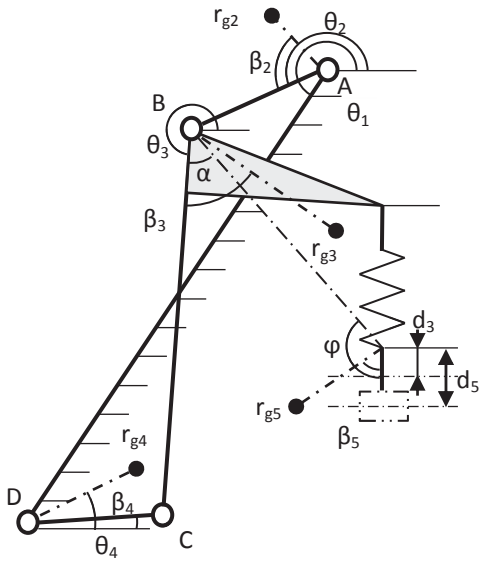

Figure 5-2 Attachment displacement during spring stretch

Eq. (5-27) formulates the dynamic performance of the entire mechanism during the normal movement; one special circumstance that the spring unit inside the coupler is triggered will incur the supplement of the potential energy from the spring added into the dynamic equation. If the spring is deformed by a distance of d ($d = d_5 - d_3$; d_3 is the distance without deformation shown in Figure 5-2) in the opening/closing stage, the potential energy of this spring can be calculated in (5-36). The attachment is stripped separately into a complex directly connecting the spring. The dynamics considering spring function in Lagrange's method can be expressed in Eq. (5-37), and the required torque from actuation is given in (5-38). The position of the attachment point and the centroid of the attachment can be respectively written in Eq. (5-39) and (5-40). Since the deformation d is rather small compared with the other items, partial items used in the dynamic equation will ignore the distance variation induced by the spring deformation, as given in (5-42) and (5-43).

$$\tau_{spr} = \frac{1}{2}kd^2 \tag{5-36}$$

Where k is the spring stiffness, and the spring is assumed to have no deformation initially.

$$\sum_{i=2}^{5}\left\{m_i\left(\ddot{x}_{gi}\frac{\partial\dot{x}_{gi}}{\partial\dot{\theta}_2}+\ddot{y}_{gi}\frac{\partial\dot{y}_{gi}}{\partial\dot{\theta}_2}\right)+I_{gi}\ddot{\theta}_i\frac{\partial\dot{\theta}_i}{\partial\dot{\theta}_2}\right\}=\tau_{act}-\tau_{load}-g\sum_{i=2}^{4}m_i\frac{\partial\dot{y}_{gi}}{\partial\dot{\theta}_2}-\frac{\partial\tau_{spr}}{\partial\theta_2} \tag{5-37}$$

$$\tau_{act}=\sum_{i=2}^{5}\left\{m_i\left(\ddot{x}_{gi}\frac{\partial\dot{x}_{gi}}{\partial\dot{\theta}_2}+\ddot{y}_{gi}\frac{\partial\dot{y}_{gi}}{\partial\dot{\theta}_2}\right)+I_{gi}\ddot{\theta}_i\frac{\partial\dot{\theta}_i}{\partial\dot{\theta}_2}\right\}+g\sum_{i=2}^{4}m_i\frac{\partial\dot{y}_{gi}}{\partial\dot{\theta}_2}+\tau_{load}+\frac{\partial\tau_{spr}}{\partial\theta_2} \tag{5-38}$$

Where $m_5, (x_{g5}, y_{g5})$ denotes the mass of the attachment and the coordinates of the centroid; and $\frac{\partial\tau_{spr}}{\partial\theta_2} = kd\frac{\partial d}{\partial\theta_2}$

$$\begin{cases} x_5 = l_{AB}\cos\theta_2 + l_{BP}\cos(\theta_3+\alpha) + d\cos(\theta_3+\alpha+\varphi) \\ y_5 = l_{AB}\sin\theta_2 + l_{BP}\sin(\theta_3+\alpha) + d\sin(\theta_3+\alpha+\varphi) \end{cases} \tag{5-39}$$

$$\begin{cases} x_{g5} = l_{AB}\cos\theta_2 + l_{BP}\cos(\theta_3+\alpha) + r_{g5}\cos(\theta_3+\alpha+\beta_5) \\ y_{g5} = l_{AB}\sin\theta_2 + l_{BP}\sin(\theta_3+\alpha) + r_{g5}\sin(\theta_3+\alpha+\beta_5) \end{cases} \tag{5-40}$$

$$\begin{cases} \ddot{x}_{g5} = \ddot{x}_{g3} - r_{g5}\left[\ddot{\theta}_3\sin(\theta_3+\alpha+\beta_5) + \dot{\theta}_3^2\cos(\theta_3+\alpha+\beta_5)\right] \\ \ddot{y}_{g5} = \ddot{y}_{g5} + r_{g5}\left[\ddot{\theta}_3\cos(\theta_3+\alpha+\beta_5) - \dot{\theta}_3^2\sin(\theta_3+\alpha+\beta_5)\right] \end{cases} \tag{5-41}$$

$$\begin{cases} \frac{\partial\dot{x}_5}{\partial\dot{\theta}_2} = -l_{AB}\sin\theta_2 - r_{g3}\frac{\partial\dot{\theta}_3}{\partial\dot{\theta}_2}\sin(\theta_3+\beta_3) \\ \frac{\partial\dot{y}_5}{\partial\dot{\theta}_2} = l_{AB}\cos\theta_2 + r_{g3}\frac{\partial\dot{\theta}_3}{\partial\dot{\theta}_2}\cos(\theta_3+\beta_3) \end{cases} \tag{5-42}$$

$$\begin{cases} \frac{\partial\dot{x}_{g5}}{\partial\dot{\theta}_2} = -l_{AB}\sin\theta_2 - r_{g3}\frac{\partial\dot{\theta}_3}{\partial\dot{\theta}_2}\sin(\theta_3+\beta_3) - r_{g5}\frac{\partial\dot{x}_5}{\partial\dot{\theta}_2}\sin(\theta_3+\alpha+\beta_5) \\ \frac{\partial\dot{y}_{g5}}{\partial\dot{\theta}_2} = l_{AB}\cos\theta_2 + r_{g3}\frac{\partial\dot{\theta}_3}{\partial\dot{\theta}_2}\cos(\theta_3+\beta_3) + r_{g5}\frac{\partial\dot{y}_5}{\partial\dot{\theta}_2}\cos(\theta_3+\alpha+\beta_5) \end{cases} \tag{5-43}$$

The gear combination used in the device has four-level reductions with the total ratio of 98; the absolute reduction ratio at each level is 12/48, 11/49, 12/33, and 14/28. The whole gear train bridging the motor and the linkage is treated as one equivalent gear pair to calculate the dynamic relationship before and after the gear system, as shown in Figure 5-3. If the efficiency of each gear pair is assumed to be ideal, the load torque T_{load} that is claimed of the mechanism can be converted to an equivalent torque T_e directly loaded on the motor shaft, as calculated in (5-44); and the total amount of the equivalent load T_{me} also includes the gear reduction system to be combined to the motor shaft in (5-45).

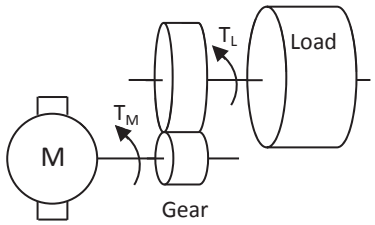

Figure 5-3 Gear in equivalent reduction

$$T_{le} = \left(\frac{12}{48} \cdot \frac{11}{49} \cdot \frac{12}{33} \cdot \frac{14}{28}\right) \cdot T_{load} \tag{5-44}$$

$$T_{me} = T_{le} + J_{ge}\ddot{\theta} \tag{5-45}$$

Where J_{ge} is the equivalent gear inertia accumulated on the motor shaft;

$$J_{ge} = J_1 + J_2\left(\frac{12}{48}\right)^2 + J_3\left(\frac{12}{48} \cdot \frac{11}{49}\right)^2 + J_4\left(\frac{12}{48} \cdot \frac{11}{49} \cdot \frac{12}{33}\right)^2 + J_5\left(\frac{12}{48} \cdot \frac{11}{49} \cdot \frac{12}{33} \cdot \frac{14}{28}\right)^2.$$

5.1.3 Validation of the Dynamic Analysis

The dynamic analysis of the entire mechanism assumes the jaw motion is carried out on the same plane where the linkage is located, which deviates from the actual scenario of planar movement on parallel planes, so the validation of the analytical process is necessitated. The analytical calculation is undertaken by valuing the variables to produce meaningful results, which are compared with results obtained from dynamic simulations in SolidWorks under the same specified input profile. Physical properties such as mass and moment of inertia are acquired from each SolidWorks part, and both structural parameters are identical as well, as given in Table 5-2.

The input profile is specified to the angular velocity of the crank, which can separately integrate and differentiate to offer the angular displacement and the angular acceleration, and accommodate the specification of the speed (rotary motor) in SolidWorks. To conveniently represent the input profile, the angular velocity of the crank is straightly given,

rather than via the inverse kinematic calculation with respect to the coupler. For one cycle, the profile for the closing phase is completely identical with that given for the opening phase with the opposite direction; and in a single phase, the crank angular velocity is specified to a constant of 1.05 rad/s, according to the general jaw movement that is completed within 2s; the starting and the ending section in one phase smoothes out the velocity variation in a constant acceleration of the same value but with respectively positive and negative direction, approximately 2.62 rad/s^2. The movement for comparison is undertaken for two cycles in both SolidWorks Simulation and the analytical calculations. The velocity profile is expressed in Eq. (5-46) and illustrated in Figure 5-4.

Table 5-2 Values of all linkage parameters

		Ground	Crank	Coupler		Follower
Denotation	Unit	DA	AB	BC	BP	CD
Length	mm	46.74	10	32	82.28	16
Angular displacement	deg	235.1	θ_2	θ_3	61.1	θ_4
Mass	g	N/A	1.51	80.54	57.78	2.29
Moment of inertia	gmm^2	N/A	54	41328.6	13550.59	135.53
Centroid radius	mm	N/A	5.81	55.33	63.9	8.13
Centroid relative angle	deg	N/A	0	53.5	55.3	0

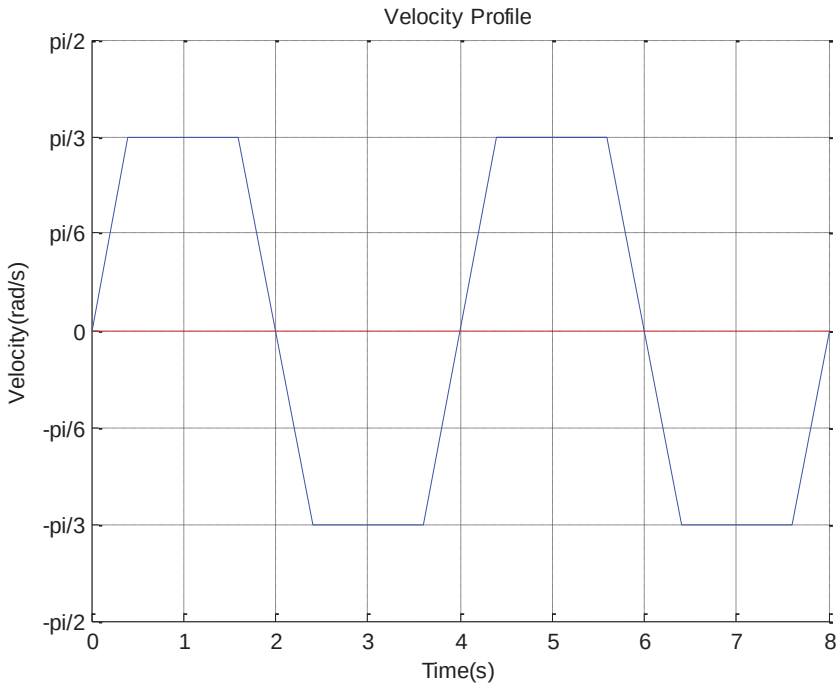

Figure 5-4 Motion profile of the crank as the input

$$\dot{\theta}_2 = \begin{cases} 5\pi/6\, t, & 2n \le t < 2n + 0.4 \\ \pi/3\,, & 2n + 0.4 \le t < 2(n+1) - 0.4 \\ \pi/3 - 5\pi/6\, t, & 2n + 1.6 \le t < 2(n+1) \end{cases} \quad (5\text{-}46)$$

Where: n is a single phase in one cycle, totally 4 phases included in the simulation.

Kinematic variables are primarily concerned, such as the angular displacement, the angular velocity and the angular acceleration of all of the links; results of all items acquired from both methods are plotted in the same figure for comparison purpose. Under the same input, Figure 5-5, Figure 5-6, Figure 5-7, and Figure 5-8 illustrate the angular displacement and the angular velocity of the coupler and the follower with respect to the time, respectively; the ones in SolidWorks give the magnitude only, which differs in the direction from the analytical results.

The angular accelerations of all three links exhibit jerks in SolidWorks results at the points of abrupt changes, in comparison with the smooth curves by analytical calculation as plotted in Figure 5-9, Figure 5-10, and Figure 5-11, which can be ascribed to an infinite jerk prescribed by dynamic solver in SolidWorks; otherwise sections of both results are matched without discrepancy.

The linear displacement of the concerned point on the coupler is not present in plot, whereas the velocities at this point in both horizontal and vertical directions that are given in Figure 5-12 and Figure 5-13 display a relative consistency between two results.

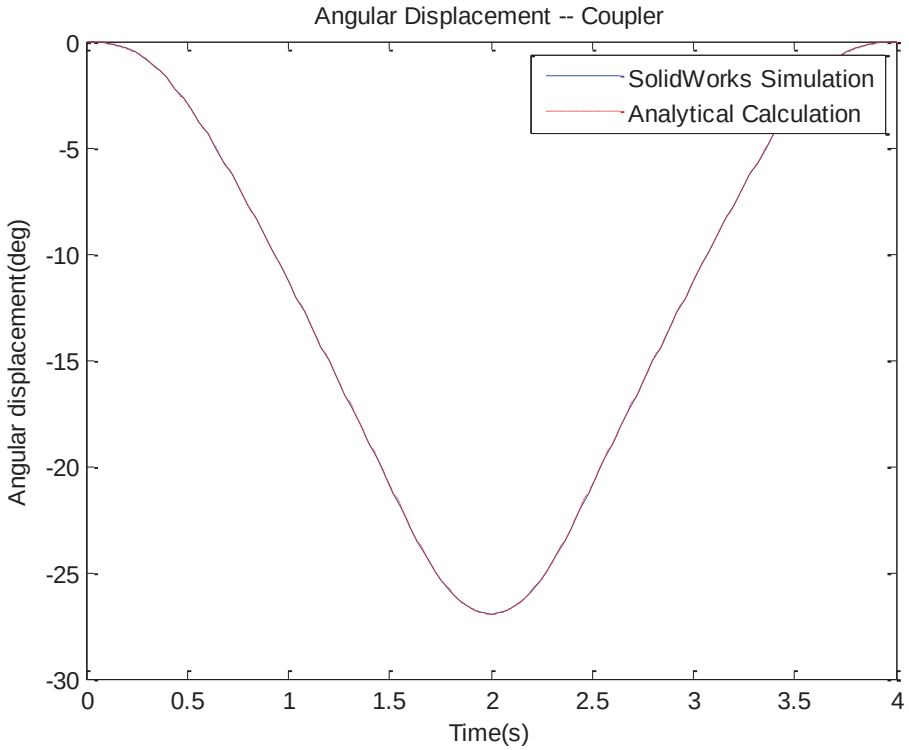

Figure 5-5 Angular displacement of the coupler

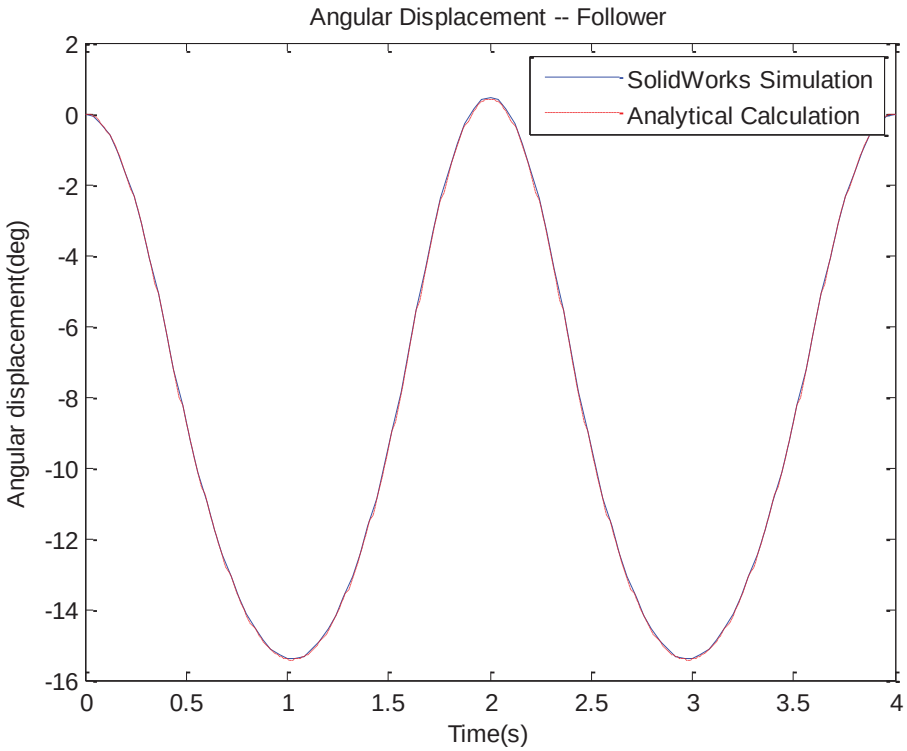

Figure 5-6 Angular displacement of the follower

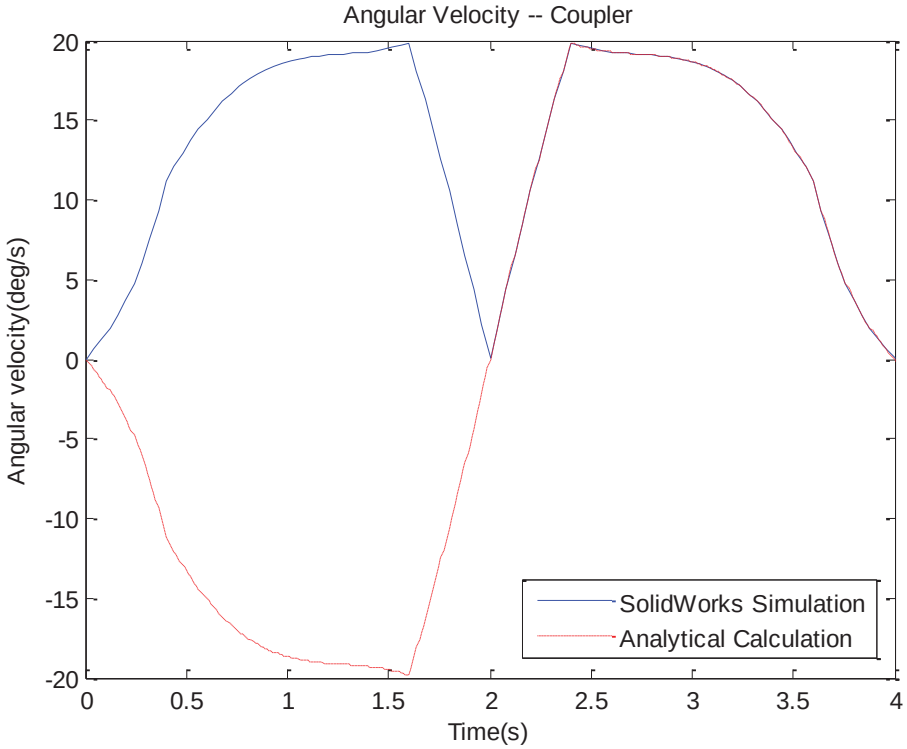

Figure 5-7 Angular velocity of the coupler

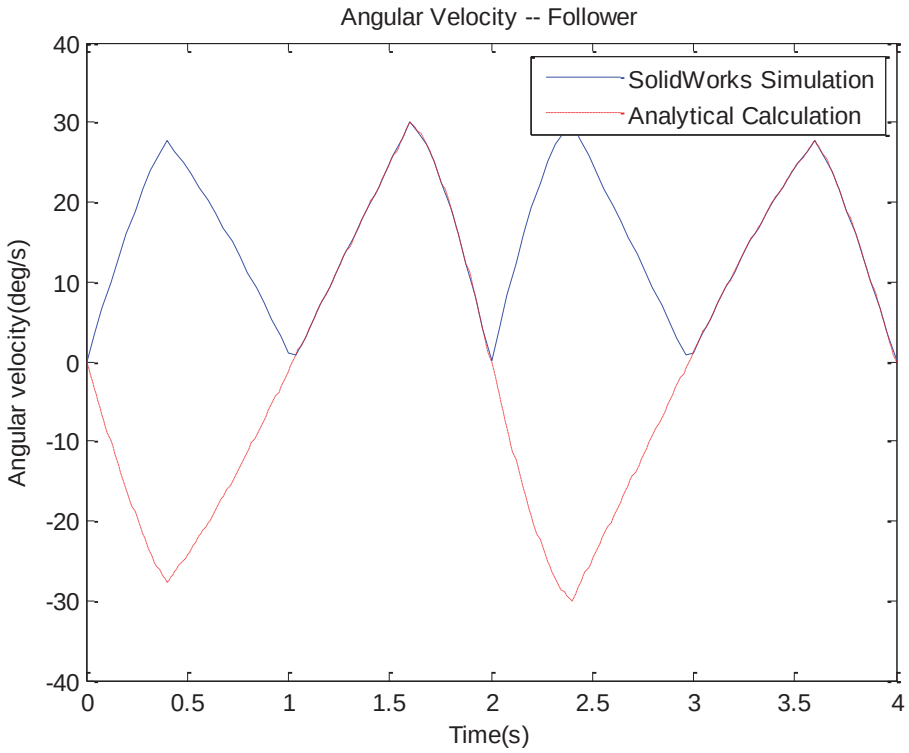

Figure 5-8 Angular velocity of the follower

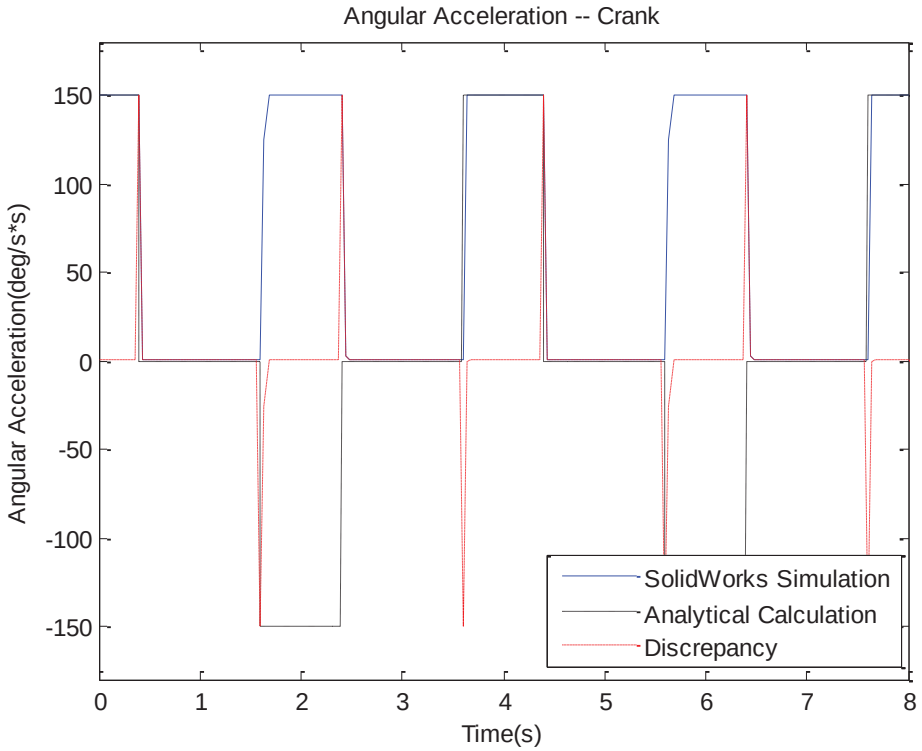

Figure 5-9 Angular acceleration of the crank

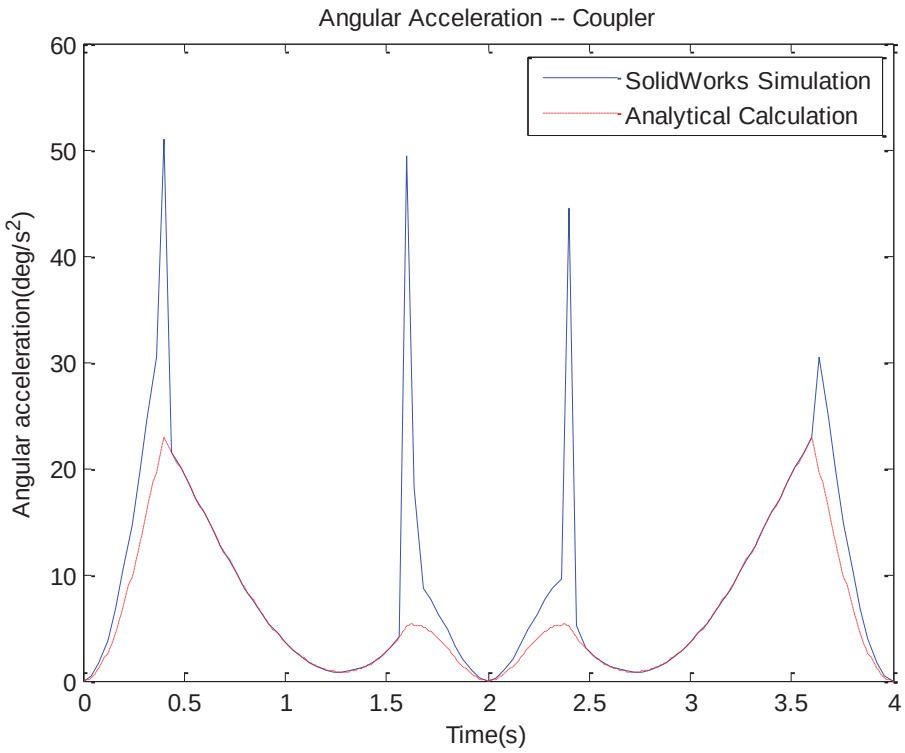

Figure 5-10 Angular acceleration of the coupler

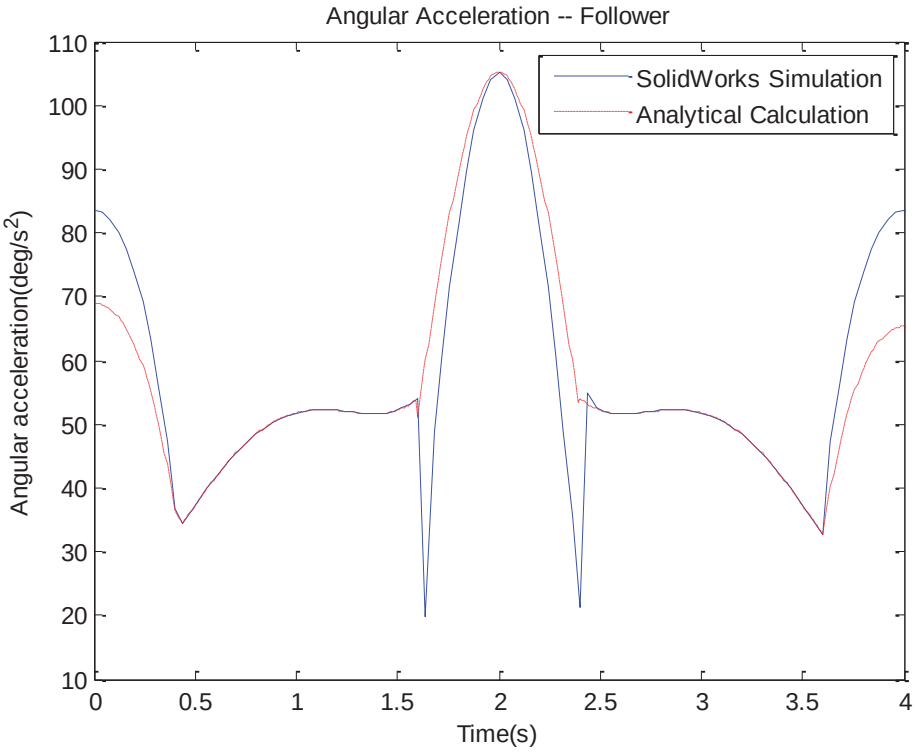

Figure 5-11 Angular acceleration of the follower

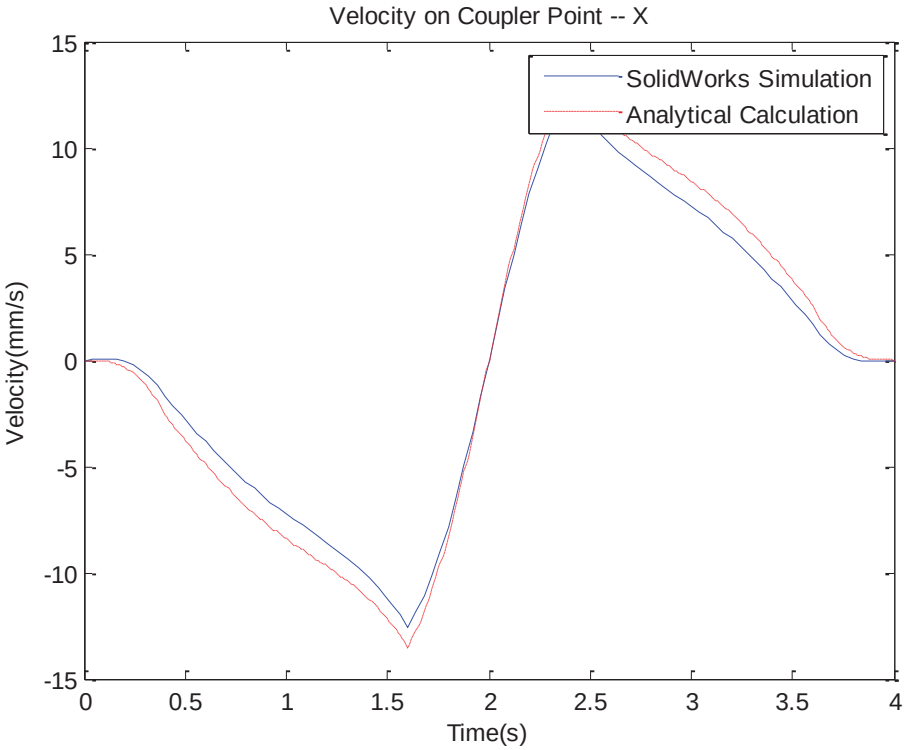

Figure 5-12 The velocity on the point in horizontal direction

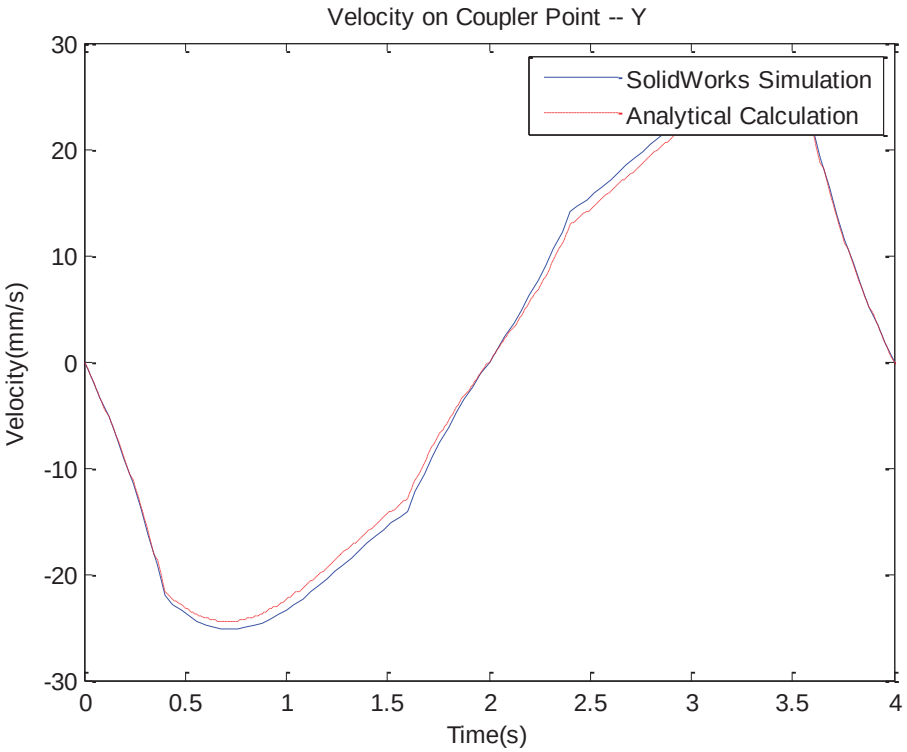

Figure 5-13 The velocity on the point in vertical direction

The above comparisons validate the kinematic calculation subject to the simplification of the same plane movement with the results from SolidWorks simulation; since both cases consider only the ideal operation of the device excluding the influence from wearing, friction, and

assembling tolerance, the kinematics of the mechanism is little affected in discretized time frame. The definition of the velocity profile is responsible for the unsmoothness of its derivative, causing the occurrence of jerks that are hardly reflected in the numerical infinite by analytical calculation of the acceleration. Alternatively, a compensating way that invokes the crank acceleration generated from SolidWorks based on the same velocity input profile can channel the consistency of results with both methods.

The required torque to actuate the movement is then compared with the motor torque obtained from SolidWorks, under two scenarios of the external force, i.e., without resistance and with a resistant constantly opposite to the direction of the mouth moving. The resistance that prevents the jaw movement has not been explicitly defined in the literature in terms of the location, nor the magnitude. According to the minimal force to open the mouth that approximates 5 N, the resistance here inflicted on the attachment is also defined as 5N, constantly pointing to the occlusion plane opposite to the movement direction, as expressed in (5-47).

$$F_r = f(x) = \begin{cases} 5, & 4n-4 \le t < 4n-2 \\ -5, & 4n-2 \le t < 4n \end{cases} \quad n = 1,2,\cdots \tag{5-47}$$

The linkage movement causes instantaneous angular varying in terms of the direction of the external force, according to the definition, and the variation is illustrated in Figure 5-14. So the force can be generalized to the expression in Eq. (5-48), and the decomposed force in the horizontal and vertical direction is expressed in (5-49), as well as in (5-50) the partial derivative at the force exerting point.

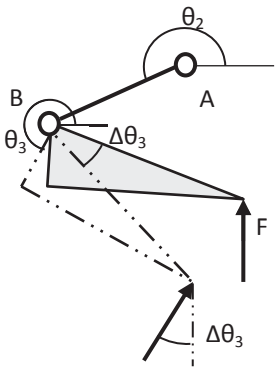

Figure 5-14 External force varying in direction

$$\tau_F = F_x \frac{\partial \dot{x}_F}{\partial \dot{\theta}_2} + F_y \frac{\partial \dot{y}_F}{\partial \dot{\theta}_2} \tag{5-48}$$

$$\begin{cases} F_x = F_r \sin \Delta\theta_3 \\ F_y = F_r \cos \Delta\theta_3 \end{cases} \tag{5-49}$$

$$\begin{cases} \dfrac{\partial \dot{x}_{F_x}}{\partial \dot{\theta}_2} = -l_{AB}\sin\theta_2 - r_F \dfrac{\partial \dot{\theta}_3}{\partial \dot{\theta}_2}\sin(\theta_3 + \beta_5) \\ \dfrac{\partial \dot{y}_{F_y}}{\partial \dot{\theta}_2} = l_{AB}\cos\theta_2 + r_F \dfrac{\partial \dot{\theta}_3}{\partial \dot{\theta}_2}\cos(\theta_3 + \beta_5) \end{cases} \quad (5\text{-}50)$$

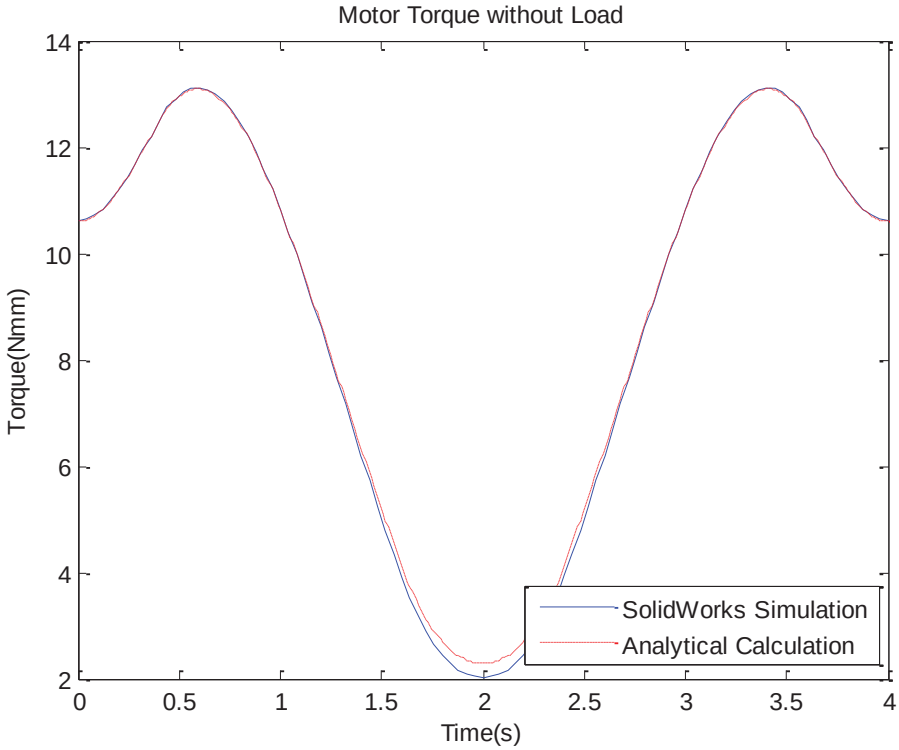

Figure 5-15 Consumed torque measured on the crank without load

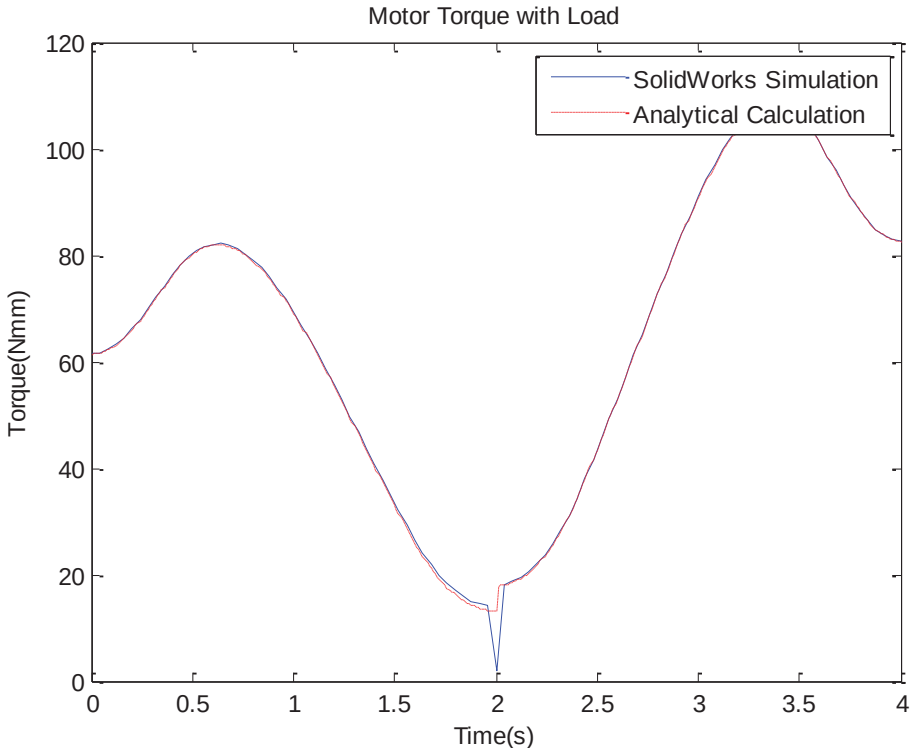

Figure 5-16 Consumed torque measured on the crank with invariant upright load

Results of dynamic study are plotted in Figure 5-15 and Figure 5-16, corresponding to the scenarios without and with resistance. Since the input still uses the same angular velocity profile that induces jerks in SolidWorks, especially at the turning point $t = 2s$ when the direction of the movement alters, the dynamic performances display small amount of inconsistency in the first comparison and a bit spike in the second one. The general sections from both methods apart from the critical points are matched together, which could justify the simplification of the parallel planar movement, as well as the correctness of the analytical calculation.

5.1.4 SimMechanics Model of Linkage System

The linkage mechanism is constructed in SimMechanics with a block diagram by combining proper blocks and joints. The global coordinate system has the origin set at the ground, under which the physical properties of each link are configured by assigning relative values of parameters in the blocks. The mass and moment of inertia of each part that are acquired from each SolidWorks part can basically be used to produce approximate results for a certain motion, but the geometry of irregular parts could not be reflected in such default configuration in SimMechanics. Therefore, the SolidWorks assembly is then linked to the SimMechanics by an add-in tool in order to export a .xml file, which can further be converted into a SimMechanics model that fully represents the physical properties of all parts. The assembly has been modified from the originally converted version to adapt the constraint condition to the real one, as a visualized model shown in Appendix Figure 8-8. The critical parameters representing the physical properties of each link are listed in Table 5-3 as configured in the SimMechanics model.

Table 5-3 Linkage parameter in SimMechanics

	Unit	Ground	Crank	Coupler	Follower	Coupler arm-1	Coupler arm-2	Jaw
X	mm	141.6	175.9	175.4	157.1	218.1	216.1	217.1
Y	mm	-134.4	-93.4	-118.2	-131.1	-138.6	-150.4	-144.5
Z	mm	31.9	17.2	12.3	18.5	-93.3	-93.3	-22.2
Length	mm	--	10.1	32.0	22.0	90	90	--
Mass	g	--	1.5134	9.5	2.75	13.8	13.8	92.2

The entire mechanism built here consists of a couple of linkages on both sides, the spring mounted on the coupler, and the attachment. In this configuration, only one side of the actuator is maintained in the model to avoid confliction of double-side actuation on the actually same rigid-body. The ideal simulation eliminates the existence of the friction during

movement in the joints or between parts in this model. The spring representing the passive compliance in the linkage is re-built by a spring block parallel with a prismatic joint which simulates the motion restraint direction along the adjustable attachment end; the positional constraints representing the tip limits are modeled by hard stops of both ends, as seen the partial model in Figure 5-18 . A unit impulse lasting 0.1s standing for an external force of 1N is imposed on the tip part, and the reaction on the joint and the tip part are illustrated in Figure 5-19. The spring constant according to the requirement is specified to 20N/m, which enables the spring to impose an extra 0.5N on the contacting point.

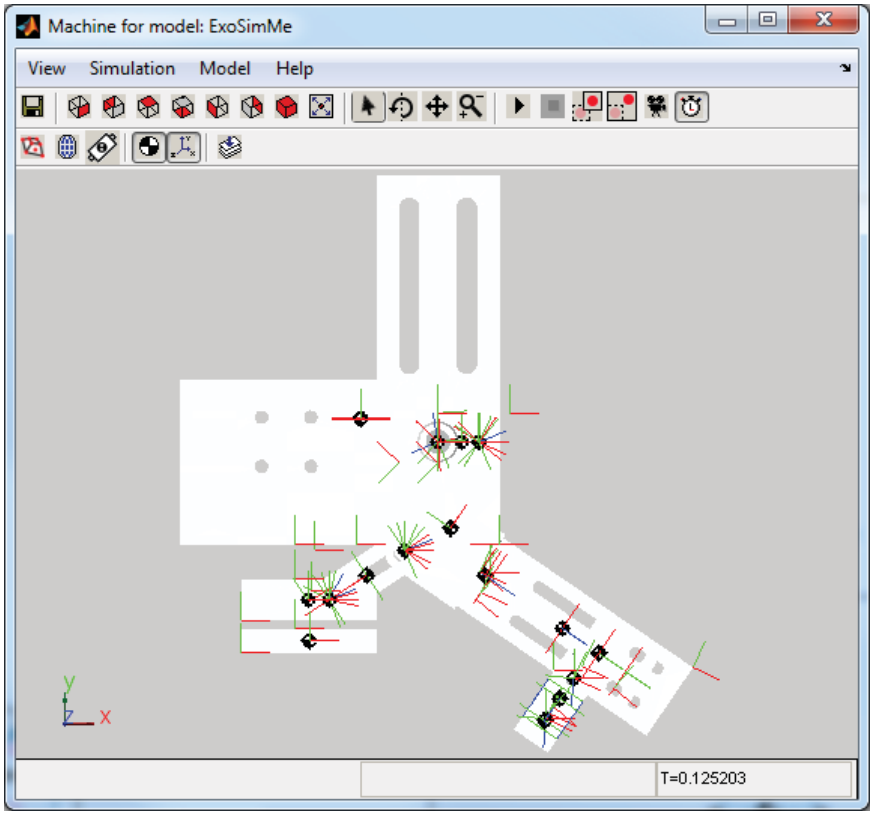

Figure 5-17 Machine model of the whole mechanism

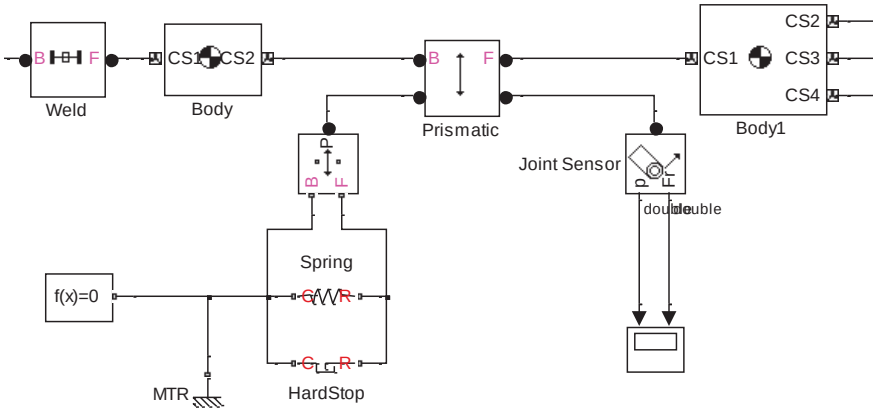

Figure 5-18 Hard stop virtually set-up in SimMechanics

An ideal actuator is attached on the crank joint, and its input is set up with respect to the specified angular velocity profile for smooth movement; a joint sensor is attached to the crank joint to detect the corresponding torque used to generate the motion, as the whole configuration shown in Figure 5-20. Body sensors and joint sensors are attached accordingly to suggest the positional conditions, which are of highly interest in the subsequent simulation in terms of the human-machine interaction, including the displacement and velocity on the IP and CP respectively, the force on the occlusal plane, and the interactive force on the condyle and chin, when the mandible is further attached. The resistance coming from the TMJs or other factors during the depression of the coupler can also be simulated into the model by adding a certain amount of the force to the coupler pointing upright to the plane by configuring the body actuator, by valuing a body actuator on the connecting bar, and the force can also be displayed by a body sensor connected on the same link, as shown in Figure 5-21; note the moment generated from the transmission of actual force applying point to the coupler is not included here.

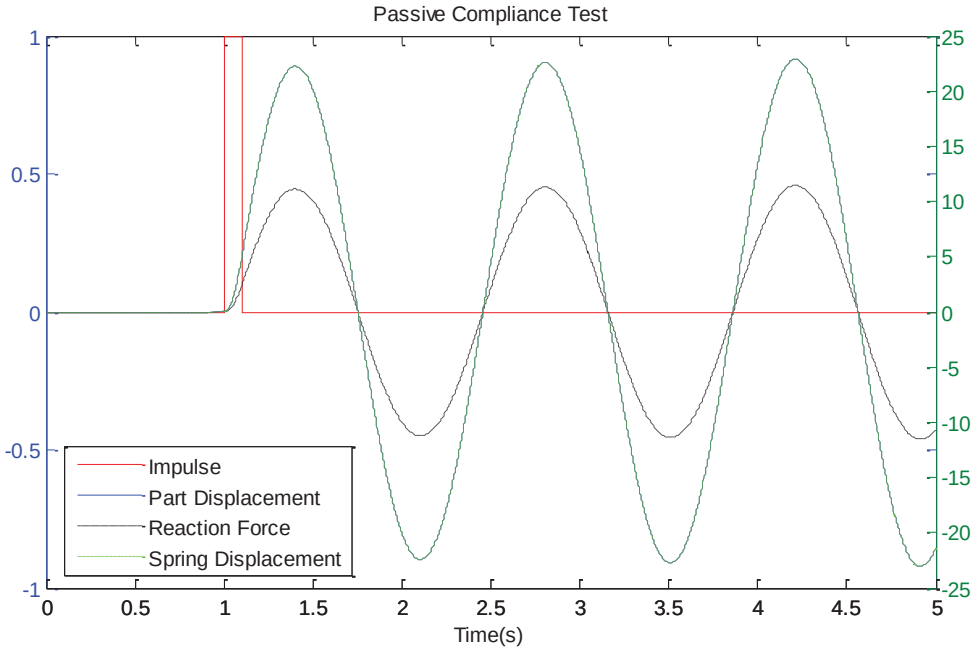

Figure 5-19 Joint and body reaction

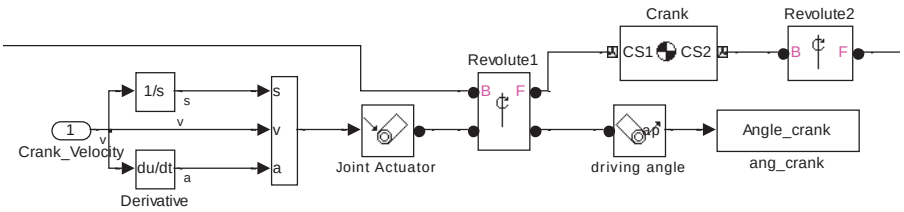

Figure 5-20 Crank joint configuration in SimMechanics

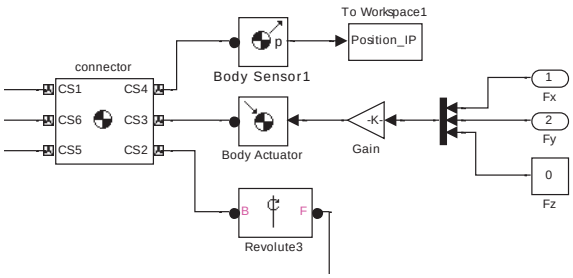

Figure 5-21 Resistance virtually set-up in SimMechanics

5.2 Simulation of the Control System

The control scheme for the whole Mechatronic hardware is envisaged to be constructed in form of the closed-loop to achieve position control of the opening distance on the incisor. The velocity during jaw movement though is considered to be a critical parameter in the training and responsible for a better efficacy, the position is chosen as the control variable to leverage two factors specialized in the jaw motion application; the opening distance of the mouth on the 1-DOF mechanism indicates the movement on the TMJ, which should be strictly monitored for the safety perspective; velocity variation based on the position control could be slightly allowable upon objective profiles, and the variation can be restrained to a certain range as the complement in the aspect of velocity regulation.

The control scheme that is configured in the closed loop will be simulated in Simulink before further implementation into the microcontroller, and its performance depends on precise representation of the plant and the actuator in modeling, in order to approach the actual conditions. Since the control system contains the motor and its actuation based control scheme, simulation of the device operation starts with the motor modeling. Controller tuning is carried out in the scenario of close-loop position control, whereas the implementation is meaningless in other cases.

5.2.1 Model of DC Motor and Simulation

A DC motor can be typically represented as a composition of electrical and mechanical equivalences as illustrated in Figure 5-22. All of the variables denoting parameters that describe the components of motor are listed in Table 5-4, and also converted in the SI unit. The electric circuit based on Kirchoff's Law is equal to the summation of the back EMF voltage, the voltage on the resistance and the inductance, as expressed in Eq. (5-51). The motor torque that is actually consumed under the input profile present can be approximately calculated according to the property of DC motor by the company of the instant current measured from the motor, as given in (5-52), which balances the mechanical part with the internal inertia in

(5-53); Figure 5-23 shows the block diagram reflective of the electromechanical system built up in Simulink mathematically.

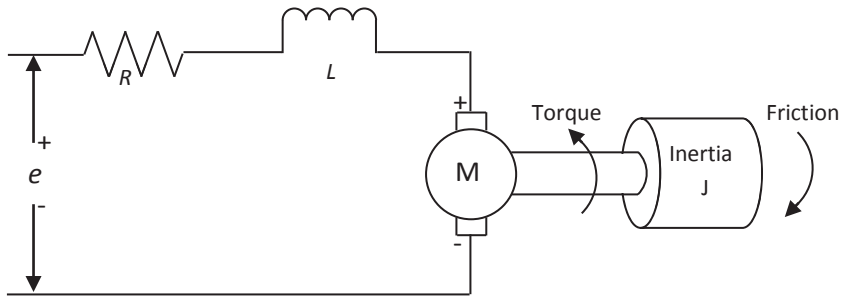

Figure 5-22 DC motor simplified electromechanical system

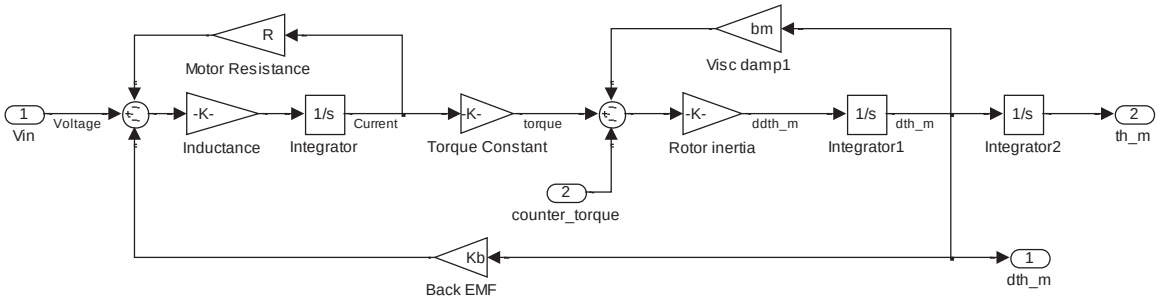

Figure 5-23 Mathematical model of DC motor

Table 5-4 Parameters in the motor

Variable		Unit	Value
Torque constant	K_m	Nm/A	$4.95 \cdot 10^{-3}$
Speed constant	K_n	$V \cdot s$	$\pi/(30 \times 1930)$
Rotor inertia	J	$N \cdot s$	$0.308 \cdot 10^{-7}$
Terminal resistance	R	Ω	12
Terminal inductance	L	H	$0.243 \cdot 10^{-3}$
Mechanical damping	b	$N \cdot m \cdot s$	$2.86 \cdot 10^{-7}$

$$e_s = e_{Bind} + e_R + e_i \tag{5-51}$$

Where:

The back emf voltage $e_{Bind} = 2\pi\, K_m\, \dot{\theta}_M$; the voltage on the resistance and inductance is $U_R = R_R\, I$, and $U_i = L_R\, \frac{d}{dt}\, I$.

$$\tau_i = K_m\, I \tag{5-52}$$

$$b\omega + J\dot{\omega} = K_m\, I \tag{5-53}$$

$$b = \frac{K_m i(t) - J\dot{\omega}(t)}{\omega(t)} = \frac{K_m I_0}{n_0} \tag{5-54}$$

Note, the mechanical damping is usually not given on the product manual, but it can be calculated by recruiting the known values at the initial point, as indicated in (5-54). In practice,

the motor torque T_a is amounted to the summation of the internal mechanical torque T_0 with the output for load T_m, which provides to the device always scaled-down with a factor of the efficiency η, as expressed in (5-55).

$$T_a = T_0 + T_m/\eta \tag{5-55}$$

Where, $T_0 = K_m I_0$.The DC motor used here is powered by 7.2V voltage in standard, while the PWM driver that provides the control signal ranging up to 5V is embedded to convert the driving voltage (Figure 5-24 (B)). The motor is physically modeled in the SimScape while applying its properties, as shown in Figure 5-24.

A

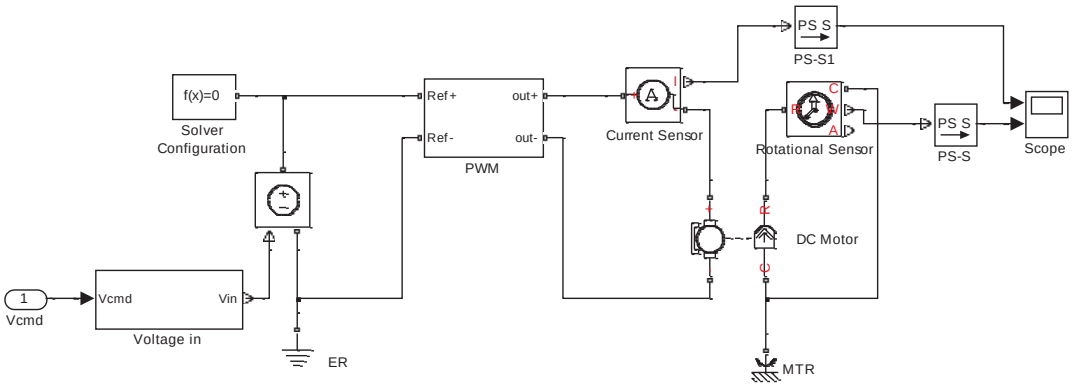

B

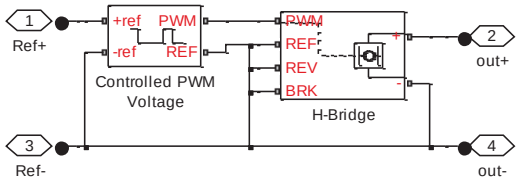

Figure 5-24 Physical model of DC motor in SimScape

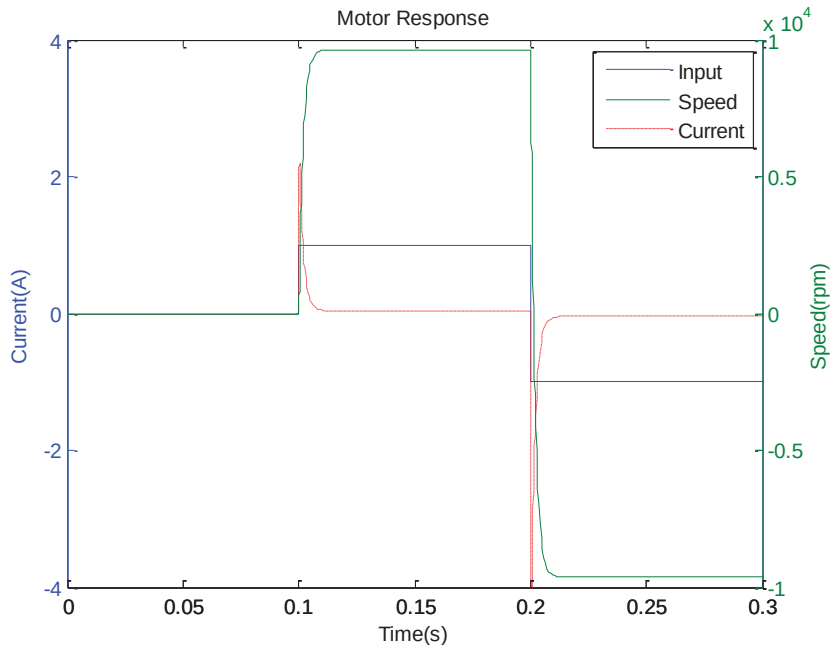

Figure 5-25 Motor response

Validation of the model is undertaken by applying of two step signals of nominal voltage to the motor. Figure 5-25 shows the motor responses with the SimScape model of the DC motor subject to step voltage of ±7.2V; the simulated shaft velocity generally matches the no load speed given in the datasheet with a slight discrepancy; but the negative current during the second step exceeds the no load current, and nearly twice as large as the peak at the first step, due to the double voltage drop.

5.2.2 Simulation of the Control System

The control system in the simulation virtually consists of one four-bar linkage, a DC motor, a feed-forward block and a PID controller; and all units are built up in the SimMechanics/SimScape/Simulink, as overviewed in Figure 5-26.

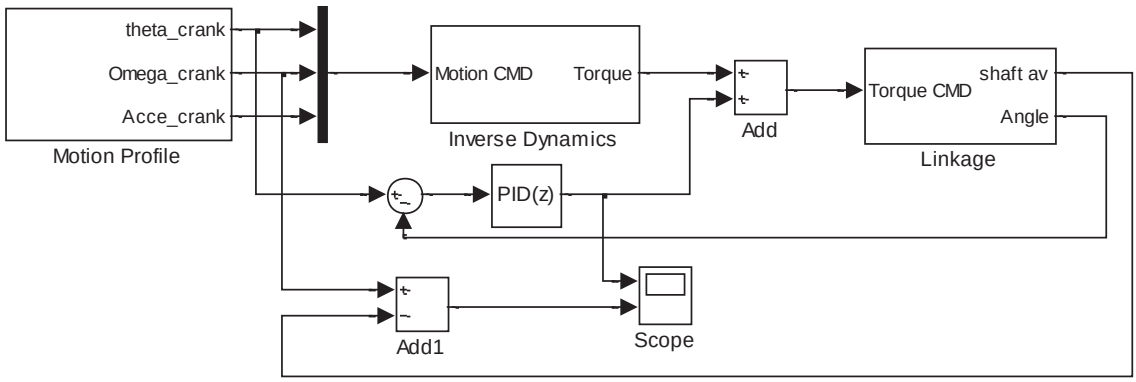

Figure 5-26 The control scheme of the linkage in Simulink

The four-bar linkage reflective of the schematic structure is dimensioned with the values of the SolidWorks parts, as seen in Figure 5-27 where some joints are modified to fit the circumstance; on the incisor spots, the movement of the device is wound back to the controller to form a closed-loop network. The DC motor as parameterized on the model replaces the ideal actuator. A discrete PID controller is planted into the closed loop, designed only to correct the error between the actual signals and the desired profile. The feed-forward block that is composed of inverse dynamics of the linkage depicts the major torque required for the specified motion, as illustrated in Figure 5-28 where the joint actuator on the crank joint accepts the motion input and sends the torque as output.

The angular velocity profile serves as the motion input to the plant, and is defined to be constant across the motion, with an acceleration and deceleration to ramp the speed change at the start and the end of the movement. A GUI in MATLAB is created to visualize the expected speed profile first for further generation; since the coupler attach directly to the jaw,

the GUI is also designed to calculate the crank profile by applying the predefined speed to the coupler via inverse kinematics, as shown in Figure 5-29.

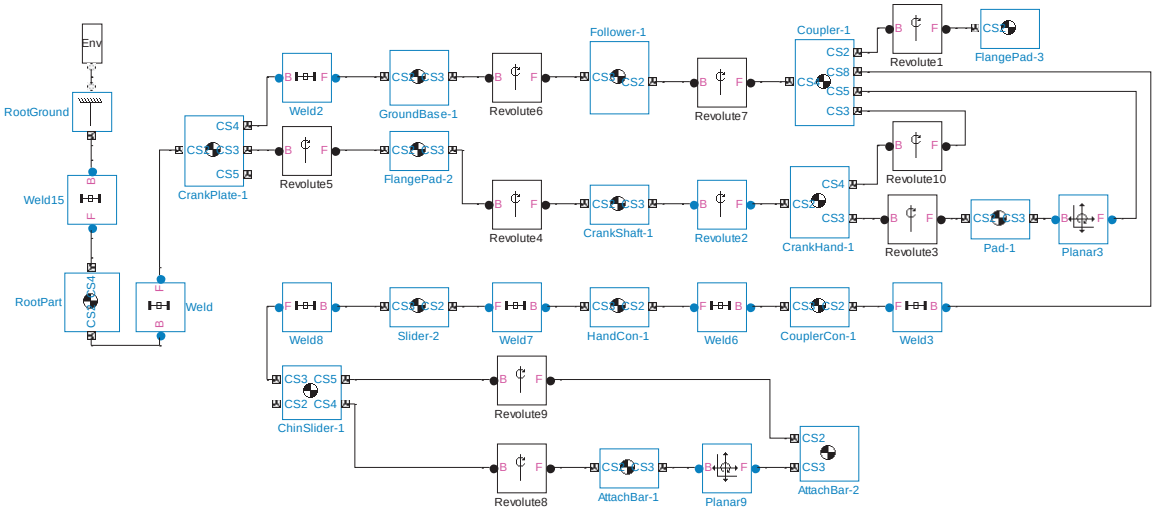

Figure 5-27 Four-bar linkage mechanism modified after conversion from SolidWorks

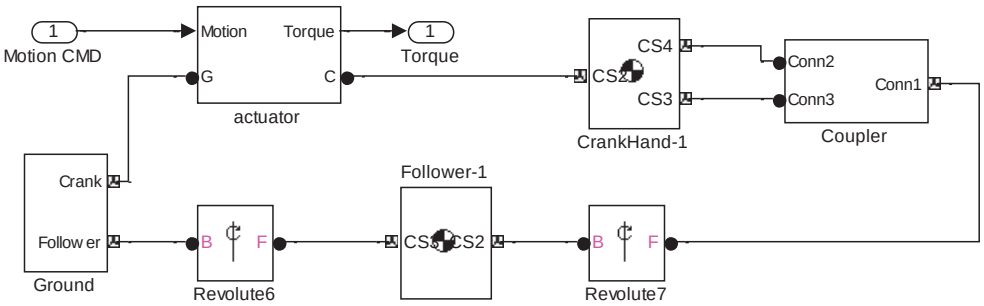

Figure 5-28 Inverse dynamics unit

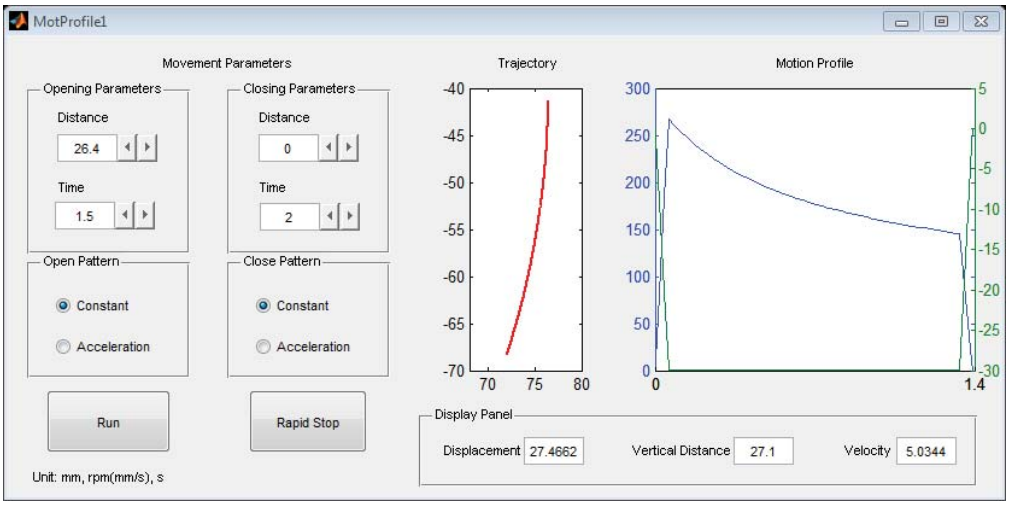

Figure 5-29 Motion profile pre-defined in a GUI

Figure 5-30 (A) provides the motion profile built up in Simulink that can be used as the angular speed of the crank, and contributes to the acceleration block by the last thread in Figure 5-30 (B) where the coupler motion is assumed as the known condition first.

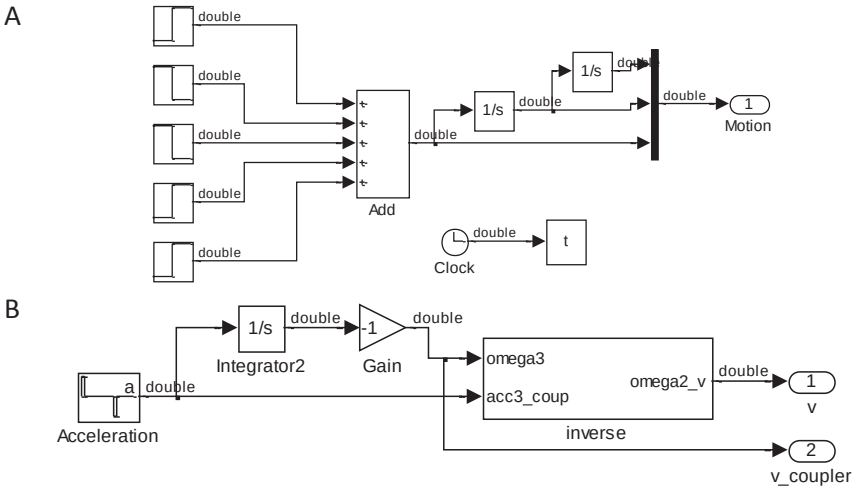

Figure 5-30 Speed profile as the input

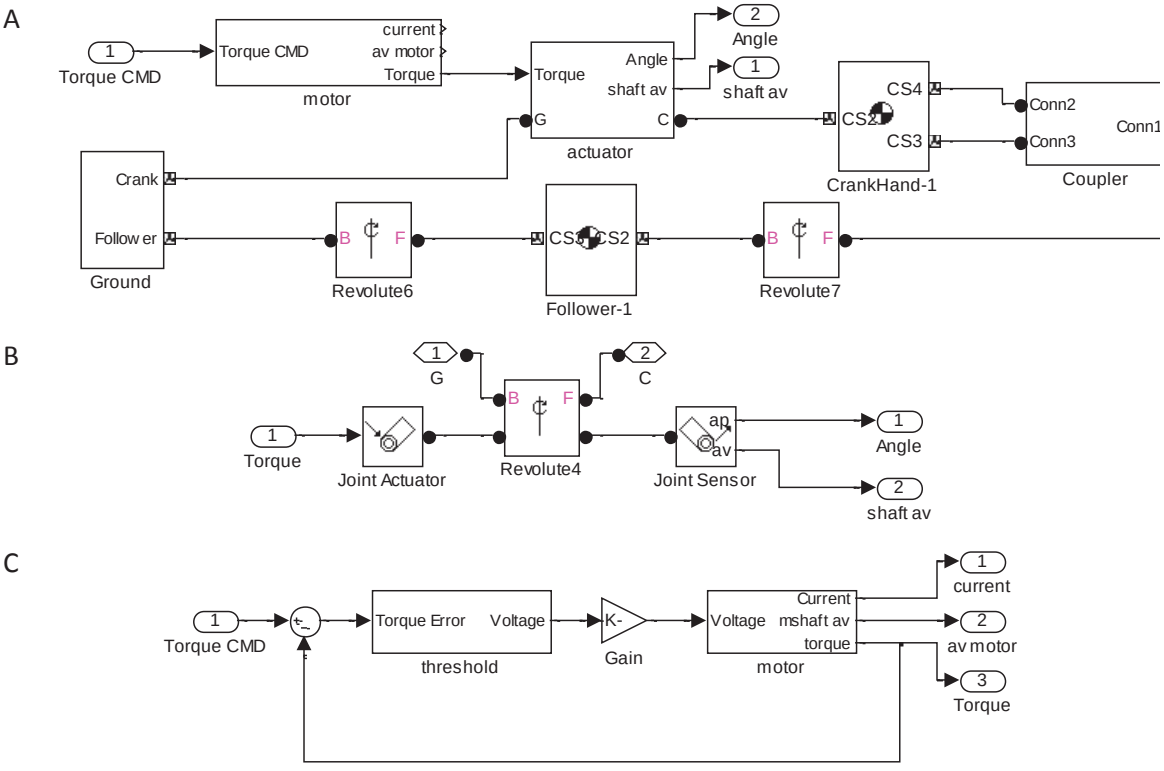

Figure 5-31 Configuration of the actuator

Figure 5-31 (A) shows the configuration of the actuator in the surrounding linkage unit; the actuator block is further pictured in (B) and the motor block is unfolded in (C). Therefore, the crank motion is firstly converted to the torque signal via feed-forward block as the input together with the rectified feedback position by PID controller; then the torque command minus counter load is sent to motor in the linkage via an amplifier.

The simulation is carried out with two scenarios, i.e. with ideal actuator and with current motor. The first trial removes the block model of the current motor, including the amplifier; the torque signal that is aggregated from the feedback is directly sent to joint actuator in the

linkage. PID tuning is not given here; the positional error and both predefined and generated angular displacement is shown on the left and right in Figure 5-32.

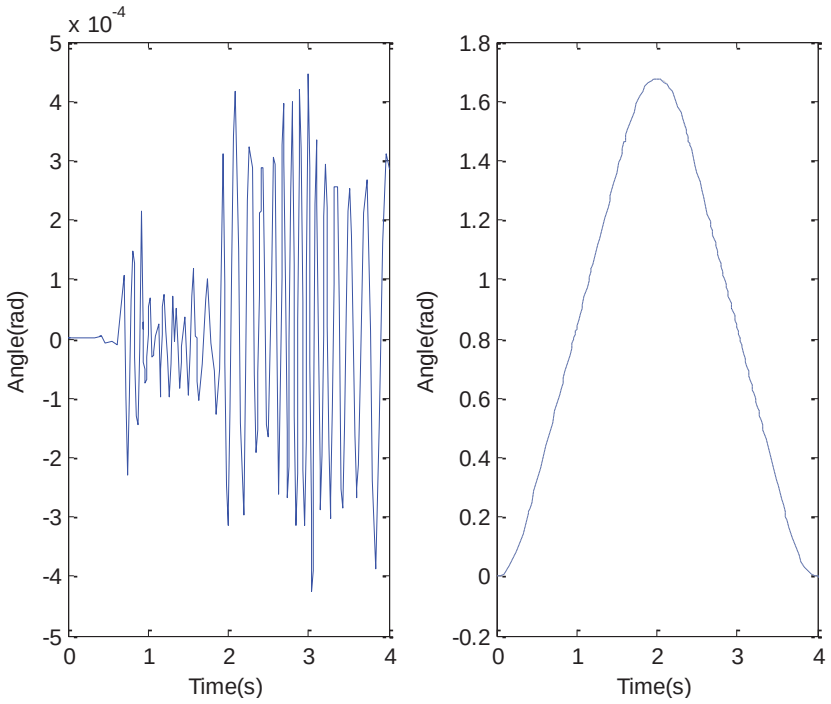

Figure 5-32 Results with ideal actuator

Figure 5-33 shows PID tuning parameters and the performance of step response in the trial with the actual motor block. Since the pre-programed motion runs about 4 s per cycle, the performance of the current controller is acceptable. The simulated angular displacement with the desired one are jointly illustrated on the right part in Figure 5-34, and the error is given on the left part. The largest error is found after the phase switching point, about 2.5° after unit conversion, suggesting a long settling time of this PID makes lag behind the abrupt change.

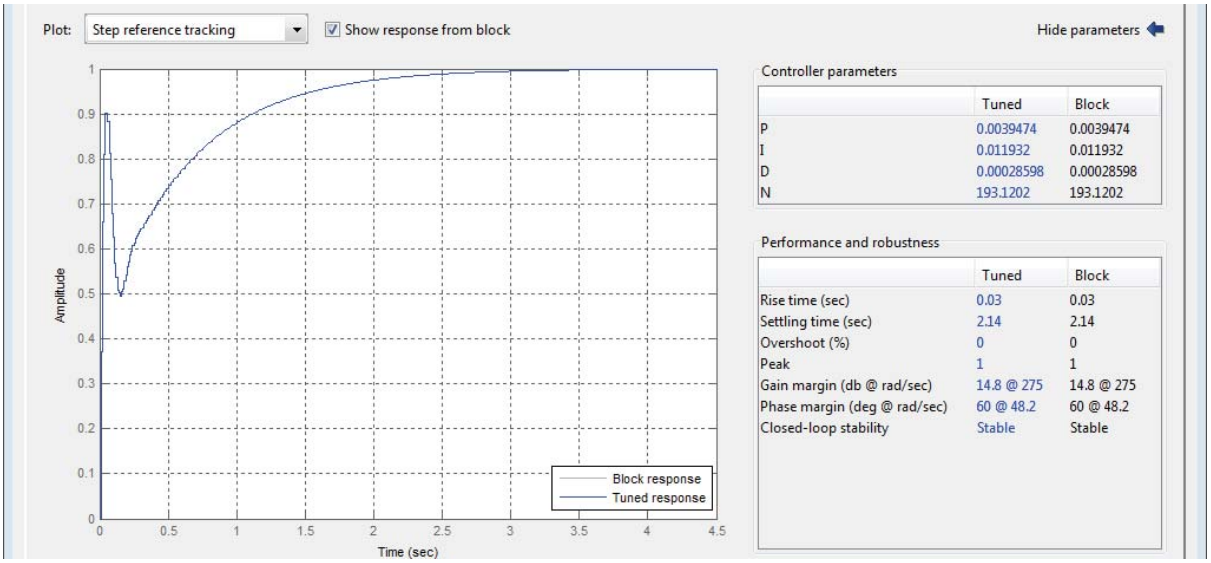

Figure 5-33 PID tuner and the applied parameters

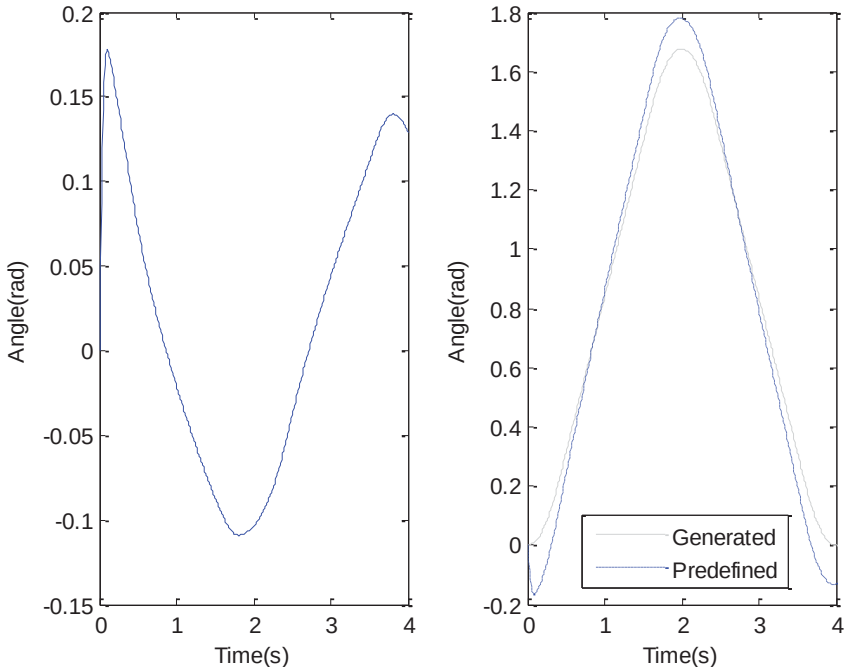

Figure 5-34 Results with actual actuator

5.3 CPG-based Control Strategy

Most of the developed exoskeletons wearable on the extremities generally adopt similar level-based hierarchical control schemes, in which the upper level is configured into a prescribed motion pattern reflecting the rehabilitative training protocols or the intrinsic behavior of the body movement. Such supervisory-level strategy singly used could place some negative influences as stated in two aspects when applied to the current device, though the protocol-embodied motion is desirably necessitated; 1) the simple pre-defined motion program lacks of the autonomous adaptability to deal with the interruption of the abnormal condition of the human-machine interaction triggered by the sensory signals; 2) meanwhile, the pre-defined motion program could not be as flexible as coupled to the mechanism that is to be switched between the mutually inhibited opening and the closing phases. Therefore, the motion program that carries over the training protocols singly as the higher level is not adequate to adapt the environmental changes. The primary objective of the control scheme in the jaw exoskeleton is to adapt the dynamic motion autonomously to achieve the voluntary activity amid the device operation.

As indicated from the perspective of neurobiology, the CPG is actually a neural oscillator that generates coordinated oscillating signals underlying the fundamental rhythmic movement in humans, such as the locomotion, respiration and mastication without resorting to the sensory input. The CPG-inspired algorithms have been increasingly implemented in the control of the biomimetic robots, particularly in regulation of locomotion in biped or quadruped robots to

achieve the adaption of the walking conditions, owing to the fact that the CPG advances in its entrainment to the natural dynamics of the interacting robotic system [188, 189]. The way to recruit the CPG-based algorithm in regulating the corresponding joint can be various, and the output of the oscillator has also been found to serve as torque control signals, phase-shift signals or joint-space signals.

Recently, the CPG-based oscillator has also been introduced in the wearable assistive orthosis to generate the control input to each actuator, so as to reach out stable locomotion subject to irregular walking conditions [190]. When it comes to the mastication, the CPG model has rarely been brought into being in the control unit among mastication robotic systems, probably due to the generally used biomimetic structure built on a parallel mechanism which is difficult to implement the joint-based CPG oscillator. However, the CPG-based neural oscillator has been attempted in practice by a virtual and a hardware setup respectively, demonstrating the competence to adapt voluntary jaw motion and the feasibility of providing input by an oscillator [191].

5.3.1 Control Strategy Description

Since the voluntary activity of the mastication relies on the CPG which generates the basic rhythm to compose the movement, inspired by the neurobiology, the CPG-based control strategy is proposed to react to the changes occurring from the sensory unit that suggests the interaction with the body amid the practice with the jaw exoskeleton; the resemblance of the natural pattern is believed to adapt the body to the complex interaction for rehabilitative exercise, and facilitates to regenerate the sensory connections.

A. Justification of Implementation

Though the feasibility of CPG-based control scheme has been practically confirmed by those existing robotic devices which employed the oscillators in variety of models, the application of the oscillator is based on some prerequisites, which have much to be justified when moved to the man-in-the-loop assistive device on the jaw, as stated below.

1) The one-DOF mechanism

   A single neural oscillation is oriented to the scenario of independently actuating a joint responsible to the relative displacement of a link, instead of the collective results with more than one actuation; and such fashion rules out the recruitment of CPG-based oscillator into parallel mechanisms, which require multiple actuators to explain the position of the floating platform. Focused on the current mechanism, the four-bar linkage though is not directly actuated relative to the open-close

distance; the one-DOF motion implicates an exclusive relationship between the displacement of the jaw and the only actuation on the crank. Therefore, theoretically the oscillator can be used in this linkage mechanism to actuate the crank.

2) Environmental adaption

The CPG algorithm is characterized of the good adaptability to environmental changes, from either sensory feedbacks or external perturbation, on top of its ability in rhythm control. The disturbance that may be imposed on the device can be fitted with two circumstances, to be adapted by the CPG; a) suddenly emerging impedance to open the jaw requires more power from the device to continue the motion, and that being suggested by contacting force sensors on the attachment can trigger the adaptive process with the CPG algorithm; b) a gradually increasing opening distance that is expected to be offered in the course of rehabilitation can be properly achieved by feeding an external input which is used to produce the desirable changes. Therefore, the environmental changes can be ascribed to the sensory information gathered from the device in place of the human body.

3) Apparatus correspondence

The correspondence between live mastication and the CPG-based assistive chewing movement can be established by linking involved variables in resemblance. For general users, the opening distance can directly stand for the amplitude of the oscillator, which can be adapted to the feedback information detected by sensors that suggests the resistance on the path resembled the food influence for mastication. The one-DOF mechanism switching between the opening and the closing phases fits the circumstance of joint control by the CPG oscillator; but muscular reflex intrinsically signifying muscle fatigue causes the rhythm alternation, which would require a corresponding apparatus in the device to make reflected.

B. Control Architecture

The objective to involve the CPG-based neural oscillator is the attempt to achieve the autonomous adaption of the motion delivered by the device to the dynamic changes in the resemblance of the natural pattern, which actually results from the coordinated anticipatory, rhythmic and voluntary muscular activities. To be specific, the motion adaption to the operation in terms of the wearer state is expected in the three points as follows, i.e.

1) The opening distance;

2) The frequency of the movement adjustment;

3) The interruptions.

The treatment-based position protocol generates original control objectives for the motion on the opening distance, which is then mapped to the crank for actuation. Each input protocol is

defined invariant along each cycle in terms of the controlled variable if chosen, not so compliant to adapt the interactive condition with the user; a CPG oscillator is introduced on the basis of protocols to retain the training features as well as govern the reaction to the disturbance, and the entire architecture of the control strategy is diagramed in Figure 5-35.

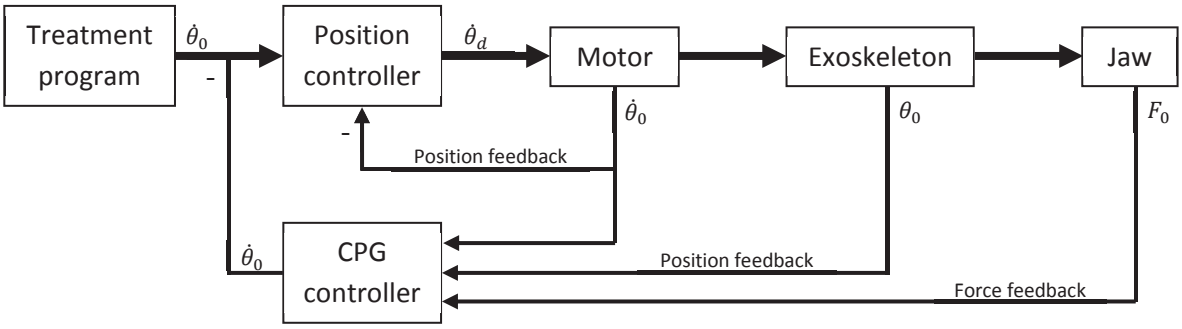

Figure 5-35 Overview of the control architecture

The actuator control is still established on the predefined position protocol, which only contributes to the piecewise operation; while the CPG oscillator governs the overall two inhibitory phases, in the aspects of the phase switch, the amplitude of each cycle, and the frequency of the movement. The oscillator produces a set of the rhythmic signals as the initial input for the cyclic movement, which is coupled to the training program to feed into the position controller; the oscillator then adjusts the motion plan in terms of the controlled variable in real-time according to the analysis of the sensory information, as a response to the interaction. The entrainment of the CPG is designated to rely on a specific rule about the position, the position and the contacting force acquired from the device and the jaw accordingly; and the opening distance can be online mapped to the joint control of the crank on the linkage via inverse kinematic computation.

C. Decision Rules

The motion is generally conducted based on the bottom control scheme, in which the position control of the crank is only achieved. The CPG algorithm will be activated when the force detected on the jaw exceeds a customized level, and then it will governs the motion in two aspects. The motion subject to the CPG control does not follow the pre-defined motion profile any more, but the position control conveyed by the displacement of each neuron in CPG.

The displacement of the crank representative of the motion of the linkage can be then adaptive by accepting the force signal brought back to the CPG controller. The force measured on the coupler will indicate the resistance level which requires more torque from the motor to compensate. CPG controller will scale it into the contextual relationship between the relative

force level and the positional signal to input into the motor, while taking over the phase switching which was originally defined in motion profile. Therefore, the CPG controller governs the entire motion control based adaptive force control.

5.3.2 Matsuoka Oscillator

A. Mathematical Model

The CPG has been mathematically modeled into different neural oscillators, of which the simplest and most widely adopted in the robotic control is the Matsuoka oscillator, due to the generation of the continuous-time signals. The basic unit in the Matsuoka oscillator is a neuron, as encircled in the dash-dotted frame in Figure 5-36; and the single neuron can be mathematically expressed with a group of nonlinear differential equations from Eq. (5-56) to Eq. (5-58).

$$T_{ri}\frac{dx_i}{dt} + x_i = -a_{ij}y_j + s_i - b_i f_i \tag{5-56}$$

$$y_i = g(x_i) \tag{5-57}$$

$$T_{ai}\frac{df_i}{dt} + f_i = {y_i}^q \tag{5-58}$$

The subscript i or j represents the ith or the jth neuron unit; for the ith neuron, x_i, is the neuron state signifying the firing rate; f_i indicates the degree of fatigue or adaptation, modulated by the adaptation firing rate b_i; s_i is the tonic input externally; y_i is the output firing rate of the neuron, $y_i = \mathrm{g}(x_i) = \max(x_i, 0)$ suggests its always being the positive part of the corresponding x_i; T_{ri} and T_{ai} are time constants respectively denoting the inner state of the rise and adaptation effect; a_{ij} represents the weight of inhibitory connection from the jth neuron to the ith neuron; so the item $a_{ij}y_j$ is the input within the inner neural network to the ith neuron; and an exponent q_i indicates the adaptation effect which is proportional to a power of the output firing rate in this neuron [192].

One oscillator can consist of at least two neurons to form a cyclic inhibitory excitation, from which a string of rhythmic signals is produced. For the simplest double-neuron oscillator as illustrated in Figure 5-36, the input can be split into the positive and the negative part, respectively feeding to the two neurons inside to active one and inhibit the other; therefore, the output of this CPG network is defined as the net value between the two neurons, i.e. $y_{out} = y_1 - y_2$. The mathematic description of the dual-neuron oscillator is built in the Simulink to facilitate the observation of the output wave, and Figure 5-37 (A) and (B) correspondingly show the single neuron and the entire oscillator.

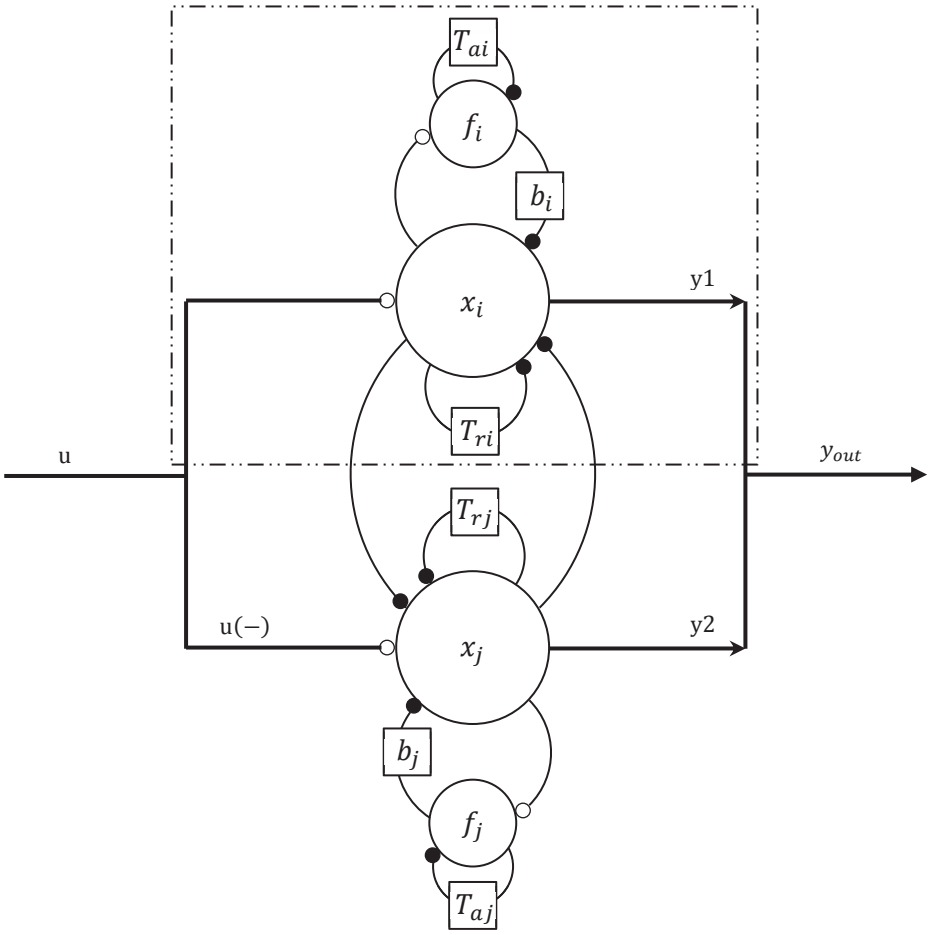

Figure 5-36 Two-neuron composed Matsuoka oscillator

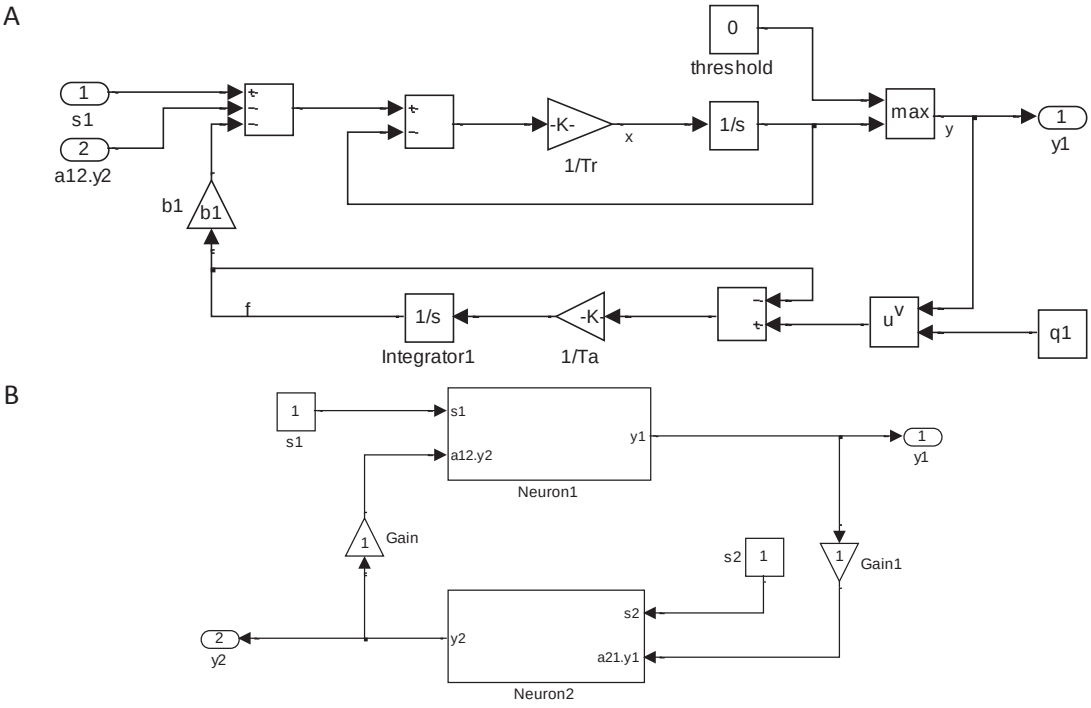

Figure 5-37 Matsuoka oscillator built in Simulink (A) single neuron (B) the entire oscillator

B. Oscillator Parameters

The Matsuoka oscillator can be entrained to the frequency of the controlled system to survive in the unpredicted input, either externally or from the sensory information, suggesting its adaptability to the environmental changes. The rhythmic output that is characterized of the pattern, the frequency and the amplitude depends on the inner neural parameters, which, on the other hand, also determine the entrainment properties of the neural oscillator. The influence of each parameter has been investigated qualitatively with the instructive findings to the waveform of the output by tuning a custom-designed GUI, since the original work did not implicate the coupled interrelation between the feedback and the output [191].

One Matsuoka oscillator of two inhibitory neurons is recruited to give a numerical indication about the influence to the performance in terms of the variance of one parameter while the others maintain still. All parameters are narrowly bounded with each own range to fit into the application, and also conform to the condition written in Eq. (5-59) to achieve the fundamental generation of a steady oscillation in the form of an assigned range or ratios. A GUI for interactive investigation is created to easily process the results (Figure 5-38); it is noted the identical parameters in both neurons assigned with the same value, offering identical neurons by default. Each parameter has been tested with discrete interval within its variation range, and the correspondingly obtained amplitude and period can be acquired by pinpointing the points of the maximum values on the waveform after an oscillating wave has been stabilized, as shown in Figure 5-39. Figure 5-40 illustrates the results for both the amplitude and the frequency for each single variable.

$$1 + \frac{T_{ri}}{T_{ai}} < a_{ij} < 1 + b_i \tag{5-59}$$

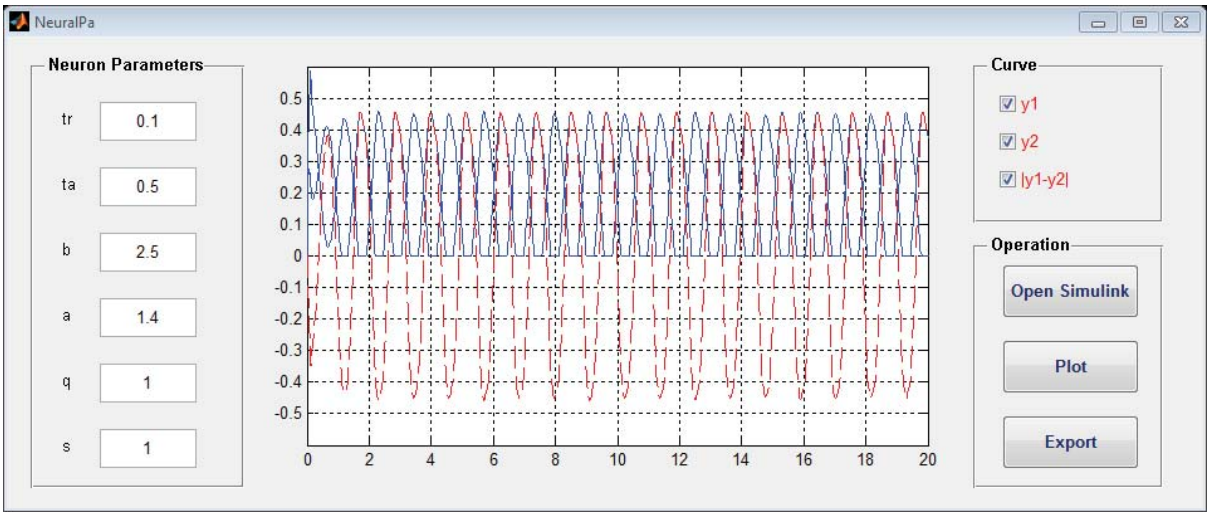

Figure 5-38 GUI for investigation of neural oscillator

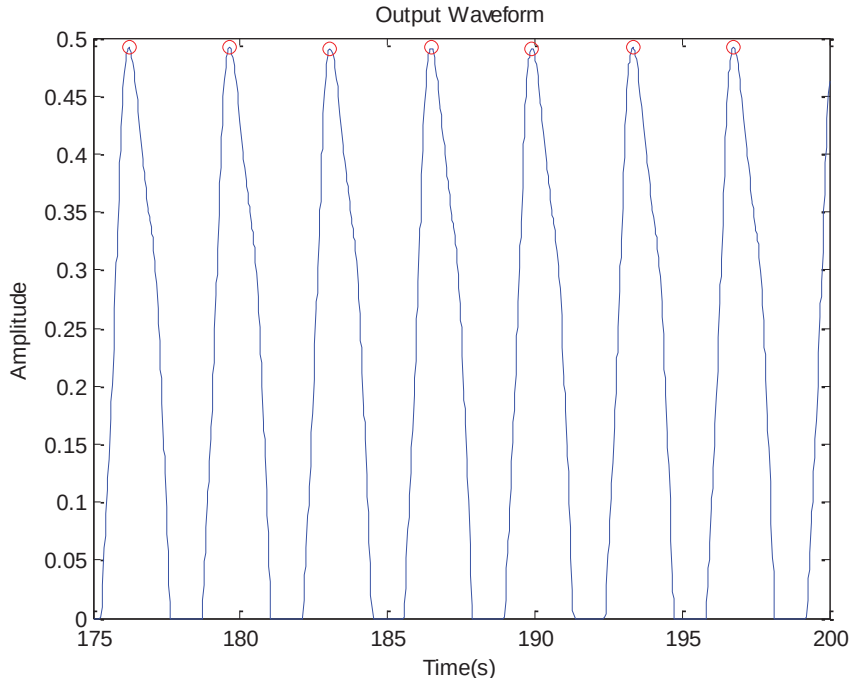

Figure 5-39 Acquisition of the waveform features

Conclusive descriptions have been illuminated with the same method above in application of this oscillator to control robotic devices [193]. The trend of the output performance basically conforms to the previous investigations for each parameter; and the discrepancy in the value may be ascribed to the selection of the other parameters with inconsistent values.

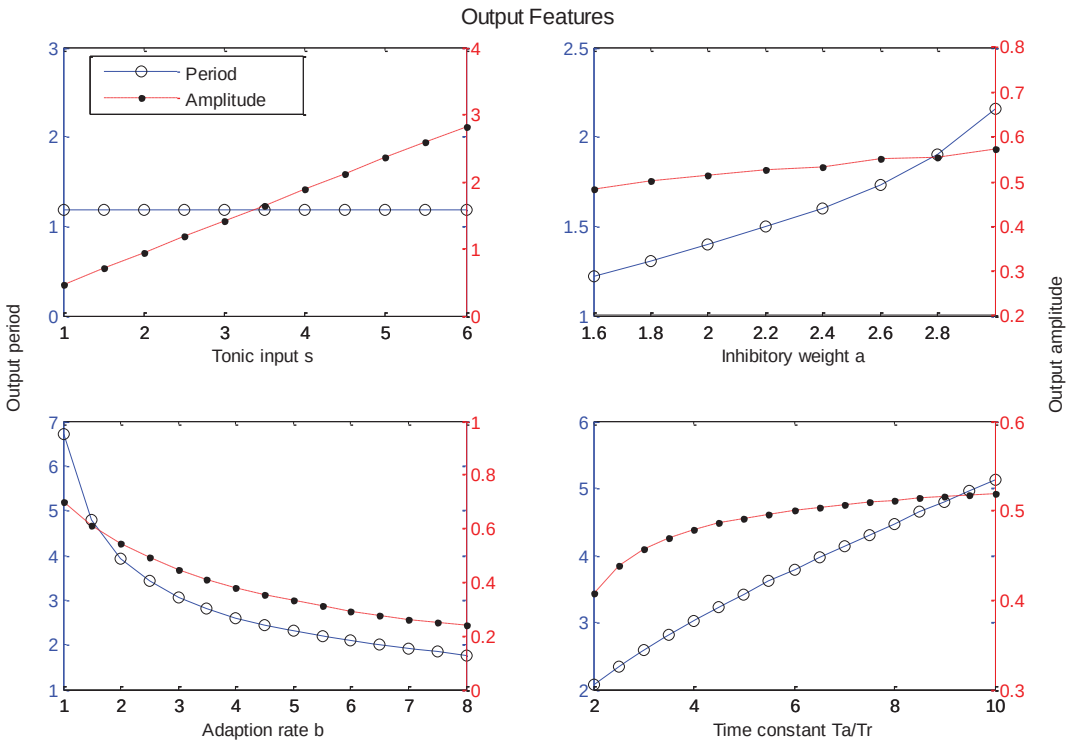

Figure 5-40 Parameter influence on the output

The ratio of two time constants (T_r) and (T_a) that should be designated within a range are correlated to the frequency of the output, but have little effect on the amplitude of the wave pattern; and the firing rate (b) is found to be negatively correlated to the period and the amplitude, which reflects a suppression of the oscillation; the external input, as represented by the tonic input here (s_i), only shows a positive correlation with the wave amplitude. Until recently, the frequency and the amplitude of the rhythmic output have been explicitly approximated as functions of the related parameters as formulated in Eq. (5-60) and (5-61) respectively, which have been validated as similar as the actual one when compared with the model-based prediction [193].

$$\omega_n = \frac{1}{T_{ai}} \sqrt{\frac{(T_{ri} + T_{ai})b_i + T_{ri}a_{ij}}{T_{ri}a_{ij}}} \tag{5-60}$$

$$A = \frac{s_i}{2\frac{T_{ri} + T_{ai}}{T_{ai}a_{ij}} - 1 + \frac{2}{\pi}(a_{ij} + b_i)\sin^{-1}\frac{T_{ri} + T_{ai}}{T_{ai}a_{ij}}} \tag{5-61}$$

Despite the constraints to the parameters that set the boundaries from the above formulations to tune the oscillator, the values of the parameters are still difficult to ascertain exactly. One set of the typical parameters for generating the stable rhythmic signals assigns values as the reference for further empirically fine tuning to fit the requirements about the outputs. One optimization system has been proposed in order to search the optimal parameters that are bounded in the oscillator to match the desired response, based on the Least-Mean-Square method by minimizing the global error between preset curve and the generated one [194].

5.4 Experimental Implementation and Trials

The control scheme has two ways for its implementation to communicate the command to the mechanism in the tests, i.e. via the PC-based hardware-in-the-loop (HIL) online control or the MCU-based offline control. Considering the practical operation requiring a certain extent of the mobility, MCU-based controller is preferably chosen in the experiment-oriented trials, which sacrifices the application of the CPG strategy as a cost, since its non-linear response is unpredictable in the plant for controller tuning.

The position-based control scheme is transplanted into the controller to test the performance in the experiments of several scenarios. Modifications of the scheme will be introduced to simplify the bulk and structure of the code.

5.4.1 Embedded Circuitry Implementation

The MCU-based electronic hardware controller stated in section 4.4 is used to carry the closed-loop control scheme orienting to the user operation in terms of the selected exercise, and its realization in the systematic level is achieved by integrating each function module. Sensors that reside in each break-out board are connected to the main board via their interfaces pins. Feed-forward controller that is originally designed to handle the major parts of the torque is not actualized in the controller, but replaced by a look-up table for each designated plan descriptive of the relationship between the motion and torque, primarily for the purpose of eliminating the task of the non-linear calculation.

The flowchart of the embedded code is diagramed in Figure 5-41. After software initialization that includes enabling all of the ports and configuring the system clock, the program starts from selecting one training mode among the pre-defined combinations from two levels via a simple UI displayed on the built-in OLED screen, as pictured in Figure 5-42 (A) and (B). When the device is launched against the chosen plan, the DAQ module synchronously sends the sensory signals to the MCU, followed by data conversion, the PID controller as the core part in this program provides the request to motor according to the error information if exists to correct the motion plan until the session is completes. Meanwhile, the watchdog module keeps monitoring the communication of the sensor to the MCU; if any sensor fails to send signal flows, the watchdog timer will be overflowed to reset the system. A real-time updated message (scanning time 1s) is also coded on the screen to indicate the current running state, as shown in Figure 5-42 (C). Parameters of the PID controller are optimally suggested in Simulink to automatically generate code for the fixed-point type arithmetic of the MCU, as shown in Figure 5-43.

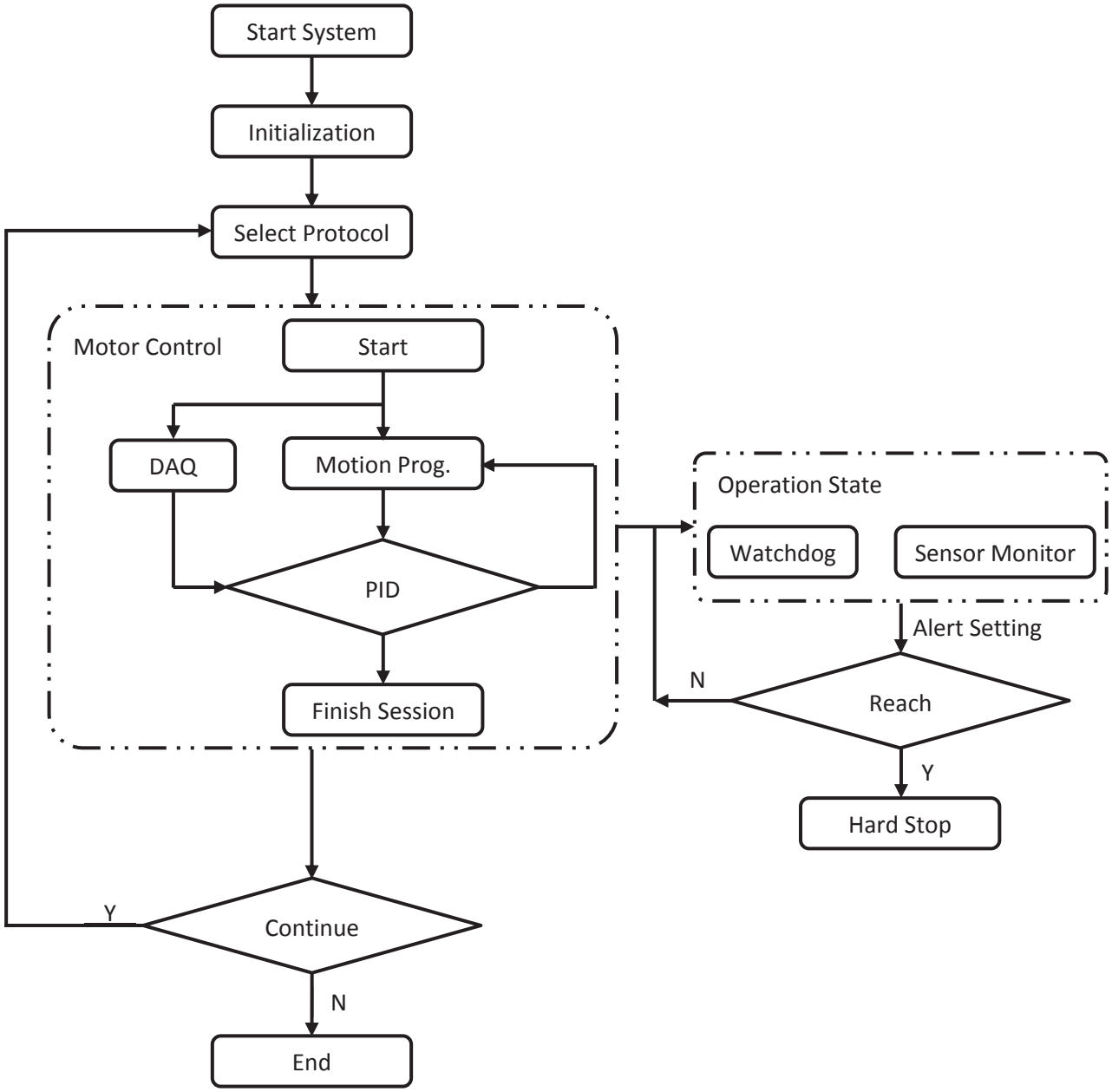

Figure 5-41 The integrated flowchart of the controller

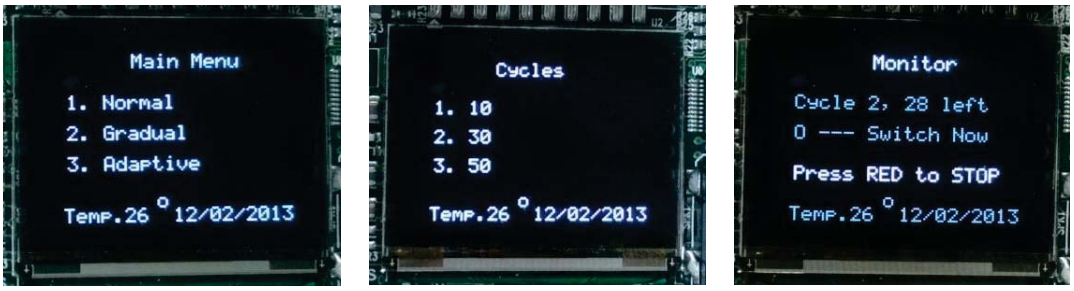

(A) (B) (C)

Figure 5-42 UI coded in the LM3S

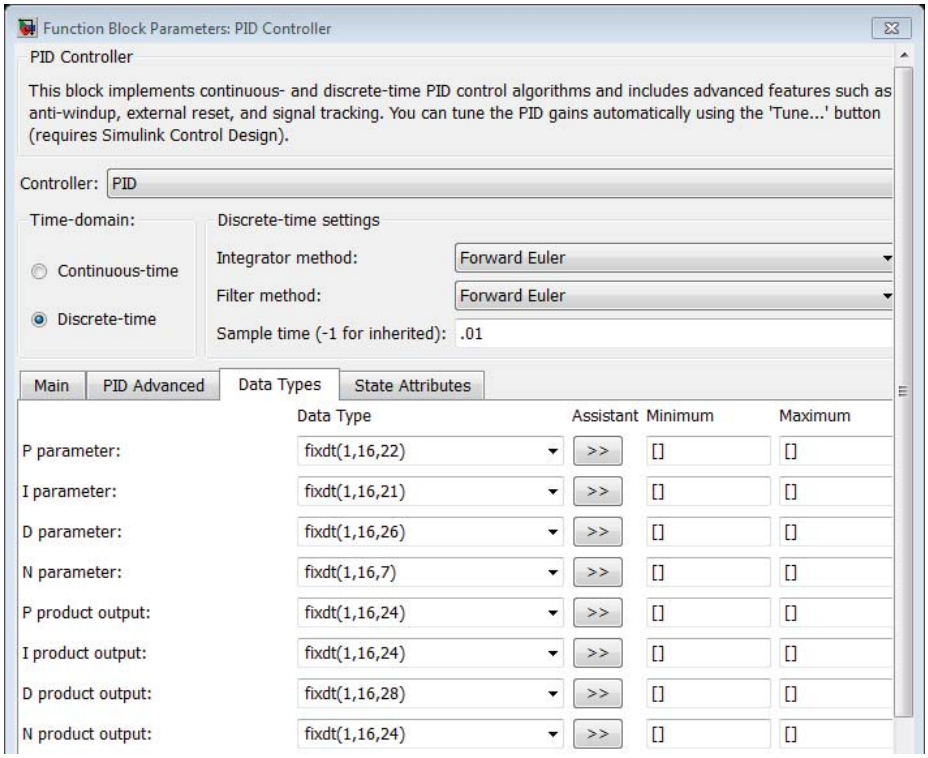

Figure 5-43 Fixed-point configuration

5.4.2 Experimental Scenarios and Results

A series of experiments are conducted to test the performance of the positional control on the jaw exoskeleton after the code is loaded to the MCU, indicating the crank angular displacement is the variable mainly concerned. All adjustable links are kept on the constant size of the original computed set without tuning during all trials in this section, expect the dimension of the follower is stayed on 21mm; the chin holder is put on the farthest side along the adjustable bars, in the way to produce the largest resistance torque; springs are not pre-tightened and in natural state.

The position feedback from sensors is simultaneously extracted out from other linked lines on each own break-out board to avoid attenuating the signals, and converted to the crank angular displacement in MATLAB after acquired via USB-6210 DAQ card; the force signals are acquired in the same way. Each scenario in this section is repeated for three times, and the result present here is from the last trial. No extra load is imposed amid the trial.

Three motion profiles comprise of the experimental scenarios, and they are one cycle of the device operation, continuous multiple cycles and intermittent multiple cycles which has 1 s in-between each cycle. The velocity profile is defined as same as the one used in the SimMechanics simulation, which contains only one cycle of depression-elevation movement; multiple cycles simply replicate the single cycle. Figure 5-44 depicts the last two motion

profiles. The trials are conducted under the open-loop set-up and the closed-loop set-up for all three scenarios; and before the code is loaded into the controller, verification of PID parameters under the fixed-point configuration is simulated on the previous SimMechanics model.

A

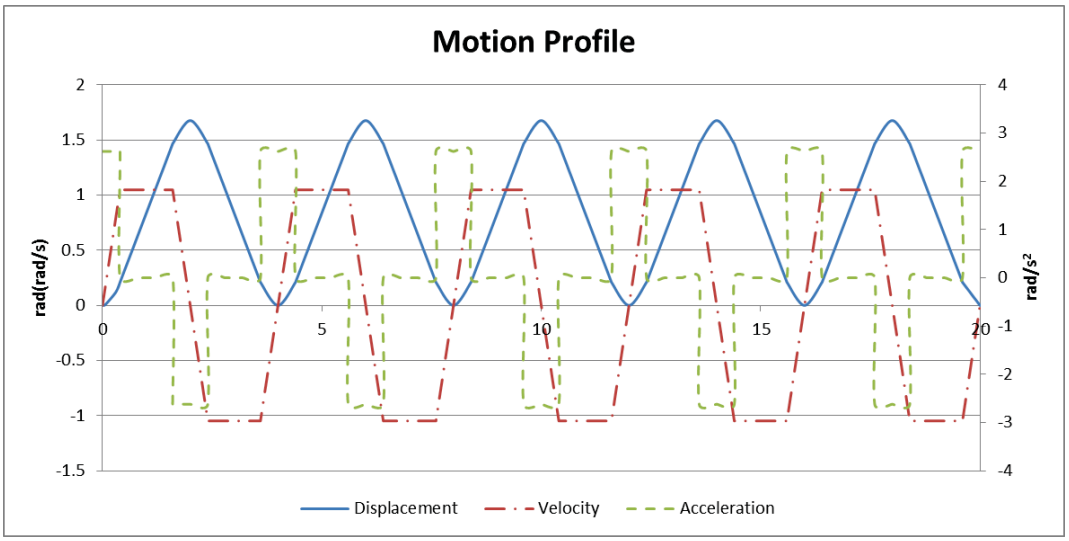

B

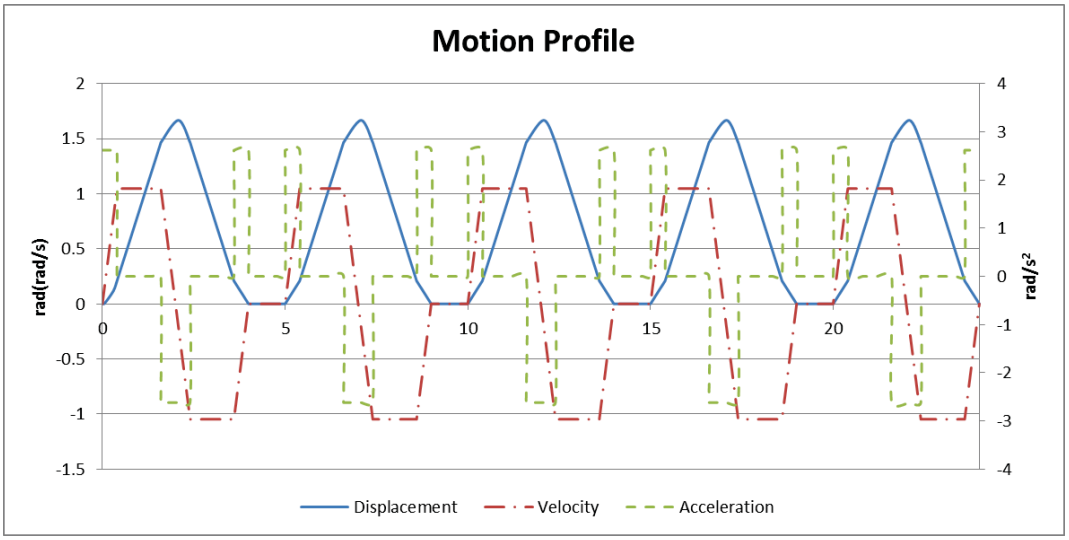

Figure 5-44 Motion profile for five cycles as illustration

A. Open-loop Set-up

Figure 5-45 depicts the simulation results with PID parameters having the given 4-digit fixed-point configuration on the top (A), and suggested digit on the bottom (B). The solid line in grey level draws the objective angular displacement with respect to the time, while dot-dash line for the actual one simulated/generated and dashed line for the discrepancy between them.

Figure 5-46 illustrates the experimental results with the open-loop set-up. In (A), the device reacts slows at the start-up, though it keeps the matching trend after 0.5s, a large error over the target is found at the corner for phase switch, about 0.17 rad, approaching the upper

bound of the safety sensor. The closing phase ends up with also an overshoot, which triggers the hall-effect sensor to stop the device. A better performance is shown in (B) after the torque-velocity relation is given a little modification; but a slow start and an overshoot in the end still exist.

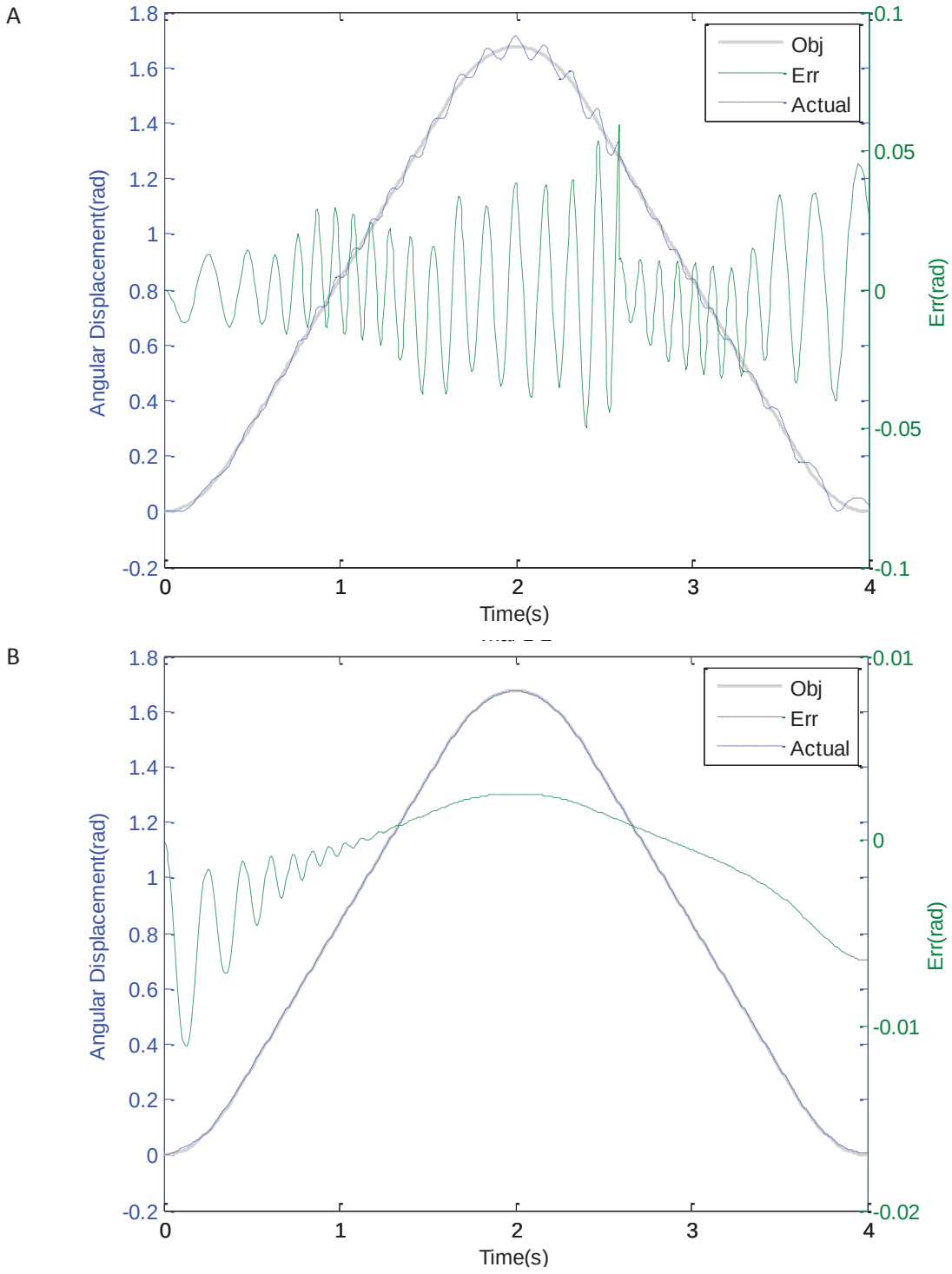

Figure 5-45 Simulation with the controller (A) before and (B) after PID tuning

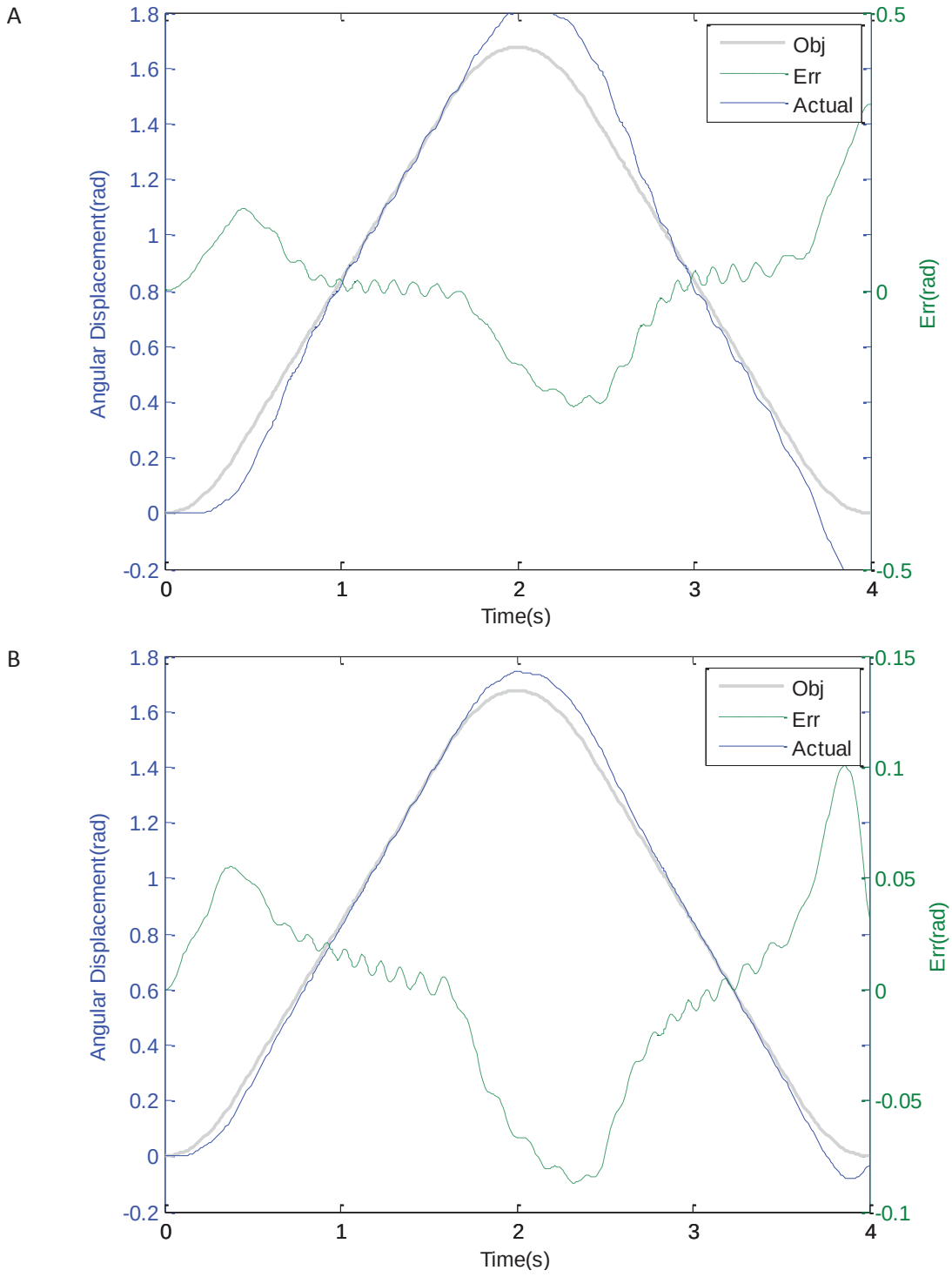

Figure 5-46 Scenario one in open-loop setup

Figure 5-47 (A) shows the experimental results of five-cycle motion. It is noticeable that the wave basically maintains the pattern of one-cycle scenario, which means the device can follow the control command. Moderate vibration occurs in the second cycle and is further deteriorated subsequently. It is likely that the torque provided according to the feed-forward block has a discrepancy compared with the actual situation, and is insufficient to drive the device.

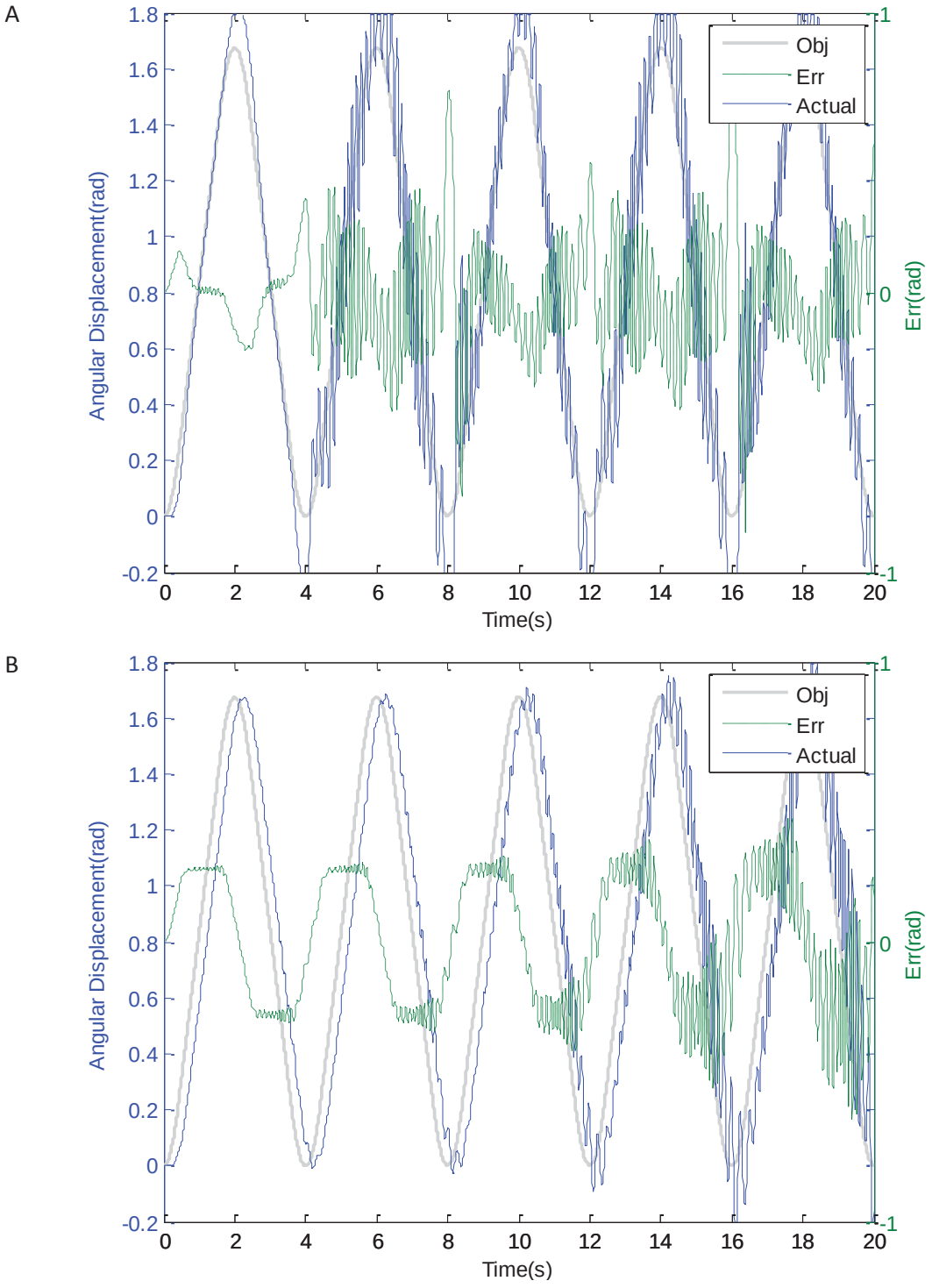

Figure 5-47 Scenario two in open-loop setup

The feed-forward torque is then modified to fit the long-duration conditions; and Figure 5-47 (B) shows an improved performance in the signal tracking but accompanied with a clear delay. Vibration can still be found from the third cycle, and is also prone to be aggravated continuously. Accumulated error without rectification could be the possible explanation of this phenomenon.

In contrast, results shown in Figure 5-48 with the same open-loop controller display an acceptable performance in the open-loop simulation of scenario 3, though a tiny shaking waveform is still found during the first several cycles, while error is incrementing during the device running; the interval in-between offers enough time for the motor to do self-correctness.

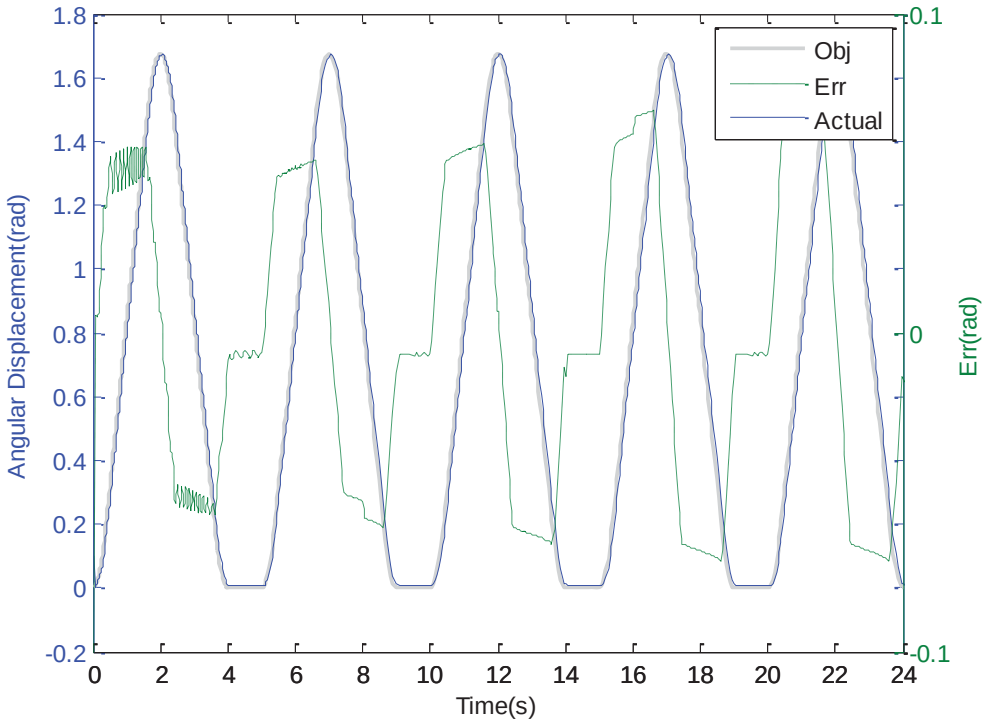

Figure 5-48 Scenario three in open-loop setup

B. Closed-loop Set-up

In this section, the closed-loop experiments are conducted on top of the same configurations in the code retained from the open-loop setup. Verification of PID parameters in the simulation will not be displayed again, but digits of the fixed-points suggested by Simulink are all applied for the following trials.

Figure 5-49 gives results of two trials of the close-loop set-up under scenario one. The measured position is found to be basically in track of the objective profile, but exhibits a small vibration of the operation in (A). The integral and the derivative value are manually enlarged via offline adjustment. The result shows the device was operating in a much smoother way, as indicated in Figure 5-49 (B); but the error across the second trial (maximally 0.04 rad) because a larger integral value is a relatively large compared to the first one.

Since the results under multiple-cycle scenario exhibit a shaky phenomenon in the open-loop trials, the PID parameters are then tuned before loaded into the controller based on the open-loop setting.

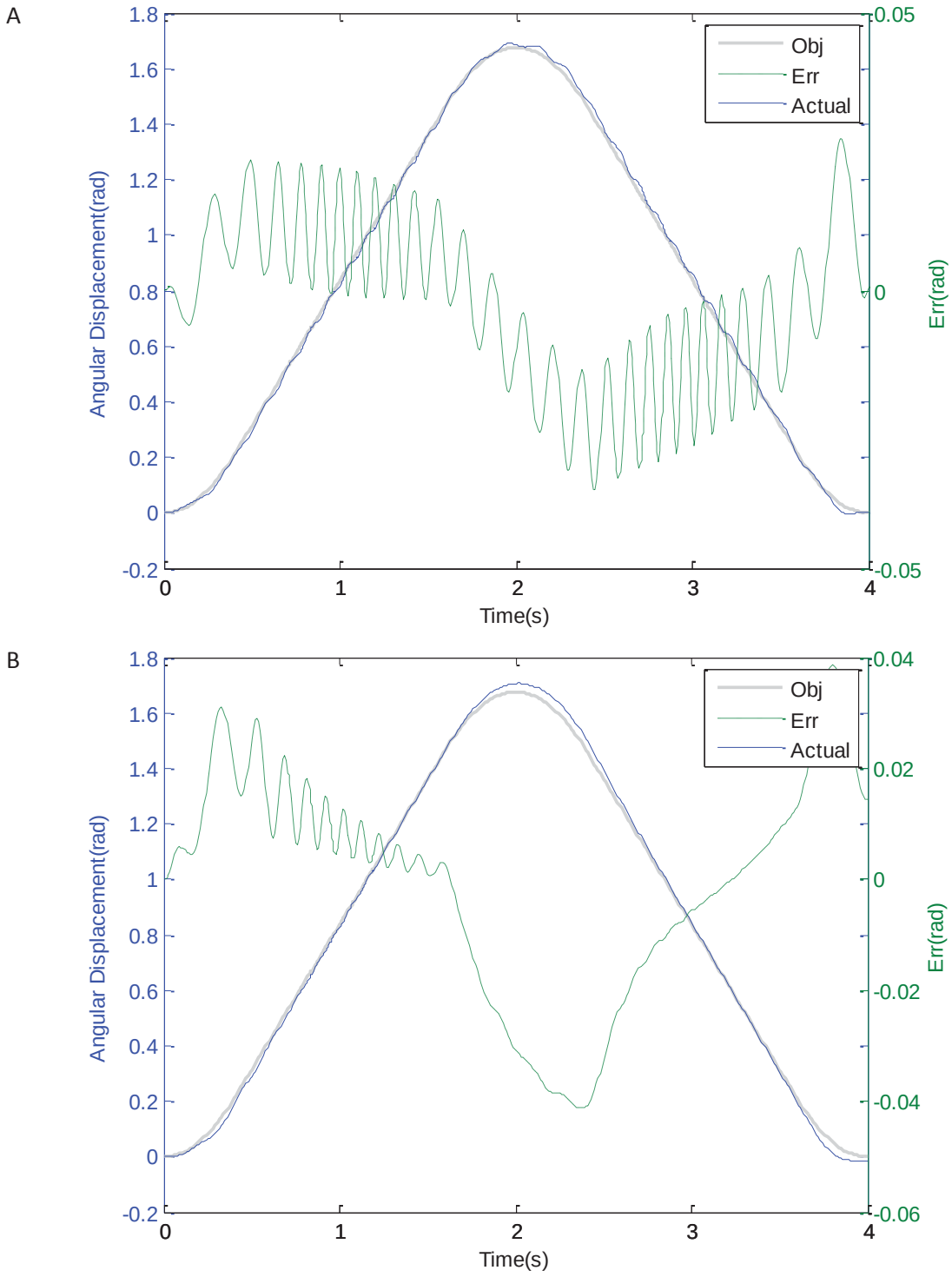

Figure 5-49 Scenario one in closed-loop setup

Figure 5-50 gives the experimental results in the closed-loop trials. It is noticed that at each phase switching point an overshoot still exists (maximally 0.04 rad), and the occurrence of

shakes this time of little amplitude also outstands distinctively during the start-up period, which has an abating trend in the following stage.

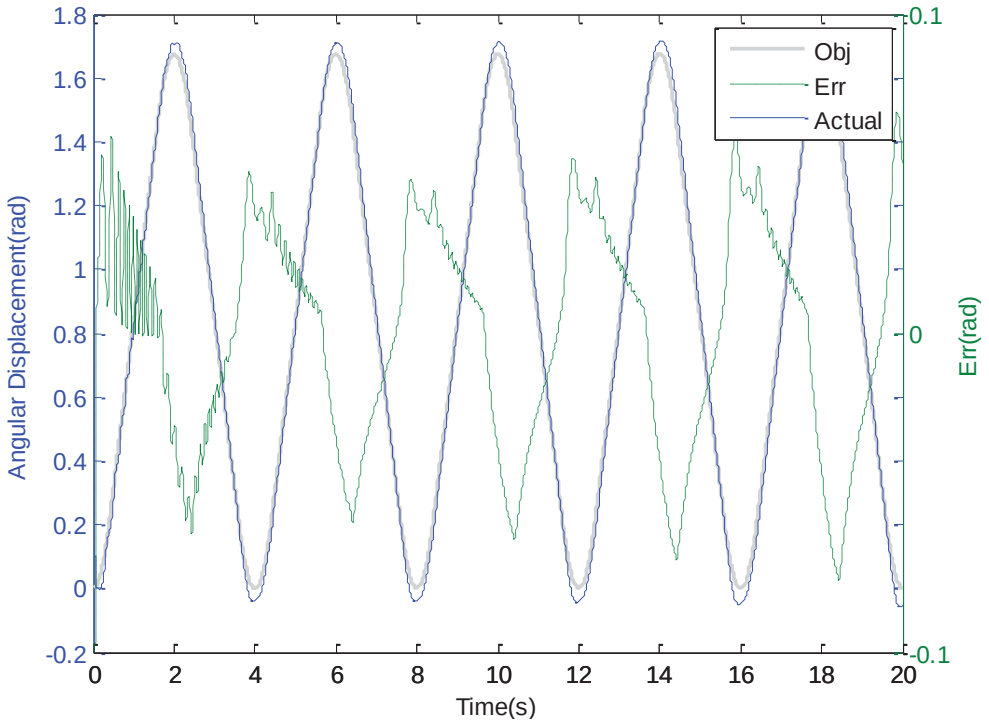

Figure 5-50 Scenario two in closed-loop setup

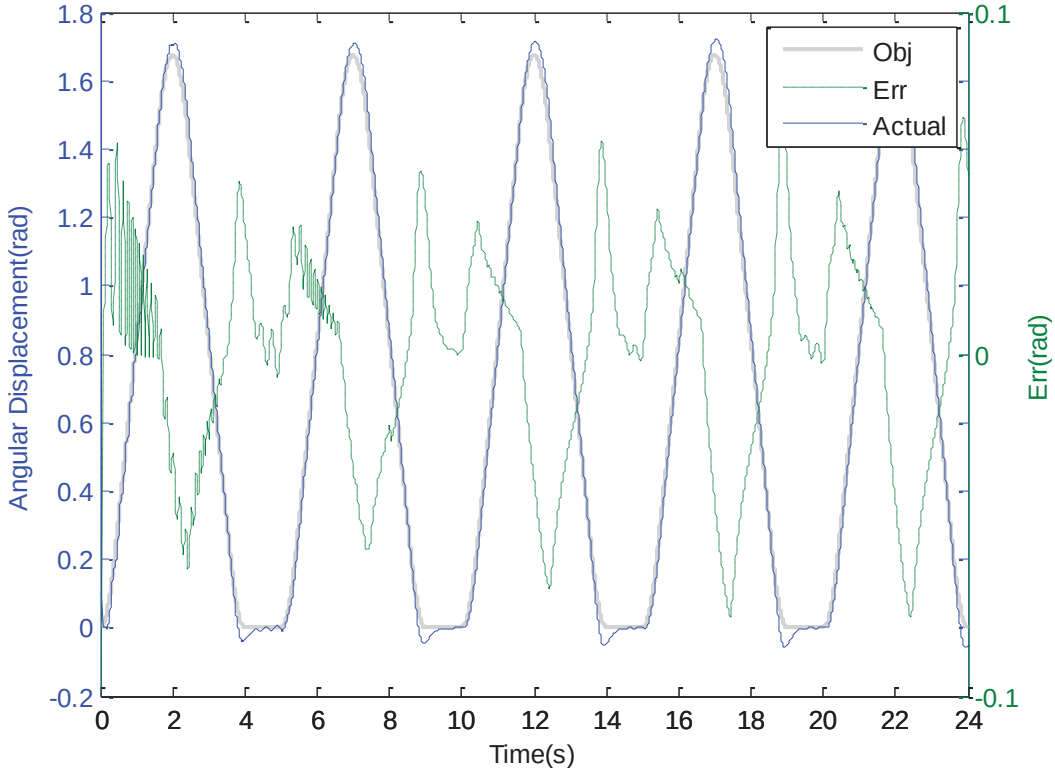

Figure 5-51 Scenario three in closed-loop setup

Figure 5-51 illustrates the experimental results of scenario three in the closed-loop trials. It shows a similar trend in terms of the positional response with the one without interval, so is the maximal error of the same level at 0.06 rad. During the intervals, the device still experiences a tiny shake of ±0.5° margin (3 increments) plus an overshoot on the end of the closing phase, which never showed up in the open-loop trials. It can be explained by the existence of the PID which adds one more signal flow to the motor compared to open-loop one.

5.5 Discussions

The dynamic analysis of the entire device underlies the implementation of the control strategy. This chapter has analyzed the kinematics and the dynamics of the entire device, which has been validated by the simulation results in SolidWorks. The entire system model has been built up in SimMechanics, to facilitate the control algorithm simulation and further implement the controller. The motor has been modeled in Simulink and simulated with verification of parameters.

The closed-loop control scheme has been proposed to achieve a position control, which consists of a feed-forward block and a feedback block. The former was implemented by the inverse dynamics of the linkage, to provide the predicted control signal; while the feedback block which is a PID controller corrected the error between the objective and the actual one. The motion profile can be predefined in a GUI which allows users to specify the motion forwardly and inversely. A couple of simulations have been done under three motion scenarios, during which PID controller was firstly tuned in Simulink.

The treatment program has been coded into the controller board, and all parameters have been inherited from the one in Simulink with fixed-point arithmetic. A simple UI to facilitate the motion selection has been coded to display in the built-in screen. Under a series of motion scenarios, the device has been tested in the performance of the positional control. The PID controller has been re-tuned to achieve the better performance in response the motor command.

Chapter 6: Evaluation of Human-Machine System

The device could not be worn on the human and run in operation before being evaluated by human-oriented tests in terms of the safety to avoid causing additional injury to wearers. Rare researches can be found to assess the influence to wearers from the biomechanical prospective due to human-machine interaction among the literature of exoskeleton development. Particularly to the replication of jaw movement, those influences subject to the jaw exoskeleton can be explicitly reflected on the attachment directly contacted to the jaw and implicitly undertaken in the inside TMJ.

In vivo measurement could not be achieved by invasive means in the circumstance of the TMJ surroundings because of its inaccessibility. Traditional approaches take more advantage of the incisor properties concerning kinematics to inversely calculate the required counterpart; in terms of the mechanical behaviors borne on the TMJ on the other hand, simulations applying FEM have been universally used pertaining to biomechanical studies. As far as potential impacts subject to wearing exoskeleton are concerned, their evaluation by means of non-invasive experiments poses a great difficulty in front of us.

This chapter starts by identifying the likely spots where detriments would occur in human-machine interaction. Then evaluation of the concerned items is undertaken by both software simulation and experiments, outcomes from which can be mutually verified by comparing the specified criteria. To approach an actual loading condition, simulations in this context consider dynamic effect from device inflicting on the wearer in the course; experiments set up in a test-rig platform. Both results are compared in discussion to obtain a general pattern and acquire critical impact factors.

6.1 Evaluation Criteria for the Interaction

Apart from the efficacy brought from the exercise practice with exoskeleton in the application view, the usage of the exoskeleton will inevitably offer many effects to the wearers during its operation in terms of the feeling of wearing, for example, the comfortableness of wearing, noise, magnetic field formed by electronic parts. The influences may be derived of the device itself, or of the interaction with the wearer; some of them project little impact to the users, while others may inflict negative consequence related to the safety whose emergence should be foreseen and prevented by further actions. Most of the effects can be interpreted with one or more factor in the design.

Basically, the influences to the wearer from the perspective of the device should be evaluated in terms of systematic aspects of the Mechatronic design per se, which is not inclusive in the discussion in this chapter, though the normal operation of the device might create some unintended effects to wearers due to the engineered malfunction, impairing the maneuverability of the device, and even the task performance as well. Imagine the scenarios that the preset exercise range is overtaken due to the unachievable limit sensor signal blaming unreliability; or the compromised effectiveness of exercise that was not fulfilled because of the less robust control system. The human-machine interaction that reflects internal reaction to the human body, however, is of our interest that is discussed in this chapter.

6.1.1 Potential Influence to Wearers

Compared to the device, the human-machine interaction gets paramount concerns on the wearing as it straightly associates with the safety and comfortableness for wearers. The negative impact could arise in the interaction between exoskeleton and wearer, which is usually placed in the independent assessment for the wearing feeling of the device; it exists in two sides, one showing up on the attachment where the jaw is gripped by the device, the other implicitly hidden in the inside TMJ where the TMD occurs. The likely harm the exoskeleton might inflict on wearers can be caused by forced movement of the jaw overstepping an acceptable ROM and imposing excessive loads upon the TMJ. Given the fact that TMJ surroundings are susceptible to injury, the potential detriments in wearing the jaw exoskeleton can be conclusively attributed to the impairments on the TMJ owing to the human-machine interaction.

Therefore, the items that are able to directly quantify the H-M interaction can be embodied to the parameters inherently reflecting the feature of the jaw movement, the travelling distances on the incisor and condyle kinematically, and the stress on the same location biomechanically, which can hardly be explanatory of the design parameters. Since the interaction that inflicts the negative influence to the wearer in aspects of biomechanics has rarely been studied over the development of the exoskeleton, the acceptable range within which allows variation for each evaluating parameter are established by referencing the literature, it is though believed the endurance of human to stand up the stress and dislocation of the joint is resilient to the pressure scenario.

6.2 Mathematical Model of the Masticatory System

Since the jaw exoskeleton which is intended to drive the lower jaw inevitably imposes some external force on the jaw in the way that is visually undetectable, the multi-body dynamic analysis is recruited in this section to non-invasively estimate their interplay subject to rigid-body motions. The dynamic study is conducted based on a computational model, enabling to embody biomechanical and physical properties of the musculoskeletal system. The loading condition can be restored in the simulation, whereas the simplification of the masticatory system will be unavoidably taken, not only in terms of the morphology, but the established kinematic model as well. The model is built up in the SimMechanics/Simulink/MATLAB for dynamic study, which contains three objectives listed below.

1) To approximately assess the effect of jaw exoskeleton interacting with the mandible by TMJ loadings as the reference;
2) To test the adaptability the condyle trajectories on the incisor trajectories experimentally;
3) To provide the estimation for further FEA study.

6.2.1 Model Definition

The model is established within the field of dynamics that excludes consideration of the deformation, and basically it consists of a bony jaw, the muscular forces from muscle, the soft tissue surrounding the jaw, and generated joint force. The maxilla or the skull is prearranged as the stationary reference that connects the lower jaw via multiple strings of muscles, and will not be explicitly visualized in the model. Though the six-DOF movement of the jaw can be undoubtedly achieved subject to a spatial configuration of muscular forces, the contact surfaces formatted on the joint and occlusal plane only constrains the sagittal-plane movement that contains three DOFs.

6.2.2 The Mandible

The mandible bone is considered as a rigid body, which is accelerated with respect to the center of gravity. The geometry of the jaw does not directly impose affection to final results, but the relative location of involved muscles that are attached on the jaw depends on its physical properties; the mandible is present in the model to form the geometry by two ways, namely, simply constructing the convex points in the Simulink, and converting SolidWorks 3D file as a representation. The lower jaw prototype that was 3D reconstructed in the SolidWorks can be used to locate the center of gravity based on the known moment of inertia, which is

adapted to the size of the 3D prototype herein from literature, as listed in Table 6-1 [94]. The mass that includes that of muscles and other tissues in the model is assigned to 440g ± 10g based on the previous published properties. The mandible is placed in gravitational field of 9.81 m/s^2 along the Y-direction in the SimMechanics.

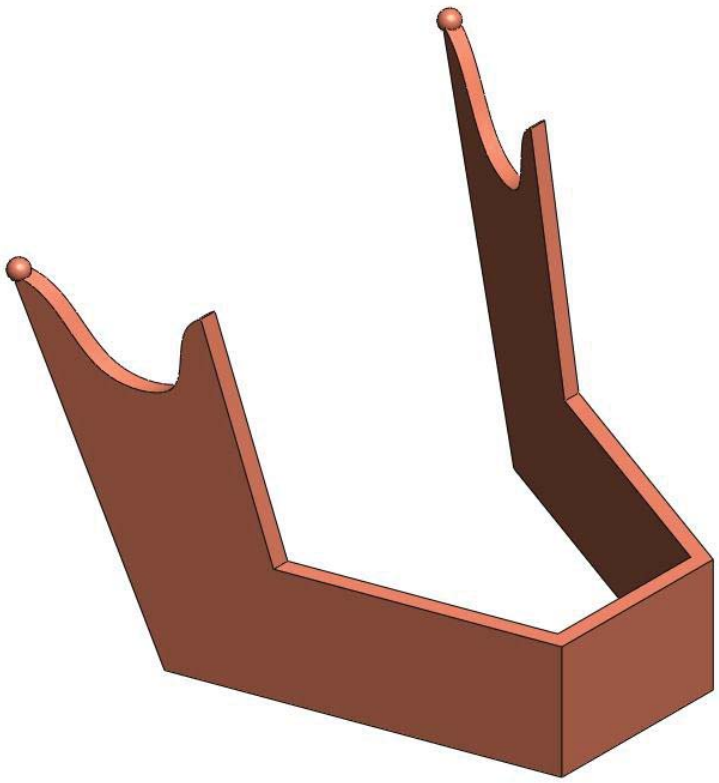

Figure 6-1 Representation of mandible in the model

Dentition that basically offers a positional constraint for occlusion is not distinctly offered, since the sagittal movement of our interest only casts a point on the occlusal plane for the normal depression-elevation of the jaw. Different from the previously modeling into an ellipsoidal surface, the condylar geometry on the jaw that affects its sliding inside the joint is also shaped by two ways, directly a single point configured in the Simulink and the one converted from SolidWorks 3D file. The contact surface in the latter is assigned frictionless and 9.2mm in the anterior-superior direction, as the whole illustration shown in Figure 6-1.

Table 6-1 Physical properties of the mandible

Center of mass (mm)			Moment of inertia (gcm^2)		
X-axis	Y-axis	Z-axis	X-axis	Y-axis	Z-axis
51.11	-49.05	0	8600	2000	6100

The guidance for the condyle movement, which is actually the bony outline of the fossa-eminence on the sagittal view, is assigned by a polynomial in Eq. (6-1), as the shown in Figure 6-2.

$$z = 3 \times \cos(x/11 \times \pi) - 3 \tag{6-1}$$

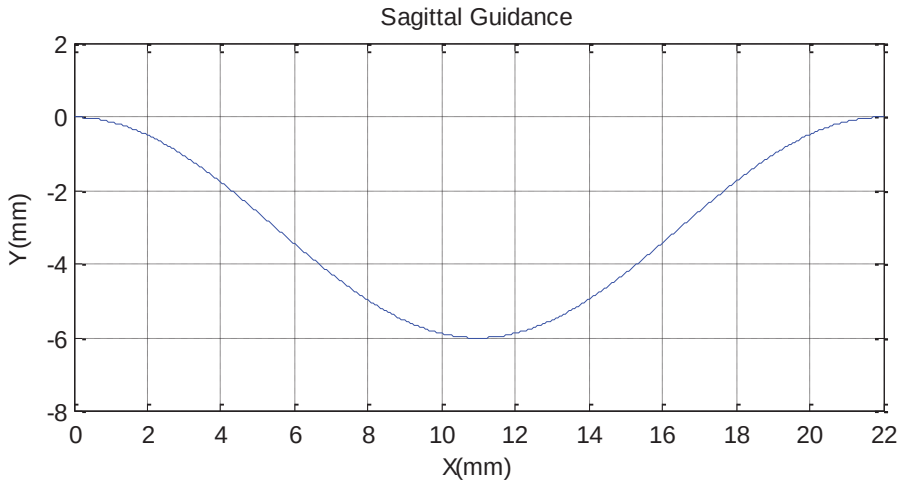

Figure 6-2 Condyle pathway guidance

6.2.3 The Muscular Force

The muscles that are involved in the mastication according to the literature exceed more than 20 portions, but only the main groups are incorporated in the entire model. The elevator simulated in the model includes the deep and superficial parts of masseters, anterior, middle and posterior parts of temporalis, and posterior part of lateral pterygoid; while the depressor includes anterior part of digastric and lateral pterygoid; as the properties of muscle groups are listed in Table 6-2, such as the muscle length for the definition of the muscle force in the model. All of the muscles are modeled to 1-D typical Hill-type actuator, each of which is fixed in the origin of the muscle portion and contract alongside the muscular line at insertion; and all of the physiological data are referred to the literature [54]. The Hill-type muscle model that has different configurations in the literature basically is modeled to contain a contractile element and elastic elements, respectively producing active and passive tensions that rely on the maximum isometric force at the sarcomere staying at the optimum length; separately, the active element correlates to it the length, the velocity and the activation level while the elongated length passing the optimum only for the passive one, as expressed in Eq. (6-2).

$$F_i(t) = F_{max}[A(t)F_L(t)F_V(t) + F_P(t)] \tag{6-2}$$

Where,

$$F_V = \begin{cases} \frac{12.5 - V_S(t)/2.73}{12.5 + V_S(t)/0.49}, & V_S(t) \geq 0 \\ 1.5 - 0.5\frac{12.5 + V_S(t)/2.73}{12.5 - 2V_S(t)/0.49}, & V_S(t) < 0 \end{cases}$$

$$F_L = 0.4128L_S(t)^3 - 4.3957L_S(t)^2 + 14.8003L_S(t) - 15.0515$$

$$F_P = 0.0014exp\left[6\frac{L_S(t) - 2.73}{2.73}\right]$$

$F_{max}, A(t), F_L(t), F_V(t), F_P(t)$ is the maximum isometric force, and the instantaneous activation, force-length relation, force-velocity relation respectively, which are formulated in [195].

Table 6-2 Muscle properties

		Muscle length (mm)	Fiber length (mm)	Sarcomere length (um)	Max. muscle length (mm)	Max. force (N)
Masseter	Superficial	45.6	24.6	2.47	61.8	204.6
	Deep	24.3	18.0	2.44	36.5	104.7
Temporalis	Anterior	49.7	27.1	2.35	69.8	231
	Posterior	52.2	25.7	2.31	72.1	166.5
Lateral pterygoid	Inferior	32.6	23.0	2.83	42.9	84.6
	Superior	31.3	21.4	2.72	42.1	28.5
Digastric	Anterior	43.2	21.4	2.75	53.7	34.8

Since the rehabilitative exercise offers power externally to dilate and shut the mouth, indicating the device is primarily designed to overcome resistance that are derived from the joint stiffness and the passive muscle force and the gravity of the mandible during depression and elevation, respectively, the passive part of the elevator force is simulated into the mandible opening process, though the active muscle force is also applied into one scenario that simulates resistance exercise.

According to Eq. (6-2), the passive muscle force is dependent on the instantaneous sarcomere length, which correlates to the fiber length; and the closing muscle length is defined maximally to reach 150% of each optimum. The length variation is generally placed all over in the fiber, since the tendon is not accountable for the extensive function, as the muscle length expressed in Eq. (6-3). Figure 6-3 shows the subsystems built in the Simulink for derivation of the instantaneous sarcomere length (A) and the passive muscle force (B), respectively. The passive force of each participant muscle is then calculated with respect to the stretched length by invoking the properties of each portion, as shown in the Figure 6-4.

$$L_{muscle_{max}} = L_{fibre_{optimum}} \times 150\% + L_{tendon}$$
$$= L\_fibre \times \frac{L_{sarcomere_{optimum}}}{L_{sarcomere}} + \left(L_{muscle} - L_{fibre}\right) \quad (6\text{-}3)$$

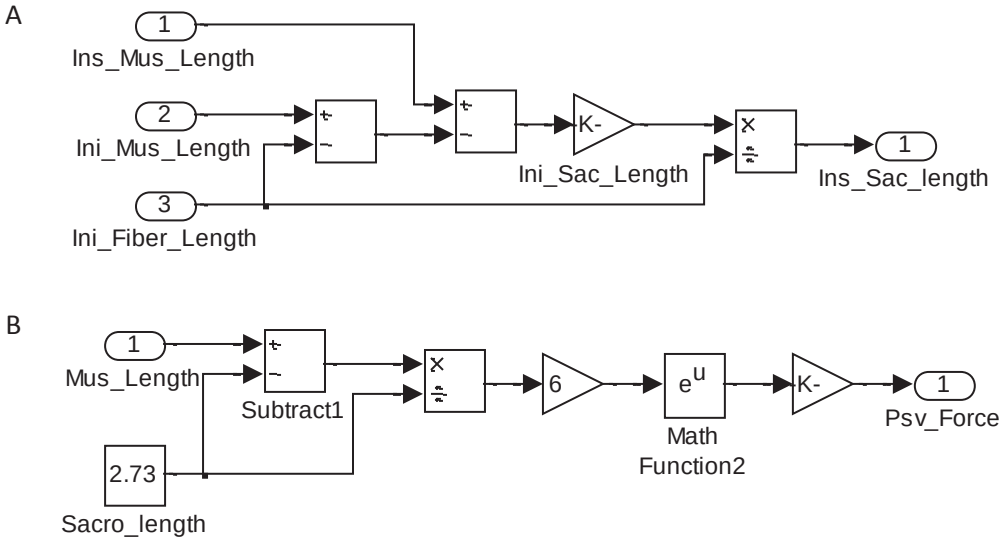

Figure 6-3 Subsystems of sarcomere length (A) and passive force (B)

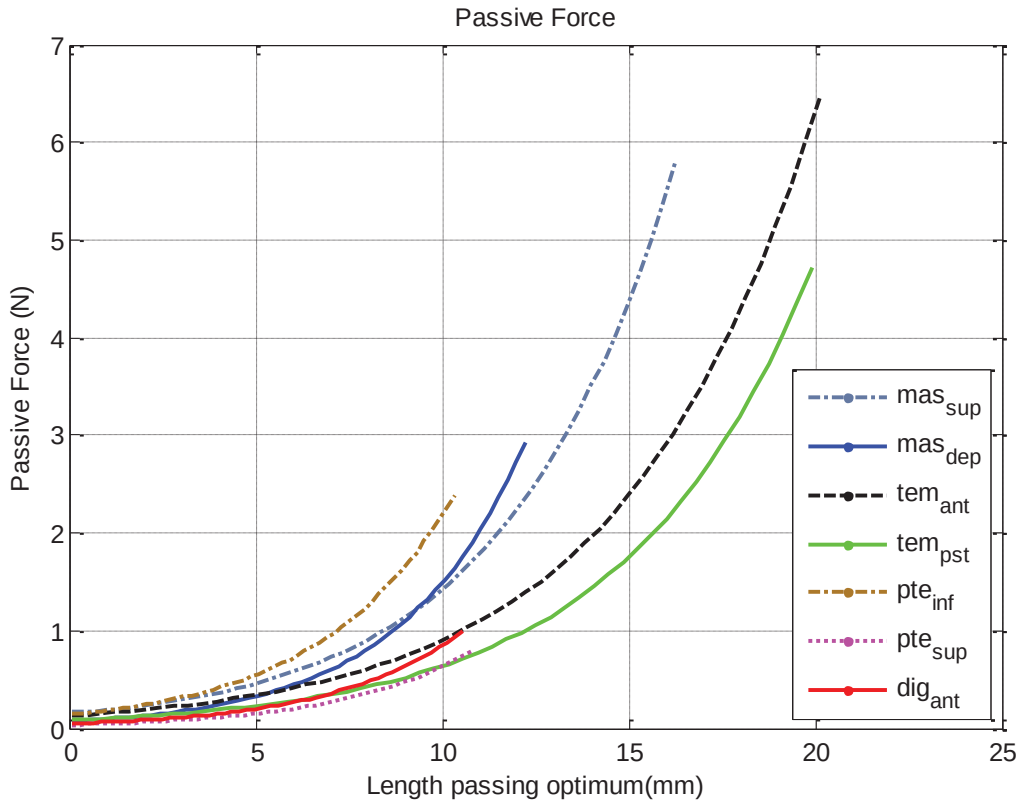

Figure 6-4 Passive Force on involved muscles

The passive muscle force singly incorporated into the muscle model is represented by an actuator against the muscle stretching direction as shown in Figure 6-5 (A). Each portion of the muscle built in Simulink as one leg connects the fixed skull and the floating jaw, which is

connected to the origin and the insertion of each participant muscle respectively; as shown in Figure 6-5 (B), the Hill-type muscle is represented by cylindrical joints from the mechanism perspective that are properly damped of relevant parameters, and the whole Simulink block is assembled as a parallel mechanism as shown in Figure 6-5 (C); according to the number of the muscle involved in the model, totally 7 sets of actuators on both sides exist in physiological location.

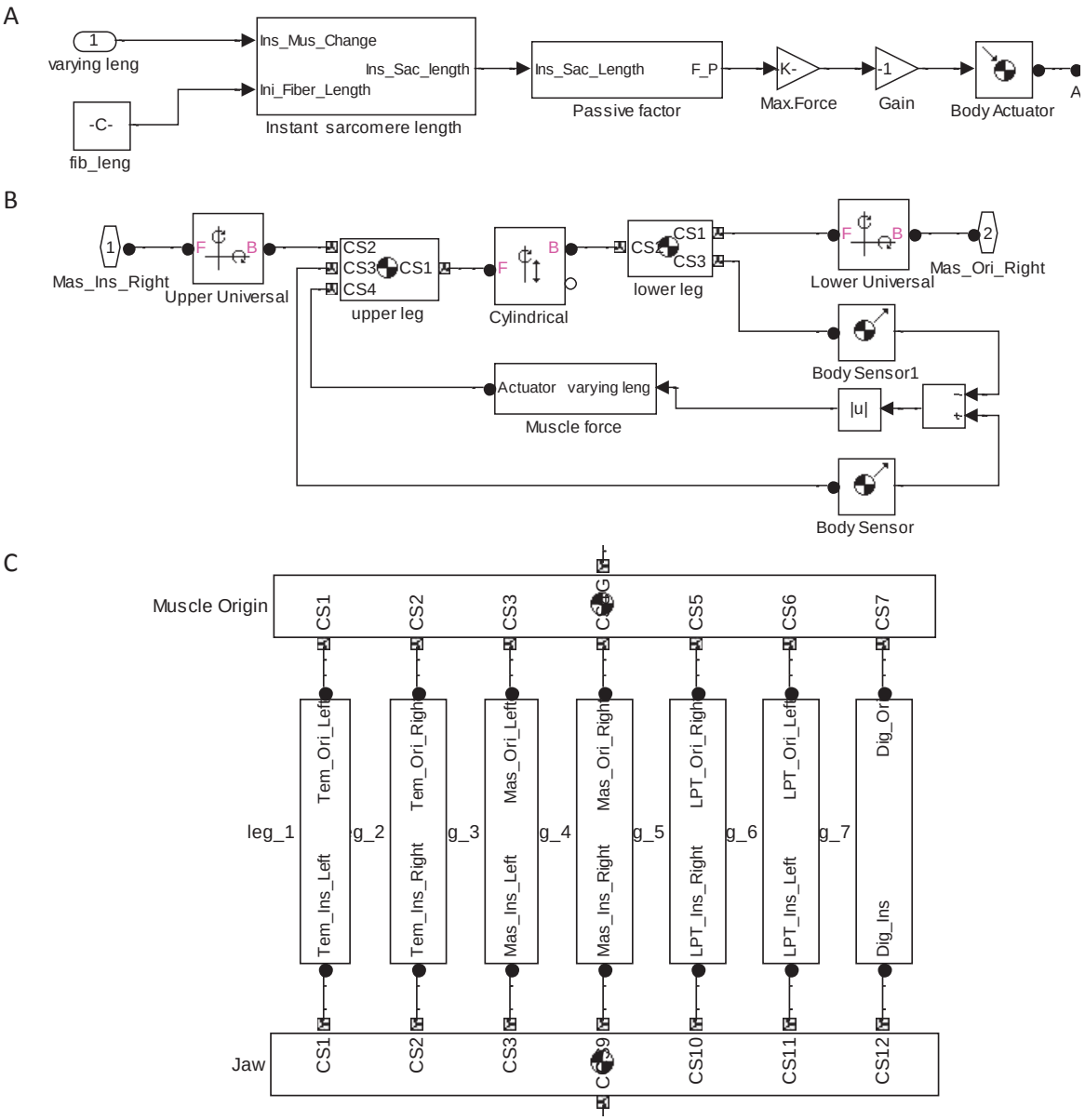

Figure 6-5 Muscle model built in Simulink

6.2.4 The Passive Element

The passive element that basically prevents the jaw from moving beyond the boundary produces its effect by deformation per se, and in the dynamic studies passive elements have normally been ruled out in the overall model probably due to the relative small force.

A. The Ligament

The ligament around the joint possesses a relative high value of stiffness, which has been applied in a range of 10-16 KN/m over different researches, so does the force it is borne that varies in a day-to-day activities. Main ligaments have been modeled as wires that are fixed on the lateral surface of the articular eminence on one side and stretches the lateral pole of the condyle on the other side [57], though no details suggest the way to model the ligament quantitatively in aspects of physiology and biomechanics.

Since the influence of the ligament only notably shows up when the jaw approaches to the border, the ligament is simulated as a passive actuator that is parameterized of the elastic modulus (E_L) by the stiffness. The model connects the lateral point on the jaw to a virtually fixed point on the skull that shares the same Y-coordinate in order to align the line of action parallel to the sagittal plane. The pattern of the action was not clearly given with respect to the elongated length; the ligament is defined to be prolonged maximally by 10% of the optimal length implicitly derived from the scenario, at which coincides the maximum open gape. The force amid the stretch is configured with respect to the largest force 5N as predefined, since the stiffness and the elastic modulus picked from the literature could not hit a consistency. The Simulink model is illustrated in Figure 6-6.

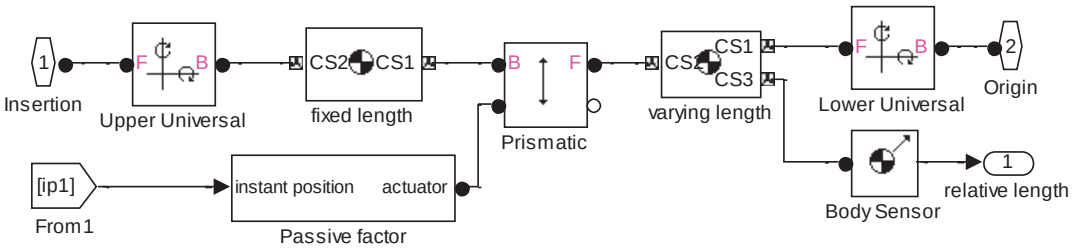

Figure 6-6 Ligament model built in Simulink

B. The Articular Disc

The articular disc has not been regularly found in dynamic simulations involved in the mandibular motion, since deformation is susceptible to occur on the incongruent surface of the articular disc when it is subject to the pressure coming from condyles that is evaluated in the stress; it is difficult to reconstruct the disc as similar as it is to present the deformation in terms of the characteristics. To reflect the likely deformation in the direction perpendicular to the fossa-eminence, the articular disc is modeled by a combination of two virtual points, one of which is fixed on the condylar point and connected to the other by a series of spring and damper by a distance of 2mm which stands for the thickness of the articular disc. The floating point is maintained in contact with the virtual boundary of the fossa-eminence by given a pre-

tightened length on the spring. This configuration on the other hand disarms the possibility to acquire the stress on the condylar point.

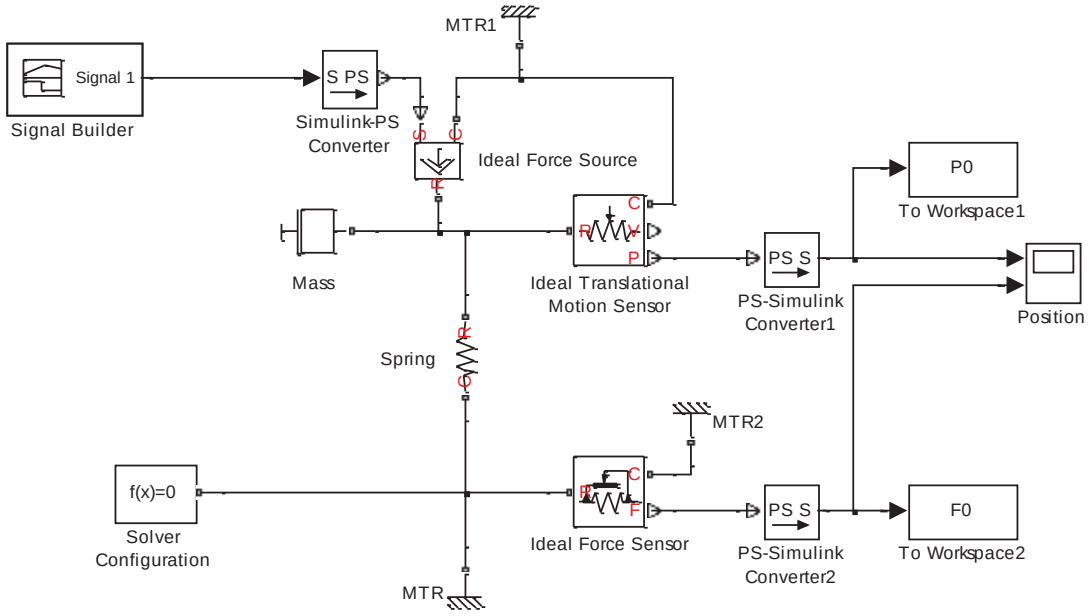

Figure 6-7 Elasticity implemented in the Simulink

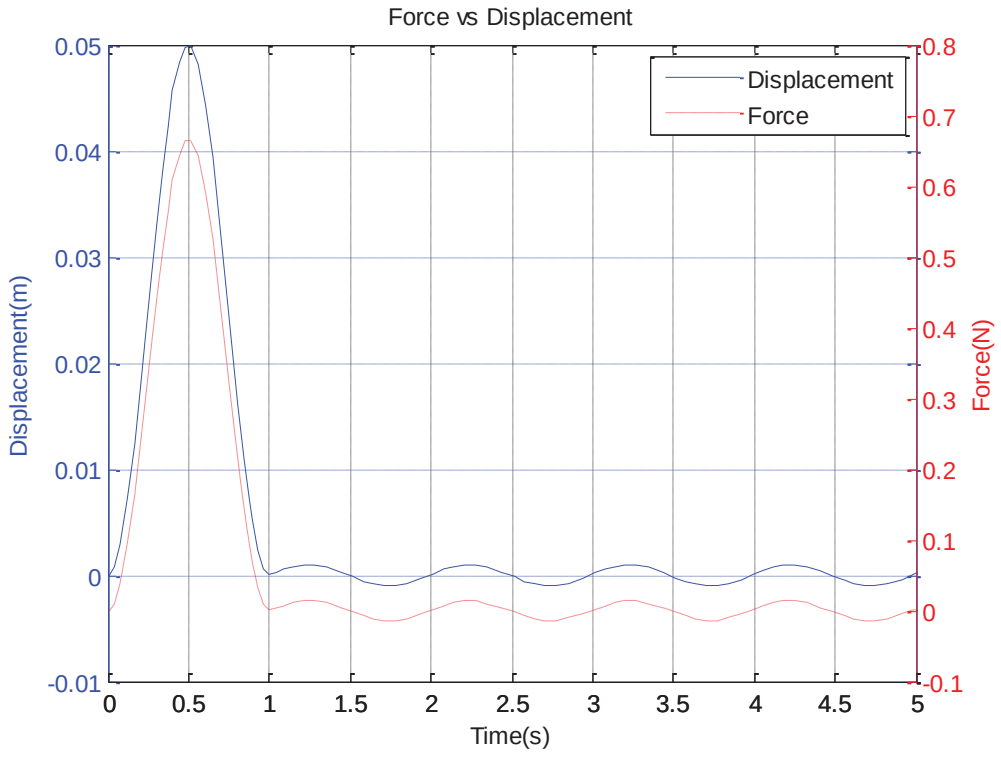

Figure 6-8 Unit response by the passive control model

The articular disc exhibits viscoelastic characteristics on top of the elasticity, so the stress-strain relationship can be described as either linear within the elastic region for the former or time-dependent within the strain limits for the latter. Both passive control models of the

articular disc are implemented by subsystem block in Simulink. Figure 6-7 and Figure 6-8, as well as Figure 6-9 and Figure 6-10 illustrate the model built and the response to a force impulse for representation of the elasticity and the viscoelasticity, respectively.

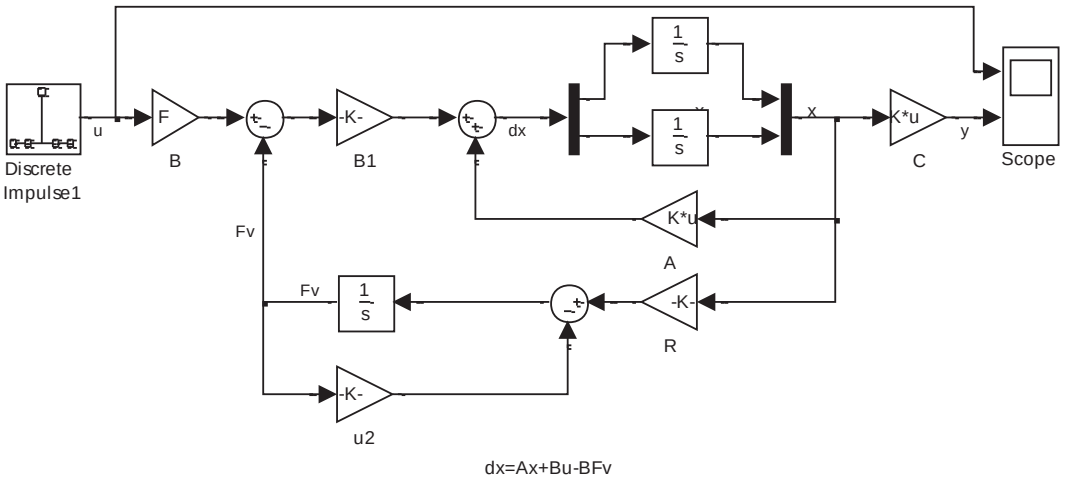

Figure 6-9 Maxwell model implemented in the Simulink

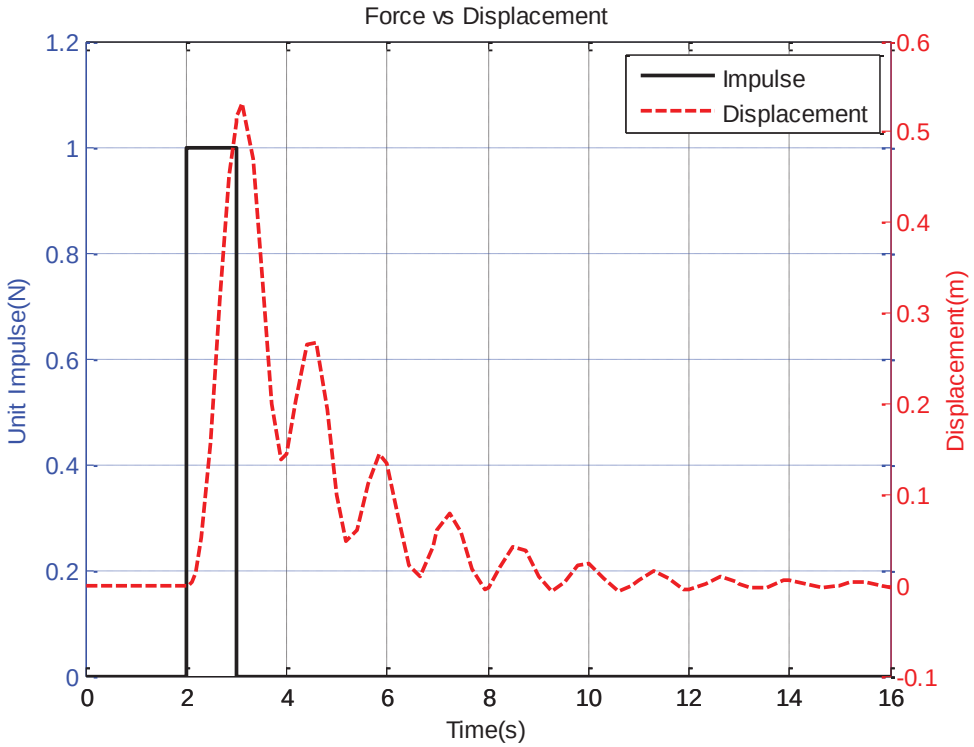

Figure 6-10 Unit response by the passive control model

The contact between the device and the mandible which actually falls on the skin around the chin is simplified in the model to three connective faces formed by four symmetric points on both sides to enclose the chin. The flexible property of the skin and tissues around the chin is not considered here.

6.2.5 Complete Model

The device model in the Simulink that was trimmed after conversion from SolidWorks is added into the entire human-machine simulation. The contact spots between the device and the jaw are specified with two points on each side of the jaw, which are configured into revolute joints, sharing the same coordinates at the initial state. Those joints are also given an allowable range of rotation modeled by the hard-stop, as seen in Figure 6-11. The overall system that is built in the Simulink is diagramed in Figure 6-12.

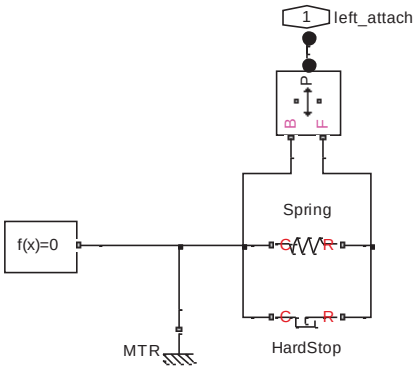

Figure 6-11 Contact configuration

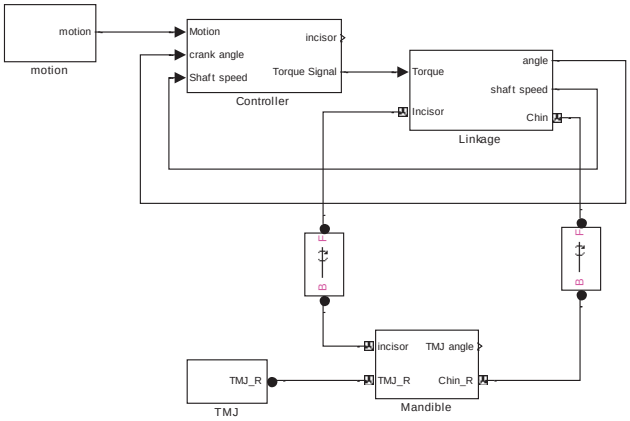

Figure 6-12 The overall model built in Simulink for dynamic study

6.3 Simulation of Human-Machine Interaction

The simulation of the human-machine interaction is carried out based on the combination of the model of each unit built in Simulink, and the objective in this section is to investigate the joint force on the TMJ when the jaw is subject to the device operation. During the simulation, each pair of involved muscles only contributes to the passive force if not specified, in resemblance of the surrounding of lost active force.

The device is specified to run under exactly the pre-defined motion profile used in Chapter 5, in one cycle and multiple cycles with interval in-between. Since it is confirmative that the

model of the device with ideal actuator behaves robust in the performance of the signal response and power provision, the kinematics of concerned points will not be investigated; instead, the simulation will be conducted based on the plant with basic controller, also for the purpose of studying the powering ability of the device.

6.3.1 Model Verification

The active muscle force can be negligible when the jaw is in relaxation, and it is also found that the passive muscle force will balance with the gravity of the mandible at a distance of about 5mm mouth open. So this state is recruited here to verify the correctness of the jaw model here.

The linkage model is firstly removed from the overall human-machine combination, and only the jaw model that is configured with passive model is kept during the simulation; double sides of the TMJ representation is also removed, since a 5mm-opening distance would not cause a large amount of translation on the condyle. The body actuators in all muscles are replaced by the joint actuators that are connected on the extensive joints as exampled in Figure 6-13, to simulate the passive muscular force that actively offer actuation in the model. The simulation starts from the jaw closing position, and lasts for 2s; the displacement of the jaw in the Y-axis direction as affected is shown in Figure 6-14.

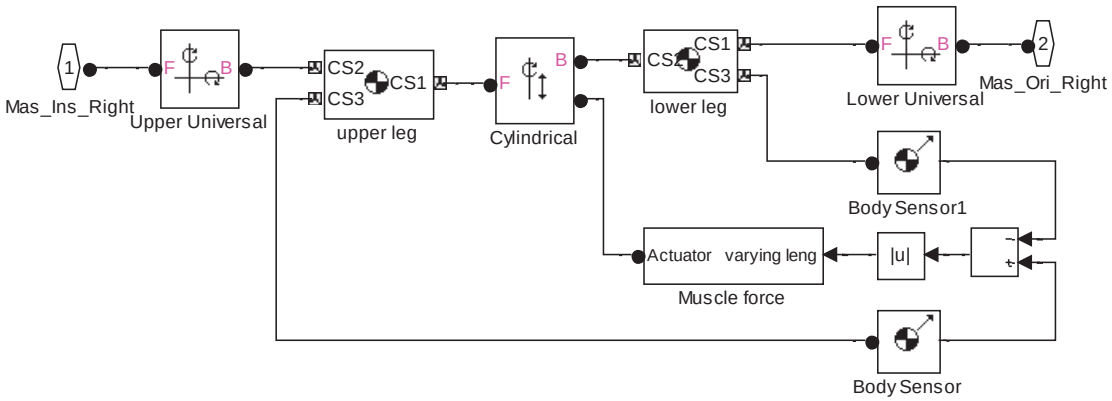

Figure 6-13 Passive force used actively

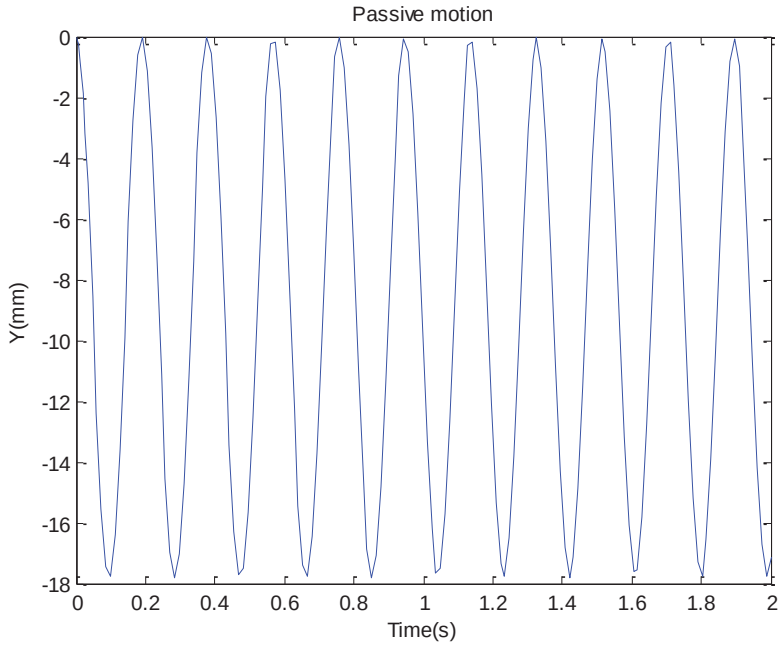

Figure 6-14 Y-axis displacement when only passive force exists

The concerned displacement shows a trend of an oscillation centering the balancing point around 9mm, which stands for the rest position of the jaw. Since the passive force is configured into a function of the stretched length of the muscle, its magnitude keeps growing up with respect to the relative height with jaw in the Y-direction; the gravity is larger than the passive force unit reaching out the balance point, then the passive force starts to shrink in increasing after the stretched length exceeds the optimum, which leads to the oscillation in the simulation. The damping property of the muscle that can hinder the further oscillation in the human is not embodied in the model, and the stretch that is hold invariant could not decrease the passive muscle force. Therefore the rest position simulated in Simulink behaves a pattern of oscillation around the actual balancing point. If only focusing on the model in Simulink, the dynamic model of the jaw movement can be acceptable.

6.3.2 Simulation and Results

The first scenario lasts for 2s for the jaw moving from the starting position to the maximum opening position forced by the linkage, and no active muscle force is added during all simulations. The second scenario contributes 5 cycles of the jaw movement, totally consuming 24s with 1s interval between each cycle. A resistance of 2N is respectively given on the first scenario exactly placed on the incisor point, while no resistance is added into the second scenario.

The joint force is obtained by reading the joint sensor on the joint connecting TMJ block. Figure 6-15 sketches the simulation results in scenario 1 without and with load represented by

(#1) and (#2) respectively. The joint force given in (#1) starting from around 10N is followed by a slight drop till roaring up about 45N. The weight changes the magnitude of the joint force in (#2) where the movement starts with an above 20N joint force, which ascends to about 90N till the simulation completes.

Figure 6-16 gives the cyclic pattern of the joint force on the TMJ, note the minus value represents the measurement direction against the preset coordinates. Focusing on only one cycle, the joint force starts from an absolute value of around 10N, which is equal to the one obtained in the first scenario, and also roars up to around 45N to reach the maximum distance the device can achieve. In the followed closing phase, the joint force generally possesses the same trend during the opening one, and it rests around the same value of the starting point during the interval till next cycle starts.

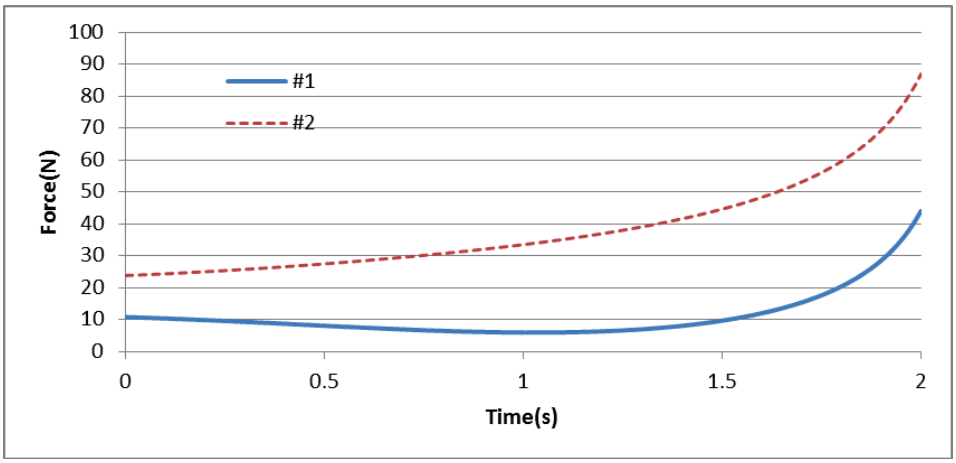

Figure 6-15 Joint force at scenario 1

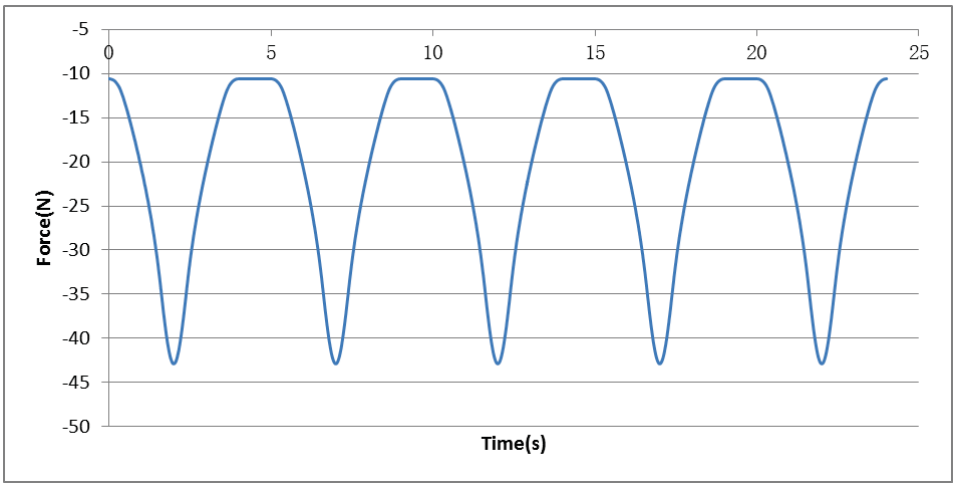

Figure 6-16 Joint force at scenario 2

6.4 Experimental-rig Construction and Set-up

The life-sized experiment that tests the performance of the device in terms of HMI on a customer-built rig can reciprocally justify the outcome from simulation, before moving onto the clinical practice with consideration of the safety of wearers. Meanwhile, the continuous movement inside the TMJ is hardly acquirable on human being by using traditional measurement methods because of the inaccessibility of the oral cavity and uncontrollable precision, which promotes to build up a realistic test-rig.

The objective of construction of this customer-oriented rig lies in two sides: 1) providing the free movement of the constrained jaw on the sagittal plane, 2) which eventually provides this rig as a platform to test the HMI of interest in terms of the motion range and loading conditions on contact sites.

6.4.1 Requirement for Test-rig Construction

Most previous jaw simulators are bio-inspired from the pattern of the masticatory muscles driving the jaw to move, therefore, mimicking the effective masticatory muscles are indispensable while the simulated muscle replacers can be further coordinated to study human mastication control structure. This test-rig is focused on the realization of the movement pattern on the sagittal plane, which does not necessitate the existence of the anthropomorphic structure of muscular actuation. The rig concentrates more on the acquisition of the online data about the HMI in order to evaluate the performance of the jaw exoskeleton in terms of the safety when the exoskeleton runs in operation. The design of the simulator is required to couple the motion reproduction on top of the measurement implementation, which discriminates this simulator from others. Though replaying the jaw movement is still the prerequisite for the justification of the exoskeleton, some requirements for the sensory unit are given priority of selection ahead considering the envisaged special movement.

The recording of continuous movement of the jaw replica is highly preferred, and it is likely to exist in relatively high frequency of the samples. The implementation of the sensory unit (distinguished with the one in exoskeleton) goes into the identical two sides as the mutual verification with the simulating results, i.e. the travelling path and the force around the incisor and the condyle, respectively, requirements of whose measurement are listed below in Table 6-3.

Table 6-3 Accuracy required in the sensory unit

	Position (mm)	Force (N)
Resolution	0.1	1
Range	60	5/50

Considering the space limited for installation, AG 500 that was used for live recording of the jaw movement is selected to track the jaw movement in terms of the interested points after ruling out other commercial tracking devices that generally require a relatively large spot for sensor installation. The overall implementation is detailed in section 6.5. Similar cause in the spatial limits on the joints narrows the force sensor selection down to the sensor exporting raw data from acquisition without post-processing; and the *Flexiforce* sensor is chosen in this application, the deployment of which is fully elaborated in section 6.6, together with the test scenarios.

6.4.2 The Test-rig Construction

Simplification on embodying all components in the masticatory system is unavoidable, and in light of the applied surrounding, it goes in the several elements that are excluded in this rig; 1) the muscles, producing active forces which represents the actuation, since muscles are assumed in weak force exertion or control to fit the context, while only passive force that emerges in the stretch is linearly assigned to the simulator; 2) the passive components, including ligaments and the articular disc that are hardly found replacement with the artificial tissue of similar material properties, as well as little affection to the movement. Therefore the test-rig under such configuration turns into a passive jaw motion simulator.

A. Prototype of the Jaw

The condyle-eminence contact plays a crucial role in measuring the joint force for the purpose of restoration of actual scenarios a relatively high accuracy, which is interpreted by a life-sized jaw and a skull replica from the same subject that are 3D printed from the reconstructed 3D model of the cadaver, as both shown in Figure 6-17 (A) and (B) respectively. The physical properties of the jaw that are likely recruited in the test are listed in Table 6-4, while the skull is fastened onto a frame and properties are not relevantly involved. Since the skull is set as the stationary reference, the coordinate system built based on this combination sets the origin as at the highest point on the jaw, which can also be recognized as the point on the skull where the jaw replica coincides to.

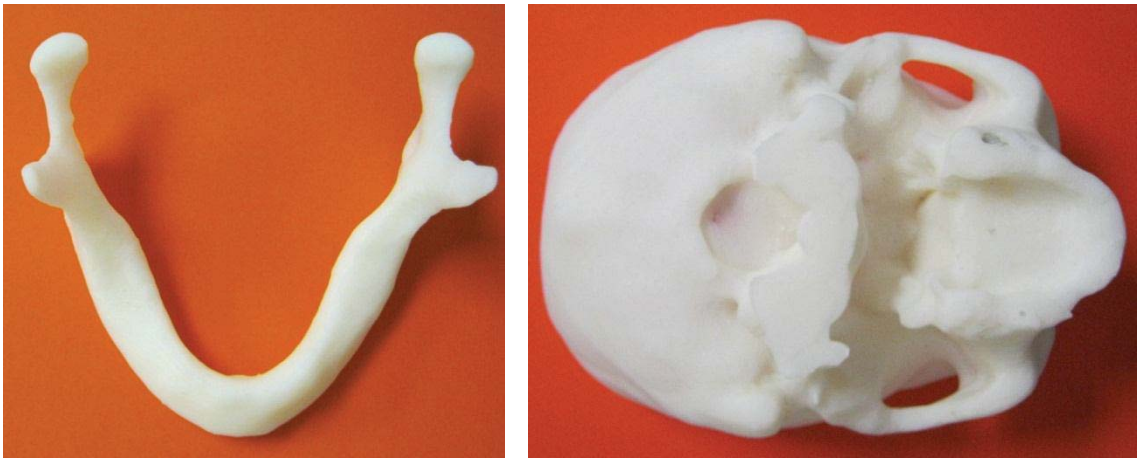

(A) (B)

Figure 6-17 3D printed (A) Jaw and (B) maxilla

Table 6-4 The physical properties of the3D printed jaw replica

	Weight	Size (mm)		
	(g)	X	Y	Z
Condyle	N/A	10	10	10
Jaw	100	82	60	45

B. Muscles

Four pairs of muscles are included in the test-rig only producing passive force with elastic materials; they are temporalis, masseter, and lateral pterygoid for the depressor and digastric for the elevator, each of which is anatomically located in a string by the origin and insertion from literature. Note the temporalis is represented three strings through its breakdown into pieces due to the pinnate shape. The passive force that is proportional to extension occurs during the opening stage for the depressor. The elevator muscle balances the gravity of the mandible replica at the vertical distance of 5mm. The maximum force borne on the artificial muscle is not defined in this context.

C. The TMJ

The TMJ complex is replaced by a joint in the test-rig featured of being frictionless during the jaw movement, which is implemented by two ways in trials of force measurement, corresponding to the respective deployment of the sensors; they are, 1) the tight contact between the condyle and the eminence without other artificial joint, indicating that no actual constraints to the jaw replica that is left free to move subject to the exoskeleton, 2) an artificial joint that is translatable in both directions contacting with the condyle which effaces the curvilinear surface of the fossa-eminence. The first option is preferred in this experimental circumstance since the curvilinear surface that can hardly be replicated by other way than 3D printing will affect the pressure between the contacting faces.

D. The Entire View of Test-rig Platform

For the initial stance which is defined at the rest position of the jaw, the mandible is contacting the skull on the condyle-eminence without clearance, which signifies the non-existence of the articular disc. Since no teeth are mounted on both replicas, the jaw replica is rigidly fixed on the exoskeleton via attaching parts; the entire view of the test-rig is shown in Figure 6-19 (A).

6.5 Trajectory Tracking Experiment

Tracking the jaw movement on the incisor is implemented by recording the trajectories of the IP on the jaw replica which is attached to the exoskeleton in operation with an Articulograph machine. The latest electromagnetic Articulograph AG500 (whole view shown in Figure 6-18), which is originally developed as the speech-movement recording device, provides a non-invasive way to enables the three-dimensional recording and visualization of movement inside the mouth. Basically, the Articulograhpy system detects locations of the sensors based on the inductive distance principle in electromagnetic fields, different frequencies of which generated by transmitters can induce a current in each sensor whose information is conveyed via receivers to calculate the location with respect to transmitters [196, 197].

AG500 enables totally 12 channels of sensors at the same time to record data of five-DOF movement (three-coordinate positions and two-orientation angles) on each with sampling rate of 200 Hz, and all sensors can be attached at any desired position and orientation. The machine has an original coordinate frame based on which to record and illustrate tracking data; the origin of the machine frame sits at the cubic center of the 300mm-radius measuring space and the directions of three axes are specified in equipment as showed in Figure 6-18; the technical specifications are optionally listed in Table 6-5.

Table 6-5 Specifications of the AG500

Specifications					
Range (mm)	X	300	Angle (°)	Φ	90
	Y	300			
	Z	300		Θ	90
	Resolution	0.3/0.5		Resolution	N/A
Frequency (Hz)			100K (sampling)		
			200 (recording)		

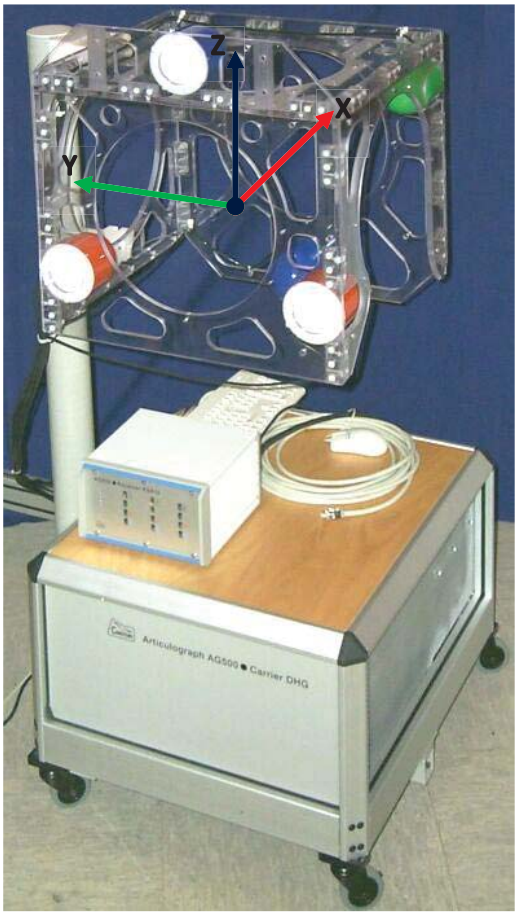

Figure 6-18 Articulograph AG500 [142]

6.5.1 Experimental Set-up and Configuration

The exoskeleton and the maxilla replica are separately fastened on the platform conforming to their relative position and are placed within the cubic space of valid measurement range in AG500. The jaw replica is firmly clamped to the attachment on the exoskeleton with a clip, and maintains a small distance in Z-direction away from the contacting surface on the maxilla to ensure free movement of the jaw without collision between the opposite surfaces when it is subject to the exoskeleton, simply for the purpose of recording the unconstrained trajectories on the CP.

8 out of 12 channels of sensors are substantially used in this experiment to record instant locations of attaching points, and to further compose of trajectories; other sensors were ruled out in the calibration stage because of inaccuracy. Usually in the cases involving human subjects 3 sensors preferably are required to be attached on the relatively non-moving spots on the head to represent the head movement which is set as the benchmark to be offset in the trajectories recorded from other sensors. In this context, though head movement does not necessarily need compensation, 3 reference sensors that are still used to offset subtle

motion of the test-rig such as likely vibration induced from motor, are glued to rear temporal bone, right and left fossa on the maxilla replica, as shown in Figure 6-19 (A-B). The other 5 sensors are glued to the several points including CP and IP on the device and the jaw to record the movement (Figure 6-19 (C-D)); their relative positions are listed in Table 6-6.

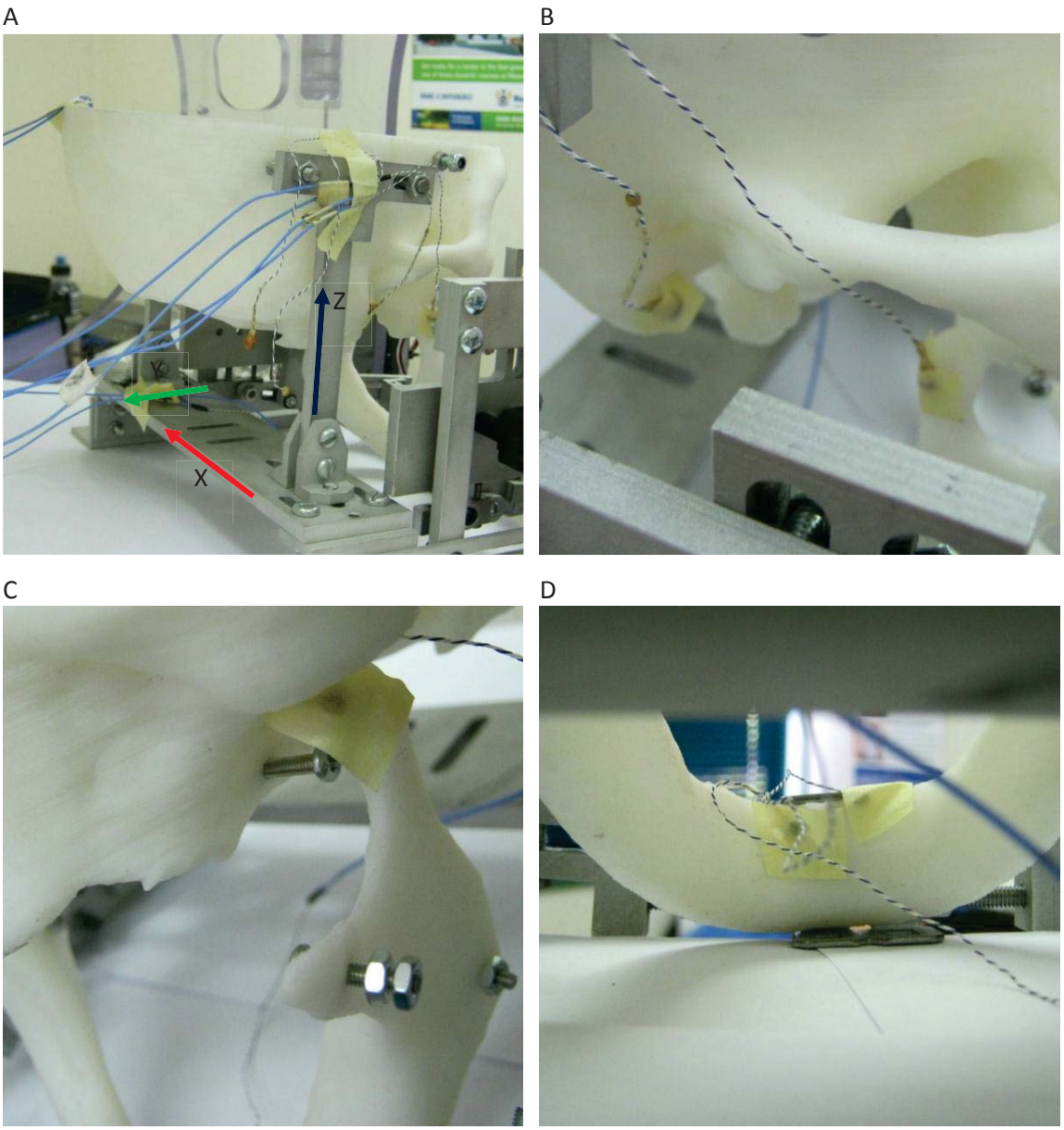

Figure 6-19 Sensor locations (A) of the overall view (B) at fossa and left condyle (C) at right condyle (D) at incisor

Table 6-6 Sensor Positions

Reference Sensor	X (mm)	Y (mm)	Z (mm)	Tracking Sensor	X (mm)	Y (mm)	Z (mm)
3	2.75	43.65	-15.77	4	129.22	-40.35	-45.14
11	-25.20	-9.07	-16.19	5	74.73	12.25	66.90
12	0.02	0.01	0.01	6	-90.08	37.53	63.05
Note: Coordinates with respect to Machine origin.				7	93.62	-9.45	-19.23
				10	117.47	24.99	-83.8
				Note: Coordinates with respect to			

6.5.2 Position Tracking Experiments

The experiments to record the trajectories on IP and both CPs are carried out with several scenarios listed in Table 6-7. The experiments that were originally designed to verify the correctness in terms of trajectories on the interested points are not equipped with high-resolution DC motors installed on the exoskeleton, which means only simple velocity profiles are provided, i.e. constant velocity of the crank and constant acceleration of the crank, driving the jaw to move back and forth. In each scenario the exoskeleton is running repetitively at least 5 rounds, depending on different trials. The ROM is preset in vertical measurement with which the running time is calculated according to the corresponding velocity profile. Loading conditions were not expected existing in the experiments to avoid the inadequate motor torque to propel the jaw causing motor failure, but the last scenario still gave a try of hanging a weight of 0.2 kg on the jaw replica, which means 2N-resistance is added on jaw closing stage.

Table 6-7 Simulation scenarios for adjustable linkage

Trial	Follower	Ground	Trial	Follower	Ground
#1	--	--	#2	--	-5
#3	--	+5	#4	Max(+6)	+10
#5	Max	Max(18)			

6.5.3 Post-processing of the Experimental Data

The test-rig platform is hardly placed in the ideal way to ensure the planar movement to stay parallel to any of three orthogonal planes in the machine frame, and the recorded data on the concerned points reflect their instantaneous coordinates at the sampling time under the global frame, which should be transformed to the coordinates in a tip frame as the jaw is usually oriented at its occlusion to demonstrate the planar trajectories. At the initial state where the jaw stops to the occlusion, the sagittal plane of the replica and the occlusal plane are assumed to be parallel to the side surfaces of each lateral pole and the large plat surface of the test-rig respectively, both sharing the same orientation. Therefore, the tip coordinate frame is set up on the test-rig at the jaw occlusion state, maintaining a constant transformation with respect to the original machine frame to compute the sagittal jaw movement before moving onto the measurement trials.

Three sensors are glued orthogonally on the edges of the test-rig to form the axes of the tip frame. Since the exoskeleton that actuates the planar movement is fastened to the test-rig, identifying the expected sagittal plane of the jaw rather than by the jaw per se, the jaw replica is assumed to share the same orientation in terms of its sagittal plane and occlusal plane on

top of the installation error. The upright edge on the test-rig is specified as the Z-axis of the tip frame; Y-axis is the other axis composing of the sagittal plane, also determined along the exoskeleton edge as shown in Figure 6-19 (A); X-axis points perpendicular to the cross product of Y- and Z-axis. AG500 is switched on running to record coordinates of these 3 sensors while the exoskeleton is also in operation to get rid of the likely head movement. The tip frame identification recording lasts for about 4 seconds and is repeated 3 times; the obtained coordinates on each point after data visualization present a little variation; the distances between three stationary sensors are averaged; and the maximum deviation evaluated as the error between the positive and negative peak distance among all trials is calculated within a range 0.5 mm.

Results show that the standard deviation (STD) of the constant distances in each sensor pair basically stays within the range of the machine resolution (0.3mm); therefore the three sensors can be considered stationary in the machine frame to establish the tip frame that sits on the test-rig. With the values of the sensors coordinates that are averaged, transformation from machine frame to test-rig frame can be represented by Eq. (6-4), one of algebraic matrixes on the new origin point is listed in Eq. (6-5), since transformation is conducted at each scenario to avoid the inaccuracy from interference.

$$ {}^{O}_{J}T = \begin{bmatrix} OA_x & OB_x & OC_x & O_x \\ OA_y & OB_y & OC_y & O_y \\ OA_z & OB_z & OC_z & O_z \\ 0 & 0 & 0 & 1 \end{bmatrix} \tag{6-4} $$

$$ {}^{O}_{J}T = \begin{bmatrix} 0.2549 & -0.7151 & -0.6509 & 38.6302 \\ -0.9212 & -0.3843 & 0.0614 & -101.2320 \\ -0.2940 & 0.5840 & -0.7567 & -112.8004 \\ 0 & 0 & 0 & 1 \end{bmatrix} \tag{6-5} $$

Therefore, coordinates of any point in the machine frame can be transformed to describe its location under the test-rig frame by Eq. (6-6).

$$ {}^{J}P = \left[{}^{O}_{J}T\right]^{-1} \cdot {}^{O}P \tag{6-6} $$

The jaw replica shares the same coordinate frame with the test-rig without a single one attached for representation in terms of its position and orientation, since basically the planar movement is only affected by on the actual sagittal plane determined by the exoskeleton rather than that in the jaw replica.

After the recorded data transformed into the test-rig frame, the trajectories is required to undergo an ideal software filtering which could get rid of the high-frequency affection derived of the AG itself and data sampling, and at the same time smooth the trajectories from the

noise. As AG recording frequency is about 200 Hz, a low-pass Butterworth IIR filter is chosen to meet the filter specification that is given to have at most 1 dB of pass-band ripple, and at least 15 dB of stop-band attenuation to keep waveforms without too much data attenuation. Parameters of the filter are calculated in the process of filter design with MATLAB and the data in all trials are filtered with this Butterworth filter before illustration. Figure 6-20 shows an example of one set of raw after transformation in the tip frame compared with filtered one. All trajectories shown below have been filtered from the raw data.

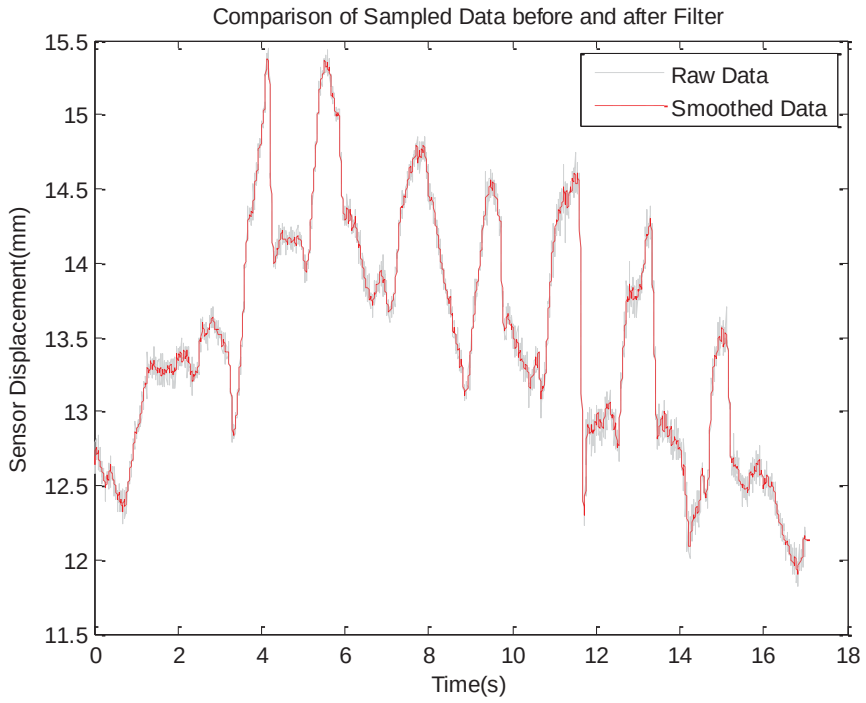

Figure 6-20 Comparison of data before and after filtering

6.5.4 Results Comparison and Discussion

The scenarios under which to conduct trials are not fully in line with the series that was specified before, and finally three scenarios of the link size combinations (of grey shading in Table 6-7) that have been successfully used to export result, since the follower is hard to stay adjustable during the experiments. Primary concerned in the measurement is the condylar displacement in the plane, and four sensors are used to acquire the condyle trajectory with a couple being attached on either side. One sensor is attached on the incisor, which is neither in according with the specified IP position $[89.51, 45.01]$ with respect to the condyle $[0,0]$.

The results are plotted in MATLAB after transformation into the plane, the planarization of the coordinates evaluated by STD and peak discrepancy has also been checked within the machine precision. Since at least five cycles are conducted in each trial, the running cycles are firstly partitioned out after filtering to ensure the curve for comparison only to contain one cycle.

Figure 6-21 to Figure 6-23 illustrates the condyle trajectories acquired on 3 out of 4 sensors in No.1 scenario, which keeps the original dimension of links. The crank is specified to rotate to the extreme position as it can, passing by an angle of around 100°. The measured trajectories on the condyle possess similar trend by and large with the one calculated theoretically, in the aspects of both range and the trajectory inclination. The wavy shape suggests the fluctuation of the tracking trajectories, which may be triggered by the motor shake brought into the measurement or unstable fixation of the device, instead of being caused by the device itself in terms of the design. The largest deviation between two groups of data is about 2mm in the superior-inferior direction, but it is not strictly calculated.

Figure 6-24 and Figure 6-25 give the comparison of the condyle trajectory on one sensor in trial 4 and 5 respectively. During these two trials, a 200g weight is hung on the attaching bar, and the crank is specified to rotate a relative 60° rather than to the extreme value. The measured trajectories on the condyle basically trace the similar trend with the theoretical one, but differentiated in the angle of inclination and a shrunk range. The smaller range suggests the correlation between the trajectory of condyle and incisor under the same movement, and it is not proportional to the crank angular displacement. The difference of the inclination angle is not evaluated quantitatively; the curves in one figure that are not sharing the same starting point could partially be accountable.

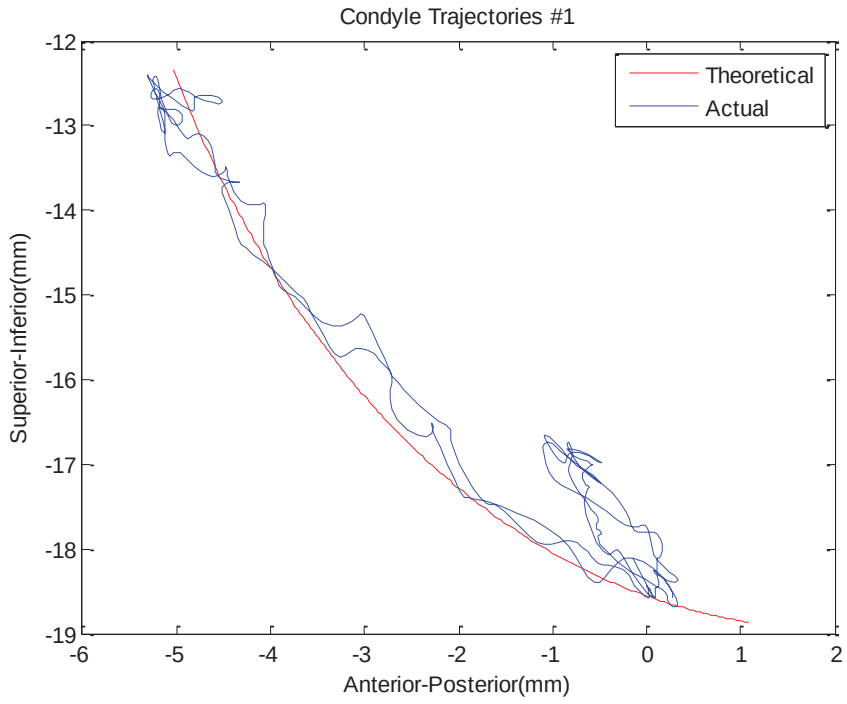

Figure 6-21 Condyle trajectory in trial 1

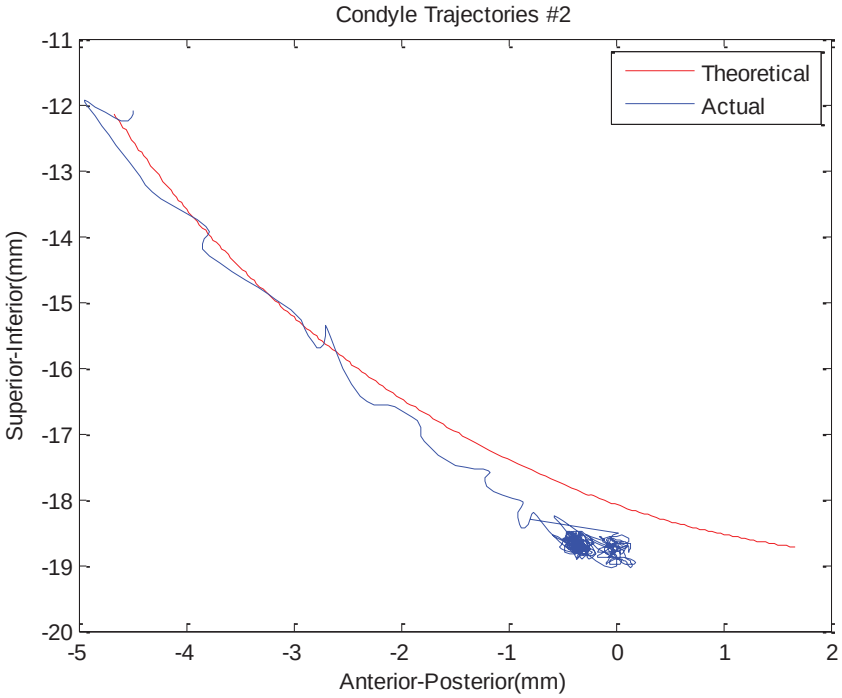

Figure 6-22 Condyle trajectory in trial 1

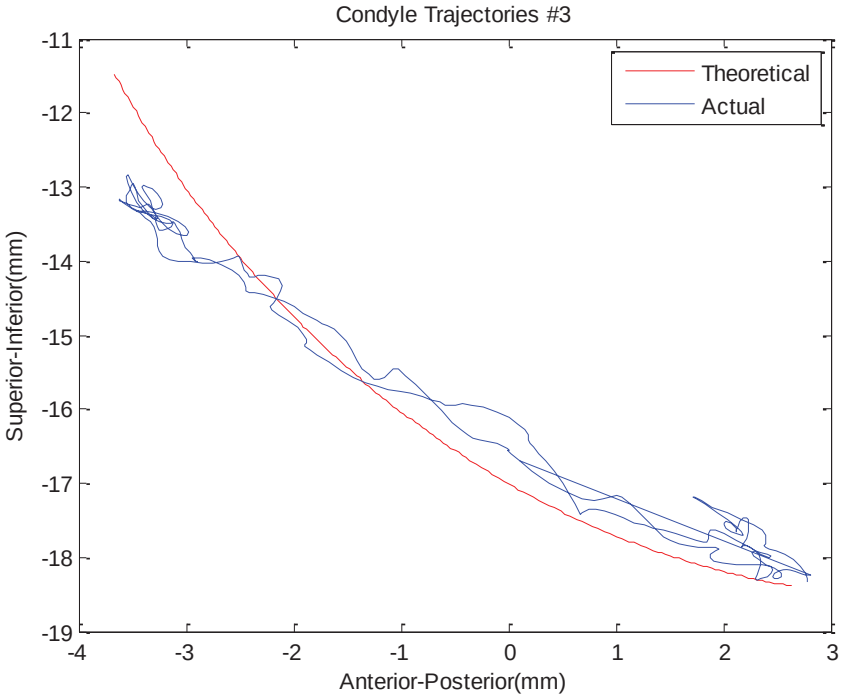

Figure 6-23 Condyle trajectory in trial 1

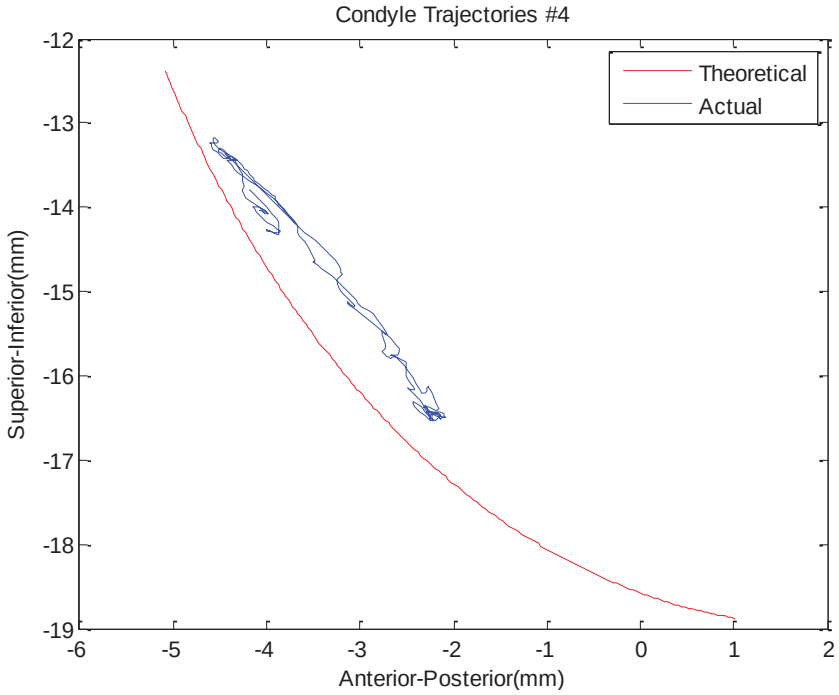

Figure 6-24 Condyle trajectory in trial 4

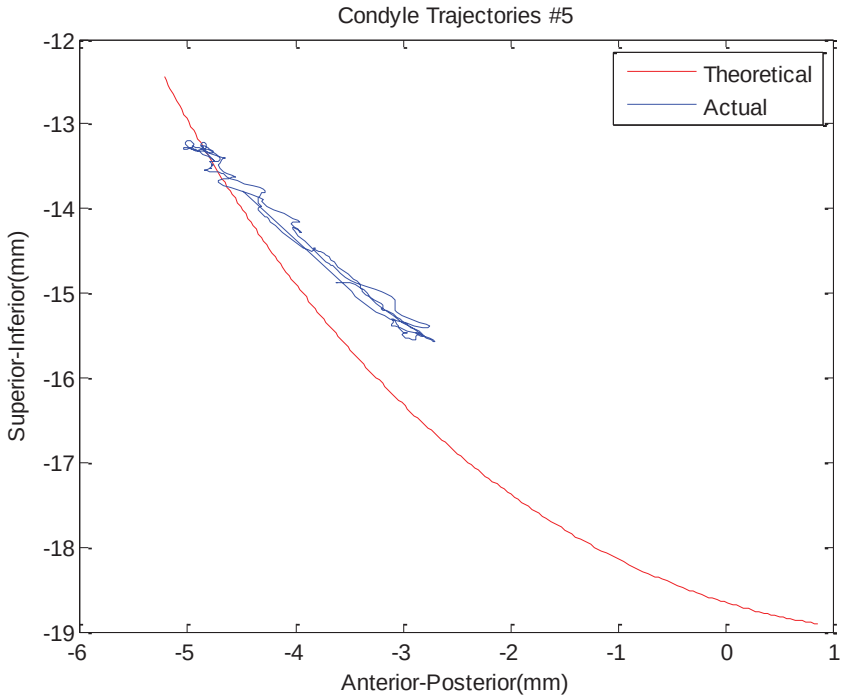

Figure 6-25 Condyle trajectory in trial 5

The incisor trajectories have been also recorded in all five trials, of which Figure 6-26 and Figure 6-27 show the transformed results of scenario No.1. The range of the actual curves is larger the calculated one, which is side confirmed by those on the condyle. The curves are basically maintained the same form of the theoretical ones. More fluctuation can be found in

the incisor side than in the condyle, which can likely be explained by the requirement of more moment on the incisor. In summary, the measurement with AG 500 can generally consider the device is able to replay the specification in terms of the motion without too excessive discrepancy compared with the theoretical one.

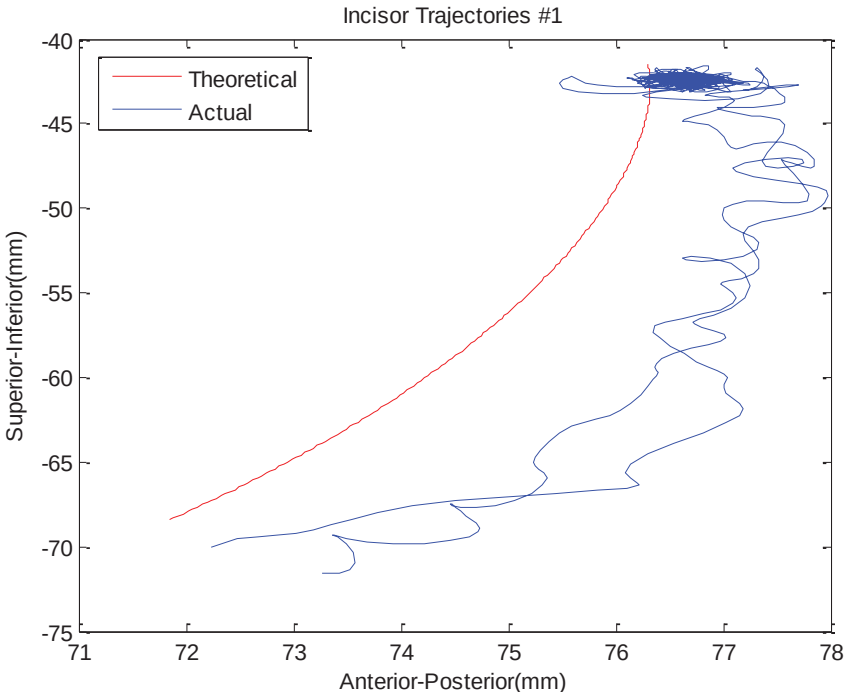

Figure 6-26 Incisor trajectory in trial 1

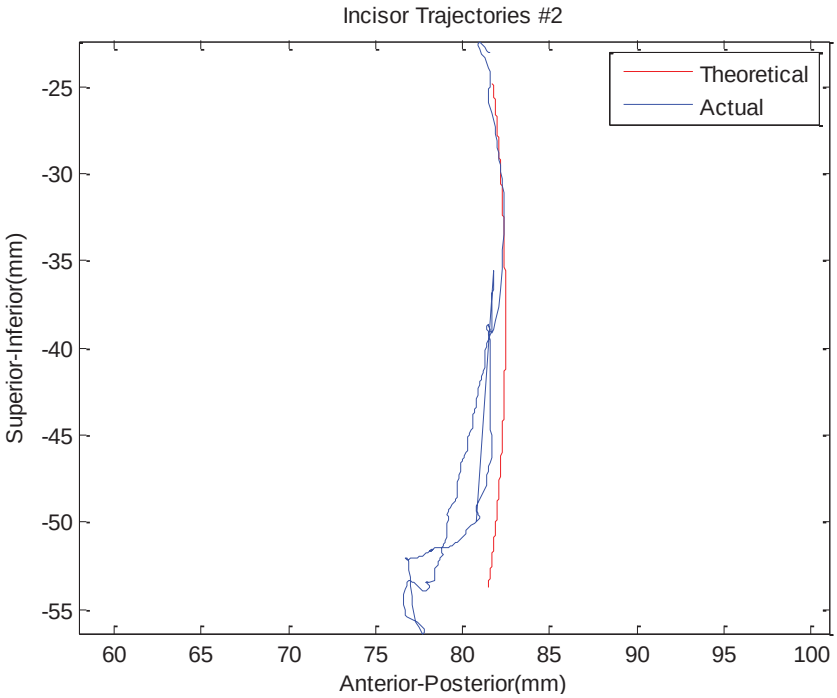

Figure 6-27 Incisor trajectory in trial 1

6.6 Trials of Force Measurement

Since TMJ surroundings are much more vulnerable than other components in the masticatory system, excessive pressure should be strictly restrained to avoid causing further detriment to the joint. Apart from the simulation that offers an insight into joint force from the dynamic prospective, the non-invasive measurement can hardly be conducted in vivo due to the inaccessibility of the area. Therefore, the test-rig which has been installed with the replica of upper jaw and lower jaw is used to measure the joint force when the mandible replica is forced to move subject to the jaw exoskeleton.

Interference of the jaw movement as caused by the incongruent eminence surface on the skull is likely to happen, and that is also the reason large force is generated during the movement if the actual trajectory stays inconsistency with the produced one. Passive muscular force is not included in the test-rig prototype.

6.6.1 Trial Set-up

Force sensors that are characterized of flexibility and curvature performance are preferred in this application, while the requirement on the size outweighs the precision of the measurement, since even in the circumstance of the test-rig; the contact between the replicas on the joint is rather tight. On the other hand, a general force level during the experiments is adequate to evaluate the effect the device may impose on user at worse.

Flexiforce sensor that satisfies requirements in the size is selected to test the joint force. Although those sensors can be attached to any surface on either eminence or the condyle, the curvilinear rate of both surfaces hinders the direct installation. To keep the curvilinear feature while attaching the sensors onto one of them, the jaw replica is partitioned into two parts along a cross-section away from the condyle about 15mm. The joint force in this trial is considered to point perpendicularly to the eminence surface at the contacting point, but the cross-section that sets the jaw apart could not assure to be always orthogonal to the instantaneous force vector. The variation to the real direction of the force will be discussed in the following section. The measured force provides only values of the magnitude rather than vector that contains direction as the actual one. According to the simulation results, the sensor type is selected the one with measuring range of 25lb.

The force testing experiment is carried out on the scenario that the device is running under the continuous cyclic movement with 1s interval in-between. The size of the device has not been adjusted during the experiment, i.e. the trajectories on the condyle will not be varied

ideally; springs are not pre-tightened and in natural state. To maintain the stability of the device while tuning the relative position between the device and the test-rig, the exoskeleton is also mounted on the same platform where the test-rig is mounted. No extra load is added during the experiment. The force signal from sensors is sent to Simulink via USB-6210 DAQ card with the same configuration stated in section 4.3.4. The scenario in this section is repeated for three times.

6.6.2 Results of Joint Force Test

Figure 6-28 shows measured voltage of samples of a 4s period for one cycle specifically singled out. During one cycle, the acquired voltage starts from 2.7V, and peaks up around 6V at the extreme opening position, followed by a symmetric pattern in the closing stage with the opening one. Without consideration of the angle variation, the voltage level stands for 15N to 60N at largest through interpolating the curve fitting equation.

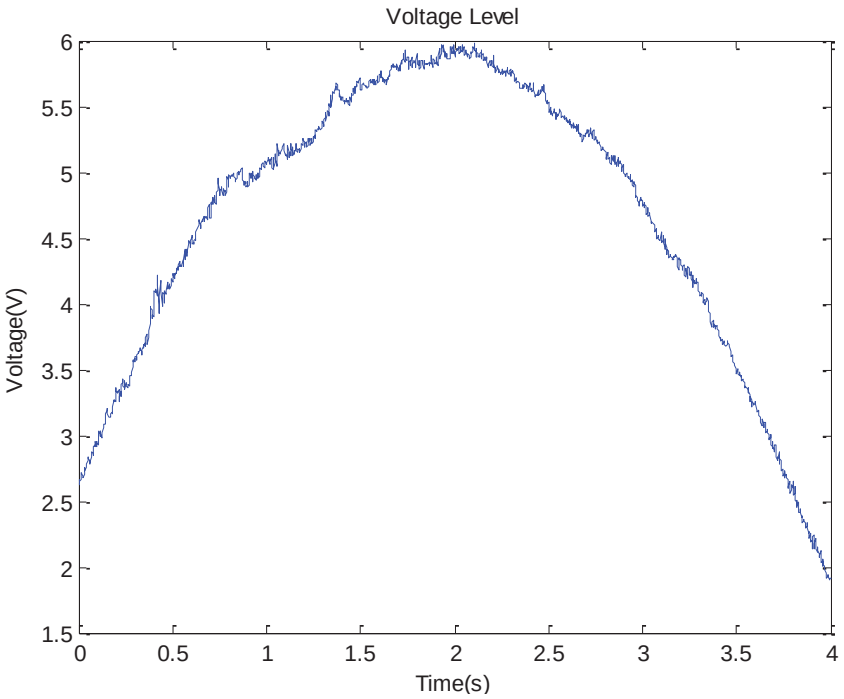

Figure 6-28 Measured joint force in one cycle

The magnitude variation has the same trend in the whole session of the experiment, as shown in Figure 6-29. From the curves in both figures, it can be seen that the voltage is varying linearly from the beginning point to the end, which is not in line with pattern the literature has investigated. But it could not rule out the possibility that continuously increasing force is required to pass the concave formed by the fossa, which can be side-proved by several spots of large impulse before the opening end that shows in Figure 6-29. During all trials, no distinct sign of the impedance to movement has been found, but the device has experienced some

vibration at the beginning of each cycle. Sudden rise can also be found in the opening phase, while the closing phase is much smoother and stiffer in the curvature.

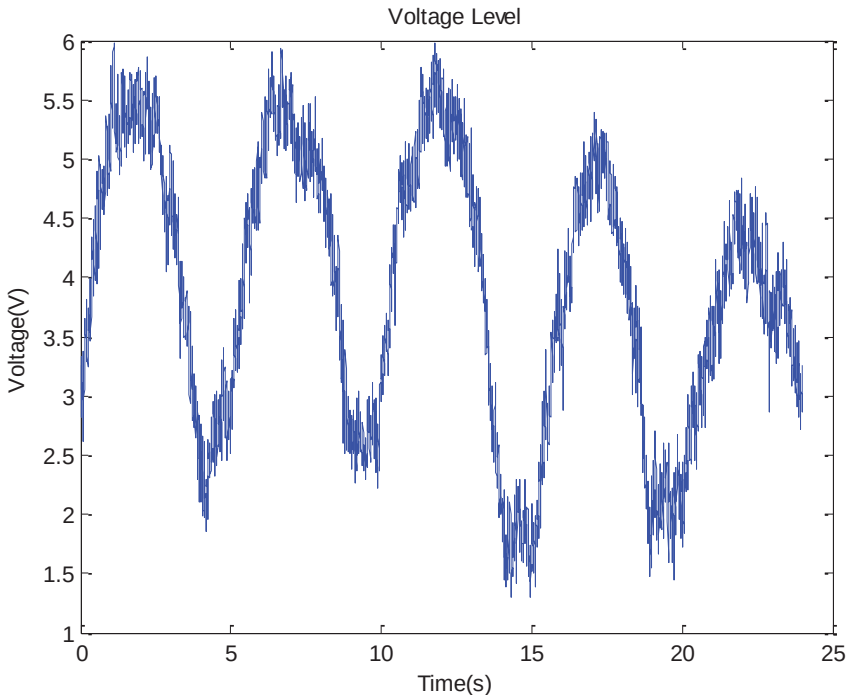

Figure 6-29 Measured joint force in continuous movement

6.6.3 Results in Control Performance

The controller performance is also evaluated in this experimental set-up that mimics the actual condition with loadings. Basically the positional variables are acquired at the same time frame when the device grasps the jaw replica to test the joint force; therefore, multiple cycles with interval in the closed-loop configuration is applied in the test. Since the loading condition that is not embodied in the feed-forward block in the simulation could pose a large difference in terms of the calculated torque, the relationship between the torque and the motion has firstly to be modified before the PID controller is tuned again. The controller simulation based on the SimMechanics model is carried out again to produce the feed-forward and PID parameters. Setups in the linkage subsystem are similar with the integrated human-machine interaction, only the feed-forward block is subject to a body actuator as configured into the same value as the linkage is subject to the mandible and the passive muscular force.

Figure 6-30 illustrates the simulation results after model modification in the closed-loop trial. The crank position in the simulation has a tiny lead compared with the predefined motion, and the maximum deviation hits up to 5°. Figure 6-31 shows the experimental result that behaves unstable at the starting section as similar as shown in the simulation. The tiny lead disappears, since PI controller is configured instead of the PID controller.

It is noticeable in Figure 6-31 that a distinctive shaking phenomenon occurs in the middle session of the closing phase with a relatively large margin of ±2.5° margin compared to the average of the error, about, which is likely be caused by the gravity of the load to be overcome in the opposite direction of the jaw movement. Figure 6-32 gives the experimental results of the crank position with the PI controller that have been refined. The vibration that occurred in the closing phase is eliminated after adjusting the PI parameters, and error has the similar pattern with the result in no loading scenarios

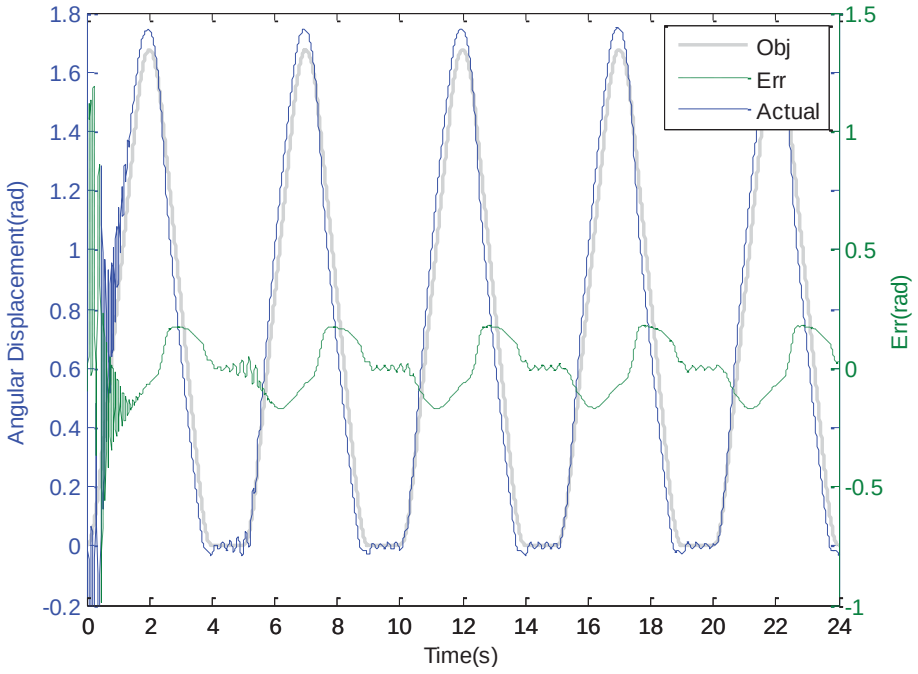

Figure 6-30 Simulation trial

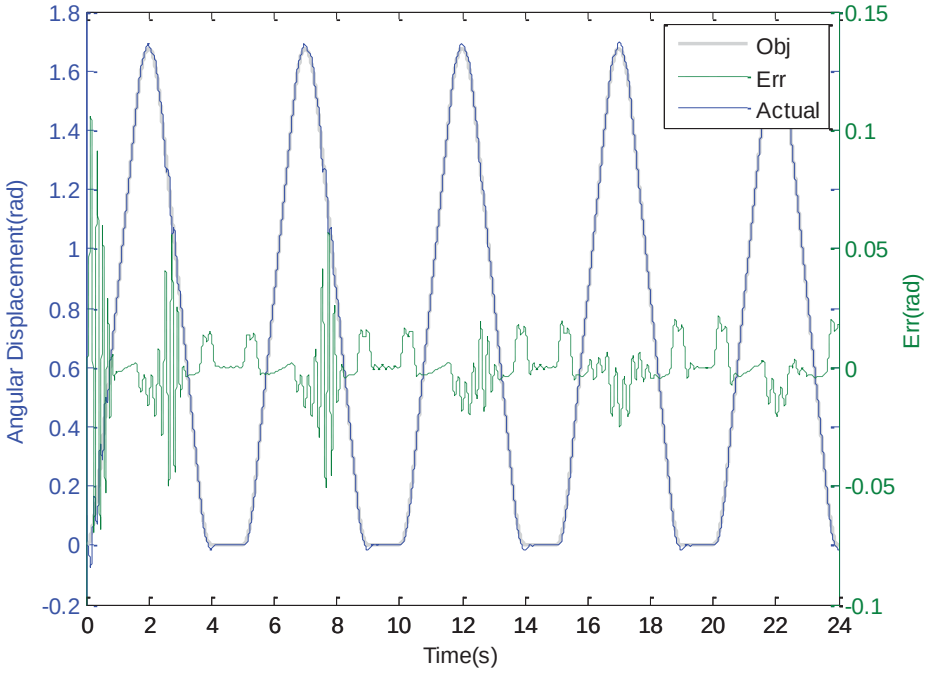

Figure 6-31 Experimental trial one

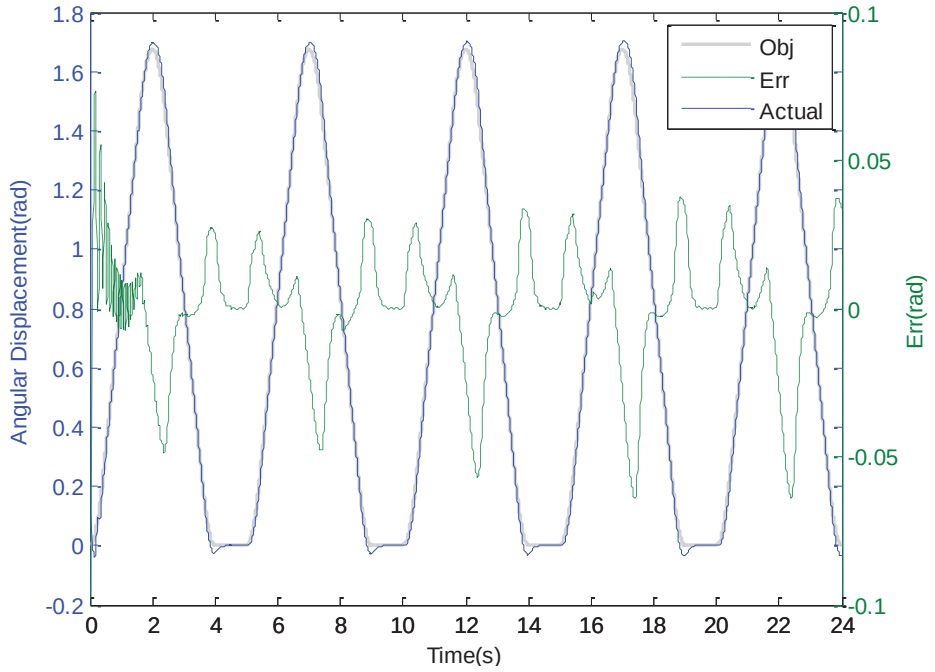

Figure 6-32 Experimental trial two

6.7 Discussions

Nothing stays more critical than the safety for a wearable device that interacts with human in daily life. For most of the researches that dominate in the development of the device, this chapter has discussed the human-machine interaction in terms of the potential detriment. The study in the area of human dynamics pays more attention in the relationship between the force and movement, which seldom touched the circumstance that involves interaction with a device. Therefore, the multi-body dynamic study can be much suitable to be recruited in this application.

6.7.1 Systematic Influence of the Method

Two methods have been recruited in the evaluation of the joint force, i.e. simulation with multi-body dynamics and experiment with a jaw replica. Neither one directly conducts the measurement on the human body, due to the inaccessibility of the inside spot, and inevitably deviates the result from the actual one. The system model in the Simulink neglects the material properties that are highlighted in the force-length relationship with respect to the time, which could severely affect the result if only focusing on the balance state. The active muscular force that plays a major part in the joint force has not been included in the simulation; but this configuration has also been found in the scenario that the jaw-closing muscles are not activated to observe the joint force. The difference of the joint force between subject to the device and one more load can be explanatory of the influence by wearing the device.

Experimental method can be much accurate in acquiring the data, but this test-rig setup has little adaptability to deal with the likely impedance. Muscle force is not implemented in the test-rig. It has been reported the passive muscle force of the jaw opener would peak up at 5 N to at the maximal opening distance. The contact inside the TMJ between the skull and the jaw has always been modeled into rigid contact without articular disc. The sensor installation would impose an internal error to the final result, due to the possible inclination angle to the force.

6.7.2 Comparison of Results

Compared with the joint force that has been referred in the literature, the result produced in this chapter either from the simulation or the experiment is far less than the maximal magnitude. The magnitude of the force level and the trend in response to the cyclic motion is similar; therefore it is considered that the method and the result in both the simulation and the experiment are mutually verified.

Three findings are summarized to account the difference between the current studies in comparison with the literature.

Firstly, the active muscle force is not included, either simulation or the experiment. The active muscle force contributes literally all force to in the mastication, which also affects the loading on the joint as well; and it is confirmed the addition of the active force will exponentially increase the joint force in the literature [198]. Therefore, it can be accountable for the smaller value in the current study.

Secondly, the joint force is rather small during the jaw opening stage if the jaw opener is activated with a tiny level, and approximately 20N according to the literature. Though the simulation results possess a similar trend for the jaw-opening stage, the force level exceeds to a large amount. Results in the jaw closing phase are closely identical; the likely explanation can be the jaw closer exerts little passive force during the closing to make the simulation configuration similar.

The experimental results provide a force level with potential inclination angle with respect to the contact force vector. During the jaw movement, the embedded sensors in the condyle are rotating with the mandible in the same phase. The force in any direction can be reflected in the sensor surface during the force transmission. Large vibration can be explained by this phenomenon.

In conclusion, the joint force obtained in the simulation and experiments that may be deviated from the actual simulation in some aspects, the force level it reflects is basically in line with the literature. The joint force when the user is subject to the device would not exert excessive force from the device.

Chapter 7: Conclusion and Future Expectations

7.1 Conclusion

The concept of a novel wearable assistive device has been proposed in this thesis, for the purpose of providing the forced movement to rehabilitate the disabled jaw movement from either neuromuscular or musculoskeltal causes, since the physical therapy has been advised to spread into the patient, owing to the distinctive efficacy.

The mandibular movement has been reviewed and analyzed based on a planar model. Instead of total replication of the jaw movement in 3D space, the requirement from the rehabilitation underlied the expected movement to be delivered in the treatment. The jaw motion has been confirmed to possess a pattern via in-vivo measurement, which has been recruited to produce a pair of typical trajectories on the condyle and incisor that determine a position of the jaw instantaneous. The adjustable four-bar linkage has been proposed to form the mechanism of the device; and the traditional linkage synthesis has been conducted by globally minimizing the structural error, achieving a set of acceptable results. The linkage has been evaluated with a SimMechanics model, generating good performance in trajectory replication. An interactive GUI program has been developed in MATLAB as a reference to assist users to tune the linkage on their own.

Based on the mechanism, the prototype of the jaw exoskeleton has been designed into a Mechatronic system with the integrated thinking. The Mechatronic construction included the mechanical, electronic and sensory subsystems. The mechanical subsystem based on the four-bar linkage has been designed in the adjustable manner, which allows adapting to the different size and correlated motion path. Passive compliance has also been designed, along with the force response of the spring-based unit. The electronic hardware has been built up based on an evaluation board, with supporting peripheral circuitry to communicate with sensory units. Each sensory unit has been implemented into the break-out board and calibrated. Before the device has been fabricated, the reliability check has been carried out in the mechanical structure of the device; and it showed the design is acceptable.

The device has been entirely modeled in SimMechanics/Simulink, including all participating units, i.e. the linkage, the motor and the controller. Kinematic and dynamic performance of the linkage has firstly been analyzed, with verified by the simulation result in SolidWorks. Then the motor has been simulated with verification of parameters. The closed-loop control

scheme has been proposed to achieve a position control; a feed-forward block provided the predictable control signal while the feedback block corrected the error between the objective and the actual one. A series of simulations has been done under three motion scenarios, which can be visualized in a GUI that was specially programmed to facilitate the motion profile selection. PID controller was tuned in Simulink, and it was further implemented into the MCU-based board. The treatment program has been coded into the controller board hardware, and a simple UI has been coded to display in the built-in screen. With the same motion scenarios, the device has been tested in the performance of the positional control. After tuning the PID on the controller, a good performance in following control commands has been achieved.

The human-machine interaction has been evaluated in the circumstance that the device is worn on the user. The range of motion and the joint force inside the TMJ of the wearer has been investigated in two ways, simulation and experiment. The masticatory system has been modeled in Simulink in order to investigate the joint force based on the mandible dynamics. The simulation result had a force level far less than 100 N compared with the one under similar scenario in the literature. A test-rig where a pair of the jaw and skull replica was mounted has been designed and fabricated, to facilitate the experimental measurement. The recording of the condyle trajectory has been carried out by employing AG500, under different link size combinations. The comparison between the theoretical trajectory and the recorded one showed the device is able to trace the specified trajectory without much discrepancy and would not create harmful influence. Following experiments have been carried out to measure the joint force and investigate the performance of the position controller when subject to the load that is close to the reality. Experimental results shows the force of a less than 100N existing during the movement. The controller has been modified in the feed-forward block to adapt the load in terms of predicted motor signal; and the comparison between the measured angular position and the motion profile suggested a good performance and power level for the device.

7.2 Future Work

Revolving around this topic, future work in the aspect of the device itself includes the refinement of the mechanical parts, the passive compliance and the attachment; the control algorithm is expected to behave adaptive to vast range of the loading condition, especially when the passive compliance is activated. Though the force acting on the jaw is not required to control in this circumstance, the reaction force is expected in full calculation to estimate the feeling from the perspective of users.

References

[1] A. Zoss, H. Kazerooni, and A. Chu, "On the mechanical design of the Berkeley Lower Extremity Exoskeleton (BLEEX)," in *Intelligent Robots and Systems, 2005. (IROS 2005). 2005 IEEE/RSJ International Conference on*, 2005, pp. 3465-3472.

[2] C. J. WALSH, K. ENDO, and H. HERR, "A QUASI-PASSIVE LEG EXOSKELETON FOR LOAD-CARRYING AUGMENTATION," *International Journal of Humanoid Robotics,* vol. 04, pp. 487-506, 2007.

[3] P. Letier, M. Avraam, S. Veillerette, M. Horodinca, M. De Bartolomei, A. Schiele, and A. Preumont, "SAM : A 7-DOF portable arm exoskeleton with local joint control," in *Intelligent Robots and Systems, 2008. IROS 2008. IEEE/RSJ International Conference on*, 2008, pp. 3501-3506.

[4] B. Blasberg and M. Greenberg, "Temporomandibular Disorders," *Burket's oral medicine diagnosis and treatment.,* pp. 271-306, 2003.

[5] B. J. Costello and S. P. Edwards, "Pediatric mandibular hypomobility: current management and controversies," *Oral and Maxillofacial Surgery Clinics of North America,* vol. 17, pp. 455-466, 2005.

[6] S. P. Lehman-Grimes, "A review of temporomandibular disorder and an analysis of mandibular motion," The University of Tennessee, 2005.

[7] V. Miller, V. Bookhan, D. Brummer, and J. Singh, "A mouth opening index for patients with temporomandibular disorders," *Journal of Oral Rehabilitation,* vol. 26, p. 534, 1999.

[8] K. Anderson, G. S. Throckmorton, P. H. Buschang, and H. Hayasaki, "The effects of bolus hardness on masticatory kinematics," *Journal of Oral Rehabilitation,* vol. 29, pp. 689-696, 2002.

[9] D. Ostry, E. Vatikiotis-Bateson, and P. Gribble, "An examination of the degrees of freedom of human jaw motion in speech and mastication," *Journal of Speech, Language and Hearing Research,* vol. 40, pp. 1341-1351, 1997.

[10] E. Vatikiotis-Bateson and D. J. Ostry, "Analysis and modeling of 3D jaw motion in speech and mastication," in *Systems, Man, and Cybernetics, 1999. IEEE SMC '99 Conference Proceedings. 1999 IEEE International Conference on*, 1999, pp. 442-447 vol.2.

[11] R. J. Fonseca, *Oral and Maxillofacial Surgery 2: Orthognathic Surgery* vol. 2: Elsevier Science Health Science Division, 2000.

[12] K. Tveteras and S. Kristensen, "REVIEW The aetiology and pathogenesis of trismus," *Clinical Otolaryngology,* vol. 11, pp. 383-387, 1986.

[13] M. Chidzonga, "Temporomandibular joint ankylosis: review of thirty-two cases," *British Journal of Oral & Maxillofacial Surgery,* vol. 37, pp. 123-126, 1999.

[14] L. Guarda-Nardini, D. Manfredini, and G. Ferronato, "Total temporomandibular joint replacement: A clinical case with a proposal for post-surgical rehabilitation," *Journal of Cranio-Maxillofacial Surgery,* vol. 36, pp. 403-409, 2008.

[15] D. Reinerman and J. Piecuch, "Long-term effects of orthognathic surgery on the temporomandibular joint: comparison of rigid and nonrigid fixation methods," *International Journal of Oral & Maxillofacial Surgery,* vol. 24, pp. 268-272, 1995.

[16] R. B. SALTER, "The Biologic Concept of Continuous Passive Motion of Synovial Joints: The First 18 Years of Basic Research and Its Clinical Application," *Clinical orthopaedics and related research,* vol. 242, pp. 12-25, 1989.

[17] E. M. Culav, C. H. Clark, and M. J. Merrilees, "Connective Tissues: Matrix Composition and Its Relevance to Physical Therapy," *Physical Therapy,* vol. 79, pp. 308-319, March 1, 1999.

[18] P. U. Dijkstra, W. W. I. Kalk, and J. L. N. Roodenburg, "Trismus in head and neck oncology: a systematic review," *Oral Oncology,* vol. 40, pp. 879-889, 2004.

[19] M. M. Lai and R. S. Howard, "Pseudobulbar palsy associated with trismus," *Postgraduate Medical Journal,* vol. 70, pp. 823-824, November 1, 1994.

[20] R. J. Sim, N. Beasley, and C. A. Milford, "Trigeminal neurinoma presenting with trismus," *The Journal of Laryngology & Otology,* vol. 113, pp. 1112-1113, 1999.

[21] M. Bakke, E. Møller, C. E. Thomsen, T. Dalager, and L. M. Werdelin, "Chewing in patients with severe neurological impairment," *Archives of Oral Biology,* vol. 52, pp. 399-403, 2007.

[22] M. J. H. Ariës, P. C. A. J. Vroomen, J. H. van der Hoeven, and J. De Keyser, "Trismus as manifestation of bilateral internal capsule genu infarction," *Clinical Neurology and Neurosurgery,* vol. 110, pp. 305-306, 2008.

[23] V. Kadyan, A. C. Clairmont, M. Engle, and S. C. Colachis, "Severe trismus as a complication of cerebrovascular accident: A case report," *Archives of physical medicine and rehabilitation,* vol. 86, pp. 594-595, 2005.

[24] E. Willoughby and N. Anderson, "Lower cranial nerve motor function in unilateral vascular lesions of the cerebral hemisphere," *British Medical Journal,* vol. 289, p. 791, 1984.

[25] P. Kemppainen, A. Waltimo, H. Palomaki, O. Salonen, M. Kononen, and M. Kaste, "Masticatory force and function in patients with hemispheric brain infarction and hemiplegia," *Journal of Dental Research,* vol. 78, pp. 1810-1814, 1999.

[26] A. Van Der Bilt, F. G. Weijnen, F. Bosman, H. W. Van Der Glas, and J. B. M. Kuks, "Controlled study of EMG activity of the jaw closers and openers during mastication in patients with myasthenia gravis," *European Journal of Oral Sciences,* vol. 109, pp. 160-164, 2001.

[27] Y. Sasakura, S. Kumasaka, T. Takahashi, and J. Shindo, "Myasthenia gravis associated with reduced masticatory function," *International Journal of Oral and Maxillofacial Surgery,* vol. 29, pp. 381-383, 2000.

[28] F. G. Weijnen, A. van der Bilt, J. H. J. Wokke, J. B. M. Kuks, H. W. van der Glas, and F. Bosman, "Maximal bite force and surface EMG in patients with myasthenia gravis," *Muscle & Nerve,* vol. 23, pp. 1694-1699, Nov 2000.

[29] F. G. Weijnen, A. van der Bilt, J. B. M. Kuks, H. W. van der Glas, I. Oudenaarde, and F. Bosman, "Masticatory performance in patients with myasthenia gravis," *Archives of Oral Biology,* vol. 47, pp. 393-398, May 2002.

[30] F. W. BOOTH, "Physiologic and Biochemical Effects of Immobilization on Muscle," *Clinical orthopaedics and related research,* vol. 219, pp. 15-20, 1987.

[31] J. S. Feine, C. G. Widmer, and J. P. Lund, "Physical therapy: A critique," *Oral surgery, oral medicine, oral pathology, oral radiology, and endodontics,* vol. 83, pp. 123-127, 1997.

[32] M. L. McNeely, S. Armijo Olivo, and D. J. Magee, "A Systematic Review of the Effectiveness of Physical Therapy Interventions for Temporomandibular Disorders," *Physical Therapy,* vol. 86, pp. 710-725, May 1, 2006.

[33] R. B. Salter, *Textbook of Disorders and Injuries of the Musculoskeletal System: An Introduction to Orthopaedics, Fractures, and Joint Injuries, Rheumatology, Metabolic Bone Disease, and Rehabilitation*: LIPPINCOTT WILLIAMS & WILKINS, 1999.

[34] S. W. O'Driscoll and N. J. Giori, "Continuous passive motion (CPM): theory and principles of clinical application," *Journal of rehabilitation research and development,* vol. 37, pp. 179-188, 2000.

[35] R. Worland, J. Arredondo, F. Angles, F. Lopez-Jimenez, and D. Jessup, "Home continuous passive motion machine versus professional physical therapy following total knee replacement," *The journal of arthroplasty,* vol. 13, pp. 784-787, 1998.

[36] C. Mavroidis, J. Nikitczuk, B. Weinberg, G. Danaher, K. Jensen, P. Pelletier, J. Prugnarola, R. Stuart, R. Arango, and M. Leahey, "Smart portable rehabilitation devices," *Journal of NeuroEngineering and Rehabilitation,* vol. 2, p. 18, 2005.

[37] B. T. Volpe, H. I. Krebs, and N. Hogan, "Is robot-aided sensorimotor training in stroke rehabilitation a realistic option?," *Current opinion in neurology,* vol. 14, pp. 745-752, 2001.

[38] S. Young and K. H. Kong, "Emerging Therapies in Stroke Rehabilitation," *Ann Acad Med Singapore,* vol. 36, pp. 58-61, 2007.

[39] D. Reinkensmeyer, P. Lum, and J. Winters, "Emerging technologies for improving access to movement therapy following neurologic injury," *Emerging and Accessible Telecommunications, Information and Healthcare Technologies,* 2001.

[40] C. Fraser, M. Power, S. Hamdy, J. Rothwell, D. Hobday, I. Hollander, P. Tyrell, A. Hobson, S. Williams, and D. Thompson, "Driving plasticity in human adult motor cortex is associated with improved motor function after brain injury," *Neuron,* vol. 34, pp. 831-840, 2002.

[41] J. W. Krakauer, "Motor learning: its relevance to stroke recovery and neurorehabilitation," *Current opinion in neurology,* vol. 19, pp. 84-90, 2006.

[42] J. Lund, "Mastication and its control by the brain stem," *Critical Reviews in Oral Biology & Medicine,* vol. 2, p. 33, 1991.

[43] M. Nakata, "Masticatory function and its effects on general health*," *International dental journal,* vol. 48, pp. 540-548, 1998.

[44] B. Sessle, K. Adachi, L. Avivi-Arber, J. Lee, H. Nishiura, D. Yao, and K. Yoshino, "Neuroplasticity of face primary motor cortex control of orofacial movements," *Archives of Oral Biology,* vol. 52, pp. 334-337, 2007.

[45] C. S. Yin, Y. J. Lee, and Y. J. Lee, "Neurological influences of the temporomandibular joint," *Journal of Bodywork and Movement Therapies,* vol. 11, pp. 285-294, 2007.

[46] E. Cohen, D. Deschler, K. Walsh, and R. Hayden, "Early use of a mechanical stretching device to improve mandibular mobility after composite resection: a pilot study," *Archives of physical medicine and rehabilitation,* vol. 86, pp. 1416-1419, 2005.

[47] P. U. Dijkstra, M. W. Sterken, R. Pater, F. K. L. Spijkervet, and J. L. N. Roodenburg, "Exercise therapy for trismus in head and neck cancer," *Oral Oncology,* vol. 43, pp. 389-394, 2007.

[48] P. Nicolakis, B. Erdogmus, A. Kopf, G. Ebenbichler, J. Kollmitzer, E. Piehslinger, and V. Fialka-Moser, "Effectiveness of exercise therapy in patients with internal derangement of the temporomandibular joint," *Journal of Oral Rehabilitation,* vol. 28, p. 1158, 2001.

[49] R. Gilmore, J. Aram, J. Powell, and R. Greenwood, "Treatment of oro-facial hypersensitivity following brain injury," *Brain Injury,* vol. 17, pp. 347-354, 2003.

[50] C.-L. LIN, Y.-C. KUO, and L.-J. LO, "DESIGN, MANUFACTURE AND CLINICAL EVALUATION OF A NEW TMJ EXERCISER," *Biomedical Engineering: Applications, Basis and Communications,* vol. 17, pp. 135-140, 2005.

[51] G. Grandi, M. Silva, C. Streit, and J. Wagner, "A mobilization regimen to prevent mandibular hypomobility in irradiated patients: An analysis and comparison of two techniques," *Med Oral Patol Oral Cir Bucal,* vol. 12, pp. E105-9, 2007.

[52] R. Drake, A. W. Vogl, and A. W. Mitchell, *Gray's anatomy for students*: Churchill Livingstone, 2009.

[53] A. G. Hannam and A. S. McMillan, "Internal Organization in the Human Jaw Muscles," *Critical Reviews in Oral Biology & Medicine,* vol. 5, pp. 55-89, January 1, 1994.

[54] T. M. G. J. van Eijden, J. A. M. Korfage, and P. Brugman, "Architecture of the human jaw-closing and jaw-opening muscles," *The Anatomical Record,* vol. 248, pp. 464-474, 1997.

[55] J. H. Koolstra, "Dynamics of the Human Masticatory System," *Critical Reviews in Oral Biology & Medicine,* vol. 13, pp. 366-376, July 1, 2002.

[56] J. H. Koolstra and T. M. G. J. van Eijden, "Three-dimensional dynamical capabilities of the human masticatory muscles," *Journal of Biomechanics,* vol. 32, pp. 145-152, 1999.

[57] J. H. Koolstra, M. Naeije, and T. M. G. J. Van Eijden, "The Three-dimensional Active Envelope of Jaw Border Movement and its Determinants," *Journal of Dental Research,* vol. 80, pp. 1908-1912, October 1, 2001.

[58] R. W. Brand, D. E. Isselhard, and E. Satin, *Anatomy of orofacial structures*: Mosby Inc, 2003.

[59] Y. Yamada, K. Yamamura, and M. Inoue, "Coordination of cranial motoneurons during mastication," *Respiratory Physiology & Neurobiology,* vol. 147, pp. 177-189, 2005.

[60] J. Lund and A. Kolta, "Generation of the Central Masticatory Pattern and Its Modification by Sensory Feedback," *Dysphagia,* vol. 21, pp. 167-174, 2006/07/01.

[61] D. Yao, K. Yamamura, N. Narita, G. M. Murray, and B. J. Sessle, "Effects of reversible cold block of face primary somatosensory cortex on orofacial movements and related face primary motor cortex neuronal activity," *Somatosensory & Motor Research,* vol. 19, pp. 261-271, 2002.

[62] A. van der Bilt, E. Weijnen, F. A. M. Ottenhoff, H. W. van der Glas, and F. Bosman, "The Role of Sensory Information in the Control of Rhythmic Open-Close Movements in Humans," *Journal of Dental Research,* vol. 74, pp. 1658-1664, October 1, 1995.

[63] K. Fushima, L. M. Gallo, M. Krebs, and S. Palla, "Analysis of the TMJ intraarticular space variation: a non-invasive insight during mastication," *Medical Engineering & Physics,* vol. 25, pp. 181-190, 2003.

[64] K. Fushima, L. Gallo, M. Krebs, and S. Palla, "Analysis of the TMJ intraarticular space variation: a non-invasive insight during mastication," *Medical Engineering and Physics,* vol. 25, pp. 181-190, 2003.

[65] J. Leader, J. Boston, R. Debski, and T. Rudy, "Mandibular kinematics represented by a non-orthogonal floating axis joint coordinate system," *Journal of Biomechanics,* vol. 36, pp. 275-281, 2003.

[66] U. Posselt, "Terminal hinge movement of the mandible," *Journal of Prosthetic Dentistry,* vol. 86, pp. 2-9, Jul 2001.

[67] V. F. Ferrario, C. Sforza, A. Miani, G. Serrao, and G. Tartaglia, "Open-close movements in the human temporomandibular joint: Does a pure rotation around the intercondylar hinge axis exist?," *Journal of Oral Rehabilitation,* vol. 23, pp. 401-408, Jun 1996.

[68] J. P. van Loon, C. H. Falkenstrom, L. G. M. de Bont, G. J. Verkerke, and B. Stegenga, "The theoretical optimal center of rotation for a temporomandibular joint prosthesis: A three-dimensional kinematic study," *Journal of Dental Research,* vol. 78, pp. 43-48, Jan 1999.

[69] J. P. Okeson, *Management of temporomandibular disorders and occlusion*: Mosby, 2007.

[70] R. Sadat-Khonsari, C. Fenske, B. Kahl-Nieke, I. Kirsch, and H. Jüde, "Mandibular Instantaneous Centers of Rotation in Patients With and Without Temporomandibular Dysfunction," *Journal of Orofacial Orthopedics / Fortschritte der Kieferorthopädie,* vol. 64, pp. 256-264, 2003/04/01 2003.

[71] X. Chen, "The instantaneous center of rotation during human jaw opening and its significance in interpreting the functional meaning of condylar translation," *American Journal of Physical Anthropology,* vol. 106, pp. 35-46, 1998.

[72] J. Chen and T. R. Katona, "The limitations of the instantaneous centre of rotation in joint research," *Journal of Oral Rehabilitation,* vol. 26, pp. 274-279, 1999.

[73] M. Yatabe, A. Zwijnenburg, C. Megens, and M. Naeije, "The kinematic center: A reference for condylar movements," *Journal of Dental Research,* vol. 74, pp. 1644-1648, Oct 1995.

[74] M. Yatabe, A. Zwijnenburg, C. C. E. J. Megens, and M. Naeije, "Movements of the Mandibular Condyle Kinematic Center during Jaw Opening and Closing," *Journal of Dental Research,* vol. 76, pp. 714-719, February 1, 1997.

[75] L. M. Gallo, D. B. Gössi, V. Colombo, and S. Palla, "Relationship between Kinematic Center and TMJ Anatomy and Function," *Journal of Dental Research,* vol. 87, pp. 726-730, August 1, 2008

[76] J. J. R. Huddleston Slater, C. M. Visscher, F. Lobbezoo, and M. Naeije, "The Intra-articular Distance within the TMJ during Free and Loaded Closing Movements," *Journal of Dental Research,* vol. 78, pp. 1815-1820, December 1, 1999.

[77] L. M. Gallo, G. B. Airoldi, R. L. Airoldi, and S. Palla, "Description of Mandibular Finite Helical Axis Pathways in Asymptomatic Subjects," *Journal of Dental Research,* vol. 76, pp. 704-713, February 1, 1997.

[78] L. M. Gallo, M. Brasi, B. Ernst, and S. Palla, "Relevance of mandibular helical axis analysis in functional and dysfunctional TMJs," *Journal of Biomechanics,* vol. 39, pp. 1716-1725, 2006.

[79] L. M. Gallo, K. Fushima, and S. Palla, "Mandibular Helical Axis Pathways during Mastication," *Journal of Dental Research,* vol. 79, pp. 1566-1572, August 1, 2000.

[80] R. Sadat-Khonsari, W. Hahn, M. Knösel, K. M. Thieme, H. Nägerl, and D. Kubein-Meesenburg, "Dimeric link chain and instantaneous centers of rotation of the mandible," *Annals of Anatomy - Anatomischer Anzeiger,* vol. 189, pp. 390-392, 2007.

[81] U. Posselt, "Movement areas of the mandible," *The Journal of Prosthetic Dentistry,* vol. 7, pp. 375-385, 1957.

[82] M. Naeije, "Local kinematic and anthropometric factors related to the maximum mouth opening in healthy individuals," *Journal of Oral Rehabilitation,* vol. 29, pp. 534-539, 2002.

[83] V. F. Ferrario, C. Sforza, N. Lovecchio, and F. Mian, "Quantification of translational and gliding components in human temporomandibular joint during mouth opening," *Archives of Oral Biology,* vol. 50, pp. 507-515, 2005.

[84] U. Posselt, *Physiology of occlusion and rehabilitation*: Blackwell Science Ltd, 1968.

[85] T. Kuboki, Y. Azuma, M. Orsini, Y. Takenami, and A. Yamashita, "Effects of sustained unilateral molar clenching on the temporomandibular joint space," *Oral Surgery, Oral Medicine, Oral Pathology, Oral Radiology and Endodontology,* vol. 82, pp. 616-624, 1996.

[86] J. Margielewicz, W. Chladek, and T. Lipski, "Kinematical analysis of mandibular motion in a sagittal plane," *Acta of Bioengineering and Biomechanics,* vol. 10, pp. 9-19, 2008.

[87] A. van der Bilt, "Human oral function: a review," *Braz J Oral Sci,* vol. 1, pp. 7-18, 2002.

[88] K. H. Travers, P. H. Buschang, H. Hayasaki, and G. S. Throckmorton, "Associations between incisor and mandibular condylar movements during maximum mouth opening in humans," *Archives of Oral Biology,* vol. 45, pp. 267-275, Apr 2000.

[89] A. Zwijnenburg, C. C. E. J. Megens, and M. Naeije, "Influence of choice of reference point on the condylar movement paths during mandibular movements," *Journal of Oral Rehabilitation,* vol. 23, pp. 832-837, 1996.

[90] T. Fukui, M. Tsuruta, K. Murata, Y. Wakimoto, H. Tokiwa, and Y. Kuwahara, "Correlation between facial morphology, mouth opening ability, and condylar movement during opening-closing jaw movements in female adults with normal occlusion," *The European Journal of Orthodontics,* vol. 24, pp. 327-336, 2002.

[91] D. Gossi, L. Gallo, E. Bahr, and S. Palla, "Dynamic intra-articular space variation in clicking TMJs," vol. 83, ed: International and American Associations for Dental Research, 2004, pp. 480-484.

[92] A. G. Hannam, "Dynamic modeling and jaw biomechanics," *Orthodontics & Craniofacial Research,* vol. 6, pp. 59-65, 2003.

[93] J. H. Koolstra and T. M. G. J. van Eijden, "Dynamics of the human masticatory muscles during a jaw open-close movement," *Journal of Biomechanics,* vol. 30, pp. 883-889, 1997.

[94] J. H. Koolstra and T. M. G. J. van Eijden, "The jaw open-close movements predicted by biomechanical modelling," *Journal of Biomechanics,* vol. 30, pp. 943-950, 1997.

[95] C. C. Peck, G. E. J. Langenbach, and A. G. Hannam, "Dynamic simulation of muscle and articular properties during human wide jaw opening," *Archives of Oral Biology,* vol. 45, pp. 963-982, 2000.

[96] C. Peck and A. Hannam, "Human jaw and muscle modelling," *Archives of Oral Biology,* vol. 52, pp. 300-304, 2007.

[97] J. Koolstra and T. van Eijden, "A method to predict muscle control in the kinematically and mechanically indeterminate human masticatory system," *Journal of Biomechanics,* vol. 34, pp. 1179-1188, 2001.

[98] B. May, S. Saha, and M. Saltzman, "A three-dimensional mathematical model of temporomandibular joint loading," *Clinical Biomechanics,* vol. 16, pp. 489-495, 2001.

[99] L. R. Iwasaki, P. E. Petsche, W. D. McCall, D. Marx, and J. C. Nickel, "Neuromuscular objectives of the human masticatory apparatus during static biting," *Archives of Oral Biology,* vol. 48, pp. 767-777, 2003.

[100] H. Hansma, G. Langenbach, J. Koolstra, and T. Van Eijden, "Passive resistance increases differentially in various jaw displacement directions," *Journal of dentistry,* vol. 34, pp. 491-497, 2006.

[101] C. C. Peck, A. S. Sooch, and A. G. Hannam, "Forces resisting jaw displacement in relaxed humans: a predominantly viscous phenomenon," *Journal of Oral Rehabilitation,* vol. 29, pp. 151-160, 2002.

[102] D. Anderson, "Measurement of stress in mastication. I," *Journal of dental research,* vol. 35, pp. 664-670, 1956.

[103] J. Pap, *A Chewing Robot Based on Parallel Mechanism--Analysis and Design: A Thesis Presented in Partial Fulfilment of the Requirements for the Degree of Master of Engineering in Mechatronics at Massey University, Palmerston North, New Zealand*: Massey University, Palmerston North, 2006.

[104] E. Helkimo and B. Ingervall, "Bite force and functional state of the masticatory system in young men," *Swedish dental journal,* vol. 2, p. 167, 1978.

[105] T. M. van Eijden, "Biomechanics of the Mandible," *Critical Reviews in Oral Biology & Medicine,* vol. 11, pp. 123-136, January 1, 2000.

[106] A. Perez del Palomar and M. Doblar, "An accurate simulation model of anteriorly displaced TMJ discs with and without reduction," *Medical Engineering & Physics,* vol. 29, pp. 216-226, 2007.

[107] E. Tanaka, K. Hanaoka, T. van Eijden, M. Tanaka, M. Watanabe, M. Nishi, N. Kawai, H. Murata, T. Hamada, and K. Tanne, "Dynamic shear properties of the temporomandibular joint disc," *Journal of Dental Research,* vol. 82, p. 228, 2003.

[108] E. Tanaka, N. Kawai, K. Hanaoka, T. van Eijden, A. Sasaki, J. Aoyama, M. Tanaka, and K. Tanne, "Shear Properties of the Temporomandibular Joint Disc in Relation to Compressive and Shear Strain," *Journal of Dental Research,* vol. 83, pp. 476-479, June 1, 2004.

[109] M. Beek, M. Aarnts, J. Koolstra, A. Feilzer, and T. Van Eijden, "Dynamic properties of the human temporomandibular joint disc," *Journal of Dental Research,* vol. 80, p. 876, 2001.

[110] E. Tanaka, D. P. Rodrigo, M. Tanaka, A. Kawaguchi, T. Shibazaki, and K. Tanne, "Stress analysis in the TMJ during jaw opening by use of a three-dimensional finite element model based on magnetic resonance images," *International Journal of Oral and Maxillofacial Surgery,* vol. 30, pp. 421-430, 2001.

[111] E. Tanaka, D. Rodrigo, Y. Miyawaki, K. Lee, K. Yamaguchi, and K. Tanne, "Stress distribution in the temporomandibular joint affected by anterior disc displacement: a three-dimensional analytic approach with the finite-element method," *Journal of oral rehabilitation,* vol. 27, pp. 754-759, 2000.

[112] J. W. DeVocht, V. K. Goel, D. L. Zeitler, and D. Lew, "A study of the control of disc movement within the temporomandibular joint using the finite element technique," *Journal of Oral and Maxillofacial Surgery,* vol. 54, pp. 1431-1437, 1996.

[113] M. Singh and M. S. Detamore, "Biomechanical properties of the mandibular condylar cartilage and their relevance to the TMJ disc," *Journal of Biomechanics,* vol. 42, pp. 405-417, 2009.

[114] R. del Pozo, E. Tanaka, M. Tanaka, M. Kato, T. Iwabe, M. Hirose, and K. Tanne, "Influence of friction at articular surfaces of the temporomandibular joint on stresses in the articular disk: a theoretical approach with the finite element method," *The Angle Orthodontist,* vol. 73, pp. 319-327, 2003.

[115] J. Lang, "Clinical anatomy of the masticatory apparatus peripharyngeal spaces," ed: G. Thieme Verlag (Stuttgart and New York and New York), 1995.

[116] M. Beek, J. H. Koolstra, L. J. van Ruijven, and T. M. G. J. van Eijden, "Three-dimensional finite element analysis of the human temporomandibular joint disc," *Journal of Biomechanics,* vol. 33, pp. 307-316, 2000.

[117] E. Tanaka, M. Tanaka, Y. Hattori, J. Aoyama, M. Watanabe, A. Sasaki, M. Sugiyama, and K. Tanne, "Biomechanical behaviour of bovine temporomandibular articular discs with age," *Archives of Oral Biology,* vol. 46, pp. 997-1003, 2001.

[118] P. S. Donzelli, L. M. Gallo, R. L. Spilker, and S. Palla, "Biphasic finite element simulation of the TMJ disc from in vivo kinematic and geometric measurements," *Journal of Biomechanics,* vol. 37, pp. 1787-1791, 2004.

[119] M. Beek, J. H. Koolstra, and T. M. G. J. van Eijden, "Human temporomandibular joint disc cartilage as a poroelastic material," *Clinical Biomechanics,* vol. 18, pp. 69-76, 2003.

[120] J. Koolstra, E. Tanaka, and T. Van Eijden, "Viscoelastic material model for the temporomandibular joint disc derived from dynamic shear tests or strain-relaxation tests," *Journal of Biomechanics,* vol. 40, pp. 2330-2334, 2007.

[121] D. M. Smith, K. R. McLachlan, and W. D. McCall, "A Numerical Model of Temporomandibular Joint Loading," *Journal of Dental Research,* vol. 65, pp. 1046-1052, August 1, 1986.

[122] J. C. Nickel, K. R. McLachlan, and D. M. Smith, "A Theoretical Model of Loading and Eminence Development of the Postnatal Human Temporomandibular Joint," *Journal of Dental Research,* vol. 67, pp. 903-910, June 1, 1988.

[123] E. Tanaka and J. H. Koolstra, "Biomechanics of the Temporomandibular Joint," *Journal of Dental Research,* vol. 87, pp. 989-991, November 1, 2008.

[124] E. Tanaka, K. Tanne, and M. Sakuda, "A three-dimensional finite element model of the mandible including the TMJ and its application to stress analysis in the TMJ during clenching," *Medical Engineering & Physics,* vol. 16, pp. 316-322, 1994.

[125] M. Abe, R. Medina-Martinez, K. Itoh, and S. Kohno, "Temporomandibular joint loading generated during bilateral static bites at molars and premolars," *Medical and Biological Engineering and Computing,* vol. 44, pp. 1017-1030, 2006.

[126] J. Chen, U. Akyuz, L. Xu, and R. M. V. Pidaparti, "Stress analysis of the human temporomandibular joint," *Medical Engineering & Physics,* vol. 20, pp. 565-572, 1998.

[127] B. Buranastidporn, M. Hisano, and K. Soma, "Effect of biomechanical disturbance of the temporomandibular joint on the prevalence of internal derangement in mandibular asymmetry," *The European Journal of Orthodontics,* vol. 28, pp. 199-205, June 1, 2006.

[128] Y. Nyashin, M. Mesnard, V. Lokhov, J. Morlier, M. Nyashin, A. Ballu, and M. Cid, "Mechanical actions and pressure in functioning of the human temporomandibular joint," *Computer Methods in Biomechanics and Biomedical Engineering,* vol. 10, pp. 187-188, 2007.

[129] G. Pileicikiene and A. Surna, "The Human Masticatory System From A Biomechanical Perspective: A Review," *Stomatologija,* vol. 6, pp. 81-84, 2004.

[130] M. Beek, J. H. Koolstra, L. J. Van Ruijven, and T. M. G. J. Van Eijden, "Three-dimensional Finite Element Analysis of the Cartilaginous Structures in the Human Temporomandibular Joint," *Journal of Dental Research,* vol. 80, pp. 1913-1918, October 1, 2001.

[131] M. Hirose, E. Tanaka, M. Tanaka, R. Fujita, Y. Kuroda, E. Yamano, T. M. G. J. Van Eijden, and K. Tanne, "Three-dimensional finite-element model of the human temporomandibular joint disc during prolonged clenching," *European Journal of Oral Sciences,* vol. 114, pp. 441-448, 2006.

[132] H. Koga, Y. Usuda, M. Matsuno, Y. Ogura, H. Ishii, J. Solis, A. Takanishi, and A. Katsumata, "Development of the Oral Rehabilitation Robot WAO-1," in *Biomedical Robotics and Biomechatronics, 2008. BioRob 2008. 2nd IEEE RAS & EMBS International Conference on*, 2008, pp. 556-561.

[133] E. Flores, S. Fels, and E. Vatikiotis-Bateson, "Chew on this: Design of a 6DOF anthropomorphic robotic jaw," in *Robot and Human interactive Communication, 2007. RO-MAN 2007. The 16th IEEE International Symposium on*, 2007, pp. 648-653.

[134] W. L. Xu, J. E. Bronlund, J. Potgieter, K. D. Foster, O. Rohrle, A. J. Pullan, and J. A. Kieser, "Review of the human masticatory system and masticatory robotics," *Mechanism and Machine Theory,* vol. 43, pp. 1353-1375, Nov 2008.

[135] S. Molnar, "Mechanical Simulation of Human Chewing Motions," *Journal of Dental Research,* vol. 47, pp. 559-563, July 1, 1968.

[136] T. Hayashi, S. Tanaka, S. Nakajima, H. Kobayashi, Y. Yamada, and M. Miyakawa, "Control mechanism of an autonomous jaw-movement simulator, JSN/1C, during open-close movement," in *Engineering in Medicine and Biology Society, 1996. Bridging Disciplines for Biomedicine. Proceedings of the 18th Annual International Conference of the IEEE*, 1996, pp. 613-614 vol.2.

[137] T. Hayashi, S. Kato, S. Yamada, S. Nakajima, Y. Yamada, and H. Kobayashi, "A physiological control of chewing-like jaw movement for robotized jaw simulator

JSN/2A," in *Engineering in Medicine and Biology Society, 2000. Proceedings of the 22nd Annual International Conference of the IEEE*, 2000, pp. 730-731 vol.1.

[138] A. Takanishi, T. Tanase, M. Kumei, and I. Kato, "Development of 3 DOF jaw robot WJ-2 as a human's mastication simulator," in *Advanced Robotics, 1991. 'Robots in Unstructured Environments', 91 ICAR., Fifth International Conference on*, 1991, pp. 277-282 vol.1.

[139] H. Takanobu, T. Tanase, A. Takanishi, and I. Kato, "Adaptive masticatory jaw motion using jaw position and biting force information," in *Multisensor Fusion and Integration for Intelligent Systems, 1994. IEEE International Conference on MFI '94.*, 1994, pp. 360-365.

[140] H. Takanobu, T. Yajima, and A. Takanishi, "Development of a mastication robot using nonlinear viscoelastic mechanism," in *Intelligent Robots and Systems, 1997. IROS '97., Proceedings of the 1997 IEEE/RSJ International Conference on*, 1997, pp. 1527-1532 vol.3.

[141] H. Takanobu, N. Kuchiki, and A. Takanishi, "Control of rapid closing motion of a robot jaw using nonlinear spring mechanism," in *Intelligent Robots and Systems 95. 'Human Robot Interaction and Cooperative Robots', Proceedings. 1995 IEEE/RSJ International Conference on*, 1995, pp. 372-377 vol.1.

[142] H. Takanobu, T. Yajima, M. Nakazawa, A. Takanishi, K. Ohtsuki, and M. Ohnishi, "Quantification of masticatory efficiency with a mastication robot," in *Robotics and Automation, 1998. Proceedings. 1998 IEEE International Conference on*, 1998, pp. 1635-1640 vol.2.

[143] H. Takanobu, T. Akizuki, A. Takanishi, K. Ohtsuki, D. Ozawa, M. Ohnishi, and A. Okino, "Jaw training robot that manipulates patient's jaw to sideway," in *Intelligent Robots and Systems, 2002. IEEE/RSJ International Conference on*, 2002, pp. 1463-1468 vol.2.

[144] B. Daumas, W. L. Xu, and J. Bronlund, "Jaw mechanism modeling and simulation," *Mechanism and Machine Theory,* vol. 40, pp. 821-833, Jul 2005.

[145] W. L. Xu, J. S. Pap, and J. Bronlund, "Design of a Biologically Inspired Parallel Robot for Foods Chewing," *Industrial Electronics, IEEE Transactions on,* vol. 55, pp. 832-841, 2008.

[146] W. L. Xu, J. D. Torrance, B. Q. Chen, J. Potgieter, J. E. Bronlund, and J. S. Pap, "Kinematics and experiments of a life-sized masticatory robot for characterizing food texture," *Ieee Transactions on Industrial Electronics,* vol. 55, pp. 2121-2132, May 2008.

[147] K. Alemzadeh and D. Raabe, "Prototyping Artificial Jaws for the Bristol Dento-Munch Robo-Simulator; `A parallel robot to test dental components and materials'," in *Engineering in Medicine and Biology Society, 2007. EMBS 2007. 29th Annual International Conference of the IEEE*, 2007, pp. 1453-1456.

[148] D. Raabe, K. Alemzadeh, A. J. L. Harrison, and A. J. Ireland, "The chewing robot: A new biologically-inspired way to evaluate dental restorative materials," in *Engineering in Medicine and Biology Society, 2009. EMBC 2009. Annual International Conference of the IEEE*, 2009, pp. 6050-6053.

[149] L. Lo, C. Lin, and Y. Chen, "A device for temporomandibular joint exercise and trismus correction: design and clinical application," *Journal of Plastic, Reconstructive & Aesthetic Surgery,* vol. 61, pp. 297-301, 2008.

[150] H. Takanobu, A. Takanishi, D. Ozawa, K. Ohtsuki, M. Ohnishi, and A. Okino, "Integrated dental robot system for mouth opening and closing training," in *Robotics and Automation, 2002. Proceedings. ICRA '02. IEEE International Conference on*, 2002, pp. 1428-1433 vol.2.

[151] H. U. Takanobu and A. Takanishi, "Dental robotics and human model," in *Neural Engineering, 2003. Conference Proceedings. First International IEEE EMBS Conference on*, 2003, pp. 671-674.

[152] H. Takanobu, K. Nakamura, A. Takanishi, K. Ohtsuki, D. Ozawa, M. Ohnishi, and A. Okino, "Human skull robot as a mechanical patient simulator for mouth opening and closing training," in *Intelligent Robots and Systems, 2001. Proceedings. 2001 IEEE/RSJ International Conference on*, 2001, pp. 2154-2159 vol.4.

[153] C. Sun, J. E. Bronlund, L. Huang, M. P. Morgenstern, and W. L. Xu, "A Linkage Chewing Machine for Food Texture Analysis," in *Mechatronics and Machine Vision in Practice, 2008. M2VIP 2008. 15th International Conference on*, 2008, pp. 299-304.

[154] C. Salles, A. Tarrega, P. Mielle, J. Maratray, P. Gorria, J. Liaboeuf, and J. J. Liodenot, "Development of a chewing simulator for food breakdown and the analysis of in vitro flavor compound release in a mouth environment," *Journal of Food Engineering,* vol. 82, pp. 189-198, 2007.

[155] R. Akhras and J. Angeles, "Unconstrained nonlinear least-square optimization of planar linkages for rigid-body guidance," *Mechanism and Machine Theory,* vol. 25, pp. 97-118, 1990.

[156] C. Chen, S. Bai, and J. Angeles, "A Comprehensive Solution Of The Classic Burmester Problem," *Transactions of the Canadian Society for Mechanical Engineering,* vol. 32, pp. 137-154, 2008.

[157] J. Yao and J. Angeles, "Computation of all optimum dyads in the approximate synthesis of planar linkages for rigid-body guidance," *Mechanism and Machine Theory,* vol. 35, pp. 1065-1078, 2000.

[158] Y. Chen and J. Fu, "A computational approach for determining location of Burmester solutions with fully rotatable cranks," *Mechanism and Machine Theory,* vol. 34, pp. 549-558, 1999.

[159] X. Che, Y. Luo, J. Yang, and Z. He, "Application of Universal Grey Algorithm to Solutions of Algebraic Based on Wu Elimination Method," in *Natural Computation, 2008. ICNC'08. Fourth International Conference on*, 2008, pp. 289-293.

[160] Y. Luo, "The Research of Mechanism Synthesis Based on Mechanical System Chaos Anti-control Methods," in *Intelligent Robotics and Applications*. vol. 5928, M. Xie, Y. Xiong, C. Xiong, H. Liu, and Z. Hu, Eds., ed: Springer Berlin Heidelberg, 2009, pp. 554-561.

[161] Y. Luo, B. Zeng, and Z. He, "Hyper-Chaotic Mathematical Programming Method and Its Application to Dodecahedron Variable Geometry Truss Manipulator," in *Advances in Neural Networks – ISNN 2009*. vol. 5551, W. Yu, H. He, and N. Zhang, Eds., ed: Springer Berlin Heidelberg, 2009, pp. 1033-1040.

[162] P. J. Martin, K. Russell, and R. S. Sodhi, "On mechanism design optimization for motion generation," *Mechanism and Machine Theory,* vol. 42, pp. 1251-1263, 2007.

[163] V. Jovanovic and K. Kazerounian, "Using chaos to obtain global solutions in computational kinematics," *TRANSACTIONS-AMERICAN SOCIETY OF MECHANICAL ENGINEERS JOURNAL OF MECHANICAL DESIGN,* vol. 120, pp. 299-304, 1998.

[164] X. Jin and C. Yong, "A Chaos-based Approach to Obtain the Global Real Solutions of Burmester Points " *China Mechanical Engineering,* pp. 74-76+6, 2002.

[165] R. Sancibrian, P. García, F. Viadero, and A. Fernández, "A general procedure based on exact gradient determination in dimensional synthesis of planar mechanisms," *Mechanism and Machine Theory,* vol. 41, pp. 212-229, 2006.

[166] P. S. Shiakolas, D. Koladiya, and J. Kebrle, "On the optimum synthesis of six-bar linkages using differential evolution and the geometric centroid of precision positions technique," *Mechanism and Machine Theory,* vol. 40, pp. 319-335, 2005.

[167] J. A. Cabrera, A. Simon, and M. Prado, "Optimal synthesis of mechanisms with genetic algorithms," *Mechanism and Machine Theory,* vol. 37, pp. 1165-1177, 2002.

[168] M. Da Lio, V. Cossalter, and R. Lot, "On the use of natural coordinates in optimal synthesis of mechanisms," *Mechanism and Machine Theory,* vol. 35, pp. 1367-1389, 2000.

[169] A. M. Dollar and H. Herr, "Lower Extremity Exoskeletons and Active Orthoses: Challenges and State-of-the-Art," *Robotics, IEEE Transactions on,* vol. 24, pp. 144-158, 2008.

[170] R. A. R. C. Gopura, K. Kiguchi, and D. S. V. Bandara, "A brief review on upper extremity robotic exoskeleton systems," in *Industrial and Information Systems (ICIIS), 2011 6th IEEE International Conference on*, 2011, pp. 346-351.

[171] F. Ozkul and D. Barkana, "Design and Control of an Upper Limb Exoskeleton Robot RehabRoby Towards Autonomous Robotic Systems." vol. 6856, R. Groß, L. Alboul, C. Melhuish, M. Witkowski, T. Prescott, and J. Penders, Eds., ed: Springer Berlin / Heidelberg, 2011, pp. 125-136.

[172] F. Martinez, I. Retolaza, A. Pujana-Arrese, A. Cenitagoya, J. Basurko, and J. Landaluze, "Design of a five actuated DoF upper limb exoskeleton oriented to workplace help," in *Biomedical Robotics and Biomechatronics, 2008. BioRob 2008. 2nd IEEE RAS & EMBS International Conference on*, 2008, pp. 169-174.

[173] A. Denève, S. Moughamir, L. Afilal, and J. Zaytoon, "Control system design of a 3-DOF upper limbs rehabilitation robot," *Computer Methods and Programs in Biomedicine,* vol. 89, pp. 202-214, 2008.

[174] C. Xiong, X. Jiang, R. Sun, X. Huang, and Y. Xiong, "Control methods for exoskeleton rehabilitation robot driven with pneumatic muscles," *Industrial Robot: An International Journal,* vol. 36, pp. 210-220, 2009.

[175] N. Tsagarakis and N. Caldwell, "A Compliant exoskeleton for multi-planar upper limb physiotherapy and training," *Advanced Robotics, Invited Paper,(submitted),* 2007.

[176] J. E. Pratt, B. T. Krupp, C. J. Morse, and S. H. Collins, "The RoboKnee: an exoskeleton for enhancing strength and endurance during walking," in *Robotics and Automation, 2004. Proceedings. ICRA '04. 2004 IEEE International Conference on*, 2004, pp. 2430-2435 Vol.3.

[177] T. Hayashi, H. Kawamoto, and Y. Sankai, "Control method of robot suit HAL working as operator's muscle using biological and dynamical information," in *Intelligent Robots and Systems, 2005. (IROS 2005). 2005 IEEE/RSJ International Conference on*, 2005, pp. 3063-3068.

[178] S. Lee and Y. Sankai, "Power assist control for walking aid with HAL-3 based on EMG and impedance adjustment around knee joint," in *Intelligent Robots and Systems, 2002. IEEE/RSJ International Conference on*, 2002, pp. 1499-1504 vol.2.

[179] T. Nef, M. Mihelj, G. Kiefer, C. Perndl, R. Muller, and R. Riener, "ARMin-exoskeleton for arm therapy in stroke patients," 2007, pp. 68-74.

[180] R. Jiménez-Fabián and O. Verlinden, "Review of control algorithms for robotic ankle systems in lower-limb orthoses, prostheses, and exoskeletons," *Medical Engineering & Physics,* vol. 34, pp. 397-408, 2012.

[181] K. Kiguchi, T. Tanaka, and T. Fukuda, "Neuro-fuzzy control of a robotic exoskeleton with EMG signals," *Fuzzy Systems, IEEE Transactions on,* vol. 12, pp. 481-490, 2004.

[182] C.-J. Yang, B. Niu, and Y. Chen, "Adaptive neuro-fuzzy control based development of a wearable exoskeleton leg for human walking power augmentation," in *Advanced Intelligent Mechatronics. Proceedings, 2005 IEEE/ASME International Conference on*, 2005, pp. 467-472.

[183] J. H. Koolstra and T. M. G. J. van Eijden, "Combined finite-element and rigid-body analysis of human jaw joint dynamics," *Journal of Biomechanics,* vol. 38, pp. 2431-2439, 2005.

[184] N. Curtis, K. Kupczik, P. O'Higgins, M. Moazen, and M. Fagan, "Predicting Skull Loading: Applying Multibody Dynamics Analysis to a Macaque Skull," *The Anatomical Record: Advances in Integrative Anatomy and Evolutionary Biology,* vol. 291, pp. 491-501, 2008.

[185] M. Moazen, N. Curtis, S. E. Evans, P. O'Higgins, and M. J. Fagan, "Combined finite element and multibody dynamics analysis of biting in a Uromastyx hardwickii lizard skull," vol. 213, ed: Blackwell Publishing Ltd, 2008, pp. 499-508.

[186] A. Pérez del Palomar and M. Doblaré, "Dynamic 3D FE modelling of the human temporomandibular joint during whiplash," *Medical Engineering & Physics,* vol. 30, pp. 700-709, 2008.

[187] D. Kubein-Meesenburg, H. Nägerl, R. Schwestka-Polly, K. M. Thieme, J. Fanghänel, and B. Miehe, "Functional conditions of the mandible: theory and physiology," *Annals of Anatomy - Anatomischer Anzeiger,* vol. 181, pp. 27-32, 1999.

[188] H. Kimura, Y. Fukuoka, and A. H. Cohen, "Adaptive Dynamic Walking of a Quadruped Robot on Natural Ground Based on Biological Concepts," *The International Journal of Robotics Research,* vol. 26, pp. 475-490, May 1, 2007.

[189] X. Wu and S. Ma, "CPG-based control of serpentine locomotion of a snake-like robot," *Mechatronics,* vol. 20, pp. 326-334, 2010.

[190] Y. Uchiyama, C. Nagai, and G. Obinata, "Simulation of human walking with powered orthosis for designing practical assistive device," in *Engineering in Medicine and Biology Society (EMBC), 2012 Annual International Conference of the IEEE*, 2012, pp. 4816-4819.

[191] W. Xu and J. Bronlund, "Neural Control of a Mastication Robot," in *Mastication Robots*. vol. 290, ed: Springer Berlin / Heidelberg, 2010, pp. 237-270.

[192] K. Matsuoka, "Sustained oscillations generated by mutually inhibiting neurons with adaptation," *Biological Cybernetics,* vol. 52, pp. 367-376, 1985.

[193] K. Matsuoka, "Analysis of a neural oscillator," *Biological Cybernetics,* vol. 104, pp. 297-304, 2011.

[194] A. M. Arsenic, "On stability and tuning of neural oscillators: application to rhythmic control of a humanoid robot," in *Neural Networks, 2004. Proceedings. 2004 IEEE International Joint Conference on*, 2004, p. 104.

[195] L. J. Ruijven and W. A. Weijs, "A new model for calculating muscle forces from electromyograms," *European Journal of Applied Physiology and Occupational Physiology,* vol. 61, pp. 479-485, 1990/12/01 1990.

[196] A. Zierdt, P. Hoole, and H. G. Tillmann, "Development of a system for three-dimensional fleshpoint measurement of speech movements," 1999.

[197] K. D. Foster, A. Woda, and M. A. Peyron, "Effect of Texture of Plastic and Elastic Model Foods on the Parameters of Mastication," *Journal of Neurophysiology,* vol. 95, pp. 3469-3479, June 1, 2006.

[198] J. Koolstra and T. Van Eijden, "Combined finite-element and rigid-body analysis of human jaw joint dynamics," *Journal of Biomechanics,* vol. 38, pp. 2431-2439, 2005.

Chapter 8: Appendix

8.1 Figures of Electronic Parts

Following figures illustrate electronic parts that are designed and fabricated in Chapter 4, including sensors and conditioning circuit boards.

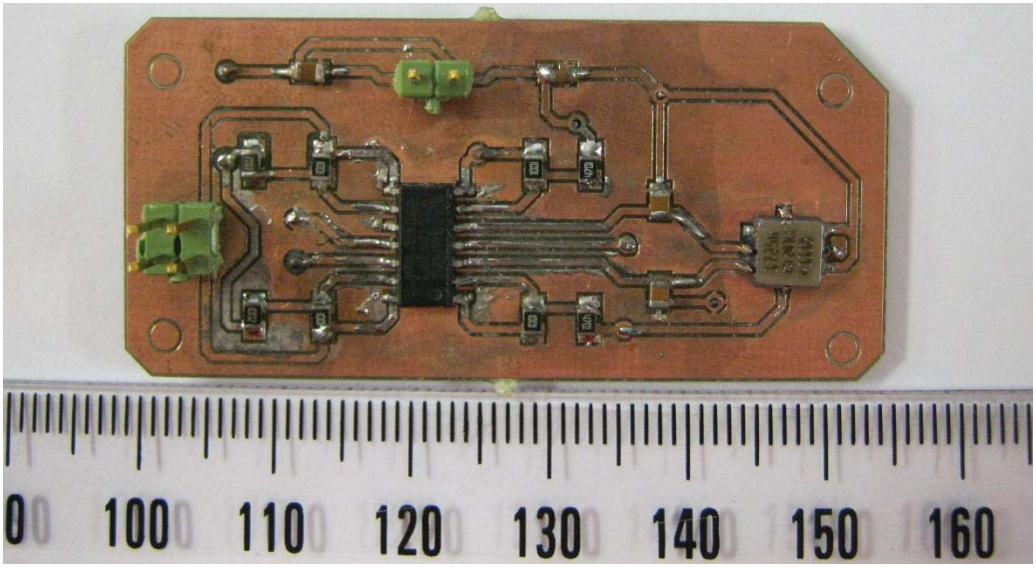

Figure 8-1 The break-out circuit board of accelerometer

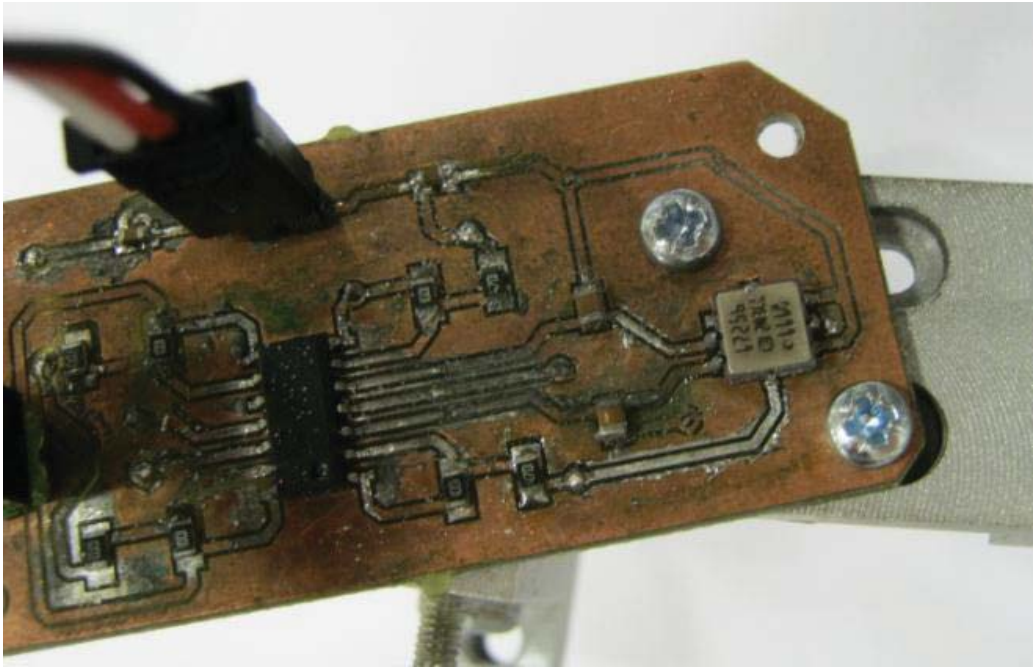

Figure 8-2 Installation of the tilt angle board on the coupler

Figure 8-3 *Flexiforce* sensor

The difference between two force conditioning boards lies in the usage of a 4-channel digital potentiometer as the resistance (R_{f}) in the board shown in Figure 8-4 (B) the value of which can be adjusted through accessing the port in the electronic system, leaving the contact force dynamic to adapt the different feeling. Figure 8-5 gives the photo of the board connecting with sensors in operation.

A B

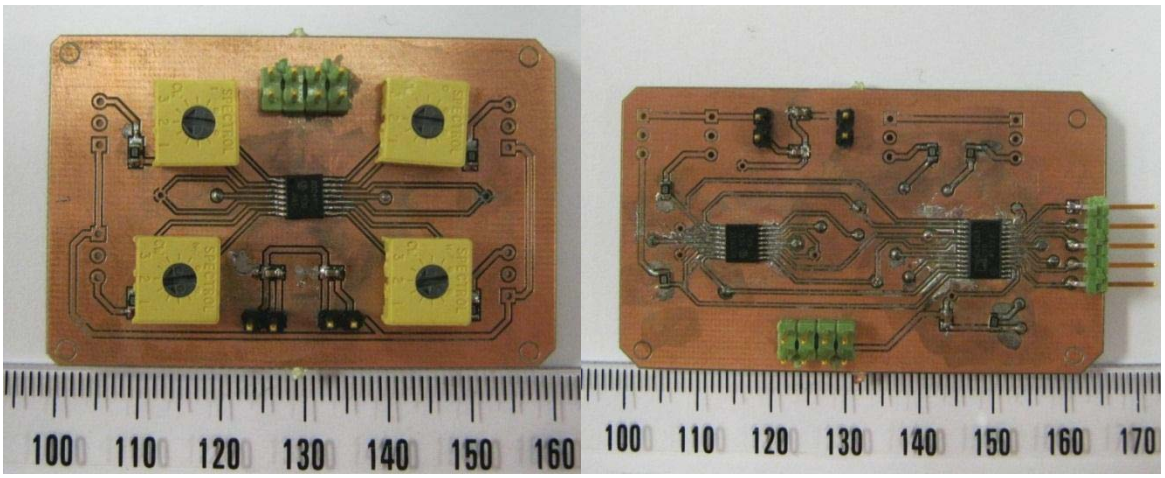

Figure 8-4 *Flexiforce* sensor break-out circuit boards

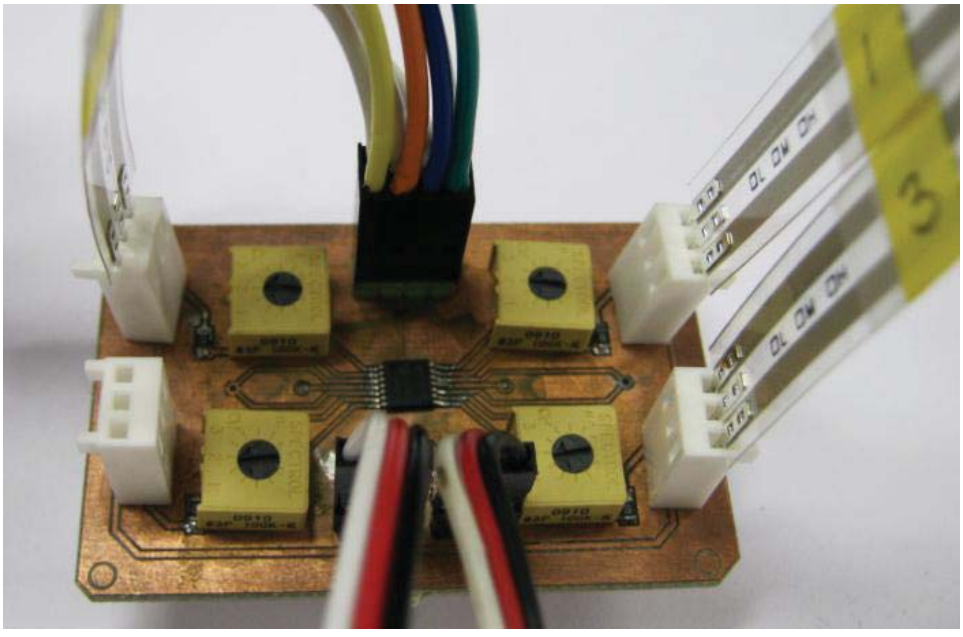

Figure 8-5 Circuit board of force sensor in operation

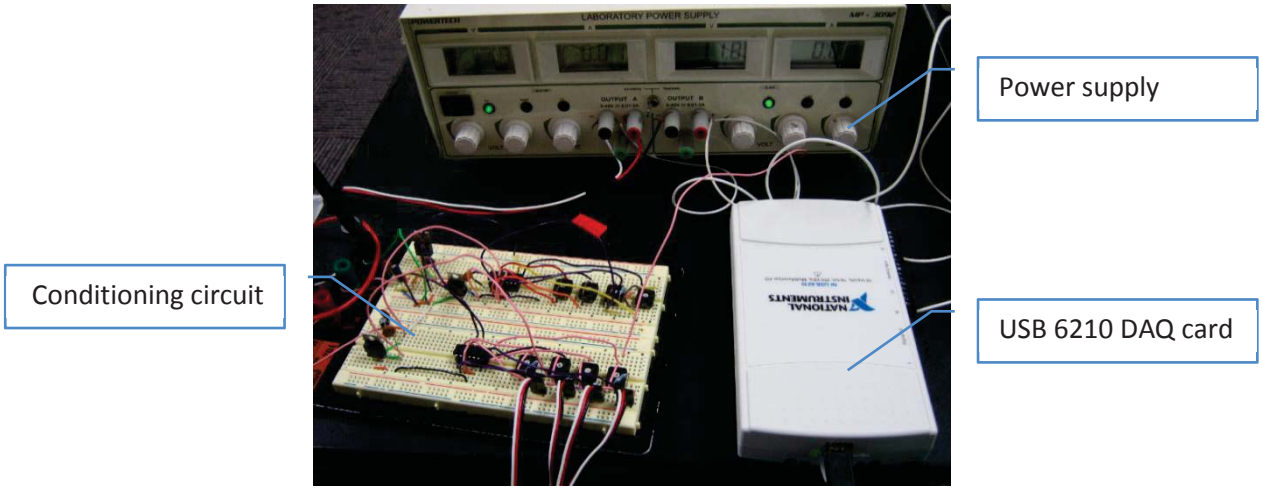

Figure 8-6 Data acquisition with USB 6210

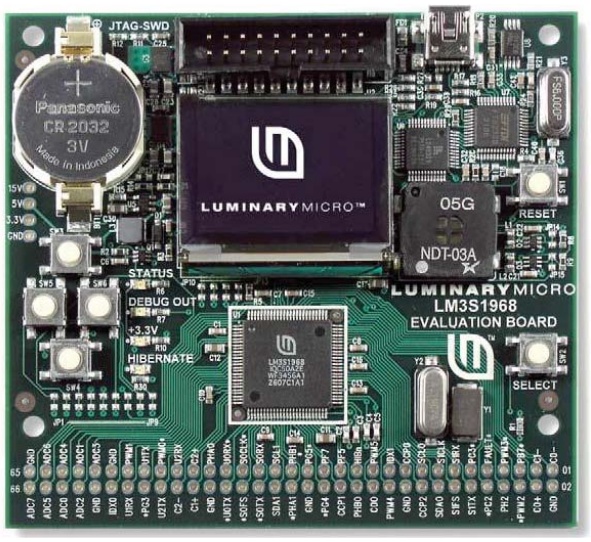

Figure 8-7 LM3S1968 board

8.2 Figures of Complete Model in SimMechanics

Following figures illustrate complete block models of the device that are built up in SimMechanics. Figure 8-8 shows the construction with ideal configurations of joints and links, while Figure 8-9 gives an illustration of the actual system converted from SolidWorks that consists of all parts in the device.

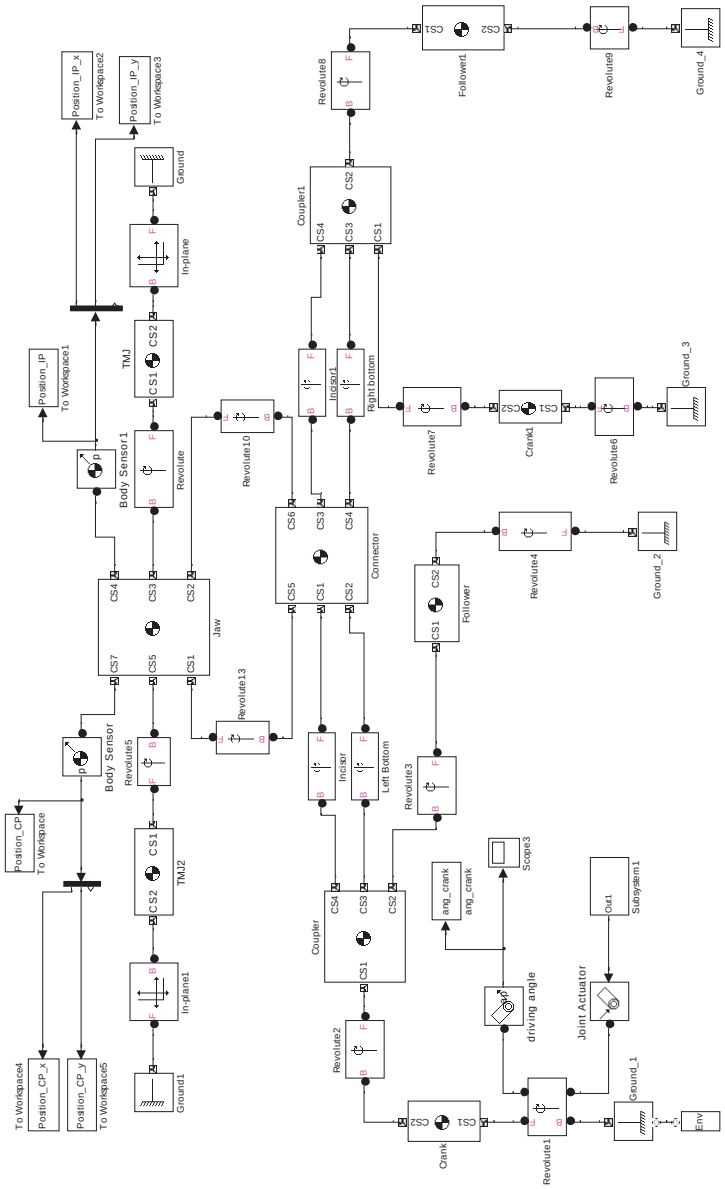

Figure 8-8 Overall linkage model built in SimMechanics

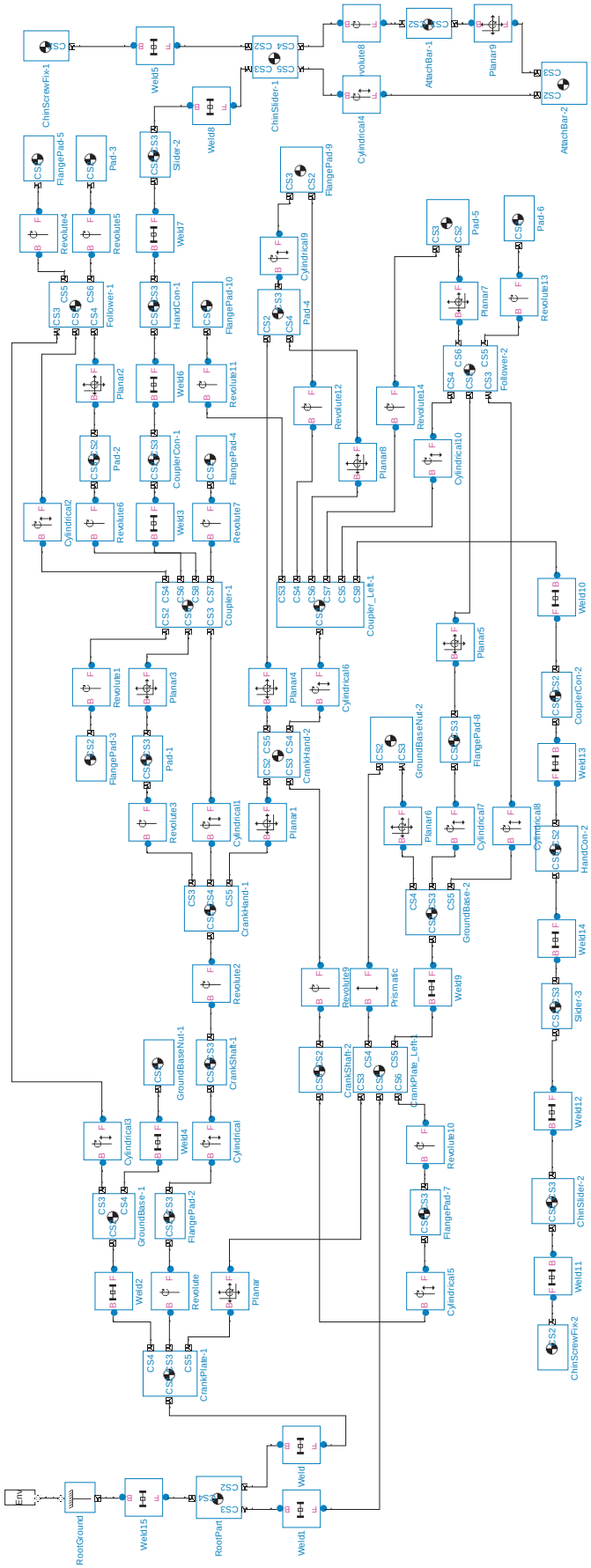

Figure 8-9 Converted block diagram in SimMechanics